THÈSE DE DOCTORAT

Soutenue à Aix-Marseille Université

MicroAlgae Processes Platform – CEA Tech Région Sud (DRT)
UMR 7265 - Institut de Biosciences et Biotechnologies d'Aix-Marseille (BIAM)

.....

Alexandre SIX

Study of polysaccharides accumulation in microalgae for bioplastic applications

.....

Discipline : Biologie Spécialité : Biologie végétale. Ecole doctorale : Sciences de la vie et de la santé.

Soutenue le 02/07/2024 devant le jury :

Céline Laroche, PR – Univ. Clermont Auvergne, CNRS, Institut Pascal	Rapportrice
Filipa Lopes, PR – Univ. Paris-Saclay, CentraleSupélec, LGPM	Rapportrice
Jean-Luc Putaux, DR – Univ. Grenoble Alpes, CNRS, CERMAV	Examinateur
Olivier Gonçalvez, PR – Univ. Nantes, Oniris, GEPEA	Examinateur
Gatien Fleury, Ingénieur-chercheur – CEA	Encadrant de thèse
Yonghua Li-Beisson, DR – Univ. Aix-Marseille, CEA, CNRS, BIAM	Directrice de thèse

Affidavit

I, undersigned, Alexandre SIX, hereby declare that the work presented in this manuscript is my own work, carried out under the scientific supervision of Yonghua LI-BEISSON and Gatien FLEURY in accordance with the principles of honesty, integrity and responsibility inherent to the research mission. The research work and the writing of this manuscript have been carried out in compliance with both the French national charter for Research Integrity and the Aix-Marseille University charter on the fight against plagiarism.

This work has not been submitted previously either in this country or in another country in the same or in a similar version to any other examination body.

Place Aix-En-Provence, date 09/02/2024.

Alexandre SIX



Cette œuvre est mise à disposition selon les termes de la Licence Creative Commons Attribution - Pas d'Utilisation Commerciale - Pas de Modification 4.0 International.

List of publications and conference attendance

Publications:

I. Six A., Dimitriades-Lemaire A., Lancelon-Pin C., Putaux J.-L., Dauvillée D., Petroutsos D., Alvarez P., Sassi J.-F., Li-Beisson Y., and Fleury G. (2024). "Red light induces starch accumulation in *Chlorella vulgaris* without a} ecting photosynthesis e ciency, unlike abiotic stresses".
Under submission process.

II. Six A., Chambonnière P., Fon-Sing S., Alvarez P., Sassi J.-F., Li-Beisson Y., and Fleury G. (2024). "Optimization of the light supply for fast starch accumulation in *Chlorella vulgaris* outdoor culture".
In preparation for submission.

III. Six A., Lancelon-Pin C., Putaux J.-L., Dauvillée D., Sassi J.-F., Le Moigne N., Li-Beisson Y., and Fleury G. (2024). "Extraction, characterization and plasticization of microalgae starch into thermoplastic starch".
In preparation for submission.

Conference attendance:

1. AlgaEurope 2023. Six A., Fleury G., Compadre. A, Dimitriades-Lemaire A., Alvarez P., Lancelon-Pin C., Putaux J.-L., Putaux J.-L., Dauvillée D., Sassi J.-F., and Li-Beisson Y. "Bridging the gap from raw microalgae to bioplastic: conversion of *Chlorella vulgaris* into thermoplastic starch"
Oral presentation.

2. PSE young scientists 2023. Six A., Fleury G., Compadre. A, Dimitriades-Lemaire A., Alvarez P., Lancelon-Pin C., Putaux J.-L., Molina-Boisseau S., Sailler P., Putaux J.-L., Dauvillée D., Sassi J.-F., and Li-Beisson Y. "Extraction and puri⁒cation of *Chlorella vulgaris* starch for bioplastic applications"
Oral presentation.

3. AlgaEurope 2022. Six A., Fleury G., Alvarez P., Delrue F., Fon-Sing S., Compadre. A, Dimitriades-Lemaire A., Dauvillée D., Petroutsos D., Sassi J.-F., and Li-Beisson Y. "Evaluation of light quality, temperature and nutritive deprivation impact onto starch accumulation in *Chlorella vulgaris*"
Poster presentation.

Summary

Biobased and biodegradable plastics offer a promising alternative to traditional plastics, aiming to reduce the pollution they cause. Among the resources used for bioplastic production, starch is highly sought after. However, the current production is limited and allocated to other uses such as food industry. In response to this demand, microalgae are emerging as high-potential starch producers.

Microalgae possess a remarkable ability to accumulate large quantities of starch in response to stress. This capacity could be industrially exploited for starch production, but requires the development of specific cultivation and extraction processes, as well as achieving positive energy and economic efficiency. The objective of this work was to study microalgae starch production and its conversion into bioplastics, aiming to better understand the challenges associated with industrial scale-up.

The experimental work initially involved comparing known methods for inducing the starch accumulation. It was demonstrated that the absence of blue light induces continuous starch accumulation without imposing stress on the culture. Based on this technique, a simpler continuous cultivation process could be developed, with similar productivity to the current two-stage method.

Furthermore, we evaluated the optimal conditions for natural light supply during the starch production phase. Under natural light and nutritional stress, microalgae cannot reach their maximum starch content without diminishing their light utilization efficiency. Thus, it is essential to find the right balance for the final starch content. Under our experimental conditions, a final starch content of approximately 50% led to a theoretically higher areal starch productivity than plants.

Finally, we developed an extraction process recovering microalgal starch with a yield of 98%. The starch recovered from microalgae was utilized to produce thermoplastic starch (TPS), marking the first demonstration of microalgal starch plasticization using industrially relevant techniques.

In conclusion, this research provides new practical knowledge on starch accumulation, outdoor cultivation, and the conversion processes of microalgae into bioplastics. It represents a step forward towards the industrial production of bioplastics from microalgae starch.

Keywords: microalgae, bioplastics, starch, starch accumulation, abiotic stress, light quality, light modelling, plasticization, thermoplastic-starch.

Résumé

Les plastiques biosourcés et biodégradables sont une alternative prometteuse pour remplacer les plastiques traditionnels et réduire la pollution qu'ils engendrent. Parmi les ressources utilisées pour la fabrication de bioplastiques, l'amidon est largement sollicité pour sa disponibilité et ses propriétés. Cependant, la production actuelle d'amidon est affectée à d'autres usages et peut difficilement être augmentée. En réponse à cette demande, les microalgues émergent comme des producteurs d'amidon à haut potentiel.

Les microalgues ont la propriété remarquable de pouvoir accumuler de grandes quantités d'amidon en réponse au stress. Cette particularité pourrait s'exploiter à des fins de production industrielle d'amidon, mais nécessite d'abord de développer des procédés de culture et d'extraction spécifiques. La difficulté majeure de ce développement est d'obtenir un bilan énergétique et économique positif. Afin de mieux appréhender les défis liés à une échelle industrielle, l'objectif de ce travail a été d'étudier la production d'amidon de microalgues et sa conversion en bioplastiques.

Le travail expérimental a d'abord consisté à comparer les méthodes connues pour induire l'accumulation d'amidon dans les chlorophycées, en utilisant *Chlorella vulgaris* CCALA924 comme cas d'utilisation. Il a été montré que l'absence de lumière bleue induit une accumulation constante d'amidon sans générer de stress pour la culture. A partir de cette technique, il serait possible de développer un procédé de culture continu plus simple et aussi productif que la méthode actuelle en deux étapes utilisée en référence dans ce travail.

D'autre part, nous avons évalué les conditions optimales d'apport en lumière naturelle durant la phase de production d'amidon qui a lieu sous stress nutritionnel. En lumière naturelle et sous stress, les microalgues ne peuvent pas atteindre leur contenu maximal d'amidon sans compromettre l'efficacité de l'utilisation de la lumière. Il est ainsi essentiel de trouver un équilibre pour le contenu final en amidon. Dans nos conditions expérimentales, un compromis sur le contenu final d'amidon d'environ 50% mène à une productivité surfacique d'amidon au moins similaire aux plantes.

Enfin, nous avons développé un procédé d'extraction de l'amidon de microalgues dont le rendement est de 98%. L'amidon extrait des microalgues a été transformé en amidon thermoplastique (TPS, pour thermoplastic starch), marquant la première démonstration de plastification d'amidon de microalgues à l'aide de techniques similaires à l'industrie.

En conclusion, cette recherche apporte de nouvelles connaissances pratiques sur l'accumulation d'amidon, sur la culture en contexte extérieur, et sur les procédés de conversion des microalgues en bioplastiques. Elle constitue une avancée vers la production industrielle de bioplastiques à partir d'amidon de microalgues.

Mots clés : microalgue, bioplastique, amidon, accumulation d'amidon, stress abiotique, qualité de la lumière, modélisation de la lumière, plastification, amidon thermo-plastique.

Acknowledgments

A PhD is a deeply personal project. During these three years, I had the chance to do what I am passionate about. But in many aspects, this PhD was more than just a research project. It was a great 3-years journey that enriched me a lot, both as a young scientist and as a person.

For sure, the quality of this experience and resulting work has been significantly influenced by the many people who supported me. I express my intense gratitude to those who contributed, whether nearby or from afar, to easing my path during this PhD. You provided me with your assistance, inspiration or guidance, and you created a supportive work environment. So for this, thank you.

First of all, I want to thank my supervisor, Gatien Fleury, for its dedication and implication throughout these years. Thank you for your insistence on rigor and excellence in our work, for your surreal availability, and for your never fading kindness. It has been a pleasure working with you. I also want to thank my thesis director, Yonghua Li-Beisson, for her guidance, her presence, and the kind advice.

Next, I obviously want to thanks all the members of the Microalgae Processes Platform. First, thank you very much Camille for your dedication and energy during your internship. Although our results have not made it into this manuscript, I appreciate your hard work and positive attitude. Alexandra, thank you for your kindness, your patient help with technical issues, and your crucial role in maintaining the laboratory. Thank you Florian for the friendly talks and your help, direct or indirect, in the laboratory. Jean-François, thank you for the pleasant conversations as desk neighbors, for your insights into the world of algae, and for staying very late at work with me, even though the revolutionary experiment I was conducting completely screwed up.

To the Nenu2PHAr team Ana, Carole, Mathis, Pablo, and Sophie, it was great working together, and I will remember vividly the moments in the greenhouse. Chloé and Anne, many thanks to both of you for your always good mood, the nice conversations, and the kind support you gave me. To my fellow PhDs, Adriana, Alejandra, and María, I appreciated very much to share with you the science, struggles, and joys that are part of the PhD life. Maria, you are now in charge of our legacy, but don't worry, we are living proof that PhDs do come to an end. Paul and Thibaut, thank you for your friendship. I will cherish the moments we have shared.

Finally, I warmly thank all the other members of the PRTT DSUD. Eliane, Juliette, and Patricia, thank you for your essential administrative support. To the team INUM and all the others, I will remember the very nice moments we shared over coffee, in the canteen, and during our sport breaks. I had great colleagues and I am proud to call many of you as my friends.

In addition to my direct colleagues, I extend my gratitude to those who made significant contributions to the content of this PhD. David, thank you for participating to my thesis committees, for welcoming me into your laboratory, for conducting amylose quantification in my samples, and for sharing the original starch extraction

protocol with me. This protocol definitely paved the way towards the pilot-scale extraction of starch. Nicolas, thank you for your reactivity and enthusiasm when we first approached you about starch plasticization, for welcoming me into your laboratory to conduct the plasticization trials, and for sharing you time and pedagogy to introduce me to the world of plastics. Jean-Luc, I greatly appreciated the time you dedicated to exchange with me about starch and electronic microscopy, and your assistance with the publication of our results. I also want to thank Jérémy Pruvost for his participation to my thesis committees.

I also thank the members of the BIAM that helped me in various circumstances: Gilles Pelletier, for introducing me to the technique of chlorophyll fluorescence; Bernard Genty, for evaluating the capabilities of my fluorometer, discussing my fluorometry results, and suggesting new experiments; Stephan Cuiné, for providing the light filters that were essential to cover glass bottles in a crucial experiment; Ousmane Dao, for kindly reviewing the photorespiration section; Maureen Saint-Sorny, for the memorable Fête de la Science weekend where we used every ounce of our energy to handle a thousand visitors at our boot.

Finally, I express my gratitude to all the members of the jury, Filipa Lopes, Céline Laroche, Olivier Gonçalvez, and Jean-Luc Putaux, for taking their time to evaluate my work. I also thank the Région PACA and the European project Nenu2PHAr for funding my PhD.

It is customary to also thank the family, and this time, I have a specific reason to do so: many thanks to my sister, Isaline Six, for the time she spent on Photoshop to create a wonderful Chlorella figure (Figure 1.2). I also thank all my family for their kind review of the introduction section, and more generally, for their continuous support.

I finally address my deepest gratitude to Cécile. It looked easy because you were there. Thank you for helping me find balance. Thank you for supporting me. Thank you for accompanying me on this journey, and beyond.

Table of content

A davit 2

List of publications and conference attendance 3

Summary 4

Résumé 5

Acknowledgments 6

Table of content 8

List of figures 12

List of tables 14

List of abbreviations 15

Introduction 16

Objectives of this PhD thesis 19

Chapter 1 - State of the art: from microalgae to bioplastics 20

1.1 Microalgae and photosynthesis 21

1.1.1 Microalgae and the model *Chlorella vulgaris* 21

1.1.2 Photosynthesis in green microalgae 25

1.1.3 Monitoring photosynthesis by fluorometry 32

1.1.4 Conclusion 35

1.2 Light management in microalgae cultivation 35

1.2.1 Light utilization and interactions in microalgae culture 35

1.2.2 Microalgae culture systems 39

1.2.3 Microalgae as converters of solar energy 43

1.2.4 Conclusion 45

1.3 Microalgal starch as building blocks for bioplastics 46

1.3.1 Starch in microalgae 46

1.3.2 Microalgal starch production 49

1.3.3 Starch recovery and plasticization 51

1.3.4 Conclusion 52

1.4 Conclusion 53

Chapter 2 - Materials & Methods 54

2.1 Microalgae cultivation (Paper I, II, III) 54
2.1.1 Strain & Medium 54
2.1.2 Growth monitoring 54
2.1.3 Cultivation in the different set-ups 55
2.2 Analytical techniques (Paper I,II,III) 57
2.2.1 Biomass and supernatant characterization 57
2.2.2 Photosystem II status 59
2.2.3 Assessment of cell rupture 60
2.2.4 Electron microscopy 60
2.3 Starch characterization (Paper I,III) 62
2.3.1 Starch structure 62
2.3.2 Small- and wide-angle X-ray scattering (SAXS and WAXS) 62
2.3.3 Differential scanning calorimetry (DSC) 62
2.3.4 Granulometry 62
2.4 Productivity and statistics (Paper I) 62
2.4.1 Calculation of productivities and conversion of total carbohydrates values into starch. 62
2.4.2 Statistical analysis 63
2.5 Relationships between light flux and starch accumulation (Paper II) .. 63
2.5.1 Calculations of photon flux per biomass PFPB 63
2.5.2 Calculations of starch accumulation parameters 63
2.5.3 Starch accumulation and light-per-biomass relationships 64
2.6 Starch extraction, plasticization and characterization 65
2.6.1 Extraction from microalgal biomass 65
2.6.2 Starch materials and control TPS 65
2.6.3 Optical microscopy observations of starch plasticization 65
2.6.4 Extrusion and injection of TPS 65
2.6.5 Tensile tests 66

Chapter 3 - Results 67

Paper I - Red light induces starch accumulation in *Chlorella vulgaris* without a} ecting photosynthesis e ciency, unlike abiotic stresses ... 68

Graphical abstract 68
Abstract 68
I.1 Motivation and research objectives 69
I.2 Results 70

I.2.1 Starch accumulation 70
I.2.2 Starch structure 74
I.2.3 Biomass composition 75
I.2.4 Photosynthetic capacity 79
I.2.5 Cell wall thickness and cell rupture 81
I.2.6 Application perspectives 83
I.3 Conclusion 85

Paper II - Optimization of the light supply for fast starch accumulation in *Chlorella vulgaris* outdoor culture 86

II.1 Motivation & research objectives 86
II.2 Results 87
II.2.1 Sudden nitrogen deprivation under laboratory conditions under long night 87
II.2.2 Impact of biomass concentration for starch accumulation under sunlight 89
II.2.3 Determination of the initial biomass concentration for optimal starch accumulation 97
II.2.4 Discussion: Model limitations and its implication for the two-stage process 100
II.3 Conclusion 102

Paper III - Microalgal starch extraction, characterization and plasticization 103

III.1 Motivation & research objectives 103
III.2 Results 104
III.2.1 Extraction of the starch-enriched microalgae 104
III.2.2 Characterization of microalgal starch 110
III.2.3 Plasticization of microalgal starch and characterization 112
III.3 Conclusion 122

Chapter 4 - General discussion and perspectives 124

4.1 Technical limitations of this work 124
4.2 Future experimental perspectives 126
4.3 General discussion 127

Conclusion 133

Appendices 135

Appendix A. Supplementary materials of Paper I.....135
Appendix B. Light input in vertical cylindrical bottle and flat panel PBR142
Appendix C. Supplementary material Paper II.....151
Appendix D. Extended summary (French) 154
Introduction 154
Etat de l'art 155
Résultats expérimentaux.....157
Discussion et perspectives 163
Conclusion.....164
References 166

List of figures

Figure 1.1: Morphological diversity of microalgae. 22
Figure 1.2: Cell morphology of the microalgae *Chlorella vulgaris*. 23
Figure 1.3: Development of cell wall during the cell cycle of Chlorella. 24
Figure 1.4: Simplified schematic representation of the electron transport chain and general light reactions of the photosynthesis. 26
Figure 1.5: Simplified representation of the role of the RuBisCo protein in the photorespiration and Calvin-Benson processes. 27
Figure 1.6: Light capture by chlorophyll molecules. 28
Figure 1.7: Mechanisms of photoprotection by non-photochemical quenching 30
Figure 1.8: Variation of pigmentation and antenna cross-section. 31
Figure 1.9: Fluorometry analysis by pulse-and-probe method. 33
Figure 1.10: Photosynthesis (P) versus irradiance (I) curve. 36
Figure 1.11: Light experienced by the microalgae cells depending on the biomass concentration. 38
Figure 1.12: Ionic forms of inorganic carbon in water, and CO_2 exchange with air-water interface. 39
Figure 1.13: Raceway and circular ponds, the two most popular open culture systems. 40
Figure 1.14: Vertical, tubular, and flat panel photobioreactors (PBR). 41
Figure 1.15: Amylose and amylopectin molecules. 46
Figure 1.16: Representation of the starch granule 47
Figure 1.17: Induction of starch accumulation. 50
Figure 1.18: The three steps of starch extraction from microalgae and the associated techniques employed in the literature. 51

Figure 2.1: Measured emission spectra of white and red LEDs 55
Figure 2.2: TEM image of cell wall from a *Chlorella vulgaris* cell 61

Figure I.1: TEM images of ultrathin section of resin-embedded *Chlorella vulgaris* cells 71
Figure I.2: Impact of abiotic factors on biomass and carbohydrate accumulation in *Chlorella vulgaris* CCALA924. 72
Figure I.3: Separation of amylopectin and amylose on CL-2B chromatography 75
Figure I.4: Changes in protein and lipid contents upon starch induction. 77
Figure I.5: Evolution of total chlorophyll concentration 78
Figure I.6: Response of cultures photosynthetic capacities to starch induction methods. 79
Figure I.7: Evolution of absorbed light energy repartition 80
Figure I.8: Variations of cell wall thickening over time and corresponding effects on cell rupture. 83

Figure II.1: Effect of long night on biomass growth after sudden nitrogen deprivation. 88
Figure II.2: Experimental set-up for outdoor culture cultivation 89
Figure II.3: Biomass growth of nitrogen-deprived cultures in 1L bottles and under natural light. 90
Figure II.4: Optical and electron microscopy pictures of *Chlorella vulgaris* cells 91
Figure II.5: Evolution of carbohydrates accumulation over the range of photon flux per biomass. 93
Figure II.6: *Chlorella vulgaris* culture after 3 days of nitrogen-starvation 94
Figure II.7: Biomass growth of nitrogen-deprived culture in 180L flat panel PBR and under natural light. 95
Figure II.8: Carbohydrates accumulation according to the photon flux per biomass 96
Figure II.9 Starch accumulation according to photon flux per biomass PFPB and to active biomass concentration Xa. 99

Figure II.10: Starch accumulation according to mean daily photon flux density I_M and to active biomass concentration Xa. 100

Figure III.1: Disruption of microalgae cells along the pressure cycles. 105
Figure III.2: Proportion of starch recovery from the initial cell lysate for several dilution. 106
Figure III.3: Purification of the crude starch pellet with water rinsing. 106
Figure III.4: Growth of the microalgae biomass after induction of starch accumulation by nitrogen deprivation 107
Figure III.5: Flowchart of the starch extraction protocol 107
Figure III.6: Starch purification with successive water rinsing. 110
Figure III.7: Microalgal starch granules observed with scanning electron microscopy (magnifications 10 000 X and 20 000 X). 110
Figure III.8: Structural characterization of the extracted microalgal starch. 111
Figure III.9: Differential scanning calorimetry of the microalgal starch. 112
Figure III.10: Optical microscopy observations of starch plasticization in glycerol with increasing temperatures, without polarizer. 114
Figure III.11: Starch plasticization in glycerol with increasing temperatures, observed by optical microscopy equipped with polarizer. 115
Figure III.12: Injected dogbone specimens of potato TPS, microalgal TPS, plasticized raw biomass, and commercial TPS. 116
Figure III.13 : Scanning electron microscopy images of the materials in their initial and plasticized forms 118
Figure III.14: Cross-section of cryo-fracturated raw biomass injected specimen. The dogbone specimen was obtained by extrusion and injection of a mix of 70%w/w entire microalgae cells and 30%w/w glycerol. Starch granules still largely intact and therefore unplasticized can be observed inside broken microalgae cells. 119
Figure III.15: Tensile mechanical properties of commercial, potato and microalgal TPS evaluated by tensile test. The p-values for the comparisons indicated in the graph are calculated with Prism 9 (Graphpad Software, LLC) and based on ANOVA Tukey's multiple comparisons test (***, $P = 0.0007$; ****, $P < 0.0001$; $7 \leqslant n \leqslant 10$) 120
Figure III.16: Tensile mechanical properties of microalgal TPS with 7.5 or 10 % additional water, evaluated by tensile test. 121

Figure 4.1: Inoculum preparation leads to reduced starch productivity. 128

Figure A.1: TEM images of ultrathin sections of resin-embedded *Chlorella vulgaris* cells 137
Figure A.2: Cell wall thickness compared to the mean diameter of the corresponding cell. 138
Figure A.3: FAME profile of *Chlorella vulgaris* CCALA924 according to four growth conditions 138
Figure A.4: Relative electron transport rate (rETR) over the starch induction time 139
Figure A.5: Thickness of the outer cell wall, measured on three regions for at least 60 cells per condition. 139
Figure A.6: Illustration of an instantaneous light curve obtained by fluorometric assay and the associated key values 140
Figure A.7: Optical density of the biological triplicates in the 4 conditions 140
Figure A.8: Measurement of the maximal quantum yield (QYmax) of the biological triplicates in the 4 conditions 141

Figure B.1: Representation of surface considered for the direct equivalent model 143
Figure B.2: Description of light beams incidence on the PBR surface 144
Figure B.3: Refraction and reflection of light at the different parts of the reactor wall. 147

List of tables

Table 1.1: Theoretical and practical estimations of solar energy conversion 44
Table 1.2: Comparison of starch and fatty acids functional properties. 48

Table I.1: Biomass, carbohydrate, and starch-equivalent productivities during 4 days 73
Table I.2: Protein, lipid and chlorophyll productivity during 4 days 76

Table II.1: Estimation of the carbohydrate accumulation outcomes simulated from different photon flux per biomass. 98

Table III.1: Content in class of compounds for initial cell lysate, separated fractions, and purified starch. The composition of non-disrupted biomass was very similar to the cell lysate. 109
Table III.2: Recovery of the class of compounds in the different fractions after the separation step 109

Table 4.1: Yield in starch or sucrose from the main crops 130

Table A.S1: Nutrient availability in culture media of control N+ and red light illumination RL 135
Table A.S2: Table characterization of biomass and compound evolution during the starch induction experiments 135
Table A.S3: Biomass growth parameters and productivities of compounds during the starch induction experiments 136
Table A.S4: Mean cell wall thickness and cellular growth rate for every growth condition 136

Table B.1: Light quantification according to the different light models. 150

Table C.1: Data set of the laboratory experiment with long nights. 151
Table C.2: Data set of the 1L-bottle experiment for the nine bottles. 153
Table C.3: Data set of the 180L PBR experiment. 153
Table C.4: Calculated values of the identification parameters 153

List of abbreviations

AP	Areal productivity
Chl$a$	Chlorophyll a
Chla/b	Ratio of chlorophyll a and chlorophyll b
Chl$b$	Chlorophyll b
DW	Dry weight
E	Young's modulus
F_M	Relative maximum fluorescence yield in dark-adapted conditions
F_M'	Relative maximum fluorescence yield during illumination
F_S	Relative fluorescence yield in steady-state illumination
HPH	High-pressure homogenizer
HT	Harsh (i.e. supra-optimal) temperature condition
LC	Light curve
N-	Nitrogen-deprived media condition
N+	Control growth condition with complete media, optimal temperature and white light illumination
OD_{880}	Optical density measured at 880 nm
PAR	Photoactive radiations
PBR	Photobioreactor
PE	Photosynthetic efficiency
PFD	Photon Flux Density ($mol_{photon}/m^2/s$)
PFPB	Photon Flux Per Biomass ($mol_{photon}/g_a/s$)
QY_{max}	Maximal quantum yield
RL	Red-light illumination condition
TPS	Thermoplastic starch
VP	Volumetric productivity
wt%	Percentage of dry weight
X_0	Initial biomass
X_a	Active biomass
ΔpH	Trans-thylakoid pH gradient
λ_{max}	Wavelength at the maximal absorbance
σ_{max}	Maximal stress
Φf,d	Sum of Φf – quantum yield of fluorescence, and Φd – quantum yield of constitutive thermal energy dissipation at steady state
ΦNPQ	Quantum yield of ΔpH- and xanthophyll-regulated thermal energy dissipation at steady-state
ΦPSII	Quantum yield of PS II photochemistry at steady-state
Im	Daily mean PFD on the reactor ($mol_{photon}/m^2/s$), calculated from actual solar measurements

Introduction

The Earth's climate is changing at an unprecedented pace, attributed to the anthropogenic release of greenhouse gas (GHG). The global temperature has already increased by 1.1°C since the industrial revolution and could reach between +1.4 and +4.4°C in 2100 depending on the reduction of GHG emissions (IPCC, 2023). These global temperatures will be the highest ever experienced by any individuals of the Homo genus. After 3 million years of evolution in a cooler climate, current population will witness the effects of climate change in the year 2100.

Climate change represents a direct threat to mankind. In many populated areas, the combined increase of temperature and humidity will make the outdoor conditions barely tolerable for the human body, with a direct risk of death for most of the year (IPCC et al., 2023). To mitigate the consequences of climate change, most nations agreed to limit global temperature increase to 1.5°C above the pre-industrial era. Achieving this goal requires a substantial drop of 5% in annual GHG emissions, comparable to the emission reduction observed in 2020 during the global lockdown, albeit requiring an additional reduction each subsequent year. Economic analysis reveals that transitioning away from fossil energy to stay below the 1.5°C limit would require a war economy as seen in the USA during WWII (Jacques et al., 2023).

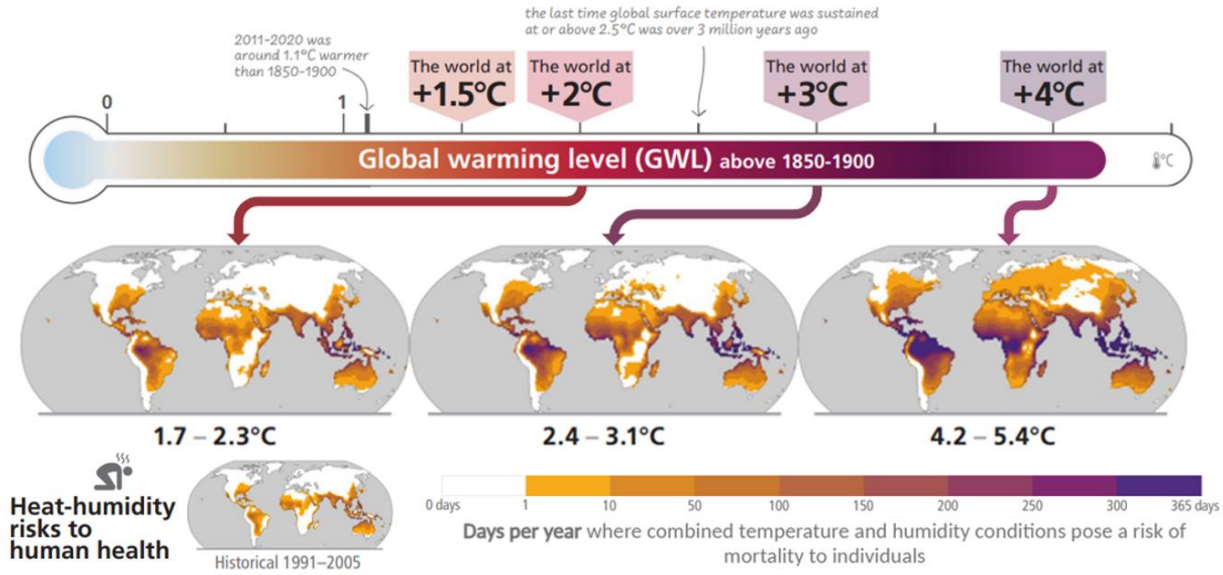

Figure 1: Projections of heat-humidity risks to human health depending on the level of global warming. Modified from (IPCC report, 2023).

Plastics production and disposal are significant contributors to global GHG emissions. In 2019, the plastic lifecycle represented 1.8 gigatons of CO_2e emissions, equivalent to 3.7% of global emissions (OECD, 2022), which is more than Brazil's total emissions. This figure is expected to rise in the future, with plastics production expected to double or triple by 2060, emitting 4.3 Gt of CO_2e (4.5% of global GHG emission). The carbon footprint of plastics is attributed for 90% to polymer production and their conversion into products, while the remaining 10% comes from their disposal.

In addition to GHG emissions, plastics are also a major source of environmental pollution. Indeed, inadequate management of the plastic end-of-life leads to continuous leakage in the environment, totaling 22 Mt globally in 2019. These continuous inflows of plastic waste accumulate in aquatic environments, reaching 139 Mt in 2019 and a staggering projection of 493 Mt by 2060.

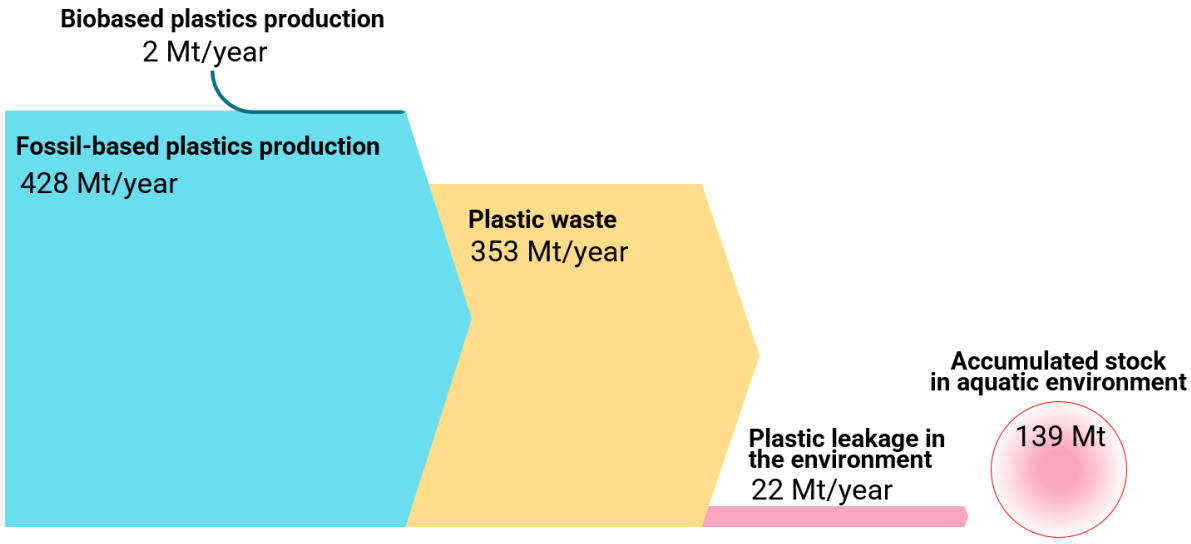

Figure 2: Life-cycle of plastics in 2019. The width of each arrow is proportional to the plastic volumes. The represented numbers are expected to double or triple by 2060. Data from (OECD report on plastics, 2023).

The detrimental impacts of plastic waste on human and ecosystems health are becoming increasingly evident. On land, plastic debris obstructs waterways and drainage systems, exacerbating the risk to spread diseases (Boelee et al., 2019), while open burning transfers the pollution burden to air and water, emitting toxic chemicals. Once leaked in the environment, plastic wastes gradually decompose in micro- or nano-plastics that can enter the human food chain via trophic transfer, with probable risks for human health. Ecosystems are also impacted, with the ubiquitous presence of plastic wastes in marine ecosystems, from polar regions (Obbard et al., 2014) to deep sea trenches (Chiba et al., 2018). Plastics debris alters habitats, endangers wildlife, and disrupts ecosystem functioning, services and productivity (Beaumont et al., 2019; Secretariat of the Convention on Biological Diversity, 2012). Plastic pollution is not only an environmental catastrophe and a concerning public health hazard; it is also economically imprudent, as productivity of ecosystems are decreased and billions of dollars in economic value are wasted through single and brief usage of plastics.

The first and most evident solution to address the plastic pollution issue is to urgently reduce our plastic usage. A secondary and parallel solution is to increase the use of biobased or biodegradable plastics, generally designated as bioplastics. Biodegradable plastics break down easily when leaked into the environment and therefore prevent the pollution at its source. Biobased plastics are derived from biomass instead of petrol resources, which could reduce the global emissions of the plastic industry provided that no increase of land use is necessary (OECD, 2022).

As the current production of biomass is limited, new feedstocks are needed to increase the bioplastic production. Microalgae have high biomass production potential: they achieve comparable yields to plants (Masojídek et al., 2013; Tredici, 2010) and exhibit the capacity to grow in wastewater or on nonagricultural land. In addition, microalgae are competitive producers of starch, a polymer and energy reserve that is a key building block for bioplastics (Brányiková et al., 2011).

However, despite microalgae have been known and used for many years, global microalgae production is still scarce. Three major challenges persist: enhancing the energy efficiency and pest control of cultures, reducing the energy cost of harvesting, and achieving low-energy and environmentally friendly extraction processes (Levasseur, 2021). Given the potential of microalgae, there is a real interest in overcoming these limitations and exploring a full capacity to produce starch by microalgae.

In literature, several works paved the way towards microalgae starch production for bioplastics applications. Brányiková and co-authors developed the induction of starch accumulation by nutritive deprivation and demonstrated that reaching high starch productivity is possible in outdoor culture (Brányiková et al., 2011). However, reports on starch induction methods other than nutritive deprivation are scarce, and the efficiency of starch accumulation regarding the natural light has never been investigated. Moreover, despite starch extraction and plasticization has been demonstrated at laboratory scale (Di Caprio et al., 2023; Gifuni, 2017a), the current processes should be simplified and scaled-up to envisage their industrialization.

Objectives of this PhD thesis

Within the context presented in the Introduction section, my PhD focused on three main tasks:

- Comparing the advantages and limitations of different methodologies for inducing starch accumulation;
- Determining the optimal light conditions for starch accumulation in outdoor conditions;
- Developing a scalable and environmentally friendly starch extraction process.

Beyond the application in bioplastics, this work on starch production also paves the way for the use of microalgae as highly efficient producers of polysaccharides, a major renewable feedstock.

The structure of this manuscript revolves around four chapters.

Chapter 1 is a literature review aiming to provide a technical background by presenting the state-of-the-art linked with the experimental work. Overall, it attempts to explain why and how microalgae could be used to produce bioplastics. To do so, it introduces some generalities around microalgae, an overview of the mechanism of photosynthesis, a description of light management, and the accumulation of starch in microalgae together with starch relevance for bioplastic production.

Chapter 2 describes the methods used during the experimental work. It is divided in six subsections that present the general and specific techniques used throughout the study.

Chapter 3 gathers the experimental results of this PhD. The results are divided into three research papers, focusing on starch accumulation induction and light quality, optimization of light supply, and starch extraction and plasticization, successively.

Chapter 4 discusses the results obtained to extend the conclusions and put them in perspectives. A critical look of the methods employed is provided, together with more general insights on the possible integration of the developed processes in the current state of the industry.

Chapter 1 - State of the art: from microalgae to bioplastics

This first chapter aims at presenting the technical background necessary for understanding the following work. It revolves around a fundamental yet not straightforward question: *How can microalgae be used to produce bioplastics ?*

The three sections of this chapter narrow down the general problematic to provide insights on the biological use of light in microalgae cells, the light management in microalgae cultures, and the relevance of microalgae starch for bioplastics. The three parts attempt to answer the following questions, successively:

- *How do microalgae synthetize biomass from light?*
- *How can light be optimally used in microalgae cultivation to enhance biomass productivity?*
- *How is microalgae biomass, particularly starch, relevant for bioplastics?*

1.1 Microalgae and photosynthesis

1.1.1 Microalgae and the model *Chlorella vulgaris*

Microalgae

Microalgae are unicellular or simple multicellular organisms using oxygenic photosynthesis. Unlike macroalgae, commonly known as seaweeds, microalgae lack complex multicellular structures. Although most microalgae are found in freshwater or marine systems, they are present in many other natural habitat: some grow on soil, ice, and animals (e.g. sloth, orca), some thrive in extreme environments with high temperature or acidity, and some form symbiotic relationships with other organisms (e.g. corals, lichens, trees)(Andersen, 2013). Microalgae species are estimated to a number of 30,000 to 1 million (Guiry, 2012). As a group, microalgae play a crucial ecological role. These microscopic organisms contribute to half of the photosynthetic conversion of solar energy on Earth (Falkowski and Knoll, 2007). The solar energy stored by microalgae as reduced carbon would reach 2.10^{21} J per year, four times more than the 5.10^{20} J of total energy consumed by human societies (Antal et al., 2013). Microalgae also release 50% of the global oxygen and fix 45 to 50 GT of organic carbon per year (Falkowski et al., 1998). Microalgae biomass accumulates in the marine systems and serves as the basis of food source of essentially all marine and freshwater animals.

Microalgae form a phylogenetically diverse group, with no precise taxonomic definition (Ruggiero et al., 2015). The term microalgae officially designates only microbial photosynthetic eukaryotes (Hamlaoui et al., 2022; Parker et al., 2008), while it used to generally refer to microbial photosynthetic organisms. In practice, some authors still use the second, more general definition (Andersen, 2013).

According to this last definition, there are two distinct groups of microalgae. The cyanobacteria have a prokaryotic cell structure and closely resemble bacteria. They evolved 3.5 billion years ago and released so much free oxygen that it fundamentally changed life on Earth (Andersen, 2013; Falkowski and Knoll, 2007). The rest of the microalgae species are eukaryotes with complex cell structure. They acquired photosynthesis approximately 2.0 billion years ago after a single endosymbiosis event. At that time, a nonphotosynthetic eukaryote engulfed a cyanobacterium, and integrated it into its cell rather than digesting it; the cyanobacterium reproduced in this cell and later became a chloroplast (Knoll et al., 2006). Prokaryotic microalgae represent a single phylum, while the eukaryotic microalgae are divided into seven main phyla (Figure 1.1). The microalgae from the Cyanobacteria, Chlorophyta (green microalgae), and Rhodophyta (red microalgae) phyla show the greatest potential for biotechnological applications (Levasseur et al., 2020).

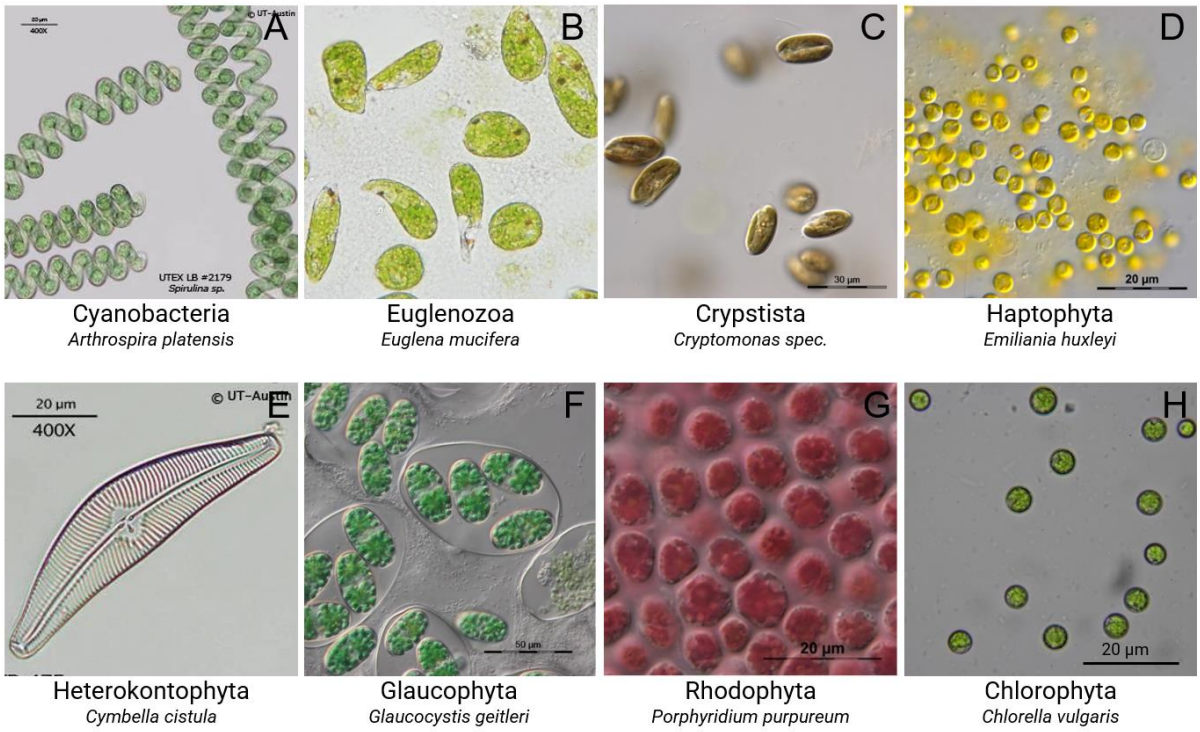

Figure 1.1: Morphological diversity of microalgae. The eight microalgae phyla are represented, with one microalgae species per phyla. Images are optical microscope pictures issued from UTEX Collection (A, E), CCALA Collection (B), SAG Collection (C, D, F, G), and from our laboratory (H).

Human usage of microalgae is ancient. Cyanobacteria were consumed in Mexico Valley in 1524 and *Spirulina* is a daily food for ethnic groups around Lake Chad (Becker, 2013). However, the modern production of microalgae biomass only began in the past century. At that time, microalgae were envisioned to become a major supply of food or biofuel for future generations. Nowadays, global microalgae production is only around 23,000 $t_{\text{dry weight}}$ per year (García et al., 2017) and microalgae applications are mainly restricted to high-value molecules or nutraceutical products (Levasseur et al., 2020). The main bottleneck of microalgae cultivation lies in the investment and operational cost of culture facilities, harvesting systems, and downstream processes. Nonetheless, engineers and scientists believe that microalgae can help to mitigate the anthropogenically generated issues of climate change, open nutrient cycles, or freshwater availability. The research currently focuses on four main research fields: high-added value molecule production, CO_2 sequestration, wastewater treatment, and production of new feedstock for biofuel or biomaterials (Levasseur, 2021). In the future, microalgae are expected to provide additional biomass in places like Saudi Arabia, where the sun and saline water availability is high, arable lands are scarce, and investment capacities are important (Benemann, 2023).

The model *Chlorella vulgaris*

One of the most promising microalgae for applications is *Chlorella vulgaris*. This species is the second most highly produced microalgae after Spirulina, with approximately 5000 tons yearly worldwide (Nethravathy et al., 2019). Along with *Chlamydomonas reinhardtii*, *Chlorella vulgaris* is widely studied as a model organism.

In addition, *Chlorella vulgaris* belongs to the Chlorophyta phylum (green microalgae), which is advantageous for biotechnological applications (Levasseur et al., 2020). In short, *Chlorella vulgaris* is robust and easily cultivable, its metabolism is well understood, and its biomass contains interesting biomolecules for potential applications. For these reasons, in this work, we restricted our focus to green microalgae only, and we chose *Chlorella vulgaris* as our experimental model.

Chlorella vulgaris is defined as a non-motile eukaryotic green microalga with small spherical or ellipsoidal cells of 2 to 10 µm. Like many microalgae, it can switch between the three nutritional modes of autotrophy, heterotrophy, and mixotrophy. While some microalgae display sexual reproduction, *Chlorella vulgaris* reproduces only asexually by autosporulation. The mother cell divides into 2 to 16 daughter cells, with an average generation time of approximately one day in autotrophy (Liu and Hu, 2013).

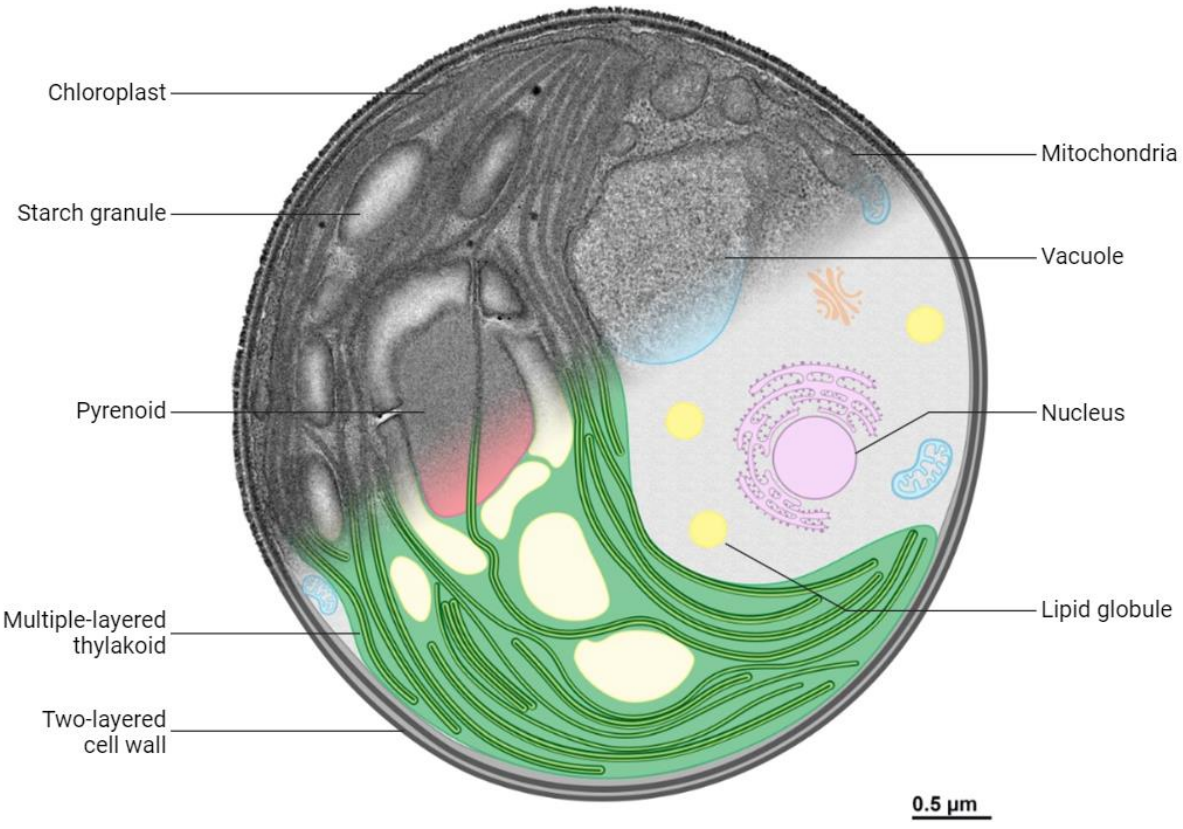

Figure 1.2: Cell morphology of the microalgae *Chlorella vulgaris*. The top half of the image depicts an actual MET picture of a *Chlorella vulgaris* CCALA924 cell grown in replete normal condition. The bottom half extends the picture to provide a more visual representation of subcellular organization.

The *Chlorella vulgaris* cell contains many subcellular organelles similar to higher plants, as depicted in Figure 1.2. Inside the cell, the cytoplasm hosts the nucleus, mitochondria, vacuoles, endoplasmic reticulum, Golgi body, and a single parietal chloroplast (Safi et al., 2014). This cup-shaped chloroplast occupies half of the cell volume and is responsible for photosynthesis and starch storage. It contains one pyrenoid penetrated by a single double-layered thylakoid and surrounded by a starch sheath (Baudelet et al., 2017; Liu and Hu, 2013). The carbon reserves of the cell are

stored either as starch granules in the chloroplast or as lipid droplets in the cytoplasm. Outside its phospholipid membrane, the cell is protected by a particularly rigid cell wall.

Cell wall of Chlorella

One major bottleneck for the industrial exploitation of *Chlorella vulgaris* is the recovery of its cellular compounds, which is hindered by its robust cell wall. Some discrepancies exist around the structure and composition of the Chlorella cell wall (Baudelet et al., 2017). This is probably due to the diversity of the Chlorella genus, among which some of the hundred described species were misidentified (Baudelet et al., 2017; Liu and Hu, 2013). The true-*Chlorella* strains have their cell wall divided in three distinct layers: an outer electron-dense layer surrounding an inner layer of lower electron density, separated by an electron-transparent interspace (Baudelet et al., 2017; Gerken et al., 2013). The cell wall is built as a succession of layered microfibrils, visible in cross-sections of adult cell walls (Duval et al., 2023; Němcová and Kalina, 2000). Hair-like structures are sometimes reported on the outside of the outer layer (Gerken et al., 2013). As shown in Figure 1.3, the cell wall is renewed after each reproduction cycle when the outer layer breaks to release the daughter cells. The inner layer is synthesized from the early cell growth stage on the surface of the plasma membrane and near the outer cell wall. After hatching, the outer layer is lost in the culture while the inner layer replaces it (Yamamoto et al., 2004).

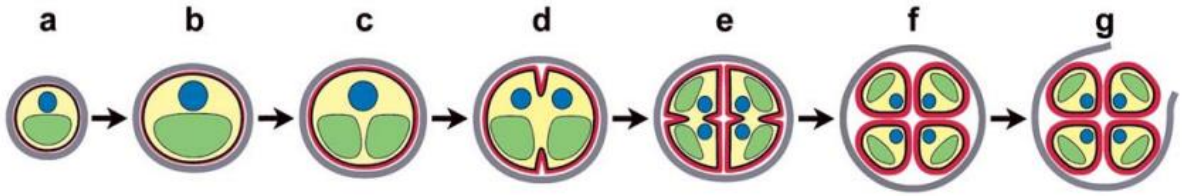

Figure 1.3: Development of cell wall during the cell cycle of Chlorella. The inner and outer cell wall layers are represented in red and grey, respectively. Reproduced from (Yamamoto et al., 2004).

The monosaccharides composition of *Chlorella vulgaris* cell wall consists mainly of galactose, rhamnose, arabinose, and glucosamine (Canelli et al., 2021a; Demir-Yilmaz et al., 2023). However, not much is known about the molecular structure of the polysaccharides or glycoproteins constituting the cell wall. Several studies suggest that chitin or chitosan would be a major constituent of the *Chlorella vulgaris* cell wall, as attested by the presence of glycosamine (Gerken et al., 2013), the identification of N-acetyl-D-glucosamine fibrils (Duval et al., 2023), and the efficacy of lysozyme and chitinase on cell wall disruption (Canelli et al., 2021b; Duval et al., 2023; Gerken et al., 2013). On the other hand, it is attested that *Chlorella vulgaris* does not contain cellulose in its cell wall (Baudelet et al., 2017), contrary to some statements (Aguirre and Bassi, 2013; Ye et al., 2023). This confusion might have arisen from the over-quantification of glucose monosaccharides, as the polysaccharides analysis reported in the literature

generally does not differentiate between storage (starch) and structural (cell wall-related) polysaccharides (Canelli et al., 2021a).

Despite some discrepancies between strains, the development and composition of the Chlorella cell wall are well described. This knowledge is crucial for designing efficient recovery processes for its intracellular biomass.

1.1.2 Photosynthesis in green microalgae

The term photosynthesis literally means building up by light (Hall and Rao, 1999; Tredici, 2010). Every living organism virtually depends directly or indirectly on photosynthesis as a source of organic matter and energy (Masojídek et al., 2013). In this process, light energy is converted into chemical energy, and energy-poor inorganic substances (CO_2, water) are converted to energy-rich organic compounds (sugar). Aside from sugar, molecular oxygen is released as a byproduct. Oxygenic photosynthesis can be simply described as:

$$CO_2 + H_2O \xrightarrow{h\upsilon} [CH_2O] + O_2 \quad (1)$$

This process is actually a cascade of chemical reactions, regrouped in two subsequent steps: light (photochemical) and carbon (biochemical) reactions. Photosynthesis also involves light capture, the protection from photodamage and the associated photoacclimation, as well as the handling of excess oxygen. These different mechanisms are described below. For further explanations on photosynthesis and its regulations in green microalgae, the reader is referred to the pedagogic and detailed review of (Levasseur, 2021) or to the in-depth review of (Mathiot, 2020).

Oxygenic photosynthesis

Photosynthesis can be assimilated to a chemical redox reaction where water, the electron donor, is oxidized and CO_2, the electron acceptor, is reduced. As CO_2 and H_2O are both very stable molecules, this electron transfer is endothermic and requires a significant amount of energy ($\Delta G^{\circ\prime}$=+479 kJ.mol-1)(Mathiot, 2020). To provide this energy, light photons are captured and their energy is transferred to special chlorophyll that eject strongly reducing electrons. After giving its electron, the photo-oxidized chlorophyll is among the most reductive biological agent known (~1.3 V). It is so reactive that water, a very stable molecule, is disassembled to replenish the electron hole in the chlorophyll molecule. As presented in Figure 1.4, the electrons pass through several carriers along the electron transport chain and reach a final acceptor, $NADP^+$, which is reduced to NADPH (Shevela et al., 2018). During its transport, the electron also induce the migration of H^+ in the stroma, which ultimately generate ATP molecules.

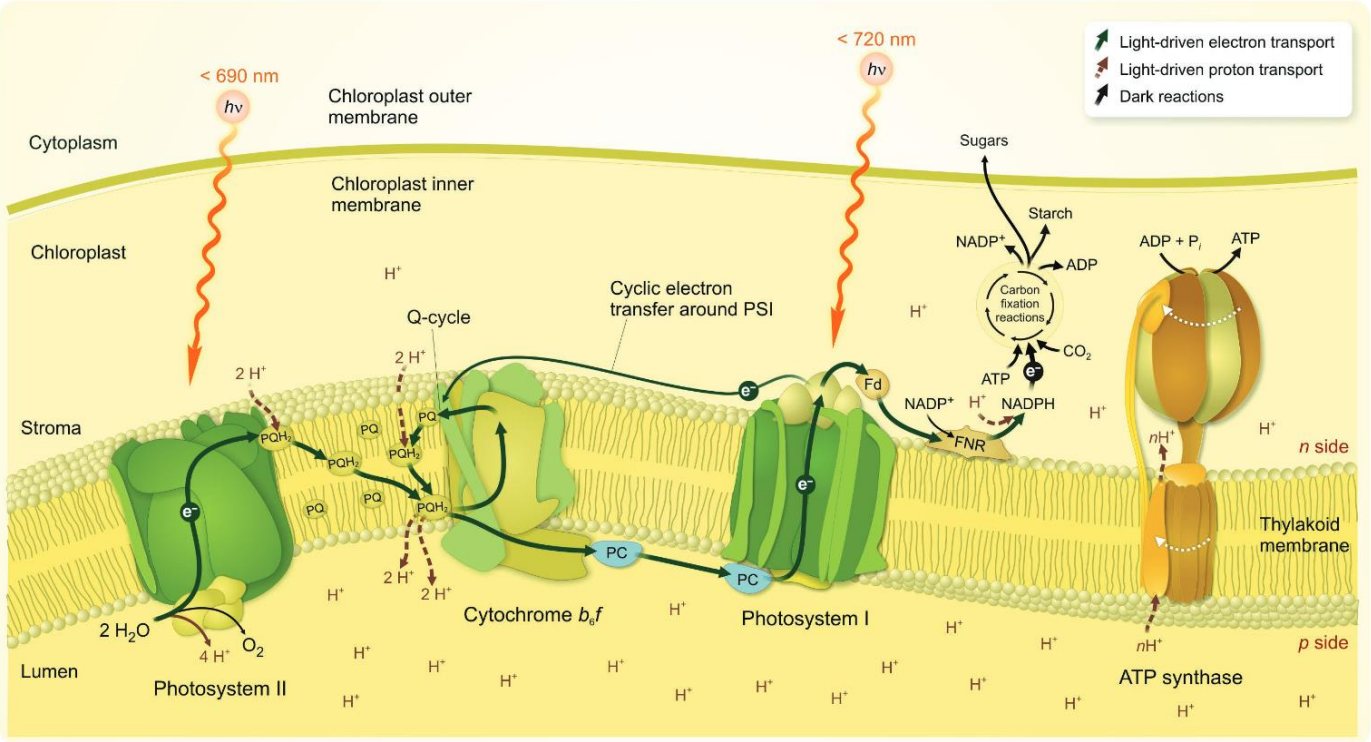

Figure 1.4: Simplified schematic representation of the electron transport chain and general light reactions of the photosynthesis. Reproduced from (Shevela et al. 2018).

Because light energy is used twice during the electron transfer, in photosystem II and photosystem I, two photons are required per transferred electron. The transfer of four electrons, requiring eight photons, leads to the formation of two NADPH and three molecules of ATP. These 2 NADPH and 3 ATP molecules are used in the carbon reactions, or Calvin-Benson cycle, to reduce 1 CO_2 molecule. This reaction is exothermic and can be represented as:

$$CO_2 + 2\,NADPH + 3\,ATP \rightarrow [CH_2O] + 2\,NADP^+ + 3\,ADP + 3\,P_i \qquad (2)$$

The maximum theoretical quantum yield of photosynthesis reactions is of 8 moles photons absorbed per 1 mole of CO_2 fixed, equivalent to $0.125\,mol_{CO_2}.mol_{photon}^{-1}$.

Energy loss by photorespiration: the detrimental effect of oxygen

Every organism relying on photosynthesis perform CO_2 fixation with the enzyme ribulose-biphosphate carboxylase/oxygenase (RuBisCo). In the first step of the Calvin–Benson cycle, RuBisCo catalyzes the carboxylation of ribulose-1,5-biphosphate (RuBP). However, carboxylation of RuBP is constantly hampered by the CO_2 vs. O_2 competition for the RubisCO catalytic sites (Levasseur, 2021; van Lun et al., 2014). If a RuBP is mistakenly oxygenated, it must be regenerated into its original form to become available again for the Calvin-Benson cycle, as illustrated in Figure 1.5.

The recovery of oxygenated RuBP is known as photorespiration. It is a complex chain reaction, involving at least the chloroplast and the mitochondria. Overall, photorespiration costs 3.25 ATP and 2 NADPH molecules per oxygenation event, and

releases one CO_2 molecule, as well as one NH_3 molecule that should be re-assimilated (Wingler et al., 2000).

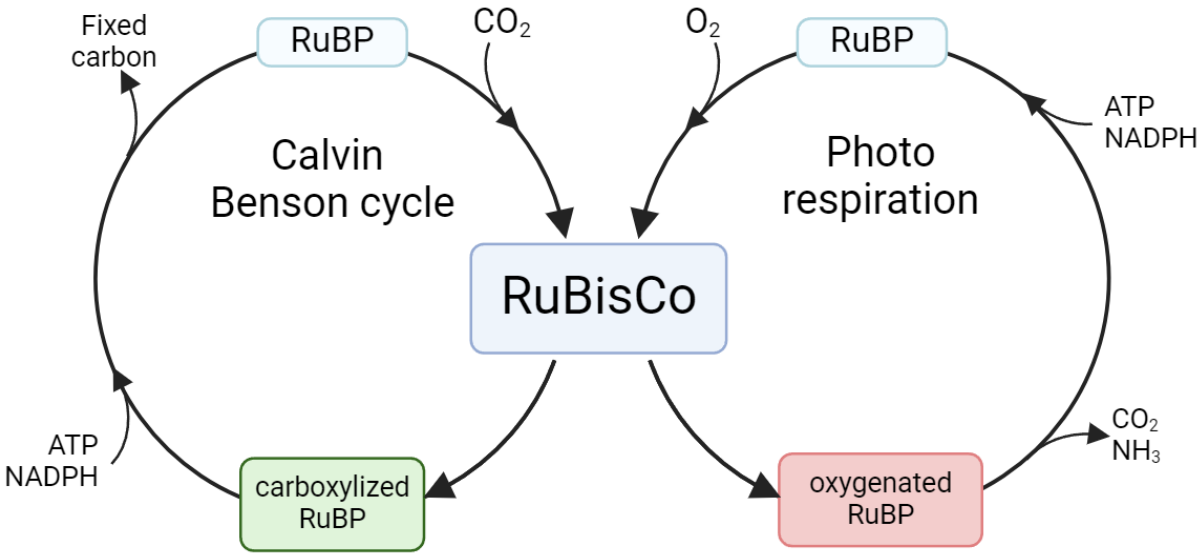

Figure 1.5: Simplified representation of the role of the RuBisCo protein in the photorespiration and Calvin-Benson processes.

Eukaryotic microalgae are equipped with a CO_2 concentrating mechanism (CCM) to concentrate and deliver CO_2 molecules to RuBisCo in a single organelle, the pyrenoid. This mechanism is thought to reduce the photorespiration; it probably evolved after the oxygen concentration increased in the atmosphere (Mathiot, 2020). Still, microalgae are subject to photorespiration in low CO_2 concentration (Tredici, 2010). Photorespiration is also triggered in case of high O_2 concentration, called hyperoxia (Neofotis et al., 2021). Oxygen build-up and hyperoxia are favored in high density cultures, where O_2 level can reach 50% or more.

Globally, photorespiration liberates an estimated 29 Gt of carbon yearly in the atmosphere (Hagemann and Bauwe, 2016). It is estimated that, under standard air composition, plants oxygenate 20 to 33 % of their RuBP molecules rather than carboxylate them (Reumann and Weber, 2006). The energy cost of RuBP recovery by photorespiration would reduce carbon fixation by 40% in plants (Tredici, 2010).

However, recent research highlights that photorespiration is not only a wasteful process, but also has beneficial aspects. For instance, photorespiration is intimately interconnected with primary carbon and nitrogen metabolism and has an important role as a recycling pathway and a protecting mechanism against photoinhibition (Busch et al., 2018; Peterhansel et al., 2010). Photorespiration would also enable cells to adapt to abiotic stress (Shi et al., 2022). Nonetheless, reducing photorespiratory losses is still beneficial despite the positive aspects of photorespiration. Indeed, the installation of alternative salvage pathways resulted in enhanced growth and biomass in *Arabidopsis thaliana* at laboratory scale (Peterhansel and Maurino, 2011).

In contrast to plants, it is theoretically simple to suppress photorespiration in microalgae culture. Indeed, in contrast with mandatory and light-independent aerobical respiration, photorespiration is only triggered after oxygenic activity of the RuBisCo

which happens at high O_2/CO_2 ratio. In the laboratory, photorespiration is suppressed by diminishing O_2 level from 21 to 2 %, or by increasing the CO_2 level from 380 ppm to 1 or 2 %. On the other hand, Tredici argue that supplying 700 ppm of CO_2 in the air would be sufficient to suppress photorespiration (Tredici, 2010). Behind the successful strategy of bulk O_2/CO_2 ratio reduction, the CCM activity has probably an important role, which still needs to be investigated. Overall, well managed microalgae cultures, with efficient oxygen removal and sufficient CO_2 supply, should completely suppress photorespiration.

Light management

Light capture

The light energy is harvested by light collecting antennas. These antennas are pigment-binding protein complex comprising the photosynthetic pigments, chlorophyll *a* and *b*. Also called light harvesting complex (LHC), the antennas are docked in the thylakoid membrane and are specifics of either photosystem I or II. Their role is to supply the light energy for photosynthesis by capturing the photons with their chlorophyll molecules as shown in Figure 1.6.

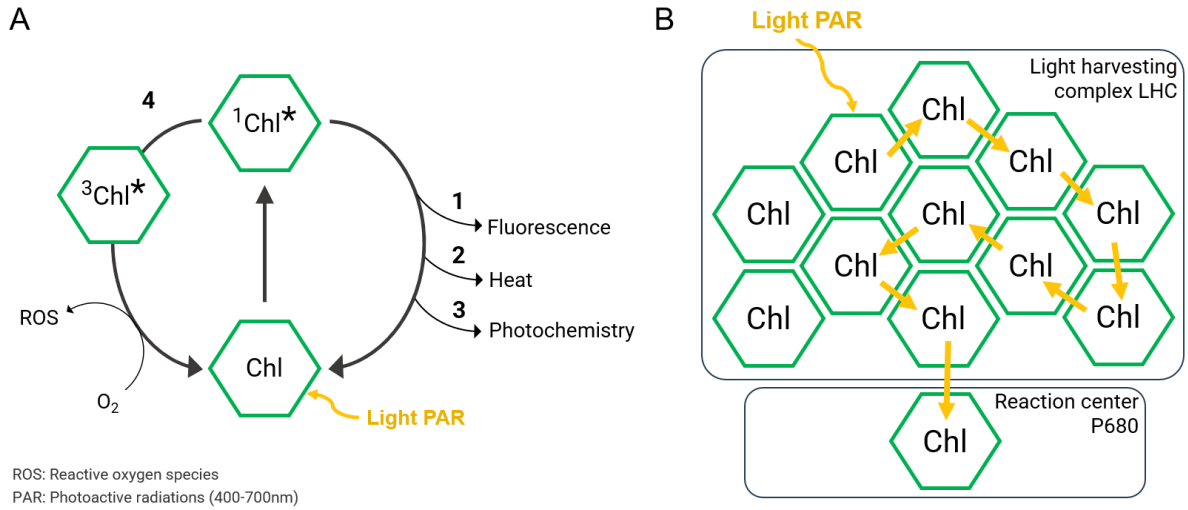

Figure 1.6: Light capture by chlorophyll molecules. (A) Fates of absorbed energy in the chlorophyll molecule. After capturing a PAR photon, the chlorophyll molecule reaches a singlet excited state ^{1}Chl*. To return to ground state, the energy is quenched by 1 fluorescence, 2 heat, or 3 photochemistry. Alternatively, the chlorophyll can reach the triplet excited state (4) that reacts with oxygen to form harmful reactive oxygen species (ROS). (B) Transfer of excitation energy in the chlorophyll molecules of the light harvesting complex (LHC). The energy reaches the special pair of chlorophyll P680 in the reaction center of the photosystem II, where it is used for photochemistry. Adapted from (Müller et al., 2001) and (Schansker, 2020).

Chlorophyll *a* and *b* capture photons over a specific range of wavelength called photoactive radiations (PAR), from 400 to 700 nm. When a PAR photon strikes an electron of a chlorophyll, the light energy is absorbed and the chlorophyll molecule goes into an excited state. The chlorophyll then returns to ground state either by heat dissipation, fluorescence light emission, or charge transfer to photochemistry (Figure

1.6.A). In contrast to chlorophyll *a*, chlorophyll *b* never emits fluorescence, because it immediately (femtosecond timescale) and irreversibly transfers its excitation energy to chlorophyll *a* (Schansker, 2020). If transferred, the excitation energy travel through the chlorophyll molecules by electromagnetic interactions (FRET mechanism) within a picosecond timescale (Figure 1.6.B). The light energy is channeled to a pair of special chlorophyll (P680) in the reaction center in photosystem II (PSII), where it is used in photochemistry reactions (Masojídek et al., 2013).

- Photodamage

Although capturing the light is necessary to allow active photosynthesis, the absorbed energy expose the cell to unavoidable damage. Indeed, at saturating light intensities, the rate of photon capture exceed by more than 100 times the rate of electron transfer resulting in a large excess of captured energy (Müller et al., 2001; Perrine et al., 2012). When the excited chlorophyll molecules return to ground state, they can create harmful reactive oxygen species (ROS) by reacting with oxygen. ROS are highly reductive and lead to oxidative damage in the surrounding molecules. The probability of forming ROS is enhanced if the chlorophyll cannot transfer their charge to photochemical reactions.

The reaction center of PSII and its protein D1 are particularly vulnerable to photodamage. Indeed, the PSII reaction center hosts the special trapping chlorophyll pair P680, which is very reactive in its photo-oxidized state P680*. If P680* is generated beyond the capacity of the electron transport chain, the lifetime of P680* increases and enhances the probability of P680* to form ROS from oxygen or to reduce directly the D1 protein (Bassi and Dall'Osto, 2021). Photons, in particular from the blue-UV range, can also break the oxygen-evolving complex of PSII, which releases its manganese ion and result in further oxidative damage in the PSII (Li et al., 2018).

Intrinsically, photodamage occurs regularly at the rate of approximately one PSII damaged per 10 million photons absorbed (Raven, 2011; Soon Chow et al., 2002). This damage probability increases for blue and UV light (Raven, 2011), as well as if the electron transport chain is damaged or overexcited (Bassi and Dall'Osto, 2021; Levasseur, 2021). At the chloroplast level, the D1 proteins are constantly repaired (Aro et al., 1993), and the inactivation of PSII (called photoinhibition) only occurs if the damage rate exceeds the repair rate (Takahashi and Murata, 2005). Yet, PSII reparation takes tens of minutes to over an hour (Raven, 2011) and is neutralized by excessive light (Erickson et al., 2015). Under high light intensities, photodamage can then easily outpace the PSII repair rate and lead to photoinhibition. Occurrence of photoinhibition can drastically reduce the photosynthesis efficiency and microalgae productivity.

- Photoprotection

To avoid photoinhibition, microalgae evolved several photoprotection mechanisms. These mechanisms are implemented in case of light overload or a reduced downstream metabolic needs to reduce the dangerous over excitation.

The first and most important photoprotection mechanism is the non-photochemical quenching, also abbreviated as NPQ. NPQ dissipates the light energy before its entry in the electron transport chain (PSII), and turns it to into harmless heat (Bassi and Dall'Osto, 2021). In short, NPQ mechanisms are triggered by the acidification of the thylakoid lumen, which is a consequence of the saturation of photosynthesis machinery. Figure 1.7 illustrates the NPQ mechanisms. First, the energy quenching qE quench the antenna system of the photosystems in a few seconds. This mechanism involves conformational changes and aggregation of the light harvesting complex, as well as the activation of xanthophyll pigment quenching qZ. Then, state transition qT alleviates the excitation pressure on PSII by relocating the PSII antenna to PSI in a few minutes (Shevela et al., 2018). After few hours or days, the PSII may be inactivated upon photodamage; this phenomenon is noted is called photoinhibition qI. Except for qI, the NPQ mechanisms are quickly reversible (Levasseur, 2021).

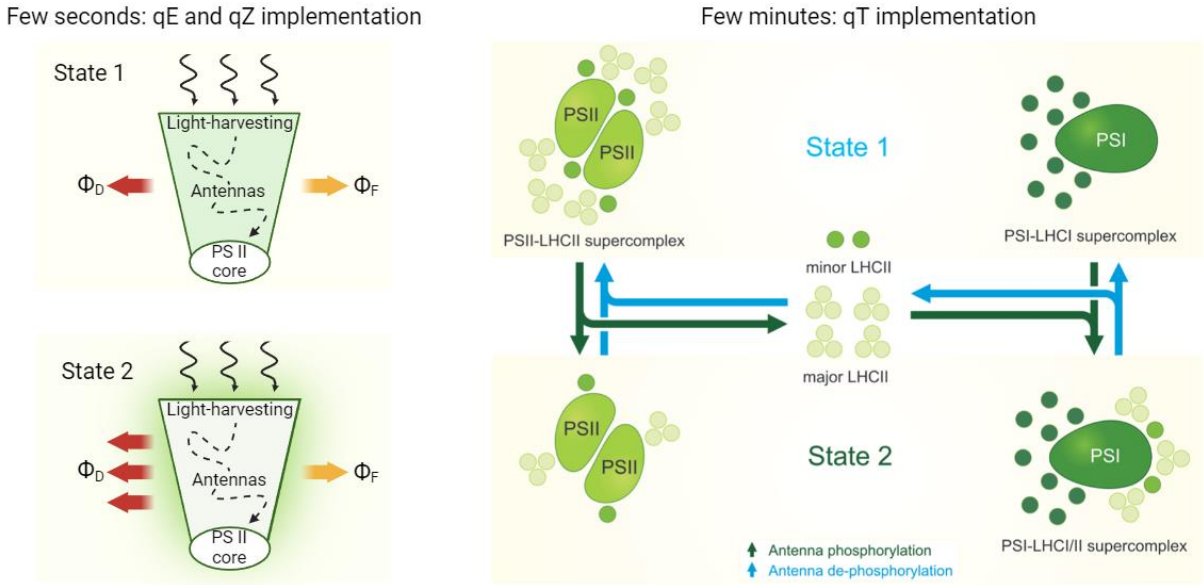

Figure 1.7: Mechanisms of photoprotection by non-photochemical quenching. The first response is the implementation of qE and qZ, which increase the thermal dissipation (Φ_D) in the antenna while the fluorescence dissipation stays constant (Φ_F). The second response in the implementation of qT, which imply the relocation of PSII antennas. Partly reproduced from (Shevela et al. 2018).

In complement with NPQ, other regulatory mechanisms can trigger electron sinks within the electron transport chain to dissipate the excessive excitation energy. These mechanisms are referred as alternative electron pathways, namely cyclic electron flow, water-water cycle and chlororespiration. Among other functions, they help preventing

photoinhibition of PSII to the expense of NADPH production (Heber and Walker, 1992; Mathiot, 2020).

- Photoacclimation and photoadaptation

Not only microalgae dynamically regulate their photosynthesis to the light conditions, but they also adapt their physiology on the long-term. This adaptation is referred as photoacclimation.

During photoacclimation to high light intensities, microalgae reduce their absorption cross-section (Torzillo and Vonshak, 2013) and modify their pigment content towards less chlorophyll and more protective carotenoids (Hu, 2013). Under low light, they increase the quantity of photosynthetic units and the size of their light-harvesting antenna (Masojídek et al., 2013). These changes occur in a few hours or days, do not involving genetic modifications, and are reversible. In contrast, photoadaptation is a long-term process where microalgae genetically adapt to their light conditions. In this case, the pigment content can vary more than during photoacclimation.

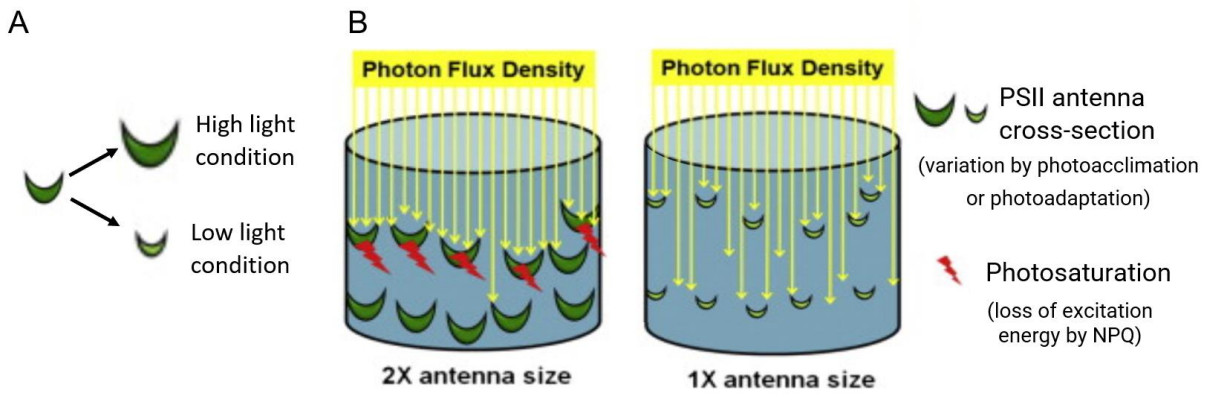

Figure 1.8: Variation of pigmentation and antenna cross-section. (A) Photoacclimation to low and high light conditions. (B) Effect of microalgae pigmentation on the light penetration and utilization in microalgae culture. Adapted from (Perrine et al., 2012).

As presented in Figure 1.8, this variation of pigmentation can drastically modify the light repartition in microalgae mass cultures. In nature, wild microalgae are naturally over-pigmented, probably to shade other phototrophs and cope with competition in mixed-species communities (Perrine et al., 2012). However, in mono-species microalgae culture, this over-light harvesting leads to photosaturation and photoinhibition, which can reduce by 40 % the conversion of solar energy (Tredici, 2010). In an artificial dense culture, the ideal microalgae should harvest only the light used for photochemistry and let the rest penetrate deeper into the culture (Masojídek et al., 2022).

To cope with this major problem, researchers are interested in obtaining photoadapted strains with minimal pigment content (Blankenship and Chen, 2013). Despite promising results of +30% biomass growth (Cazzaniga et al., 2014; Dall'Osto

et al., 2019; Perrine et al., 2012), the development of photoadapted strains with reduced antennas is not straightforward. Indeed, the light antenna also function for photoprotection (NPQ mechanisms), and should be at least partly conserved (Perrine et al., 2012). In addition, the deployment of these engineered strains in outdoor large cultures showed contrasting results in productivity (Masojídek et al., 2022). Nonetheless, photoadapted mutants with reduced pigmentation hold great promise to increase the yield of microalgae cultures.

1.1.3 Monitoring photosynthesis by fluorometry

Probing photosynthesis through chlorophyll fluorescence

Fluorometry is a technique to probe the workings of photosynthesis. For some, it is almost magical in its capability (Schansker, 2020). By shining a beam of light on a microalgae culture or a leaf and measuring the re-emitted light, it is possible to measure not only the activity of photosynthesis but also its active regulatory mechanisms. Beyond photosynthesis itself, fluorometry also informs on the physiological state. For instance, if a stress has damaged the photosynthesis apparatus or induced non-photochemical quenching (NPQ), it could be detected by fluorometry.

This technique relies on the fluorescence of the chlorophyll *a*. As stated above, the absorbed light energy has three fates in the chlorophyll molecule: transferred to photochemistry (P), lost as heat (H), or emitted as fluorescence (F), where $P + H + F = 1$ (Müller et al., 2001). In the case where the photosynthetic apparatus is blocked, we have $P = 0$ accompanied by a proportional increase of H and F, so that $H + F = 1$ (Masojídek et al., 2013). As the increase of F and H are proportional, the increase of F directly represents the energy that appeared upon photosynthesis apparatus blockage, i.e. the energy that was previously quenched by photochemistry P. In other words, measuring the proportional increase of the fluorescence F before and after the closure of the photosynthetic apparatus directly informs us on the energy that is basally quenched by photochemistry P under normal functioning of photosynthesis.

The fluorescence before and after closure of the photosynthetic apparatus is referred to as F_0 and F_M, respectively. They are measured by the pulse amplitude modulation (PAM) technique. The instrument emits three types of light: saturating pulsed light to close all PSII, actinic (continuous) light to activate photosynthesis, and modulated light to induce small fluorescence peaks of calibrated amplitude. The advantage of PAM fluorometry is that it only register the fluorescence induced by the µs measurement pulses from modulated light, and is not influenced by the saturating and actinic light induction of fluorescence (Schansker, 2020).

Fluorometry measurement

The measurement of F_0 and F_M proceed as follows. First, the sample is let in the dark several minutes to ensure that all PSII are activated (open). A low actinic light is applied to induce the basal fluorescence F_0, usually restituting between 2-10% of the absorbed energy (Schansker, 2020). At this stage, all PSII are considered open because

the low light stimulate the PSII at a lower frequency than PSII re-open after electron transfer. Then, the closure of the photosynthetic apparatus is performed by a short pulse of saturating light. As the practical turnover time of one electron in the PSII is of ~5ms (Schansker, 2020), the light pulse transiently inactivate (close) all PSII reaction centers. During this short time, the fluorescence emission of chlorophyll increases to its maximal level F_M. Following the F_M measurement, the addition of actinic light can activate the regulatory mechanisms like non photochemical quenching (NPQ). In that case, the dissipation of energy as heat is favored and the fluorescence emission decrease (Erickson et al., 2015). Therefore, the following saturating pulses yield lower fluorescence than F_M, referred as F_M' (Van Kooten and Snel, 1990). An example of this "pulse-and-probe" approach is presented in Figure 1.9.

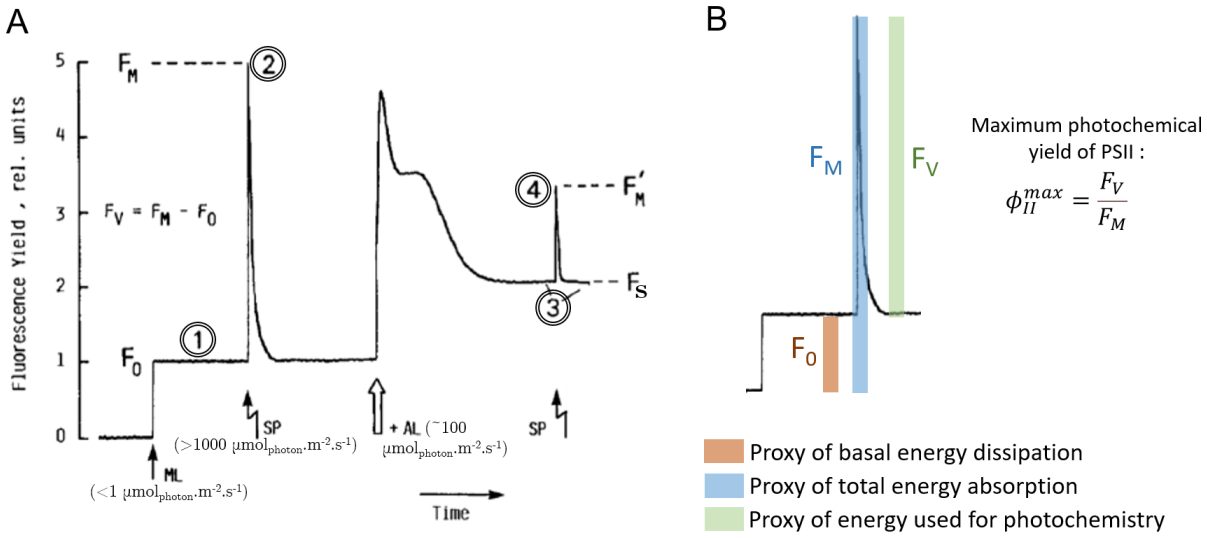

Figure 1.9: Fluorometry analysis by pulse-and-probe method. (A) ML: measuring light (<1µmol$_{photon}$.m^{-2}.s^{-1}); SP: saturating pulse (>1000 µmol$_{photon}$.m^{-2}.s^{-1}); AL: continuous actinic light (~100µmol$_{photon}$.m^{-2}.s^{-1}). Under weak measuring light (ML), the dark-adapted sample emits a minimal yield of fluorescence F_0, with all PSII centers open (1). The application of a saturating pulse (SP) rapidly closes all PSII centers, transiently suppressing the photochemical quenching (2): the fluorescence yield reaches its maximal level Fm. After the onset of a continuous illumination (AL), the system reaches a partly-excited state with a portion of PSII centers closed, characterized by a fluorescence emission Fs ranging between F_0 and Fm (3). The application of an additional SP yields the Fm' level (4). The relative decrease in Fm' from the maximal fluorescence yield at dark (Fm) quantifies the light induced NPQ mechanisms. In a first approximation, the lower the Fm' level in the light, the higher the NPQ induction. (B) Representation of photochemical yield calculation. Figure and legend adapted from (Mathiot 2020); figure originally from van Kooten and Snel 1990.

The values F_0, F_M, and F_M' lead to the calculation of photochemical yield and NPQ. As previously mentioned, heat and fluorescence quenching are considered to increase proportionally under short pulse excitation event. This hypothesis allows us to completely neglect the thermal dissipation and consider, as an extreme simplification, that fluorescence is the only energy dissipation mean together with photochemical quenching. With this in mind, it is clear that the minimal fluorescence F_0 , which is the state where all PSII are open, represents the total loss of absorbed energy, i.e. that is not used for photochemistry (Figure 1.9.B). F_M corresponds to the maximal fluorescence

and, as it reflects the maximum light absorption capacity, to the total and maximum energy absorbed. Their difference $F_M - F_0$ represents the energy used (or quenched) in photochemistry. Therefore, the photochemical quantum yield of PSII (ϕ_{II}), which is the fraction of total energy going to photochemistry, can be expressed as $\frac{F_M - F_0}{F_M} = \frac{F_V}{F_M}$ where F_V is defined as the variable fluorescence. For dark-adapted sample, the photochemical yield ϕ_{II} is maximum, with $\phi_{II}^{max} = \frac{F_V}{F_M}$. The ϕ_{II}^{max} is also referred as F_V/F_M or QY. To sum up, the parameter F_V/F_M equates the maximum quantum yield of PSII when all reaction centers are open. This calculation assumes that both F_0 and the variable fluorescence F_V are emitted by PSII only. It was shown that this is not the case and that in C3 plants on average 30% of F_0 is due to PSI fluorescence and in C4 plants this is 50-55% (Schansker, 2020).

In the case where sample is not dark-adapted but light-adapted, its PSII are partly close, and the operating photochemical yield is $\phi_{II} = \frac{F_M{}' - F_S}{F_M{}'}$ (Mathiot, 2020). The light illumination also triggers NPQ mechanisms, which correspond to a switch in the proportion of fluorescence and heat quenching. This translates as an $F_M{}'$ lower than F_M. The NPQ is evaluated as the difference $F_M - F_M{}'$ relative to the maximal fluorescence: $NPQ = \frac{F_M - F_M{}'}{F_M}$ (Huot and Babin, 2010). Alternatively, the non-photochemical quenching is also sometimes defined as a yield, expressed as $\Phi_{NPQ} = \frac{F_S}{F_M{}'} - \frac{F_S}{F_M}$. This expression is deduced from the energy balance $\Phi_{II} + \Phi_{f,d} + \Phi_{NPQ} = 1$, where the yield of non-regulated dissipation $\Phi_{f,d}$ is calculated as $\Phi_{f,d} = \frac{F_S}{F_M}$.

The operating photochemical yield can be used to express the PSII electron transport rate $ETR_{II} = a \cdot \phi_{II} \cdot PFD$. Here, a is the coefficient corresponding to the fraction of incident light absorbed by the PSII and PFD is the incident photon flux density. As the determination of a is not straightforward, standard a values are routinely used to express the relative electron transport rate rETR (Mathiot, 2020).

In its landmark work, Genty et al., 1989 demonstrated the correlation between the operating ϕ_{II} and the capture of CO_2. ϕ_{II} was also found proportional to the quantum yield of O_2 evolution for an important range of irradiance, except very low-light intensities (Burlacot et al., 2018). This demonstrates the relatability of fluorometry as a proxy of the photochemical yield.

In summary, fluorescence is a powerful technique to measure the photosynthesis quantum yield and non-photochemical quenching. It is fast, non-invasive, portable, and bring interesting insights on the photosynthesis and its regulation. Fluorometry is useful to the microalgae cultivator that wants a reliable and quick indication of the health of its culture, and also offers a window on the in-depth mechanisms of photosynthesis regulation.

1.1.4 Conclusion

Microalgae are a diverse group of microscopic phototrophs. Among them, the model *Chlorella vulgaris* holds relevance for industrial cultivation, despite its robust cell wall. *Chlorella vulgaris* uses photosynthesis to convert light energy into biochemical energy. This energy is used to fix CO_2 and generate microalgae biomass. However, the photosynthetic machinery is vulnerable to intense light. To dissipate the excess excitation energy, microalgae implement within seconds or minutes several regulatory mechanisms, such as non-photochemical quenching (NPQ). Despite these defenses, prolonged exposure to high light intensities can lead to a damaged state called photoinhibition. To monitor this phenomenon, fluorometry offers a valuable tool to probe the workings of photosynthesis, notably the maximal photon quantum yield, called QY or F_V/F_M.

Aside from understanding how light energy is used by microalgae, it is crucially important to comprehend the actual achievable productivity of microalgae. Microalgae have unique optical characteristics as microscopic and light-absorbing phototrophs. In the field, this particularity introduces several considerations in their cultivation, particularly in terms of light management.

1.2 Light management in microalgae cultivation

1.2.1 Light utilization and interactions in microalgae culture

Foreword on microalgae trophic mode

Similarly to other microorganisms, some microalgae have the ability to grow solely on preexisting organic matter. This nutrition mode is referred as heterotrophic growth, and is relevant for industrial biotechnology. Indeed, the heterotrophic growth of microalgae allow to yield very high cell density (>60 g_{DW}/L) and also rely on the robust technology of bacterial fermentation. From a technological point of view, the heterotrophic production of microalgae is no different from other fermentation processes. The only change is the output products, as microalgae exhibit a wide range of biochemical components, including some unique and high-value compounds such as pigments.

On the other hand, microalgae are phototrophs able to fix carbon and produce biochemical energy from the light. Even though growth kinetics is lower than in heterotrophy, the phototroph mode allow microalgae to grow without any organic matter. In this case microalgae are a source of biomass instead of an intermediate, and therefore can be compared to plant crops. It also exists an intermediate trophic mode, called mixotrophy. Here, microalgae growth is improved by absorbing not only light energy and inorganic carbon but also organic matter. Interestingly, waste from other processes can be used to provide this organic matter; however, it can expose the culture to contamination. Mixotrophy is a promising process, and research is ongoing to demonstrate its applicability.

Despite the potential interest in heterotrophic and mixotrophic modes, this work will exclusively focus on the phototrophic cultivation of microalgae.

Microalgae response to light intensities

The level of light utilization by microalgae primarily depends on the rate of photosynthesis. The latter evolves accordingly to two parameters: the rate of photon absorption and the efficiency at which these absorbed photons are converted into biochemical energy. Light absorption depends on the absorption cross-section of cells and irradiance, while the conversion efficiency depends on photosynthetic reactions and their regulation (Tredici, 2010).

In order to analyze the response of microalgae to their light environment, it is common to draw the curve representing the evolution of photosynthesis according to the irradiance (Figure 1.10). This curve is noted PI-curve for photosynthesis (P) relative to irradiance (I). It is divided in three zones: the photolimited, photosaturated, and photoinhibited regions (Figure 1.10). At very low irradiance, the light is too low to overcome respiration and net photosynthesis output is negative. At I_c, the irradiance of compensation, energy consumption of respiration is compensated by photosynthesis production. When irradiance increases, the photosynthesis response to irradiance is linear, following the slope α. In this state the culture is photolimited, meaning that photosynthetic apparatus are not saturated and that each additional impinging photon is readily used. However, if irradiance increases again, the photosynthesis production stops to evolve linearly: some absorbed light energy is not converted by photosynthesis and is rather dissipated by NPQ mechanisms. At irradiance I_k, that is defined as the intersection point of the line P_m and slope α, the photosaturation zone begins. Here, photosynthesis reaches its maximum capacity with no possibility to use any additional photon. The net photosynthesis productivity cease to increase with the irradiance and reach a plateau of value P_m. If the irradiance further increase, the photoinhibition zone is reached, resulting in damage on photosynthesis apparatus and reduction of productivity.

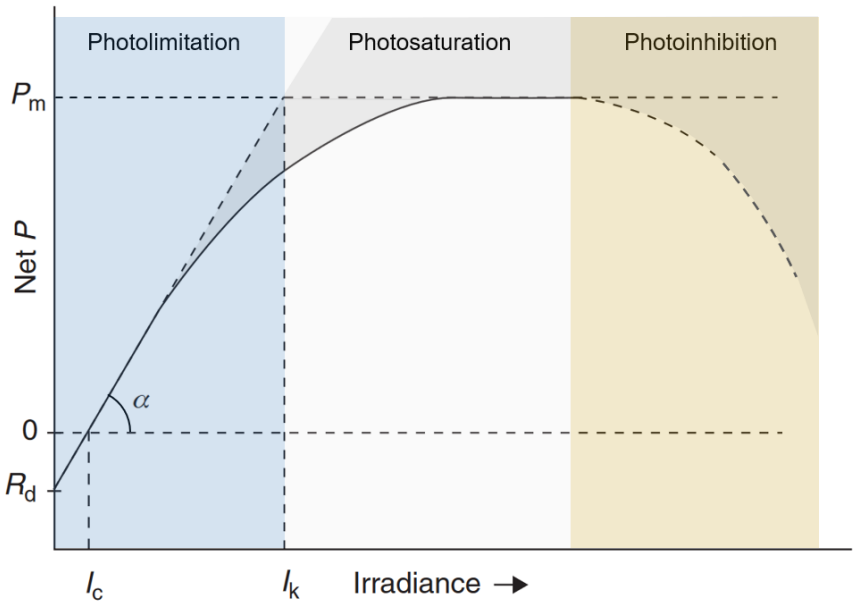

Figure 1.10: Photosynthesis (P) versus irradiance (I) curve. I_c: compensation irradiance; I_k: saturation irradiance; R_d: dark respiration; P_m: maximum photosynthesis; α: initial slope or maximal photosynthesis efficiency. The dark area represents the energy loss for photosynthesis. Modified from (Torzillo et Vonshak, 2013).

In practice, the PI curve is drawn by stimulating a microalgae culture with a calibrated range of light intensities and measuring the response of photosynthesis production. The latter is often approached with a proxy like O_2 evolution or the electron transfer rate as measured with fluorometry.

On the one hand, the PI-curve has a practical interest. It helps to analyze the response of microalgae to the light, but also their adaptation to environmental conditions. Indeed, the shape of the PI-curve change accordingly to photoacclimation of the cells, as reviewed in (Levasseur, 2021; Torzillo and Vonshak, 2013).

On the other hand, the PI-curve is a good illustration to understand the trade-off between the maximum light utilization and microalgae productivity. Indeed, the curve clearly shows that the maximum photosynthesis output P_m is reached under photosaturation. At P_m, a lot of absorbed photons are wasted, with a low productivity per irradiance ratio. Conversely, the productivity per irradiance ratio is maximal when the PI curve is linear, following the slope α at the beginning of the photolimitation zone. Here, photon dissipation is minimal but absolute photosynthesis output is low. In summary, at low irradiance the light utilization is optimal while photosynthesis productivity is low, and conversely at high irradiance.

This notion is important because, in outdoor mass culture, the limiting resource is the incident light. Therefore, microalgae cultures should aim at converting light with the highest possible efficiency. As shown by the PI-curve, low irradiance is adequate for this objective. However, the availability of light in a microalgae culture is not straightforwardly linked with the incident light on its surface. One should also account for light repartition and homogeneity in the culture.

Light repartition in microalgae culture

In microalgae mass culture, one of the main problematic is the efficient use of light. This require to avoid photosaturation and photoinhibition by using low irradiance. However, in most cases the sunlight input cannot be modified. The only leverage left is to increase the biomass concentration to lower the photon-per-microalgae cells ratio. With this approach, the culture experience low irradiance (low photon-per-microalgae) even under intense sunlight, reaching up to 2000 $\mu mol_{photon}.m^{-2}.s^{-1}$.

However, the statement 'low photon-per-microalgae equals low irradiance' is at best an extreme simplification. In reality, the light repartition is not homogeneous within the reactor. The light is progressively absorbed by the cells, which means that cells are exposed to different light intensities. Therefore, in outdoor cultivation where incident sunlight is intense, the culture is inevitably partly photoinhibited and photosaturated, and can even be exposed to dark zones in case of high density culture (Figure 1.11).

Modifying the biomass concentration cannot avoid the photoinhibition and photosaturation zones to appear. However, increasing the biomass concentration can reduce the relative importance of these zones in the culture vessel, as light would be more absorbed in the very first layers of the culture.

Figure 1.11 illustrates the importance of choosing the right biomass concentration. The optimal biomass concentration (case b) limits the light waste by transmittance and the prevalence of photosaturation-photoinhibition zone (contrary to case a). In addition, it also prevents the formation of dark respiration zone (contrary to case c). Due to light repartition and agitation, the light experienced by the optimally-concentrated cells is mainly in the photolimitation zone.

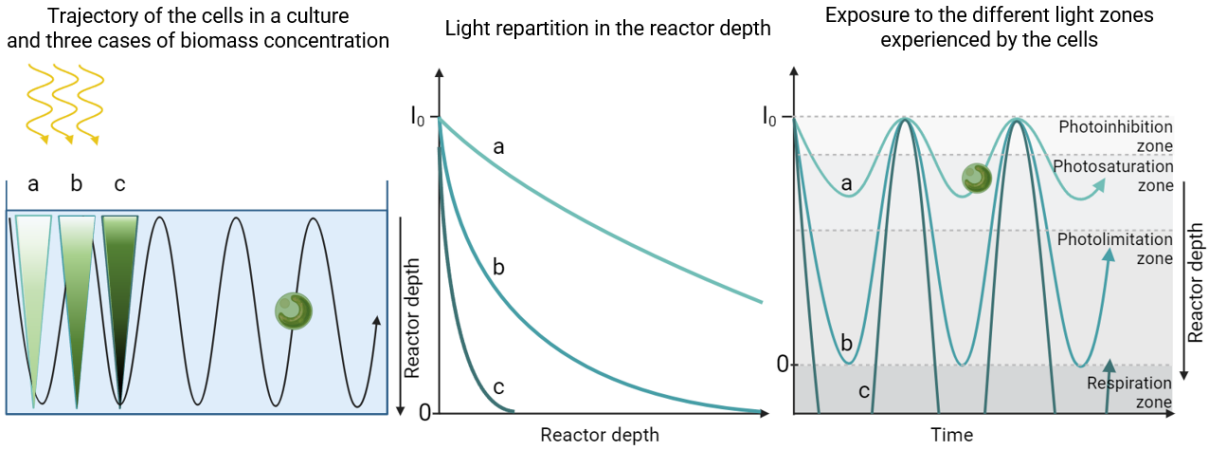

Figure 1.11: Light experienced by the microalgae cells depending on the biomass concentration. The three biomass concentrations are a (very dilute, light reaches and get through the reactor rear), b (intermediate, light is totally absorbed at the level of the reactor rear), and c (very dense, light is totally absorbed and the bottom part of the culture is dark volume). As cells are constantly moving due to agitation, they encounter different light zones (Demory et al., 2018), with different proportion depending on the light repartition in the reactor, and therefore on biomass concentration. Inspired from (Tredici, 2010) and (Levasseur, 2021).

According to the theory, the light repartition is of much importance. This relevance was experimentally demonstrated by Artu, 2016, who has shown that similar photon-per-microalgae ratio obtained with different light repartition (different culture vessels and light intensities) actually result in different biomass productivities (Artu, 2016).

Still, even if the light fractions in the reactor are well balanced, the inhomogeneity of light remains an intrinsic problem of microalgae cultivation. The first issue is that microalgae are mainly exposed to low irradiance (photolimitation zone). The cells inevitably react with photoacclimation, which results in developing larger optical cross section in a few hours, even if microalgae were previously high-light adapted. This shade-adaptation has three major negative consequences: microalgae get easily photosaturated and waste light, they may suffer from photoinhibition, and cells strongly shade each other (Tredici, 2010). The second issue is the unavoidable creation of photoinhibition-photosaturation zone. The losses due to photoinhibition and photosaturation are thought to reduce the photosynthetic efficiency by around 40% (Tredici, 2010).

In summary, the light repartition within a culture is highly important. Despite the inherent drawbacks of light inhomogeneity, selecting the appropriate biomass concentration is a crucial step toward achieving an efficient microalgae culture. Additionally, the choice of culture system is another important factor, as it influences not only light distribution but also other relevant parameters.

1.2.2 Microalgae culture systems

Importance of non-light parameters

Microalgae cultivation requires to monitor many factors related to their fitness and productivity. In addition to the light that provides the energy for microalgae growth, other environmental conditions should be adapted and optimized. If at least one environmental parameter is inadequate, microalgae will switch to a stress state. Triggering stress metabolism may be suitable in some cases, like for starch accumulation; however, it may also induce a cessation of cellular division.

Amongst the important parameters, a microalgae culture require specific temperature, pH and salinity adapted to a given microalga species. In addition, the oxygen concentration should be maintained at low level to limit photorespiration. Finally, enough nutrients with balanced macro- and micro-elements should provide the necessary building blocks for microalgae growth. Considering their relevance for this work, the nutrient and temperature parameters are detailed hereafter.

Nutrients are essential for microalgae growth. The macronutrients (>1% of dry biomass) are C, N, P, Ca, Mg, S, K; all of them are essential for cellular metabolism (Artu, 2016). Carbon, constituting around 50%$_{wt}$ of microalgae biomass, is supplied either in the gaseous (CO_2) or solid (HCO_3^- or CO_3^{2-}) form. Gaseous CO_2 injections are also used to decrease the pH in the culture. The CO_2 is better retained in the culture at high pH (>9) as it dissolved into the HCO_3^- or CO_3^{2-} forms (Kaplan, 1986). Nitrogen constitute 7-10% of dry biomass. It is provided in the form of ammonia, nitrate, nitrite, or urea depending on the species. Some microalgae can directly fix gaseous N_2, but this process is energy intensive and at the expense of growth. In addition, micronutrients and trace elements (Fe, B, Cu, Mn, Zn, Mo, Mb, V, Co, Ni, Si, Se, Al, Rb, Li, and Se) are essential. For some species, vitamins or growth factors have to be added. In general, the nutrients added to a culture media are based on the biomass elementary composition from the relevant microalgae species. If overdosed, nutrients can have toxic effect, as in the case of iron (Hu, 2013).

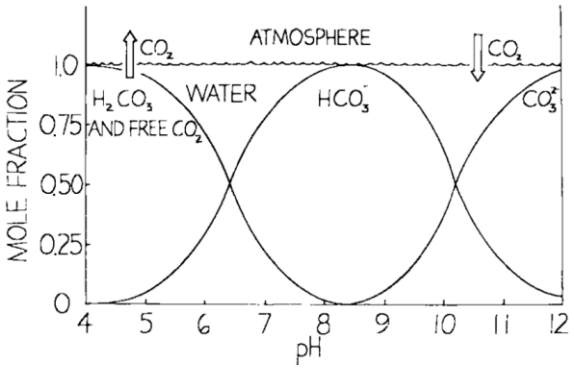

Figure 1.12: Ionic forms of inorganic carbon in water, and CO_2 exchange with air-water interface. Extracted from (Kaplan, 1986).

Temperature changes the rate of the chemical and biochemical reactions, therefore modifying microalgae composition (Hu, 2013). The optimal growth temperature of microalgae variates accordingly with the species and the strain. For *Chlorella vulgaris*, it is estimated between 20 and 30°C (Converti et al., 2009; Varshney et al., 2015). At

optimal temperature, the enzymatic and biochemical activity is optimal and the cellular growth rate is maximum. Growth at non-optimal temperature may modify the levels in unsaturated fatty acids (Nishida and Murata, 1996; Xin et al., 2011), in chlorophyll *a* (da Silva Ferreira and Sant'Anna, 2016; Thompson et al., 1992) and total carotenoids (Liu and Lee, 2000), or in starch (Ivanov et al., 2021; Nakamura and Miyachi, 1982; Zachleder et al., 2021). The reduction of metabolism speed at low temperature was shown to be an efficient strategy to alleviate respiration during the night. Edmundson and Huesemann demonstrated that after 10h in darkness at 25°C the microalga *Nannochloropsis salina* losses 20% of dry weight, while only 2% at 10°C (Edmundson and Huesemann, 2015).

Photobioreactors and open cultivation systems

The efficiency of any microalgae cultivation rely mainly on the culture system employed. Indeed, the system of culture determines light availability (depth and orientation), environmental parameters (mixing, CO_2 supply, O_2 removal, pH & temperature regulation), as well as the occurrence of contamination (exposition to open air). There is two types of culture system: open systems and photobioreactors (PBR).

The global production of microalgae is mainly issued from open systems like raceways, circular ponds, or lakes. Some lakes are natural habitats of microalgae, from which they can be regularly harvested during seasonal blooms (Abdulqader et al., 2000; Carmichael et al., 2000). Conversely, raceways and circular ponds are artificially built, and are ponds of low depth (Figure 1.13) equipped with an agitation system (Y. Shen et al., 2009). These open systems are not energy intensive and have been proven to be efficient for large scale cultivation (Tredici, 2010), but it also has its own drawbacks, for example high water evaporation, and contamination by competitors or predators (Zittelli et al., 2013). As a result, open cultivation is performed almost exclusively on robust strains that can overcome contamination by growing with high growth rate like *Chlorella vulgaris* or in selective conditions like *Arthrospira platensis* (spirulina) (Harun et al., 2010).

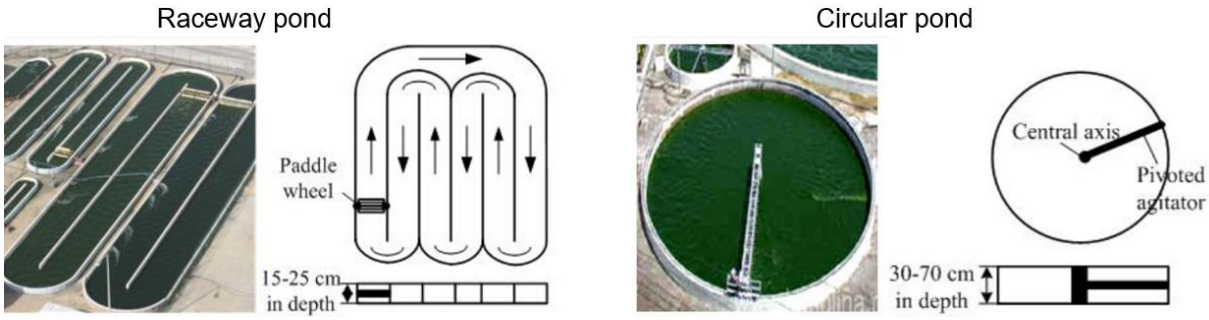

Figure 1.13: Raceway and circular ponds, the two most popular open culture systems. Reproduced from (Shen et al., 2009).

In contrast to open systems, photobioreactors (PBRs) offer a closed and controlled environment to grow specific microalgae strains (Ross et al., 2021). PBRs are defined as culture systems for phototrophs in which photons need to pass through the transparent walls of the reactor (Tredici, 2010; Zittelli et al., 2013). In general, their design aims to maximize the surface exposure to light. For this, several geometry have

been developed: vertical columns; tubular (serpentine, manifold, helical); vertical or inclined flat panel. PBRs can be built in various materials, from glass to disposable plastic, and the construction cost of low cost PBRs is not necessarily higher than for open systems (Tredici, 2010). Briefly, the main advantages of PBRs over open systems are reduced contamination, lower water footprint, control of culture parameters, efficient gas exchange (e.g. CO_2-enriched air bubbling for CO_2 supply and O_2 removal), as well as higher surface-per-volume ratio (Tredici, 2004).

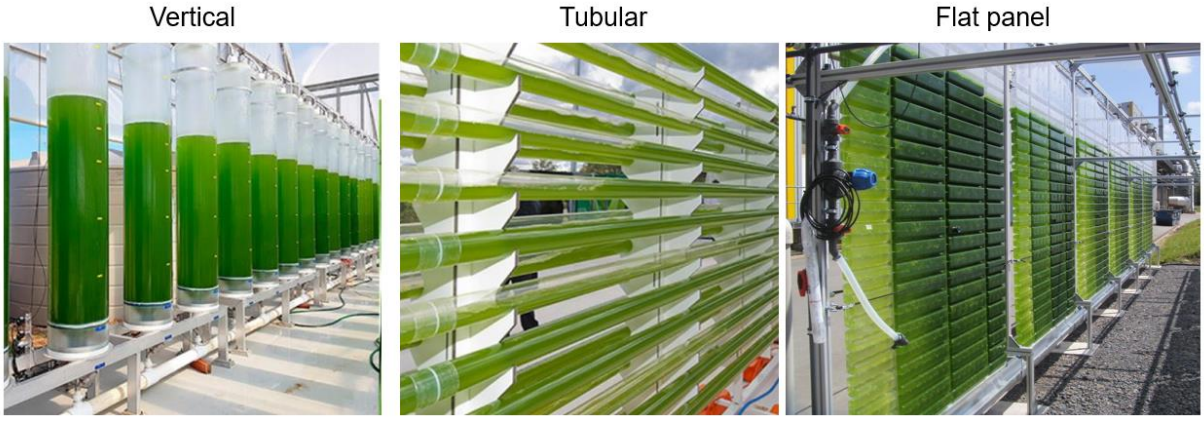

Figure 1.14: Vertical, tubular, and flat panel photobioreactors (PBR). Pictures from Ross et al. 2021 (vertical & tubular) and Subitec (flat panel).

Cultivating microalgae in PBR is much more expensive than in open culture systems. First, the installation cost of PBR is often higher than open systems. Secondly, PBR are more costly to operate, with significant energy expenditures for mixing by air bubbling and cooling by water-spraying. According to Tredici 2010, air bubbling in PBR would consume 2000 $MJ.ha^{-1}.day^{-1}$, against 200 $MJ.ha^{-1}.day^{-1}$ for paddle mixing in raceway ponds (Weissman et al., 1988), which represent up to 50% and 5% of the energy stored in the biomass, respectively (Tredici, 2010).

On the other hand, harvesting the biomass produced in PBR could be less energy consuming. Indeed, biomass concentration reach up to 8-13 g/L (Münkel et al., 2013; Pulz, 2001) in PBR against around 0.2-0.5 g/L in open systems (Levasseur, 2021; Pulz, 2001). Centrifugation, one of the most common harvesting methods, brings about 100 g/L cell density. Starting with a biomass concentration of one tenth the objective (in PBR) instead of one hundredth (in open system) surely saves some harvest cost.

PBRs and open systems are thus very different in terms of cost, operation, and biomass growth. The combination of these systems, with PBRs ensuring inoculum production and open systems performing the large cultivation, is viewed as a promising strategy for cost-effective biomass production (Rodolfi et al., 2009; Tredici, 2004). Besides, coupling of PBRs to open systems could be, for example, adapted to the two-stage depletion strategy for starch accumulation.

Quantification of culture productivity

Microalgae can be grown in various context and with different culture systems. In order to estimate and compare the productivity of microalgae cultures, one should use the relevant tools. The productivity of a microalgae culture is expressed regarding either its volume, its ground surface, or its energy conversion efficiency.

The volumetric productivity (VP) is the biomass produced per reactor volume per time unit ($g.L^{-1}.d^{-1}$). As the produced biomass depends on the absorbed photons, VP is directly linked to the number of photons entering the reactor volume per time unit ($mol_{photon}.L^{-1}.d^{-1}$). This entry of photons regarding to the volume is mainly influenced by the shape of the reactor, particularly its surface-per-volume ratio (S/V). Therefore, VP is by definition directly linked to the S/V of the reactor (Zittelli et al., 2013). That explains why a reactor with high S/V (like flat-panel PBR) performs higher VP than culture system with lower S/V (like raceways). However, high S/V reactor may perform high VP concomitantly with poor photosynthetic or areal efficiency; for instance a very small volume can yield high VP but waste a lot of light by transmittance or photosaturation.

The ground productivity (or areal productivity AP) is the biomass produced per reactor occupation surface per time unit ($g.m^{-2}.d^{-1}$). AP is linked to the incident flux of photon ($mol_{photon}.m^{-2}.d^{-1}$), and is therefore associated with the global solar irradiance, dependent of the season and latitude. It is trivial that the calculation of AP requires the estimation of the occupation surface of the culture. However, the latter is not always straightforward to obtain, in particular for PBRs. The occupation surface should consider the total surface of the production plant, including in the case of vertical PBRs the empty spaces left because of shadow casting.

A third way to express the productivity is photosynthetic efficiency (PE). Straightforwardly, PE represents the proportion of incident solar energy that is stored as chemical energy within the biomass. Conventionally, the total solar energy is considered, encompassing the visible light as well as the ultraviolet and infrared spectrum, despite their inability to be utilized for photosynthesis. PE is useful to evaluate the performance regarding the light capture, and also to compare different culture systems and locations.

Finally, the cellular growth rate is also commonly used to express the performance of outdoor microalgae culture. However, it is often ignored that high growth rate are not necessarily associated with high productivities (Zittelli et al., 2013). Intrinsically, high growth rate are reached at photosaturating irradiance (see PI-curve, Figure 1.10), while mass microalgae cultures are typically placed under photolimiting condition to capture all effective photon and maximize VP and PE (Zittelli et al., 2013). For instance, maximizing cellular growth rate in an indoor culture would require a cell density so low that most of the impinging photons would pass through unused (Tredici, 2010). Therefore, aiming to maximize the cellular growth rate alone is not a correct target for achieving high culture performance in mass microalgae culture. More generally, one should keep in mind that microalgae performances measured under

photosaturation in the laboratory are not representative of performances under photolimitation in outdoor mass culture.

1.2.3 Microalgae as converters of solar energy

Efficiency of photosynthesis in microalgae

As introduced above, knowing the efficiency of photosynthesis in microalgae culture is a way to quantify the effciency at which solar energy is stored in microalgae. Knowing the attainable photosynthetic efficiency is of great interest, because it can be used to estimate the minimal area required to produce a given quantity of biomass from an incident photon flux.

Thanks to our knowledge of photosynthesis processes, it is possible to estimate a maximum theoretical value for photosynthesis efficiency, called PE_{max}. The minimal requirement of photosynthesis is 8 photons per fixed CO_2, although some authors report the real minimal would rather be around 10 photons (Janssen, 2016). This means that 8 moles of absorbed PAR photons, totaling 1728 kJ (216 $kJ.mol^{-1}$* 8), produce 1 mole of fixed CO_2, corresponding to 460 kJ (one sixth of glucose energy content, 2760 kJ/mol). Considering that PAR photons only represents 42.3% of sunlight energy, we obtain a theoretical PE_{max} of 11.3% (Janssen, 2016). Using slightly different values, Tredici obtained a theoretical PE_{max} of 12.4% (Tredici, 2010).

In practice, this theoretical PE_{max} is largely over-estimated. Indeed, the conversion of energy from photons to biochemical energy and the fixation of CO_2 are two distinct and independent processes. Therefore, the photosynthesis energy is not only used for CO_2 fixation but also for many other cell processes. Moreover, apart from this deviation in the produced energy, the production of biochemical energy can also be diminished if either photon absorption or energy conversion in the photosynthesis machinery is reduced. Overall, it was estimated that the photosynthetic efficiency is reduced by 10% because of light reflection, by 40% because of photosaturation and photoinhibition, and by 20% because of respiration (Tredici, 2010). In practical conditions the photosynthesis efficiency would then vary between 4.9% and 5.4% (Janssen, 2016; Tredici, 2010). Still, these PE values could be significantly reduced if more energy-dense biomass compounds were accumulated instead of carbohydrates.

Microalgae yield productivity and comparison with major crops

From a technological point of view, microalgae have compelling interest as solar energy converters. However, the relevance of using microalgae should be accessed by comparing their photosynthetic efficiency with other available technologies, such as plant crops or solar panels.

In the field, long-term cultures of microalgae fail to reach photosynthetic efficiency of 5%. Outdoors experiments of at least annual duration range from 20 to 80 $t.ha^{-1}.yr^{-1}$ (5 to 22 $g.m^{-2}.day^{-1}$) in open systems (Zittelli et al., 2013). Considering a daily irradiance of 17 $MJ.m^{-2}.day^{-1}$ (annual U.S. average is approximately 18), and an energy content of 20-23 $kJ.g^{-1}$ of dry biomass, the practical photosynthesis efficiency of microalgae culture would then be around 0.6-3.0%.

In plants, the attainable photosynthesis efficiency was estimated to be in the same range as microalgae, with 4.3-5.3% (Tredici, 2010). However, for several reasons the actual long-term PE of plant crops is much lower. Sugar cane, one of the most efficient crops known, show maximal conversion efficiencies around 3.3% (Tredici, 2010).

In addition to photosynthetic efficiency, the areal productivity also appear as similar between microalgae and plants. If microalgae productivity can range from 20 to 80 $t.ha^{-1}.yr^{-1}$, biomass yield in commercial open ponds usually do not exceed 30 $t.ha^{-1}.yr^{-1}$ (Carlsson et al., 2007). This is comparable with tropical plant crops where typical yields of 20-25 $t.ha^{-1}.yr^{-1}$ (sugar beet, maize, sorghum, sugarcane) are routinely obtained, with highest yields around 80 $t.ha^{-1}.yr^{-1}$ for sugarcane.

In comparison, photovoltaic solar panels seem to better perform at energy conversion (Table 1.1). However, the energy produced by photovoltaic cells is in an instable form (electricity) and should be further converted for storage. As presented in Table 1.1, electricity can be stored in H_2 after splitting H_2O by electrolysis with high efficiency (Blankenship et al., 2011), despite that some authors argue that this conversion is not so simple in practice (Shevela et al., 2017). Solar panels can also be used to generate biomass through a combination of photovoltaic electricity generation, carbon capture, carbon fixation by electrocatalysis, and microbial growth. This technique would be more efficient than pure photoautotrophic growth with plants or microalgae (Hann et al., 2022; Leger et al., 2021). Yet, these systems of 'artificial photosynthesis' aiming to convert solar energy into chemical energy are still to be implemented and tested at a larger scale.

	Microalgae	C3/C4 plants	Photovoltaic cells (silicon, single-junction)	
Type of storage	Biomass	Biomass	None (electricity)	H_2
Theoretical maximal solar energy conversion	11.3%[1] - 12.4%[2]	12.4%/8.2%[2]	32%[3]	14%[3]
Estimation of attainable solar energy conversion	4.9%[1] - 5.4%[2]	4.3%/5.3%[2]	~20%[4]	10%[3]
Solar energy conversion achieved in the field	<3.0%[2]	<3.3%[2]	12%[5]	unknown
Solar energy conversion achieved at industrial scale	unknown	1%[3]	4.1-5.6%[4,*]	unknown

[1](Janssen, 2016) [2](Tredici, 2010) [3](Blankenship et al., 2011) [4](Leger et al., 2021) [5](Alsema, 1998) *data from >600 production sites

Table 1.1: Theoretical and practical estimations of solar energy conversion in microalgae, plants, and solar panels. The solar energy conversion corresponds to photosynthesis efficiency (PE) for microalgae and plants, while it corresponds to electricity or H2 conversion for

photovoltaic cells. H_2 is obtained from H_2O splitting by electrolysis, and is a relevant mean to store the photovoltaic electricity (Blankenship et al., 2011).

In summary, both theoretical considerations and field experience indicate that microalgae perform at levels similar to plants as solar energy converters. To counteract photosaturation and enhance microalgae productivity, various possibilities are being considered, including light dilution systems or genetically improved strains with reduced antenna size (Blankenship and Chen, 2013; Tredici, 2010). In the current state of strain availability and culture technology, the decision to choose microalgae over plants may be influenced by their special metabolites and their ability to grow on waste waters or non-agricultural lands.

1.2.4 Conclusion

Microalgae cultivation primarily relies on effective light management. The photosynthesis-relative-to-irradiance curve (PI-curve) reveals three states of light utilization: photolimitation, photosaturation, and photoinhibition. If photoinhibition is to be avoided, photolimitation and photosaturation can both turn out to be optimal conditions, depending on the desired outcome. Photosaturation leads to the highest photosynthesis output, while photolimitation brings the highest light-use efficiency. However, in outdoor culture systems the photolimitation is the preferred state, as the objective is to use all incoming photons.

A major bottleneck of microalgae cultivation is that, even with proper management of culture parameters and sufficient agitation, the culture productivity is greatly diminished because of photosaturation and photoinhibition occurring in the first layers of the culture. In practice, industrial cultivation of microalgae is not more efficient than that of plants in terms of solar energy conversion, and should be preferred for other reasons.

Indeed, microalgae cultivation presents several distinct advantages over plants. For instance, the metabolic activity of green microalgae like *Chlorella vulgaris* can be quickly redirected towards starch accumulation for the production of bioplastics.

1.3 Microalgal starch as building blocks for bioplastics

Microalgae cultures necessitate proper light management. However, beyond the optimization of the overall culture productivity, it is also possible to influence the biomass composition of microalgae and reorient metabolism toward the accumulation of compounds of interest. Indeed, microalgae have the compelling capacity to preferably accumulate one compound or another depending on the strain and culture conditions. This particularity can be used to, for example, boost massively starch accumulation in microalgae.

1.3.1 Starch in microalgae

Various types of storage polysaccharides exist in microalgae, and not every microalgae are able to synthetize starch, depending on their phylum. In this section, we will focus only on starch produced by green microalgae from the Chlorophyta phylum.

Structural organization of starch

Starch is of huge importance for human societies, as it provides 80% of the world's calories (Keeling and Myers, 2010). In plant kingdom, starch is the most represented form of carbohydrate storage. Its origins are very ancient, as the starch synthesis enzymes first appeared in red and green microalgae more than 1.5 billion years ago (Keeling and Myers, 2010). Starch metabolism is also remarkably conserved from the algae to the plant (Deschamps et al., 2008), which shows how starch was important throughout the evolution of these organisms.

In bacteria or animal cells, carbohydrates are stored as glycogen. Like glycogen, starch is a polymer of glucose with α-1,4 and α-1,6 linkage. However, starch is by far a more efficient carbohydrate polymer for long-term storage. Thanks to its highly organized structure, starch is dense and insoluble, which allow storing high quantity of energy in a small space without perturbing the cell osmolarity (Dauvillée, 2001).

Starch is actually composed of two molecules: the linear amylose and the branched amylopectin. Despite both being polymer of glucose, amylose and amylopectin have different structure, as illustrated in Figure 1.15. Amylose is linear and helicoidal because its glucose subunits mainly form α-1,4 linkages, while amylopectin is highly branched due to the presence of numerous branching points α-1,6. Native starch granules contains 20-30% amylose and 70-80% amylopectin, together with 1% of other compounds like lipids, proteins and minerals.

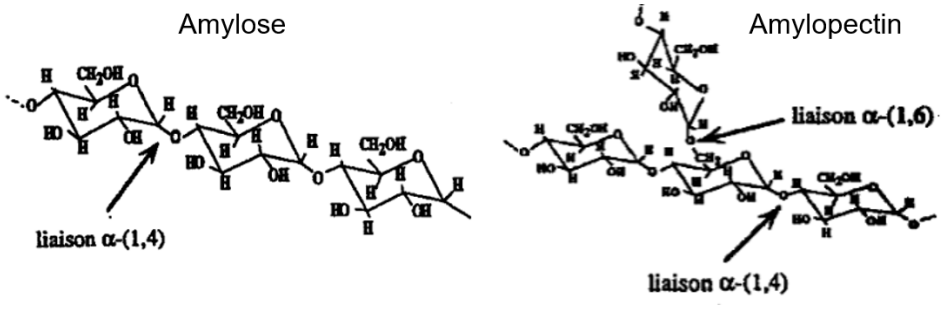

Figure 1.15: Amylose and amylopectin molecules. Their structure differs only depending on the linkage of their glucose subunits. From (Dauvillée, 2001).

Starch is biosynthesized as a highly organized granule of semicrystalline structure as depicted in Figure 1.16. The starch granules vary in shape and size, usually between 5-100 µm of diameter, depending on their botanical origin (CERMAV, 2016). They are composed of a succession of amorphous regions and crystalline lamellae. This crystalline areas are formed by the assembly of double helices from amylopectin short branches (Lourdin et al., 2015). The packing of these double helices is either compact with a low water content (A-type starch), or relatively open with an hydrated helicoidal core (B-type starch) (Tester et al., 2004). This difference in double helices packing changes the crystallinity, which allow to differentiate A- and B-type starches with X-ray diffraction spectra. Some plants produce a third crystallinity type, namely C-type, that is an intermediate structure of A- and B-type starches. The A-type mainly occurs in cereal starches, the B-type in tubers starches, and the C-type in legume seed starches (Y. Zhang et al., 2014).

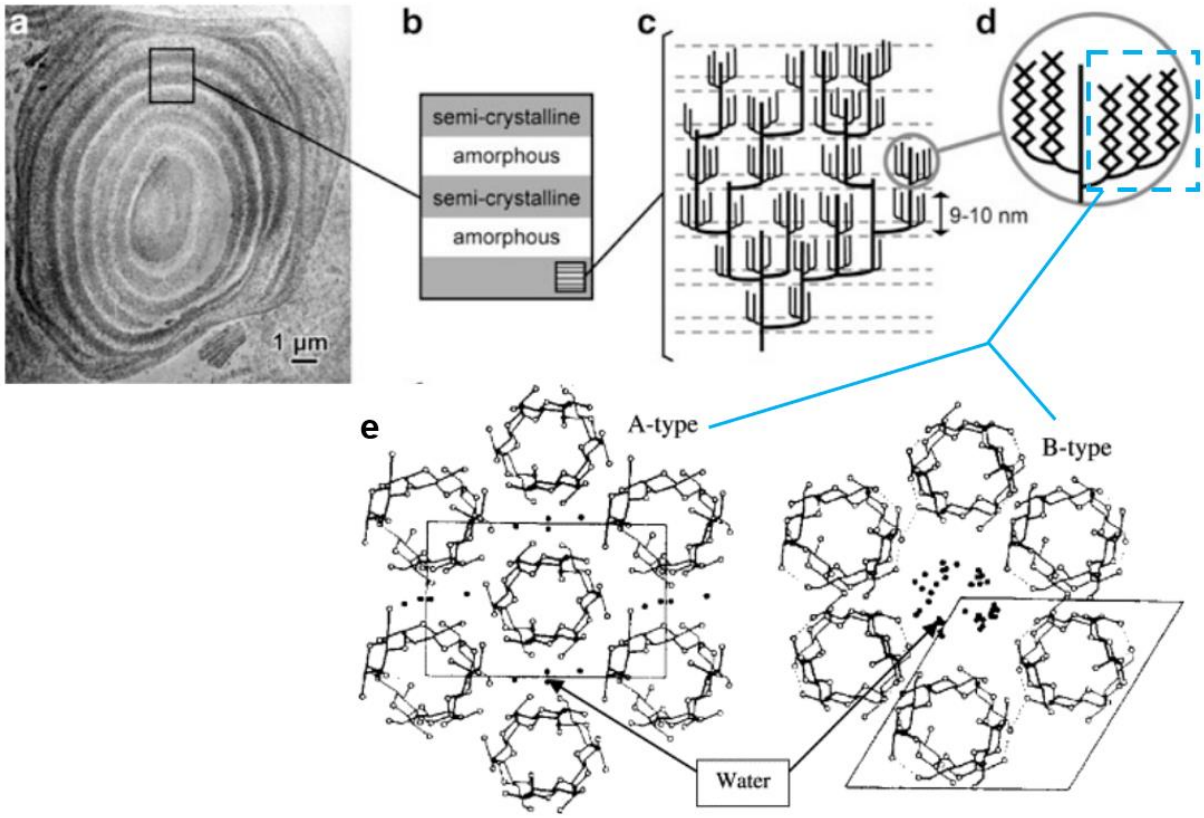

Figure 1.16: Representation of the starch granule from amorphous-crystalline rings to amylopectin and double helix crystalline assembly. (a) Waxy maize starch granule; (b) alternation of amorphous and semicrystalline growth rings; (c) clustered model of amylopectin; (d) detail of one cluster showing the formation of double helices from the short branches of amylopectin; (e) the two possible crystalline organization of double helices. Legend and figures (a-d) from (Lourdin et al., 2015) and figure (e) from (Tester et al., 2004).

Starch as modulable energy reserve

Photoautotrophs store their energy either in the form of carbohydrate polymers or triacylglycerols. Both are efficient strategies, and lipids and carbohydrates are usually concomitantly synthetized. The prevalence of starch or lipid storage in an organism depends on a genetically defined preference, but also on the immediate metabolic requirements or the environmental context. Indeed, the benefits issued from starch or fatty acids are different, as the two have different functional properties (Table 1.2).

	Starch	Fatty acids
Energy density (ATP recoverable per carbon)	ATP=~5*C (Rich, 2003)	ATP=7*C-6 (even-numbered fatty acid) ATP=7*C-19 (odd-numbered fatty acid) (Jain et al., 2021)
Reductant requirements for synthesis	1.75 ATP/NADPH consumption (Mathiot, 2020)	1.37 – 1.14 ATP/NADPH (for C16 and C18, resp.) (Mathiot, 2020)
Localization	Chloroplast	Lipid globules, chloroplast or cytoplasm
Supplementary functions	None	Major metabolite precursors

Table 1.2: Comparison of starch and fatty acids functional properties.

In green microalgae, the starch is dynamically accumulating and degrading along the day-night cycle. This process results in a low basal level of starch for microalgae growing in optimal conditions. However, when impaired in their growth, microalgae tends to over-accumulate energy reserve. This emergency energy storage helps quenching harmful excitation energy in the short term, and also prepare microalgae to replenish their growth in the long term.

The energy can accumulate either in the form of starch or lipid. The prevalence of starch or lipid typically depends on the strain and the duration of the stress (Ramírez-Romero et al., 2022; Vitova et al., 2015). Importantly, lipid and starch accumulation are not directly competitive but rather dynamically follow each other. First, the starch accumulates and then fuels a transition towards lipid accumulation (Nordin et al., 2020). This shift towards triacylglycerol ensure a secondary energy reserve for long-term survival of microalgae under stress (Hu, 2013). Some microalgae strains of one species will preferentially accumulate starch and maintain a low lipid content, while some others of the same species will do the opposite (Vitova et al., 2015). For instance, the strain *Chlorella vulgaris* CCALA924 used in this work likely belong to the starch-accumulating group (Brányiková et al., 2011).

1.3.2 Microalgal starch production

Starch is one of the most important source of polysaccharides for the industry. The industrial starch market was of $56B in 2020 (Adewale et al., 2022). Applications of starch are diverse but primarily concern the food, paper and pharmaceutical industries, representing 57, 29, and 5 % of market value, respectively. Corn is the dominant crop source with 71 % of market value, followed by potato, cassava, and wheat (7, 7, and 4 %, respectively). For now, industrial production of starch from microalgae does not exist, but microalgae hold great promise as starch producers.

Induction of starch overproduction in microalgae

In addition to developmental or physiological needs, any stress factor affecting cell division triggers starch accumulation. Namely, starch-accumulation inducers are cell division inhibitors like cycloheximide or deuterium (Brányiková et al., 2011; Zachleder et al., 2021), nutrient deprivation (Xu et al., 2022), supra-optimal temperature (Zachleder and Brányiková, 2014) or light quality (Yuan, 2022).

Macronutrient deprivation (N, P, S) is generally acknowledged to be the most efficient strategy for starch accumulation. Phosphorous is not much used, as it triggers high starch accumulation but is not optimal for both productivity and ease of operation (Ran et al., 2019). In contrast, sulfur starvation is recommended for its stable and high starch accumulation with sustained photosynthesis efficiency (Brányiková et al., 2011; Vitova et al., 2015). In comparison, nitrogen starvation is considered more harmful for the cells despite high accumulation of starch (Ran et al., 2019). However, the comparison of nitrogen and sulfur starvation in two different strains of *Chlorella vulgaris* led to contradictory starch accumulation results (Brányiková et al., 2011; Yuan et al., 2018). Among these various methods, nitrogen starvation is the most potent and commonly used one to study the process of carbon reserve accumulation, leading to starch accumulation up to 60 % in Chlorella species (Cheng et al., 2017).

Supra-optimal temperature triggers starch accumulation in *Chlamydomonas reinhardtii* and *Parachlorella kessleri* when algae are grown at 39 or 40 °C, respectively (Ivanov et al., 2021; Zachleder et al., 2021). The impact of temperature on starch production is less studied, but is interesting for application in closed PBR systems under natural light, where the temperature increases naturally with solar light availability.

In addition, light quality manipulation is proposed as a way to favor the accumulation of certain biochemical in the cell. On the one hand, changing light quality cannot be properly considered as a stress, as changing light quality can improve growth dynamics in *Chlorella vulgaris* (Kim et al., 2014; Metsoviti et al., 2019). On the other hand, applying only red-light also increases the carbohydrate content in *Chlamydomonas reinhardtii* and in *Chlorella* biofilms (Yagi et al., 1994; Yuan et al., 2020). This phenomenon is probably due to the absence of blue light photons. Indeed, the addition of a small amount of blue light reverses the carbohydrate accumulation promoted under red-light (Miyachi et al., 1978). This could be either due to an inhibition of carbohydrate synthesis by blue light, or because blue light activates the catabolism of carbohydrate, as observed in *Chlorella* (Kowallik and Schätzle, 1980).

Altogether, nitrogen deprivation, supra-optimal temperature, and light quality represent three promising strategies to induce starch accumulation, as illustrated in Figure 1.17.

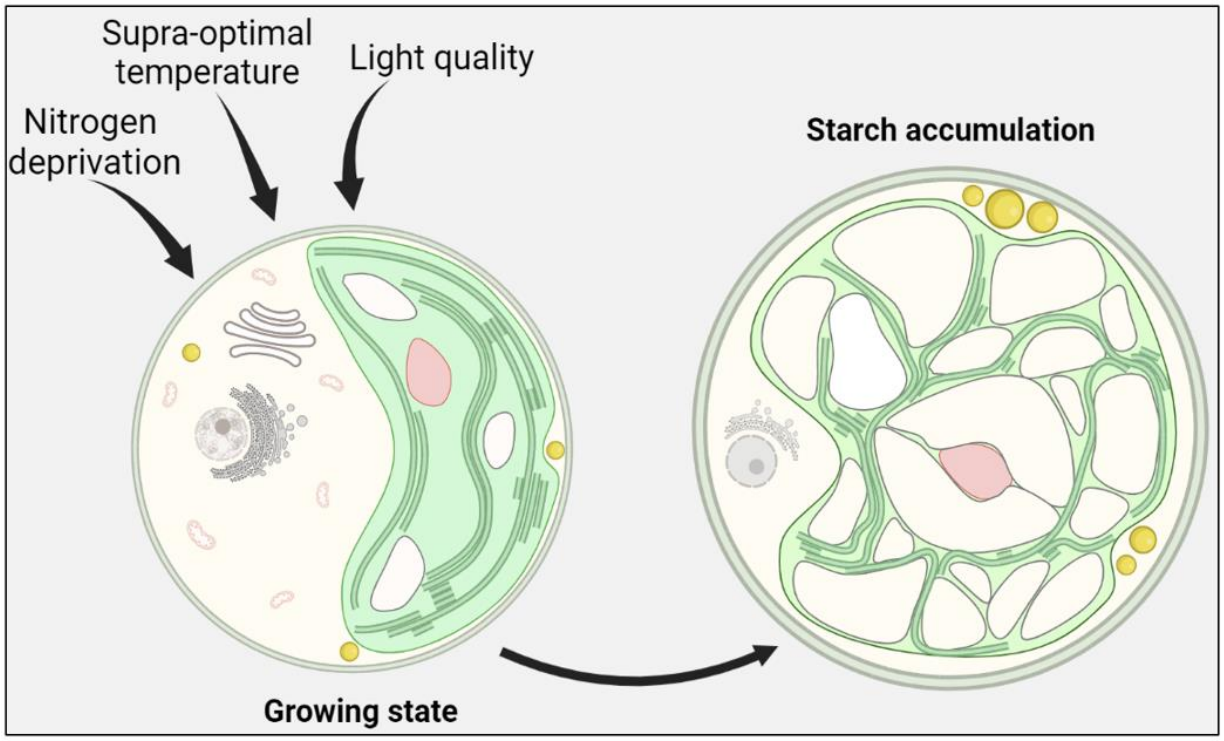

Figure 1.17: Induction of starch accumulation. The green microalga *Chlorella vulgaris* triggers starch accumulation in response to one of the three starch inducers.

Cultivation strategy for starch accumulation

Stress is often used to increase the production of one microalgae metabolite, such as starch. However, the introduction of unfavorable conditions (salinity, nutrient, or temperature) not only reduce the overall biomass productivity. It also introduces instability in the culture, which can lead to contamination and culture collapse (Hu, 2013). Therefore, a two-stage cultivation strategy was proposed to separate the phase of maximum biomass productivity from the phase of accumulation of the desired product.

One of the most common and convenient process to induce starch accumulation is the nutrient deprivation coupled with a two-stage cultivation. Indeed, the main bottleneck of the nutrient deprivation approach is that it not only redirect the energy from the cell cycle processes towards starch accumulation, but also limits protein synthesis and photosynthesis efficiency. To overcome this health degradation, the culture takes place in two steps. First, the cells are grown in optimal conditions for biomass production (complete mineral medium, optimal light, temperature). Next, the algal cultures are exposed to stress to induce the accumulation of starch, often by dilution of the culture with depleted medium (Brányiková et al., 2011; Cheng et al., 2017; Vitova et al., 2015). In addition, culture dilution increases light availability in the culture and is therefore favorable to starch accumulation.

1.3.3 Starch recovery and plasticization

Downstream process of microalgae for starch recovery

After growing and accumulating starch in microalgae, the next step involves harvesting the cells and extracting the starch from their cell walls. Although the harvest phase is also one of the major bottlenecks in microalgae biotechnology, it is not a focus of this study and the following section will only focus on starch extraction.

Starch extraction from microalgae cells typically consists of three consecutive steps: disruption, separation, and purification.

- The disruption phase consists in breaking the cell walls to release the intracellular content of microalgae. For microalgae with fragile cell walls like Spirulina or *Chlamydomonas reinhardtii*, ultrasonication or biomass freezing/thawing cycle is sufficient. For robust microalgae cells, such as *Chlorella vulgaris*, disruption is commonly achieved through chemical hydrolysis, enzymatic treatment, or mechanical stress (Brányiková et al., 2011; Gerken et al., 2013; Yap et al., 2016). The mechanical cell disruption of microalgae principally rely on bead milling, high-pressure homogenization, or French-press.
- The separation phase entails the separation of starch granules from the other components present in the cell lysate (Di Caprio et al., 2023; Gifuni, 2017b; Suarez Ruiz et al., 2020a). It relies on the high density of starch granules, that enable easy recovery by centrifugation.
- The starch purification typically involves the removal of remaining debris in the separated starch. In case of laboratory application, washing is typically extensive and rely on Percoll gradient centrifugation (Delrue et al., 1992). Likely, this extend of purity is not required for applications such as bioplastics. Other purification approaches have been tried, with acetone or ethanol extraction, and aqueous two-phase systems (Di Caprio et al., 2023; Gifuni, 2017b; Suarez Ruiz et al., 2020a, 2020b). Yet, these methods are quite complex and fail to achieve both high purity and recovery yield.

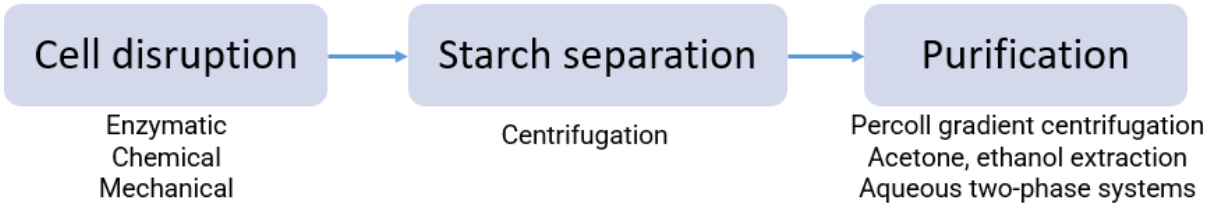

Figure 1.18: The three steps of starch extraction from microalgae and the associated techniques employed in the literature.

Importantly, the starch extraction process should not only facilitate the efficient recovery of starch but also enable the retrieval of other valuable biomass compounds, including pigments, lipids, and proteins. This biorefinery concept aims to fully valorize the microalgal biomass.

From extracted starch to bioplastics

Once extracted and purified, the microalgal starch can be directed toward a use in bioplastics. As detailed below, there is two ways to turn starch into bioplastics.

Starch owns two major attributes that makes it suitable for bioplastics production. Indeed, starch is both an energy reserve and a polymeric material. On the one hand, starch is almost only composed of glucose, a molecule that can easily fuel many organic processes. On the other hand, the structural organization of the glucose polymer confers to starch interesting material properties. These two characteristics give rise to two ways of producing bioplastics from starch.

A first way to generate bioplastics from starch is through fermentation. Indeed, starch can feed fermentation processes to yield other organic compounds, such as bioplastic monomers. In the scope of the European project Nenu2phar, which funded half of this PhD project, the microalgal starch was depolymerized into glucose syrup and fed to a specific bacteria, yielding the high-value bioplastic poly-hydroxyalkanoates (PHA). Glucose syrup from starch can also be used in any other fermentation processes (De Troostembergh, 2001; Peters, 2006), for instance to produce lactic acid that can be polymerized into polylactic acid (PLA).

Alternatively, starch can be directly turned into bioplastics thanks to its polymeric nature. Starch demonstrates thermoplastic properties once processed with plasticizers, elevated temperatures, and shear stress (Y. Zhang et al., 2014). If properly processed, the native granular starch is transformed into thermoplastic starch (TPS). The main plasticizer is glycerol and should represent 20-30% of final weight; residual water naturally present in native starch also acts as plasticizer. Shear and temperature are controlled with a screw extruder, typically in the range of 100-150°C. TPS is easily biodegradable and is already industrially produced, mainly into packaging films (Polman et al., 2021). For more details about the properties and production process of TPS, the interesting reader is referred to the review of Zhang et al. 2014 (Y. Zhang et al., 2014).

In this work, we focused on the second way, the direct plasticization, to produce thermoplastic starch from the microalgal starch.

1.3.4 Conclusion

Starch is both an energy reserve molecule and a polymer with interesting properties. This dual nature makes starch relevant for bioplastic production. Indeed, starch glucose chains can be directly plasticized after adding a plasticizer, or can be depolymerized in its glucose subunits to feed fermentation processes and yield other plasticizable molecules.

Green microalgae naturally produce starch, and overproduce it in case of stress. Based on this physiological specificity, biotechnological process were developed to grow starch from microalgae. Once produced, starch is extracted and purified from the microalgae cells, even though current processes are complex and lack of efficiency. Similarly, plasticization of microalgal starch into thermoplastic starch has only been conducted at very low scale.

1.4 Conclusion

Microalgae are a diverse group of organisms with a high potential for biotechnology. The model *Chlorella vulgaris* was selected to explore the feasibility of producing bioplastics with microalgae, both for its industrial relevance and its ability to accumulate high amount of starch. Like other microalgae, *Chlorella vulgaris* conducts photosynthesis to convert light energy into biomass. However, the machinery of photosynthesis is sensitive to intense light, and requires protective regulatory mechanisms. As a consequence, microalgae in high light use only a portion of the light while dissipating the rest mostly as heat.

Effective light management is of primary importance in microalgae cultivation. However, handling the light in outdoor context is not straightforward. By nature, photolimitation and photoinhibition zones are inherently present in cultures exposed to sunlight. One approach to increase light utilization efficiency is to adjust the biomass concentration to minimize photolimitation and photoinhibition zones, while preventing the apparition of dark zones where respiration prevails. Despite these limitations, microalgae share comparable potential as solar energy converters than plants.

Microalgae have a distinct advantage over plants in starch production, as they are able to redirect their metabolism to quickly over accumulate starch at high concentration. This accumulation can be induced by several factors, including nutrient starvation. Following the induction, the microalgae store most of photosynthesis-derived energy in the form of starch. After cultivation and harvest, the microalgae biomass must be processed to separate each compound and recover the starch. The dual nature of starch, which is both an energy reserve and a polymer material, makes it suitable to produce various bioplastics with different processes.

Chapter 2 - Materials & Methods

2.1 Microalgae cultivation (Paper I, II, III)

2.1.1 Strain & Medium

Chlorella vulgaris CCALA924 was purchased from the Culture Collection of Autotrophic Organisms (CCALA, Czech Republic). This strain was originally identified as a promising starch producer by (Brányiková et al., 2011). The nutritive medium was a modified version of the Beijerinck medium, containing 26.15 mM $NaNO_3$, 0.34 mM $CaCl_2{\cdot}2H_2O$, 0.41 mM $MgSO_4{\cdot}7H_2O$, 0.52 mM K_2HPO_4, 0.39 mM KH_2PO_4, 0.18 mM BO_3H_3, 0.077 mM $ZnSO_4{\cdot}7H_2O$, 0.026 mM $MnCl_2{\cdot}4H_2O$, 0.018 mM $FeSO_4{\cdot}7H_2O$, 0.007 mM $CoCl_2{\cdot}6H_2O$, 0.006 mM $CuSO_4{\cdot}5H_2O$, 0.001 mM $Mo_7O_24(NH_4)6{\cdot}4H_2O$, 19.98 mM $C_7H_{15}NO_4S$ (MOPS buffer). The pH was adjusted to 6.8 with 1 M NaOH (around 6 $mL.L^{-1}$). For nitrogen-deprived media, $NaNO_3$ was omitted. The cells were routinely maintained in these conditions by applying a weekly dilution, until the acclimation phase started.

2.1.2 Growth monitoring

Microalgae growth was monitored by the determination of the number and size of the cells, $OD_{880\ nm}$ (optical density measured at 880 nm), and dry weight were both used. $OD_{880\ nm}$ was evaluated by measuring the optical absorption in 1 cm light path cuvettes (ref 11602609, ThermoFisher, USA) with a spectrophotometer (UV-Vis Epoch2, BioTek Instruments, USA). Cellular density and volume were determined using a particle sizer and counter (Multisizer 4 Counter, Beckman Coulter, USA). Depending on the optical density of the sample, between 50 and 100 µL of 10-fold pre-diluted culture was suspended in 10 mL of filtered saline water (Isoton® II Diluent, Beckman Coulter, USA). The cellular exponential growth rate µ was calculated as $\mu=ln(C_2/C_1)/(t_2-t_1)$ with C_x the cell concentration at time t_x (in days). The dry weight (DW) in suspension was determined from 4–5 mL of culture. Briefly, culture aliquots were centrifuged at 4500 *g* for 10 min at 4 °C. The pellets were washed with pure water and centrifuged again to eliminate any remaining mineral solutes. The washed pellets were transferred to pre-weighed and pre-dried aluminum cups. The samples were then stored in a ventilated oven at 105 °C for 24 h. The loss in weight upon drying was measured with Mettler Toleto XSR205DU (Greifensee, Switzerland), max 220 g, d 0.01 mg/ 0.1mg and used to calculate DW and corresponding concentration. The supernatant of the centrifuged culture was recovered to determine nitrate, phosphate and sulfate concentrations by ion chromatography (940 Professional IC Vario, Metrohm, Switzerland) as described in section 2.2.1.

2.1.3 Cultivation in the different set-ups

Laboratory incubator & starch induction in laboratory (Paper I)

Before starting the starch accumulation experiment, exponential phase cultures were acclimated to the control conditions. In addition to photoperiod and CO_2 concentration, the control conditions included growth in complete medium, a temperature of 25 °C and white-light illumination. This acclimation phase lasted for 4 days, during which the cultures grew approximately from 0.3 to 1.6 OD_{880}.

For every conditions tested, the inoculum culture was centrifuged at 4500 *g* (Allegra X15R, rotor model: SX4750A, Beckman Coulters, USA) for 5 min. The supernatant was discarded and the biomass pellet was resuspended in fresh medium. In the case of nitrogen starvation, the renewed medium was nitrogen-free. For supra-optimal temperature, the incubator temperature was adjusted to 39 °C. For red-light illumination, a special set-up of 4 red LEDs (LH CPxP, Osram, Germany) was installed in the incubator.

Emission spectra measurements (BTS256-E, Gigahertz-Optik GmbH, Germany) confirmed that red LEDs emitted within the red color range only (600-700 nm), whereas white LEDs emitted in the photosynthetically active radiations and near infrared range (400-800 nm), as illustrated in Figure 2.1. The photon flux density was measured in 15 points of the incubator bottom surface with an ULM-500 light meter and its MQS-B flat sensor (Walz, Germany). Despite differences in light homogeneity, the mean photon flux density was similar for the white LEDs of the incubator and the red LEDs, with respectively 184 μmol_{photon} m^{-2} s^{-1} and 197 μmol_{photon} m^{-2} s^{-1} (n=15).

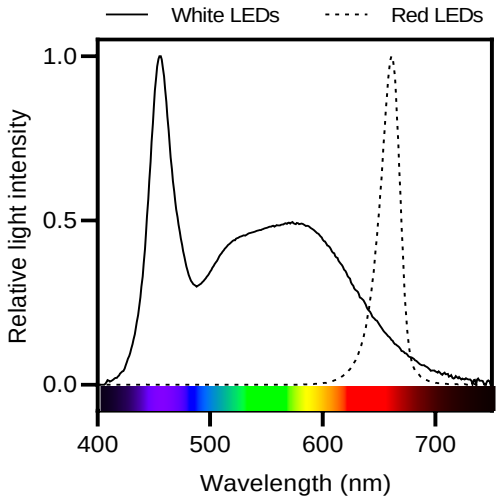

Figure 2.1: Measured emission spectra of white and red LEDs, used in N+, N-, HT experiments and for RL starch induction, respectively.

Outdoor 1L-bottle test bench (Paper II)

Small-scale microalgae cultures were grown in 1L borosilicate glass bottles (Duran, Germany) outdoors in Saint-Paul-lez-Durance (France) within a test bench comprising three mini-greenhouses. These greenhouses were covered with 180 µm thick anti-UV-treated PE plastic film (Filclair, France). Inside each mini-greenhouse, a temperature-regulated water bath accommodated four bottles, with a connecting tube ensuring homogeneous water levels between the three mini-greenhouses. The bottles were positioned on a north-south axis, with the south-facing bottle dedicated to shadow casting and the other to culture. Water temperature was regulated by a Tunze® Silence 1073.020 pump (30W, max flow 2,400 L.h-1), chilled by an Aquavie® ICE 400 (180W cooling capacity), and heated by 100W Eiheim® Thermocontrol. Water-bath temperatures were monitored and maintained between 18°C and 28°C throughout the experiment. An air-CO_2 (3% CO_2 v/v) bubbling ensure sufficient mixing to prevent precipitation in the cultures.

The culture used to start the 1L-bottle experiment was pre-cultivated for one week within the 1L-bottle test bench, achieving a biomass concentration of 3.30 ± 0.05 g/L. Ionic chromatography analysis confirmed the presence of high nitrate and phosphate levels in the medium (data not shown). After centrifugation, the medium was discarded, and the biomass pellet was resuspended in a nitrogen-depleted Beijerinck medium (see Strain & Medium section) to reach the desired biomass concentration. The bottles requiring light intensity reduction were equipped with PAR-uniform light filters (LEE colors, United-Kingdom) of transmittance 50 % and 75 %.

Outdoor pilot-scale PBR (Paper II)

Pilot-scale cultures were conducted in a 180L flat panel airlift photobioreactor (PBR) manufactured by Subitec GmbH. This PBR design features a special geometry for reduced light path and achieves effective culture mixing through air bubbling (Bergmann et al., 2013). The PBR was placed within a greenhouse in Saint-Paul-lez-Durance (France), illuminated by natural sunlight and constructed with double-layered 16 mm alveolar polycarbonate walls and a roof covered with two layers of 180 µm thick anti-UV-treated PE plastic film (Filclair, France).

The culture used to start the pilot-scale experiment was previously grown in a similar 180L flat panel airlift PBR where it reached a biomass concentration of 3.72 ± 0.13 g/L. The medium was attested to still contain high concentration of nitrate and phosphate by kit Hach analysis (data not shown). A volume of 26 L of culture was sampled and centrifuged for 10 min (10 °C, 12200 *g*) with an Avanti J-265 XP (Beckman Coulter, USA). The biomass was then resuspended in nitrogen-depleted Beijerinck medium (see Strain & Medium section) within a 180L flat panel airlift PBR. Once the experiment was started, the culture temperature was maintained below 30°C with a water aspersion system and never decreased below 22°C during the night. The pH level was continuously adjusted using CO_2 enrichment of the input air bubbling, which induced a pH variation between 6 and 8.5.

Pilot-scale microalgae production for starch extraction (Paper III)

The microalgae *Chlorella vulgaris* CCALA924 were cultivated under natural sunlight inside a greenhouse in Saint-Paul-lez-Durance (France). The culture was grown in a 180L flat panel airlift photobioreactor (PBR) manufactured by Subitec GmbH, Germany. This PBR was operated with a pH range of 7.0-7.5, an air flow of 1500 nL/h enriched with 2 % of CO_2 and a temperature regulated below 30 °C by water aspersion. Beijrinck medium adapted with NaNO3 was used.

Continuous flow pump of 269g/L $NaNO_3$ allowed maintaining a concentration of approximately 150mg/L NO_3^- during the 6 days of growth phase. NO_3^- concentration was regularly checked by ion chromatography (940 Professional IC Vario, Metrohm, Switzerland). The pump was stop on the morning of day 0 to trigger nutrient stress and starch accumulation. NO_3^- concentration was null on the afternoon, and culture was harvested on the morning of day 4. 170 L of culture were concentrated by approximately ten fold with SANI membrane filtration (Vibro I, SANI Membranes, Danemark). The pre-concentrated culture was centrifuged for three times (10000 *g*, 10 min) in 1L buckets (Avanti J-265 XP, Beckman Coulter, USA). At each step, supernatant was discarded, the biomass pellet was kept and new pre-concentrated culture was added. The biomass reached a concentration of approximately 40% DW and was stored at -20°C.

2.2 Analytical techniques (Paper I,II,III)

2.2.1 Biomass and supernatant characterization

During sampling, known volumes of culture were centrifuged, frozen at -20 °C and dried (lyophilizer COSMOS 20K, Cryotec™, France). The samples were then hermetically sealed and stored in the dark at -20 °C until analysis. In some cases where volume-based sampling were not feasible, the freeze-dried samples were carefully weighted before analysis with a Mettler Toleto XSR205DU (Greifensee, Switzerland).

Carbohydrates content and starch-equivalent content

The starch accumulation was evaluated by the quantification of total carbohydrates. The total carbohydrates were measured using the protocol developed by (DuBois et al., 1956). Briefly, samples of 1–3 mg of lyophilized biomass were digested in 1.25 M H_2SO_4 (0.5 mL mg^{-1} DW) at 100.5 °C for 3 h. The digestate was diluted in ultra-pure water to a final volume of 0.5 mL and mixed with 500 µL of 5 % (w/v) phenol solution and 2.5 mL of 95 % H_2SO_4. The total carbohydrate in the suspension was determined by comparing the light absorption at 483 nm with a glucose calibration curve.

To take into account the added H_2O molecule during starch hydrolysis into glucose, the carbohydrate values were adjusted by a factor of 0.9 to obtain the starch-equivalent content (Brányiková et al., 2011). Starch-equivalent content based on total carbohydrates quantification is to be differentiated from the starch content analyzed with enzymatic kit, as described in the section below.

Starch content and non-glucose carbohydrates

Starch concentration was determined using the Enzytec Starch kit (R-Biopharm, Germany). Boiled starches or supernatants were diluted and treated with amyloglucosidase for a 15-minute digestion at 55 °C in 100 mM citrate buffer at pH 4.6. Subsequently, the glucose content was assessed following the introduction of hexokinase and glucose-6-phosphate dehydrogenase in a buffer comprising pH 7.6, 250 mM triethanolamine, 3.5 mM $NADP^+$, and 11 mM ATP. The determination was based on the increase in absorbance at 340 nm, indicative of the reduction of NADP+ to NADPH, H+ (Findinier et al., 2017). The glucose was converted into starch concentration by applying a factor of 0.9 accounting for the water molecule expulsed during the polymerization of glucose into starch.

The concentration of non-glucose carbohydrates was calculated as the difference between glucose and total carbohydrate concentrations. The total carbohydrate concentration was analyzed according to the Dubois' method (see above section).

Protein content

The protein content in the microalgae was measured using total nitrogen amount as a proxy, as described in (Chambonniere et al., 2022). To evaluate total nitrogen (TN) and total carbon (TC) contents in the biomass, about 10 mg of dry biomass were sampled in the liquid culture, centrifuged, and washed. The resulting pellet was freeze-dried, and the dry pellet was manually ground with a mortar, to homogenize the particle size. The dry biomass was then suspended in a 50-mL bottle and kept under magnetic stirring to prevent precipitation. The analyses were carried out on the Shimadzu TOC-LCSH system (Shimadzu™, Japan) equipped with an 8-channel OCT-L autosampler and a TNM-L Total Nitrogen module. After combustion at 720 °C in a quartz tube, the O_2 carrier gas (Alphagaz Air 1 provided by Air Liquide, France) led to infrared detection (NDIR) thermostated at 65 °C, used for total carbon (TC), and to a chemiluminescence detection module for total nitrogen (TN). The flow was set at 150 mLn min^{-1}. The protein fraction in the algal biomass was computed assuming a nitrogen-to-protein ratio of 5.04, as reported for *Chlorella vulgaris* (Templeton and Laurens, 2015).

Lipid content

The lipid content and profile were assessed by total fatty acids analysis using GC-FID (GC-2010 Pro AOC-20i/AOC-20s, Shimadzu™, Japan). Lyophilized biomass samples (2–10 mg) underwent transmethylation to produce fatty acid methyl esters (FAMEs). Briefly, the samples were suspended in 3 mL of a transesterification agent (1.25 M hydrogen chloride in methanol, Ref: 17935, Supelco, USA) and combined with 0.2 mL of a 3 $mg.L^{-1}$ TAG C15:0 solution (Tripentadecanoin, reference T4257, Sigma-Aldrich™, USA) in anhydrous hexane 95% (296090, Sigma-Aldrich™, USA) as an internal standard. This mixture was incubated at 85 °C for 1 h. Subsequently, 3 mL of HPLC-grade hexane was added, followed by vigorous mixing with 1 mL ultra-pure water. After centrifugation (524 *g*, 5 min), the upper hexane phase was collected for GC analysis. The total lipid content was calculated by comparing the sum of peak

areas to that of the internal standard. Compound identification utilized retention times and validation with a set of standards of 37 FAMEs (Ref: CRM47885, Supelco, USA).

Pigment content

The pigment content was measured by the colorimetric method of (Wellburn, 1994) after pigment extraction in dimethyl sulfoxide (DMSO). Briefly, pure DMSO was added in samples of 0.5–1.5 mg of freeze-dried biomass to reach 2 mL mg^{-1} DW. Samples were heated in the dark at 60 °C for 40 min. After centrifugation, the optical density of supernatant was measured at 450, 649 and 665 nm in 1-cm lightpath cuvette (ref 11602609, ThermoFisher, USA) using a UV-Vis Epoch2 (BioTek Instruments, USA). Concentrations in chlorophyll *a*, chlorophyll *b* and total carotenoids were calculated according to the equations reported by Wellburn (Wellburn, 1994):

$$\text{Chl}a\ (\mu g\ mL^{-1}) = 12.19 * A_{665} - 3.45 * A_{649}$$
$$\text{Chl}b\ (\mu g\ mL^{-1}) = 21.99 * A_{649} - 5.32 * A_{665}$$
$$\text{TotCar}\ (\mu g\ mL^{-1}) = (1000 * A_{480} - 2.14\ \text{Chl}a - 70.16\ \text{Chl}b)/220$$

from (Wellburn, 1994) spectrophotometer range 1-4 nm

With Chl*a* and Chl*b* the chlorophyll *a* and *b* concentrations, respectively, TotCar the total carotenoid concentration, and A_{665}, A_{649}, and A_{480} the absorbance at 665, 649, and 480 nm, respectively. The total chlorophyll content was calculated as the sum of chlorophyll *a* and chlorophyll *b* contents.

Ashes content

At least 100 mg of pre-weighted samples were placed in a muffle oven (Model LE, Nabertherm, Germany). Temperature was gradually increased to 550 °C during 1 h and was then maintained for 2 h. Subsequently, ashes from the pre-weighted samples were recovered and weighted.

Nutrient characterization

The ion concentrations were measured with a Metrohm 940 Professional IC Vario ion chromatograph (Herisau, Switzerland) equipped with Metrohm Suppressor Module (MSM) for conductivity detection, and a Metrosep A Supp 7 column (dimensions: 250 × 4.0 mm, 5.0 µm particle size). The flow rate of the elution solution (3.6 mM Na_2CO_3) was set at 0.7 m min^{-1} and the run time was 35 min. The standard curve was determined with nitrate, phosphate and sulfate standards (ref. 74246, 38364, 90071 purchased from Sigma-Aldrich, Buchs, Switzerland) in the range of 2-40 mg L^{-1}. Each sample was diluted to be within the calibration range.

2.2.2 Photosystem II status

The photosynthetic apparatus status was qualified at the photosystem II (PSII) level using quantum yield protocol (QY_{max}), non-photochemical quenching protocol (NPQ3) and light curve assay (LC3) of the AquaPen-C AP 100-C fluorometer (Photon Systems Instruments, Czech Republic). Protocols details are described in the manufacturer manual and user guide. The fluorometer was set with the following parameters: measuring color of 630 nm, measuring flash pulse of 1000 $\mu mol_{photon}\ m^{-2}\ s^{-1}$, saturating pulse of 1500 $\mu mol_{photon}\ m^{-2}\ s^{-1}$, actinic light of 100 $\mu mol_{photon}\ m^{-2}\ s^{-1}$.

Soon after culture sampling, fresh microalgae cultures were diluted to an OD_{880} of 0.1–0.3 in 1 cm cuvette and placed in dark at room temperature for at least 5 min. After dark adaptation and the opening of PSII reaction centers, the response of chlorophyll *a* fluorescence to the different patterns of light stimulus was measured. The three measurement protocols were conducted once per condition and time. As the maximal quantum yield (QY_{max}) was measured for each of the three protocols, the reported results of QY_{max} were calculated from triplicates.

Partitioning of absorbed light energy was calculated from the parameters F_S, F_M, F_M' – relative fluorescence yield in steady-state illumination (actinic light), relative maximum fluorescence yield in dark-adapted conditions or during illumination (actinic light), respectively (Hendrickson et al., 2004). First, the fraction of photons absorbed by the PSII antenna allocated to PSII and photosynthetic electron transport was calculated as $\Phi PSII = 1 - F_S/F_M'$. The fraction lost by either constitutive energetic dissipation via heat or via fluorescence, i.e. the non-regulated and non-photochemical energy dissipation (f, d), was calculated as $\Phi f,d = F_S/F_M$. Finally, the fraction of regulated energy dissipation due to trans-thylakoid pH gradient- (ΔpH) and/or xanthophyll-dependent non-photochemical quenching (NPQ) was calculated as $\Phi NPQ = F_S/F_M' - F_S/F_M$. These three yields represent the complete energy partitioning, with $\Phi PSII+\Phi f,d+\Phi NPQ=1$.

2.2.3 Assessment of cell rupture

In this case, samples of biomass were stored at -20 °C without freeze-drying to preserve the integrity of cell structures. Thawed biomass samples were diluted to the desired concentration in pure water and cells disrupted by a high-pressure homogenizer (HPH, CF2 Cell Disruptor, Constant Systems Ltd., England) at 250 MPa. The biomass broth was retrieved and passed in HPH for several additional cycles. Cell concentration was measured in triplicate with a particle counter (Multisizer 4 Counter, Beckman Coulter, USA) after each disruption cycle. Particles outside the typical cell size range of *Chlorella vulgaris*, from 2.6 to 10 µm, were excluded. The cell rupture was calculated as the ratio of the disappeared cell concentration (difference in present and initial cell concentration) and the initial cell concentration.

2.2.4 Electron microscopy

Transmission electron microscopy

At 0, 40 and 88 h of treatment, the cells were fixed in suspension with a solution of 2.5 % glutaraldehyde and 0.1 M PBS (pH 7.2). Aliquots were post-fixed with reduced osmium tetroxide / potassium ferrocyanide (1 % OsO_4 / 1.5 % $K_3Fe(CN)_6$), then treated with 1 % tannic acid in 0.1 M PBS, infiltrated with an ethanol/Epon resin mixture, and embedded in Epon (Electron Microscopy Sciences, USA). Thin sections (70-nm-thick) were cut with a diamond knife in a Leica UC6 ultramicrotome. The sections were collected on carbon-coated copper grids, stained with uranyl acetate and lead citrate, and observed with a JEOL JEM-2100-Plus microscope operating at an accelerating voltage of 200 kV. Images were recorded with a Gatan Rio 16 camera. The cell wall thickness was measured using the ImageJ software (National institutes of Health, USA) in 3 separate regions on a single cell. This thickness corresponds to the

inner layer of the cell wall only. The distinction between inner and outer layers of the cell wall is described in Figure 2.2.

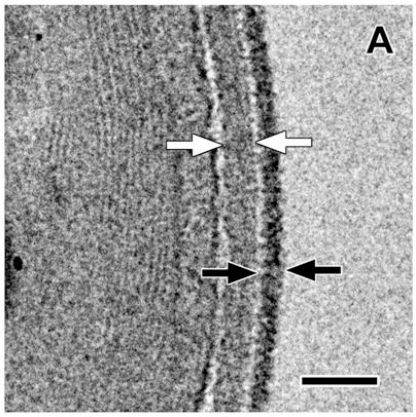

Figure 2.2: TEM image of cell wall from a *Chlorella vulgaris* cell grown in replete conditions. The cell walls are composed of two layers. The inner cell wall is the layer on the inside of the cell (white arrows), while the outer cell wall presents a hairy-like and electron dense structure (black arrows). Scale bar correspond to 200 nm.

At least 60 individual cells per condition and per time were analyzed, and the value and standard deviation reported for each cell wall thickness measurement are therefore issued from at least 180 measurements. Since the height of the section inside one cell can vary and may result in wrong measurement of the wall thickness, we assumed that the largest cells in the section would be mostly cut in their center. In that case, the cell wall was perpendicular to the plane of the section and the measured wall thickness was assumed to be meaningful. However, considering the variability of the cell diameter, we checked that, within the population of cells sections that were measured, there was not a clear correlation between the apparent cell size and cell wall thickness (Figure A.2).

Scanning electron microscopy (SEM)

- #### Starch granules

A droplet of a dilute starch granule suspension was air-dried on carbon tape fixed on a metallic stub. After a coating of the surface with Au/Pd in a Safematic CCU-010-HV sputter coater, secondary electron images were recorded with a Thermo Scientific FEI Quanta 250 microscope equipped with a field-emission gun and operating at 2.5 kV.

- #### Plasticized materials

Scanning Electron Microscopy (SEM) observations of the injected specimens cross-section were performed with a Quanta 200 FEG (FEI, Netherlands) after cryo-fracturation in liquid nitrogen and carbon coating using a Carbon Evaporator Device CED030 (Balzers).

2.3 Starch characterization (Paper I,III)

2.3.1 Starch structure

Starch granules were extracted from the microalgae after complete cell rupture with a high-pressure homogenizer (HPH, CF2 Cell Disruptor, Constant Systems Ltd., England) at 250 MPa for 5 cycles. The biomass broth was centrifuged for 5 min at 4500 *g* to pellet the starch granules. The supernatant was discarded and the pellet was resuspended in 1 mL of Percoll® (GE Healthcare Bio-Science AB, Sweden). After strong agitation followed by centrifugation, the supernatant of biomass debris and Percoll® was carefully removed. The starch pellet was rinsed in pure water and freeze-dried. Amylose and amylopectin were separated by gel permeation chromatography on a Sepharose CL-2B column (0.5 cm inner diameter, 65 cm length) eluted in 10 mM NaOH and the wavelength at the maximum absorbance of the iodine polysaccharide complex (λ_{max}) was measured for each 300 µL fraction as in (Delrue et al., 1992).

2.3.2 Small- and wide-angle X-ray scattering (SAXS and WAXS)

An aqueous suspension of native starch granules was centrifuged. The pellet was allowed to desorb in a chamber maintaining a 95 % relative humidity (r.h.) for 5 days and poured into a 1-mm outer diameter glass capillary. The capillary was flame-sealed and X-rayed in transmission in a Warhus vacuum chamber (Ni-filtered CuKα radiation, $\lambda = 0.1542$ nm). WAXS and SAXS two-dimensional patterns were recorded on Fujifilm imaging plates at sample-to-detector distances of 4.5 and 29 cm, respectively, and read with a Fujifilm BAS 1800-II bioanalyzer. Scattering profiles were calculated as radial averages of the 2D patterns.

2.3.3 Di} erential scanning calorimetry (DSC)

Starch granules (*ca.* 10 mg) were poured into a 60 mL stainless steel pan to which 30 mg of deionized water was added. The pan was hermetically sealed, accurately weighted, and allowed to equilibrate overnight. The sample pan was scanned against a pan containing 40 mg water in a TA Instruments Q200 differential scanning calorimeter. The sample was heated from 20 to 140 °C, then cooled down to 20 °C, and immediately reheated to 140 °C, all steps carried out at a rate of 5 °C.min^{-1}.

2.3.4 Granulometry

The particle size distribution was evaluated by light scattering using a Horiba LA950 laser granulometer (0.05 - 3000 µm size range). The starch granule suspension was added dropwise in the circulation loop to achieve an obscuration rate between 10 and 70%. The size distribution was determined using Mie's theory, assuming a refractive index of 1.55 for starch and 1.33 for water, and calculating a particle diameter equivalent to that of a sphere of similar volume.

2.4 Productivity and statistics (Paper I)

2.4.1 Calculation of productivities and conversion of total carbohydrates values into starch.

Productivity of biomass, carbohydrates, lipid, protein and pigment were calculated as $(C_2 - C_1)/(t_2 - t_1)$, with C_i the concentration at time t_i (in hours). In the following,

reported productivities are calculated from t_1=0 and t_2=88 h. Other periods are summarized in Table A.S3.

The measurements and calculation of carbohydrates productivities were used to evaluate the starch productivities. For that, we took the hypothesis that the measured increase of carbohydrate content during our experiments is only linked with starch increase. Furthermore, we converted the carbohydrate values into starch by multiplying by a factor of 0.9, to take into account the added H_2O molecules during starch hydrolysis into glucose, as proposed for instance in (Brányiková et al., 2011).

2.4.2 Statistical analysis

Statistical significance was assessed using the ANOVA test with Prism 9 (Graphpad Software, LLC). When the null hypothesis was rejected ($p < 0.05$), data were further analyzed using Tukey's multiple comparison test. The following results are presented as the average of the technical replicate (n = 3), while the error bars account for the standard deviation.

2.5 Relationships between light flux and starch accumulation (Paper II)

2.5.1 Calculations of photon flux per biomass PFPB

The photon flux per biomass $PFPB$ (in $\mu mol_{photon}/g_{Xa}/s$) is calculated from the mean total incident light flux density I_m ($\mu mol_{photon}/m^2/s$), the active biomass concentration X_a (g/L) as defined in the section 2.5.2, and the surface-per-volume ratio a in m^{-1}:

$$PFPB = \frac{I_m}{X_a} \times a \tag{3}$$

The surface-per-volume ratio a was calculated by considering the total surface of the culture S divided by the culture volume V. In the case of the 1L borosilicate bottle and the flat panel 180L PBR, S was calculated as the sum of cylinder and top surface, and as the sum of both faces, respectively. V is considered to be equal to the working volume, i.e. 1L and 180L.

2.5.2 Calculations of starch accumulation parameters

Starch accumulation was monitored through the carbohydrate content, the relative productivity of carbohydrates P_{CHO}^{rel} and the photosynthesis efficiency of carbohydrate conversion PE_{CHO}. The carbohydrate content was calculated from the dry weight concentration of the biomass according to the Dubois method (see section 2.2.1). The relative productivity of carbohydrates was calculated in regards to the dry weight concentration of active biomass Xa (g/L), approximated as the initial biomass concentration X_0:

$$P_{CHO}^{rel} = \frac{P_c}{X_a} \tag{4}$$

$$X_a \cong X_0 \tag{5}$$

With P_{CHO} the volumetric carbohydrates productivity calculated from the carbohydrate concentration X_{CHO} at the time t:

$$P_{CHO} = \frac{X_{CHO\,t_2} - X_{CHO\,t_1}}{t_2 - t_1} \quad (6)$$

The photosynthesis efficiency PE_{CHO} is the fraction of received light energy stored as chemical energy in the form of carbohydrates. Here, carbohydrates were considered to be only glucose. The received light energy was calculated from the quantity of incident PAR photon, using the light models described in Appendix B, and considering that every incident photon had the energy of 680 nm photon as suggested by Janssen (Janssen, 2016).

$$PE_{CHO} = \frac{P_{CHO} \times \Delta t \times V \times \varepsilon_{glucose}}{I_m \times \Delta t \times S \times \varepsilon_{680nm}} = \frac{P_{CHO} \times \varepsilon_{glucose}}{a \times I_m \times \varepsilon_{680nm}} \quad (7)$$

With Δt the period duration (s), a the surface-per-volume ratio (m^{-1}), I_m the received light flux density on the PBR rear ($\mu mol_{photon}/m^2/s$), $\varepsilon_{glucose}$ the mass energy content of glucose (kJ/mol) and ε_{680nm} the molar energy content of 680nm photon equals to 175.9 kJ/mol.

2.5.3 Starch accumulation and light-per-biomass relationships

The relationship between starch accumulation and light-per-biomass is represented through three different equations, one for each starch accumulation parameter. The three starch accumulation parameters are the carbohydrate content (C_{CHO}, % DW), the relative carbohydrate productivity (P_{CHO}^{rel}, $g_{carbohydrates}/g_{Xa}/h$), and the photosynthesis efficiency (PE_{CHO}, %), and are expressed according to the photon flux per biomass ($PBPF$, $\mu mol_{photon}/g_{Xa}/s$), as described in the Equation (8), (9), and (10), respectively.

$$C_{CHO} = C_{CHO}^{min} + \frac{C_{CHO}^{max} \times K_{C1} \times PBPF}{1 + K_{C1} PBPF + K_{C2} PBPF^2} \quad (8)$$

Where C_{CHO}^{min} is a constant value corresponding to the initial carbohydrates content, and C_{CHO}^{max}, K_{C1}, K_{C2} are parameters to be determined.

$$P_{CHO}^{rel} = \frac{P_{CHO}^{rel,max} \times K_{P1} \times PBPF}{1 + K_{P1} PBPF + K_{P2} PBPF^2} \quad (9)$$

Where $P_{CHO}^{rel,max}$, K_{P1}, K_{P2} are parameters to be determined.

$$PE_{CHO} = \frac{PE_{CHO}^{max}}{1 + K_1^{PE} \cdot PBPF^{K_2^{PE}}} \quad (10)$$

Where PE_{CHO}^{max} is a constant value corresponding to the theoretical maximal photosynthesis efficiency, and K_1^{PE}, K_2^{PE} are parameters to be determined.

Parameters are determined by least square method using the solver function of Microsoft® Excel 2016. Their calculated values are reported in Appendix C (Table C.4).

2.6 Starch extraction, plasticization and characterization

2.6.1 Extraction from microalgal biomass

The thawed starch-enriched biomass was diluted to 10% DW in pure water. The suspended cells were disrupted with high pressure homogenization (HPH, CF2 Cell Disruptor, Constant Systems Ltd., England) at 250 MPa for 5 cycles. Cell lysate was centrifuged at 15900 g for 10 min at 5 °C (Avanti J-265 XP, Beckman Coulter, USA). The starch pellet was recovered, resuspended at a concentration of 5L of pure water per kg of wet starch with magnetic stirring, and centrifuged at 15900 g for 5 min at 5 °C. This rinsing was repeated twice. The purified starch was freeze-dried for conservation purposes.

2.6.2 Starch materials and control TPS

Three types of materials, i.e. potato starch, microalgal starch and raw biomass, were used to conduct the plasticization study. Potato starch was a commercial grade from Avebe, Netherlands, of which some characterizations can be found in literature (Avebe, 2017; Kim, 1996; van Soest et al., 1996; B. Zhang et al., 2014). Microalgal starch corresponds to the purified starch from the pilot-scale process, after freeze-drying (section 2.6.1). Due to higher dryness, microalgal starch was also complemented with 10% water (final weight). Raw biomass corresponds to the entire starch-enriched microalgae cells that were used for microalgal starch extraction, in their freeze-dried form. Water content in the three materials was analyzed with an infrared moisture analyzer MA35 (Sartorius, Germany), using approximately 1 g per measurement and three replicates per material, after three days of sample stabilization in a chamber maintaining 50 % of relative humidity (r.h.). Pure glycerol was added to the three materials to achieve a starch material / glycerol ratio of 70% / 30 %, and let to rest overnight at 4 °C. Finally, commercial TPS (NP WS 001, NaturePlast, France) was used as a control for studying TPS processing and properties.

2.6.3 Optical microscopy observations of starch plasticization

Plasticization of the three materials (potato starch, microalgal starch and raw biomass) in glycerol under static conditions (i.e. no shearing applied) was studied with an optical microscope in transmitted light (Laborlux 11 POL S, Leitz, Germany) equipped with a microscope heating stage (LTS420, Linkam, UK). The use of polarized light and gypsum retardation plate enabled the observation of birefringent structures, i.e. crystalized starch. Videos were recorded with a digital camera (Leica DFC 420, 5 megapixel CCD) piloted by the software Replay® (Microvision Instruments, France). Samples of potato starch, microalgal starch and raw biomass were placed under two glass plates in presence of large excess of glycerol. A heating cycle at 5 °C.min^{-1} was applied to the mixture up to 160 °C.

2.6.4 Extrusion and injection of TPS

The starch material and glycerol mixtures were split in 12-14 g batches, sufficient to fill the mixing chamber of the twin-screw extruder (microcompounder model MC5, Xplore, Netherlands). Twin-screw extrusion is a well-established and up-scalable method for thermoplastic processing, used to mix, additivate and/or plasticize

polymers, creating homogeneous blends. The starch material mixed with glycerol was directly plasticized at temperatures of 120 °C and 140 °C, with screw speed of 100 rpm and mixing time of 2 minutes. The extrudates obtained under each processing condition were collected and injected into tensile specimens with a sequential injection molding machine (Zamak Mercator, Poland) according to the ISO 527-2 1BA specifications. Sheath temperature was 140°C, the mold temperature 40-45°C and the injection pressure 5.5 bar.

2.6.5 Tensile tests

Tensile properties of the resulting TPS specimens were measured according to ISO 527 standard with a Zwick TH 010 testing machine. Before testing, the injected specimens rested for three days in a room regulated at 23°C and 45%r.h., and tensile tests were performed with a temperature and humidity variating between 23-24°C and 41-46%r.h., respectively. For each sample, the thickness and width were precisely measured on three different parts of the specimen, and the mean values were used for stress calculations. The parameters used to establish the stress-strain curves and determine the Young's modulus, ultimate tensile strength and strain at break were a pre-stress of 0.5N and a strain rate of 60 $\%_{\text{specimen length}}$/min. At least 7 samples per blend were tested.

Chapter 3 - Results

The technical background revealed three critical steps for the production of bioplastics from microalgal starch: the induction of starch accumulation, the proper light management in cultures, and the extraction, purification, and plasticization of the microalgae starch.

This third chapter is divided into three research papers. Each paper is dedicated to one of the above mentioned critical step, with the global objective to understand and develop the overall production process of bioplastic from microalgae starch.

Consequently, this chapter focuses on addressing the following research questions:

- *Paper I - What is the best inducer of starch accumulation in terms of overall starch productivity?*
- *Paper II - Which illumination condition leads to the most optimal starch accumulation under outdoor conditions?*
- *Paper III - How can we achieve a high yield and high-purity starch extraction from the robust microalgae Chlorella vulgaris?*

Paper I - Red light induces starch accumulation in *Chlorella vulgaris* without affecting photosynthesis efficiency, unlike abiotic stresses

This Paper is under revision for publication in Algal research (February, 2024)

Graphical abstract

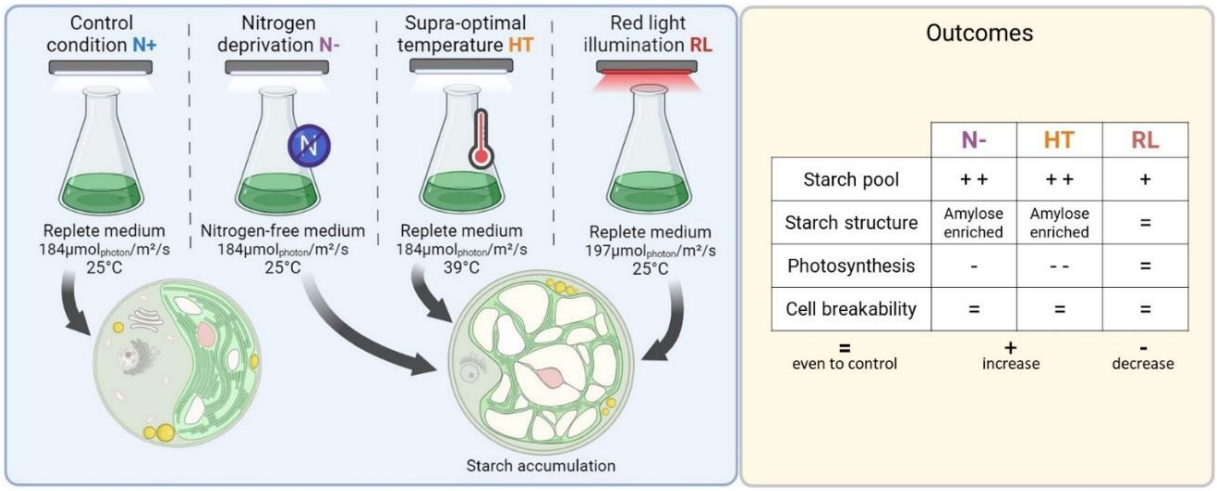

Abstract

Microalgae show great promise as sources of starch, one of the most widely consumed molecules. In this study, we evaluated the impact of three starch-inducing factors, namely nitrogen deprivation, supra-optimal temperature, and red-light, on the physiology and starch accumulation capacity of *Chlorella vulgaris*. This starch accumulation is monitored through the measurement of total carbohydrate increase and TEM imaging.

Nitrogen deprivation and supra-optimal temperature of 39 °C resulted in carbohydrate contents of 69.7 and 64.3 % of dry weight (DW). This constituted a 5.3- and 3.3-fold increase in carbohydrate productivity compared to the control, after 4 days of cultivation. During this period, carbohydrates represented more than 80 % of the produced material (DW basis). However, nitrogen deprivation and supra-optimal temperature were accompanied by extensive stress, leading to lower cell division rates and damage of the photosynthetic apparatus. Red-light illumination resulted in a more moderate production of carbohydrates. After 4 days of cultivation, carbohydrates content reached 46.8%, representing a 3.0-fold increase in productivity compared to control. The composition of the starch formed under red-light was surprisingly poor in amylose, similar to transitory-type starch rather than storage starch. Red-light illumination also resulted in a 5-fold reduction in lipid productivity. Most notably, the starch accumulation under red-light was sustained over a 7-day period without affecting the rate of cell division and quantum yield efficiency.

To the best of our knowledge, red-light is the only factor reported so far to induce important starch accumulation without hindering cell division, even after long-term

exposure (7 days). Furthermore, all three conditions induced a cell wall thickening, albeit without affecting the recovery of accumulated starch by high-pressure homogenization. These results highlight the potential of red-light as starch inducer in *Chlorella vulgaris* and open perspectives for the production of starch-based bioplastics from microalgae.

I.1 Motivation and research objectives

The demand for alternatives to oil-based products is steadily increasing. In this regard, polysaccharides sourced from biomass are promising options. However, the current pool of biomass is limited and needs to be expanded. Microalgae offer an intriguing solution, as they possess the ability to rapidly shift their metabolism towards massive carbon reserve production under stress conditions. This unique trait can be harnessed in biotechnological processes, such as through nutrient depletion or exposure to supra-optimal temperatures.

In this study, we evaluated the response of the microalga *Chlorella vulgaris* CCALA924 to three starch induction methods: nitrogen starvation, supra-optimal temperature, and red-light illumination. While these starch inducers have been documented in previous literature, a comprehensive comparison of these methods has remained unaddressed. This study aims to bridge this gap by providing a detailed analysis and comparison of these three inducers. To achieve this, we investigated starch accumulation kinetics and analyzed starch structure, photosynthetic apparatus status, and biomass composition. Additionally, we assessed starch recovery from the microalgae by examining cell rupture under high-pressure homogenization.

Contributions

Alexandre Six: Conceptualization, Methodology, Validation, Formal analysis, Investigation, Writing – original draft. Alexandra Dimitriades-Lemaire: Methodology, Investigation, Resources. Christine Lancelon-Pin: Methodology, Investigation. Jean-Luc Putaux: Investigation, Writing - review & editing. David Dauvillée: Investigation, Writing - review & editing. Dimitris Petroutsos: Conceptualization, Writing - review & editing. Pablo Alvarez: Project administration, Resources. Jean-François Sassi: Project administration, Funding acquisition, Supervision, Writing - review & editing. Yonghua Li-Beisson: Supervision, Writing - review & editing. Gatien Fleury: Conceptualization, Methodology, Resources, Funding acquisition, Supervision, Writing - review & editing.

I.2 Results

Chlorella vulgaris was grown under 4 different culture conditions to evaluate the effect of the abiotic factors on starch accumulation. The conditions were: replete medium (N+) considered as the control condition, nitrogen-depleted medium (N-), supra-optimal temperature (called HT for harsh temperature), and red-light (RL). The microalgae were grown under long night periods of 8 h, and with high initial DW concentration. Cultures were sampled both before and after the night-period over 4 days, and once after 7 days (160 h). N+ and N- cultures were also sampled after 14 days (320 h) for lipid analysis. Media in the N+ and RL conditions became sulfur-depleted by the end of the day 4 (88 h), as attested by ionic chromatography (Table A.S1). Therefore, N+ should not be considered as proper replete-medium control on day 7.

I.2.1 Starch accumulation

Each inducer efficiently triggered starch accumulation, as visible in TEM images (Figure I.1). While the control N+ showed no accumulation of starch granules, the number of starch granules notably increased after 2 days (40 h) of nitrogen deprivation (N-), supra-optimal temperature (HT) or red-light illumination (RL). The presence of starch granules within the cells further increased in N- and HT after 4 days (88 h), eventually filling up most of the cellular volume in N-. Two types of starch granules were observed: pyrenoidal and stromal starch granules, which had a similar aspect for all starch induction methods.

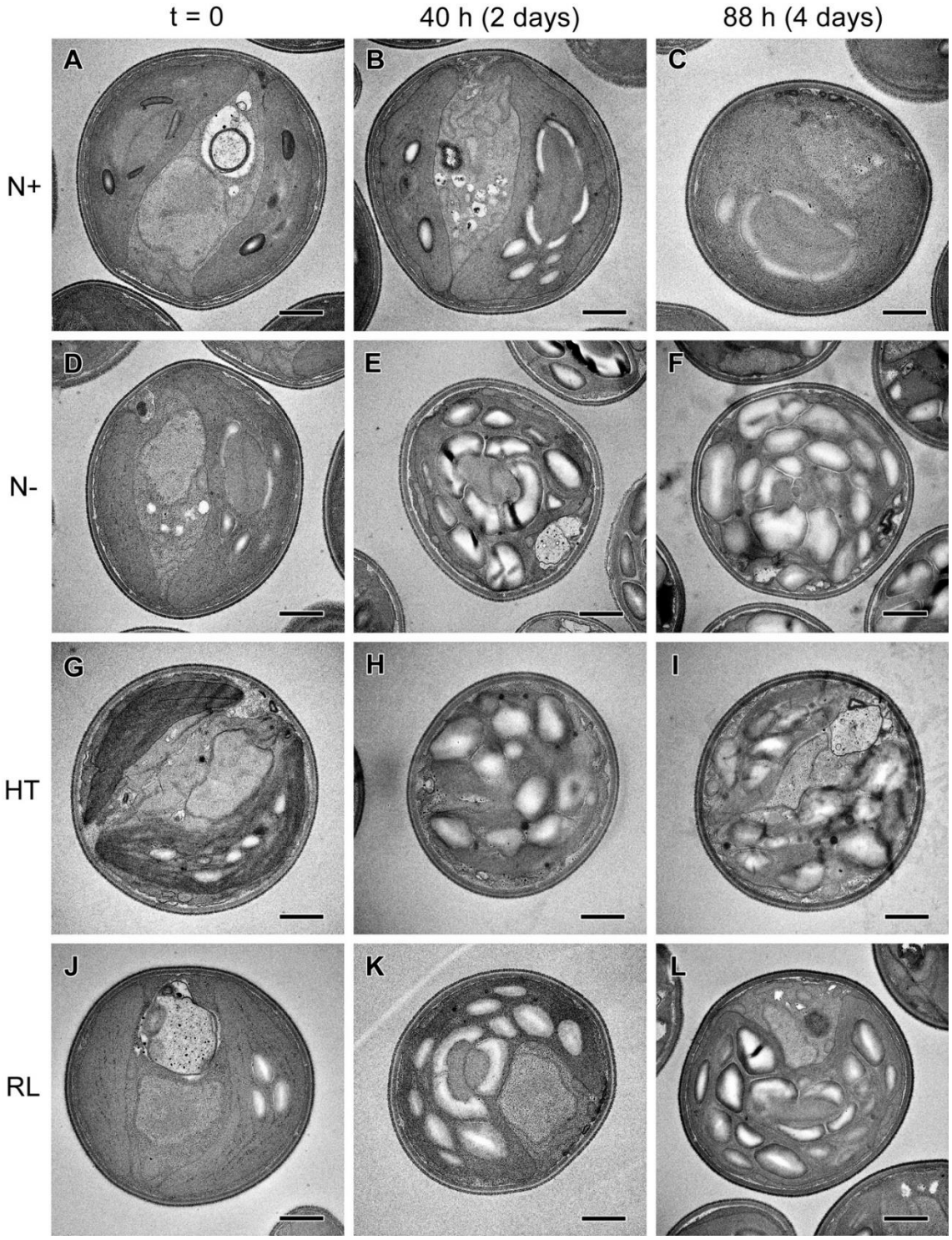

Figure I.1: TEM images of ultrathin section of resin-embedded *Chlorella vulgaris* cells after 0, 44 and 88 h of starch induction. Starch granules (in white) are visible in the chloroplast, and increased rapidly in number and size from 44 h for N-, HT and RL. Scale bars correspond to 1 µm.

Figure I.2 illustrates the starch accumulation during growth. All cultures started at 0 h with the same biomass concentration of 0.9 g L^{-1}. In the case of control N+, the biomass DW concentration reached 6 g L^{-1} after 7 days (160 h). Surprisingly, the DW concentration evolved differently depending on the applied induction method. During the first three days, the DW concentration was the highest in N-, followed by RL, then

HT and the control N+ (significant difference, $p<0.001$) (Figure I.2A). However, after 3 days, the DW concentration kept on increasing regularly only for N+ and RL, whereas the increase in DW concentration slowed down from day 3 for HT, and from day 4 for N-. The DW concentration even decreased after day 4 for HT. Overall, the dry weight biomass productivities over the first four days (88 h) were significantly higher in N- and RL (0.72 g L^{-1} d^{-1} and 0.67 g L^{-1} d^{-1}, respectively) than in N+ (0.58 g L^{-1} d^{-1}) ($p < 0.0001$).

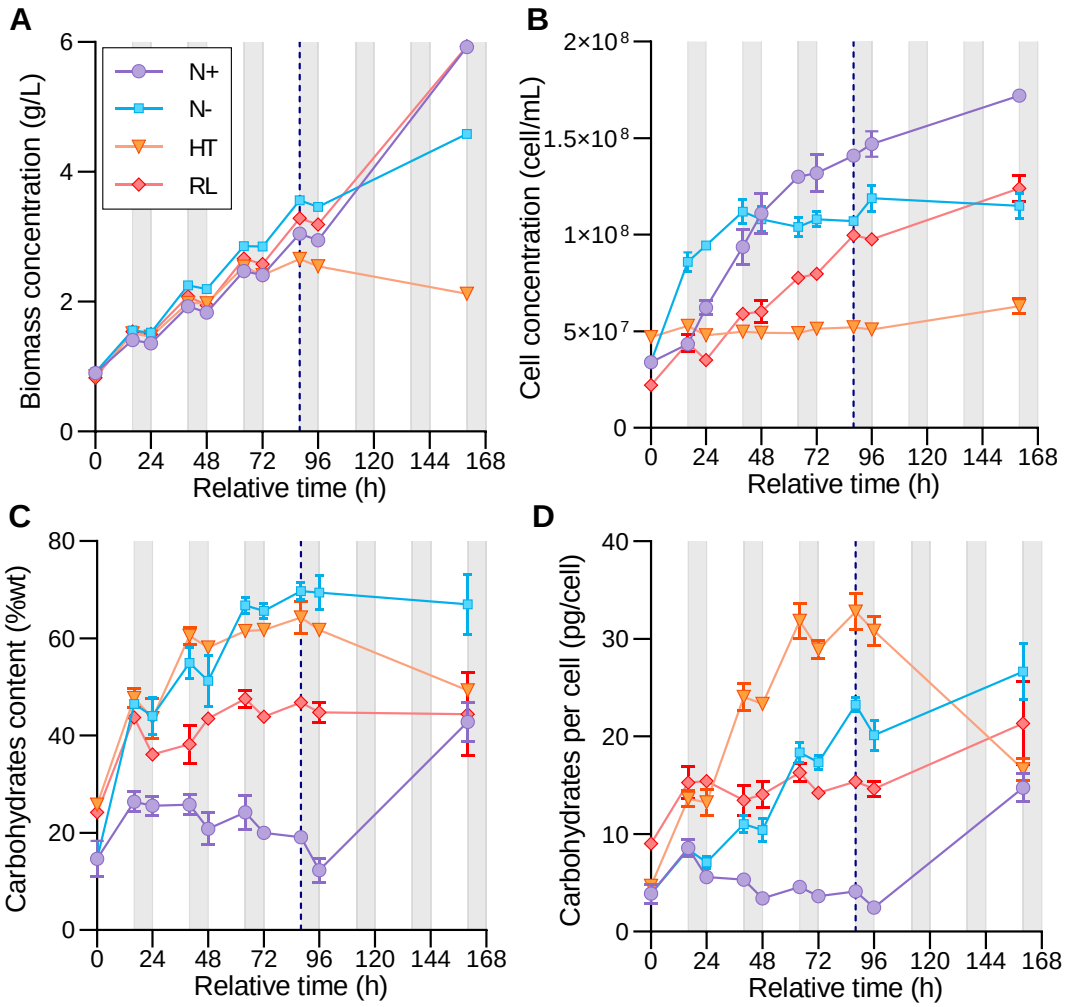

Figure I.2: Impact of abiotic factors on biomass and carbohydrate accumulation in *Chlorella vulgaris* CCALA924. (A) Biomass dry weight concentration, (B) cell concentration, and (C) carbohydrate content. The carbohydrate content per cell (D) was determined from cell and carbohydrate concentrations. Sulfur was naturally depleted at 88 h in the control culture N+ (dotted vertical line), which explains the high amount of starch observed after 96 h of cultivation in C and D. Shaded regions represent the 8-h night periods.

The starch induction method also had an impact on cellular division (Figure I.2.B). In control N+, the cell concentration regularly increased after a short lag phase during day 1. In N-, the cell concentration doubled during the first two days and then

completely stopped increasing. More remarkably, HT completely inhibited cell division from the beginning. RL behaved similarly to control N+ (Turkey's multiple comparison test, $p = 0.92$), with significantly close exponential cellular growth rates of 0.59 ± 0.01 d^{-1} and 0.61 ± 0.03 d^{-1} after 40 h for RL and N+, respectively (Table A.S3).

For control culture N+, the carbohydrate content remained stable during 4 days (96 h), between 14.7 ± 3.7 and 25.8 ± 2.0 wt% (Figure I.2.C). After day 4 (96 h), the medium became depleted in sulfur and carbohydrates therefore increased up to 42.8 ± 4.1 wt% on day 7. Nitrogen-depleted cultures (N-) had the fastest and highest accumulation of carbohydrates (significant content difference at day 4, $p<0.001$), with a considerable increase in carbohydrate content at day 1, from 14.7 ± 3.7 to 46.5 ± 0.8 wt% in only 16 h. This accumulation continued up to day 4 (88 h) when it reached 69.7 ± 3.5 wt%. From day 4 to 7, the carbohydrate content remained constant. HT cultures followed the same trend of fast and high carbohydrate accumulation. However, from day 4 to 7, the carbohydrate content decreased from 61.7 ± 0.3 to 49.3 ± 1.1 wt%. RL cultures also induced a fast starch accumulation during day 1, with a carbohydrate content increase from 24.2 ± 0.6 to 43.7 ± 0.9 wt% in 16 h. After 16 h, the carbohydrate content remained stable around 45 wt%, even between days 4 and 7 where the control N+ showed an increase in carbohydrate content due to the natural sulfur depletion of the medium. Finally, carbohydrate productivities over 4 days (88 h) in N-, HT, and RL were 0.64, 0.40, and 0.36 g L^{-1} d^{-1}, respectively (Table I.1). These values represent a 5.3-fold, 3.3-fold, and 3-fold increase, respectively, compared to control N+ (0.12 g L^{-1} d^{-1}).

	Productivity during 4 days (88 h) (mg L^{-1} d^{-1})			
	N+	N-	HT	RL
Dry weight biomass	584.3 ± 2.0	723.0 ± 12.1	493.4 ± 9.9	670.2 ± 4.2
Carbohydrates	122.8 ± 4.5	640.8 ± 19.6	406.2 ± 25.8	364.5 ± 2.8
Starch-equivalent	101.5 ± 4.1	576.7 ± 17.6	365.6 ± 23.2	328.1 ± 2.5

Table I.1: Biomass, carbohydrate, and starch-equivalent productivities during 4 days (88h). The detailed content and productivities are reported in Table A.S3

In other works, the *Chlorella vulgaris* carbohydrate productivity reached 0.92 and 0.69 g L^{-1} d^{-1} for the CO_2-adapted strain AE10 (Cheng et al., 2017; Yuan et al., 2018) and 0.82 g L^{-1} day^{-1} for CCALA924 (Brányiková et al., 2011) under various nutrient deprivation and continuous light. The productivities reported in our work are slightly lower (Table I.1) but can be explained by the lower light intensity and the 8-h night-period applied. In addition to weight loss and starch consumption due to uncompensated respiration, this 8-h night-period decreased photosynthesis by a third within a 24-h cycle. For instance, in N- condition, the initial carbohydrate productivity reached 970 ± 47 mg L^{-1} d^{-1} within the first 16 h, but decreased to 611 ± 23 mg L^{-1} d^{-1} over the entire first 24 h, representing a 37 % decrease. For N-, HT, and RL conditions, the decrease in productivity due to the extended 8-h night period ranged between 35 and 50 % over the course of 4 days.

Interestingly, the carbohydrate content per cell was lower for N- than for supra-optimal temperature HT, with maximum values of respectively 23.2 ± 0.7 vs. 32.8 ± 1.8 pg cell^{-1} at 88 h (Figure I.2.D). Meanwhile, the carbohydrate content in RL cells increased only on day 1, from around 10 to 15 pg cell^{-1}, and remained stable until 96 h. Control N+ increased its cellular carbohydrate content during day 1, possibly due to the increased light availability or medium renewal at the start of culture. Then, the carbohydrate content per cell decreased and varied between 8.6 ± 0.8 pg cell^{-1} at 16 h and 2.5 ± 0.5 pg cell^{-1} at 96 h. After day 4, and the onset of sulfate depletion, the cellular carbohydrate content increased at day 7 (160 h) for both N+ and RL, reaching respectively 14.7 ± 1.4 and 21.3 ± 4.3 pg cell^{-1}. This increase in cellular carbohydrate content in RL was not concomitant with an overall increase of carbohydrate synthesis, but rather with a general increase of cell dry weight. Indeed, the carbohydrate productivity remained stable between 96 and 160 h, while the exponential growth rate decreased (Table A.S3).

These results demonstrated that the three selected inducers efficiently triggered starch production in *Chlorella vulgaris* CCALA924, consistent with several previously published works on other green microalgae (Ran et al., 2019; Yuan et al., 2023; Zachleder et al., 2021). Nitrogen deprivation resulted in the highest carbohydrate accumulation, with a carbohydrate content remaining high and stable from day 4 to 7. In contrast, the supra-optimal temperature induced a rapid accumulation with the highest cellular content, but the carbohydrate content significantly decreased from day 4. The red-light illumination resulted in a lower but constant carbohydrate content associated with a high biomass production, and tripled its carbohydrate productivity comparing to the control N+ over the first four days.

According to the literature, all known starch induction methods inhibited cell division, including nitrogen starvation and supra-optimal temperature (Zachleder and Brányiková, 2014; Zachleder et al., 2021). Here, cell division immediately stopped after being exposed under supra-optimal temperature and after 2 days of nitrogen starvation. However, we observed that cell division continued for the entire 7-day period under red light, in parallel to starch accumulation.

Intriguingly, the natural sulfur depletion occurring on day 4 had different effects on the control and red-light cultures. Indeed, from day 4 to 7, the carbohydrate content tripled in N+ but remained stable in RL. This lack of a typical increase in carbohydrate content upon sulfur depletion could suggest that red light may possibly modify the response to nutrient deprivation, which would require further investigations.

I.2.2 Starch structure

Starch granules produced in the four conditions were extracted from the cells harvested after 7 days (160 h) of cultivation. The starch was analyzed by gel permeation chromatography (Figure I.3). Iodine staining of eluted fractions revealed distinct amylopectin and amylose fractions, comparable to those previously found in *Chlorella sorokiniana* and *Chlamydomonas reinhardtii* (Dauvillée et al., 2001; Vonlanthen et al., 2015), with a λ_{max} of the iodine-amylopectin complex ranging from 539 to 560 nm.

Qualitatively, starches produced in N+ and RL conditions contain similar very low amounts of amylose, while N- and HT conditions resulted in an apparent increase of this polysaccharide subfraction.

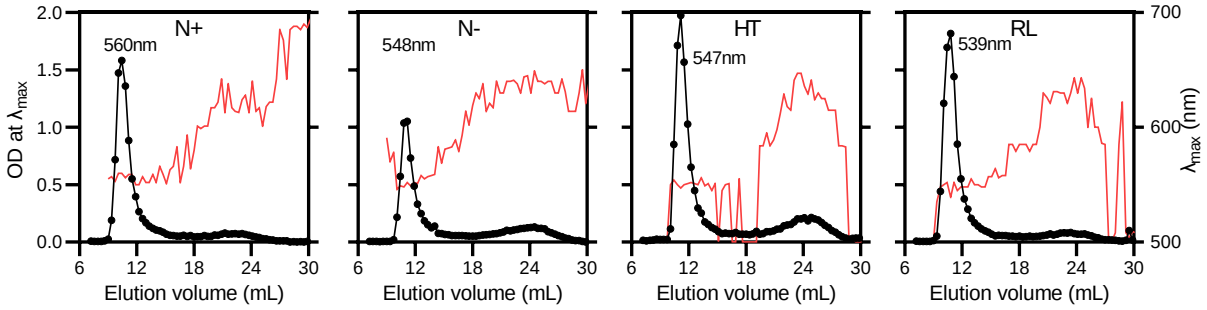

Figure I.3: Separation of amylopectin and amylose on CL-2B chromatography. Starch was extracted at day 7 (160h). Maximal absorbance of the polysaccharide/iodine complex (black circles) was measured between 500 and 700 nm for each fraction and the wavelength at maximal absorbance determined (λ_{max} in nm, red line). The gel permeation chromatography excluded the high molecular weight amylopectin (1st peak; between 8 and 15 mL of elution); while lower molecular weight amylose was eluted later (2nd peak, after 18 mL of elution). The λ_{max} of the iodine-amylopectin complex for each condition are indicated on the corresponding graphs.

In *Chlamydomonas reinhardtii*, different types of starches are produced depending on growth conditions. During active division, transitory starch mainly accumulates around the pyrenoid which is responsible for CO_2 fixation. Conversely, nitrogen starvation results in a massive accumulation of storage starch in the stroma (Findinier et al., 2019). Transitory and storage starches differ in amylopectin structure (chain length distribution) and amylose content (higher in storage-like starch) (Libessart et al., 1995). Hence, the increase in amylose content in N- and HT can be attributed to the accumulation of stromal storage starch granules, as supported by TEM observation (Figure I.1). The absence of a noticeable amylose content increase in RL-produced starch suggests the accumulation of only transitory starch. However, TEM images revealed the presence of stromal granules in RL similar to HT and N-, whereas pyrenoidal starch granules exhibited no sign of hypertrophy, in contrast to the findings in a particular *Chlamydomonas* mutant (Findinier et al., 2019). Therefore, the stromal starch accumulation coupled with a low amylose content under red-light illumination may indicate that the carbon flux is not massively oriented towards the accumulation of storage compounds. This view is supported by the fact that the cells did not fully redirect their energy toward starch accumulation in response of the absence of blue light, even when nutrient depletion occurred after 4 days (Figure I.2.C).

I.2.3 Biomass composition

Apart from carbohydrates, the three main compounds of microalgal biomass are proteins, lipids and pigments. At 0 h, the protein content was approximately 50 wt% for N+, N- and RL, while it couldn't be properly measured for HT due to analytical problems (Figure I.4.A). To perform the comparative calculations, we, assumed the

initial protein content to be similar to the other conditions (approximately 50 wt%). After 4 days (88 h), the protein content was 37.7 ± 1.2 and 35.0 ± 1.0 wt% in N+ and RL, respectively, and only 10.4 ± 0.4 and 14.3 ± 1.0 wt% for N- and HT. Additionally, protein productivity, calculated taking into account the created biomass together with its protein content after 4 days (88 h) was of 183.7 and 200.7 mg $L^{-1}d^{-1}$ in N+ and RL respectively, compared to -28.8 mg $L^{-1}d^{-1}$ for N- and -12.4 mg $L^{-1}d^{-1}$ for HT (Table I.2). Therefore, the protein synthesis was negatively impacted by nitrogen deprivation and supra-optimal temperature but was slightly favored by red-light illumination compared to the reference. Nevertheless, the N-content of the reference decreased significantly (more than 10%) during the first 4 days, which was not expected. This protein content decrease may be linked with the measured increase in carbohydrates in the control during the first day.

Regarding nitrogen deprivation, Li et al. observed that the protein content decreased in *Chlorella vulgaris* of at least 2-fold after 7 days (Li et al., 2016). Under supra-optimal temperature, contrary to our results, Zachleder et al. (Zachleder et al., 2021) reported a significant protein increase of 8-fold in *Parachlorella kessleri* after 48 h at 40 °C. In the case of red-light illumination, Yuan et al. (Yuan et al., 2020) measured a stable protein content after 6 days in *Chlorella* biofilms. Therefore, in our case, the marked reduction of protein synthesis observed in HT is intriguing. This outcome indicates a specific sensitivity of *Chlorella vulgaris* CCALA 924 to sustained exposure to supra-optimal temperatures, especially when combined with the alternating patterns of night and day.

Table I.2: Protein, lipid and chlorophyll productivity during 4 days (88 h).

	Productivity during 4 days (88 h) (mg $L^{-1}d^{-1}$)			
	N+	N-	HT	RL
Protein	183.7 ± 10.3	-28.8 ± 3.7	-12.4 ± 8.8	200.7 ± 9.3
Lipid	53.2 ± 4.9	43.3 ± 6.9	30.4 ± 3.2	10.2 ± 4.2
Total chlorophyll	28.1 ± 0.4	-0.3 ± 0.5	0.0 ± 0.7	17.9 ± 0.8

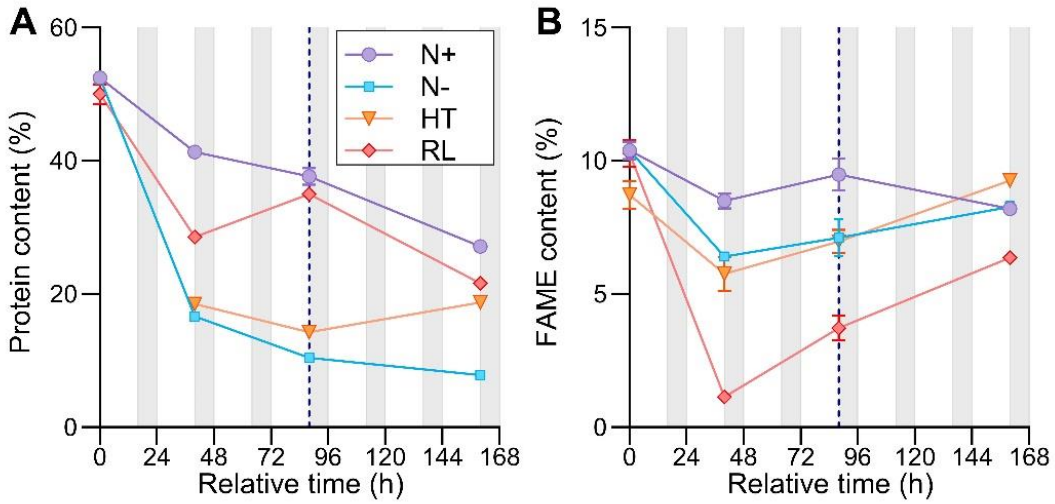

Figure I.4: Changes in protein and lipid contents upon starch induction. The dotted vertical line indicates natural sulfur depletion in N+ at 88 h. Shaded area represent the 8-h night periods.

Regarding lipid accumulation, *Chlorella vulgaris* CCALA924 did not exhibit any response to the three starch induction methods. At 0 h, the lipid content in biomass was approximately 10 wt% and subsequently remained relatively stable for the control N+ (Figure I.4.B). From day 2 (40 h), the lipid content decreased for all induction methods, with the most important decrease occurring for RL, dropping below 5 wt%. Such a quick and high variation could also be linked with analytical problems during sampling preparation (the technical replicates are similar). Moreover, the RL culture produced 10.2 mg $L^{-1}d^{-1}$ lipids over 4 days (88 h), whereas N+ and N- cultures produced 53.2 and 43.3 mg $L^{-1}d^{-1}$, respectively (significant difference, $p<0.001$). Besides, the fatty acid profiles at day 7 (160 h) showed relatively low differences (Supplementary Material Figure S3).

The decrease in lipid content under red-light illumination was unexpected, as it was shown to remain stable in *Chlorella* biofilms (Yuan et al., 2020). Moreover, this lower lipid synthesis cannot be only explained by the redirection of available energy towards starch synthesis. Indeed, the lipid productivities of N- and HT were at least 3-fold higher than RL, although concomitantly producing higher amounts of starch. This finding may suggests that blue light is essential to up-regulate lipid synthesis as shown in other microalgae species (Zhang et al., 2022), although the underlying molecular mechanisms remain to be determined.

Interestingly, lipid contents never exceeded 10 wt%, and did not increase after 7 days of nitrogen deprivation or supra-optimal temperature. Moreover, after 14 days of cultivation, the lipid content was still low in N+ and N- cultures, reaching 7.7 ± 0.2 and 10.5 ± 0.2 %, respectively. These observations differ from another report in Chlorellaceae, where the lipid content was typically in the range of 25 to 50 % after 12 days of nutrient depletion (Ramírez-Romero et al., 2022). Therefore, *Chlorella vulgaris* CCALA924 may be a low lipid-accumulating strain comparing to other Chlorella

strains. Traditionally, *Chlorella vulgaris* exhibits a two-stage response to nitrogen stress, with lipid accumulation succeeding to starch synthesis. This transition from starch to lipid storage is involving two pathways: chloroplastic triacylglycerol synthesis and glycerolipid metabolism (Nordin et al., 2020). Despite its visible ability to synthetize lipids (Table I.2), *Chlorella vulgaris* CCALA924 might lack the genetic tools to transit from starch to lipid accumulation. Yet, this hypothesis should be further investigated to explain this intriguing absence of lipid induction, especially under those favorable conditions of high light and nutrient depletion.

Another important component of green microalgal biomass is the pool of photosynthetic pigments, namely chlorophyll *a* and *b* and carotenoids. We focused on the quantification of total chlorophyll, calculated as the sum of chlorophyll *a* and *b*. The total chlorophyll concentration in cultures remained stable for the beginning for N- and HT, while it increased continuously for N+ and RL cultures (Figure I.5.A). Total chlorophyll productivities over 4 days were null or even negative for N- and HT, but were of 28.1 ± 0.4 and 17.9 ± 0.8 mg $L^{-1}d^{-1}$ for N+ and RL cultures, respectively (Table I.2). Therefore, the chlorophyll synthesis was suppressed in the case of nitrogen starvation and supra-optimal temperature, while it was only slightly reduced by red-light illumination.

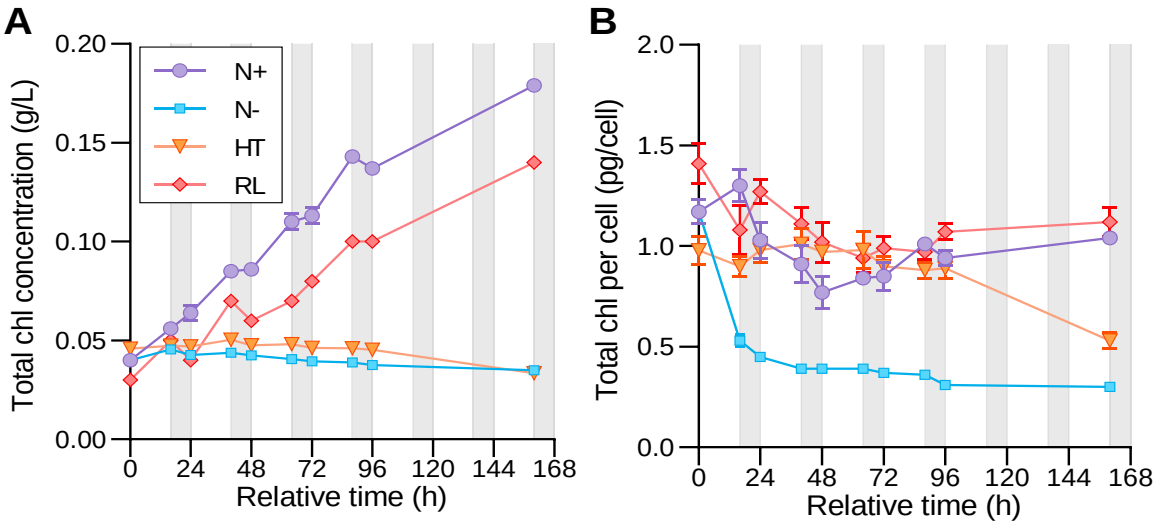

Figure I.5: Evolution of total chlorophyll concentration in the culture and per cell for the different starch induction methods.

The observed decrease in chlorophyll synthesis during nitrogen deprivation and red-light illumination aligns with literature (Li et al., 2016; Yuan et al., 2020). Regarding supra-optimal temperature conditions, a similar decrease in pigment content in cells affected by harsh temperatures was described for diatoms and higher plants (da Silva Ferreira and Sant'Anna, 2016; Kumar Tewari and Charan Tripathy, 1998).

The analyses of biomass composition have shown that starch was not the sole biomass constituent impacted by the three induction methods. Indeed, the synthesis of proteins and chlorophylls was significantly affected during nitrogen starvation and

supra-optimal temperature, with near-to-zero or even negative productivities. Furthermore, the lipid synthesis was also strongly affected, as illustrated by the 5-fold productivity reduction under red-light illumination.

I.2.4 Photosynthetic capacity

The photosynthetic capacity provides direct insights into the ability of microalgae to convert light energy and utilize it to synthesize starch. The maximal quantum yield (QY_{max}) represents the fraction of absorbed light energy entering photosystem II (PSII) to produce photochemical energy, with the assumption of full PSII opening (Baker, 2008). A decrease in QY_{max} is typically associated with damage to the photosynthetic apparatus (Levasseur et al., 2023). In Figure I.6.A, QY_{max} is around 0.72 at 0 h for all starch induction methods, indicating a healthy functioning photosynthetic apparatus. However, N- and HT cultures show a severe drop in QY_{max} from 0.69 ± 0.01 and 0.70 ± 0.00 at 48 h, to 0.15 ± 0.04 and 0.06 ± 0.02 at 160 h, respectively. In the meantime, N+ and RL cultures maintain a stable QY_{max} throughout the experiment. Interestingly, the evolution of the relative electron transport rate showed a similar pattern with QY_{max}, decreasing in N- and HT, while remaining stable in N+ and RL (Figure A.4). The decrease of QY_{max} in N- and HT is expected from the literature, as the decrease in protein synthesis affects the renewal of the essential D1 protein and the chlorophyll-binding protein CP47 within the PSII core (Markou et al., 2017).

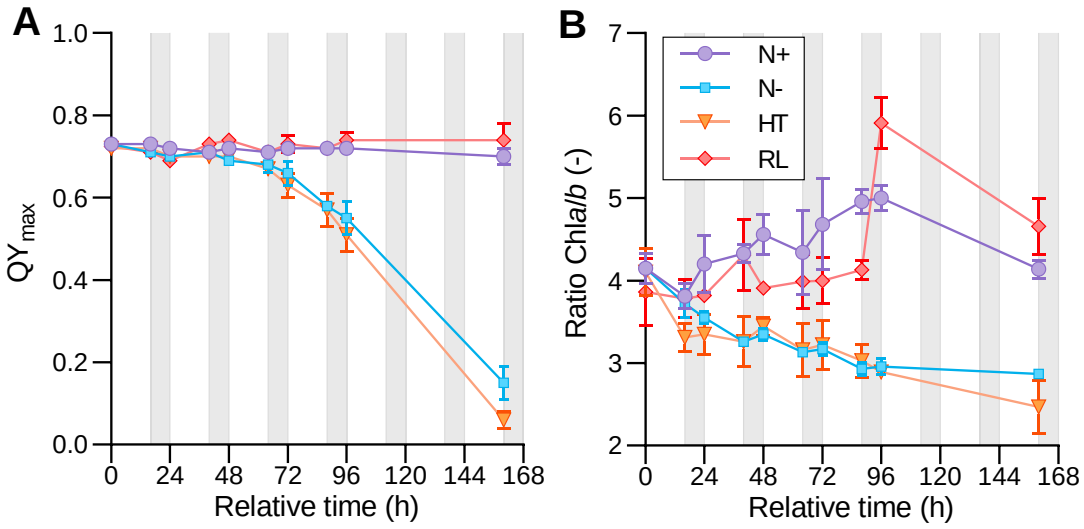

Figure I.6: Response of cultures photosynthetic capacities to starch induction methods. (A) Maximal photochemical efficiency. (B) Chlorophyll a/b ratio used as a proxy of the antenna size.

In addition to QY_{max}, which provides a broad assessment of the state of photosynthetic apparatus, we further explored the response of the key regulatory mechanisms of non-photochemical quenching (NPQ). NPQ refers to protective regulatory mechanisms leading to the dissipation of excessive absorbed light energy into harmless heat. Therefore, the extent of NPQ activation informs about the level of

stress experienced by the photosynthetic apparatus, as well as its capacity to quench excessive energy. Energy partitioning at steady-state during the fluorescence measurements revealed that NPQ was activated for all induction methods from 0 h (Figure I.7). In N+ and RL, the amount of energy quenched by NPQ (ΦNPQ) remained stable, around 10 %. In N-, ΦNPQ rapidly and gradually increased, which was seemingly associated with an equivalent decrease in PSII energy uptake (ΦPSII). In HT, ΦNPQ remained low and even decreased from day 3 (72 h) to almost zero at 96 h. This absence of NPQ implementation suggests a significant deterioration in cell health. Overall, protective mechanisms of NPQ appear mildly-activated in N+ and RL, highly-activated in N-, and under-activated in HT.

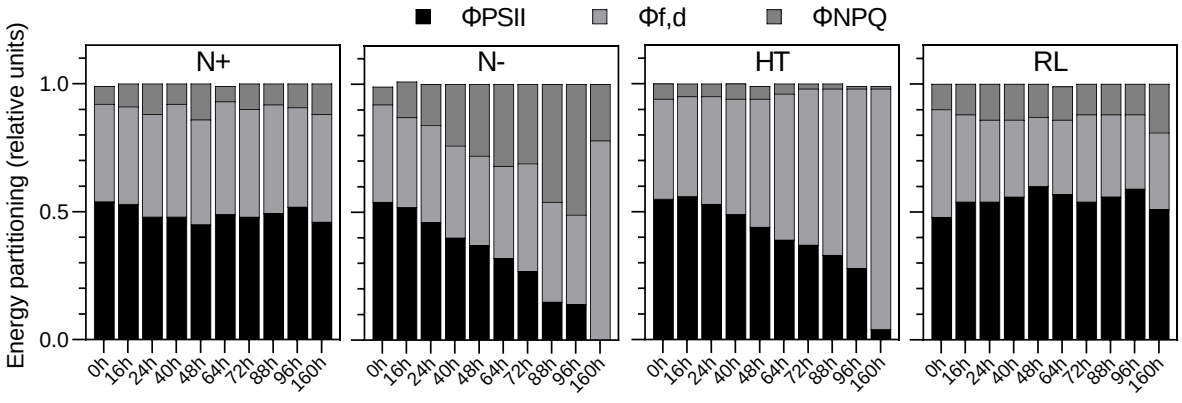

Figure I.7: Evolution of absorbed light energy repartition through PSII photochemistry (ΦPSII) (black), fluorescence and constitutive thermal dissipation (Φf,d) (light grey) and regulated thermal dissipation (ΦNPQ) (dark grey) during steady-state photosynthesis.

A complementary approach for examining the behavior of the photosynthetic apparatus involves assessing the cell ability to harvest light via their photocollective pigments. First, the cellular chlorophyll content ranged between 1 and 1.5 pg cell^{-1} at 0 h for all induction methods (Figure I.5.B). For N+ and RL cultures, chlorophyll per cell remained stable around 1.0 pg cell^{-1} until day 7 (160 h), in contrast to HT where it rapidly decreased from day 4 (96 h). For N-, the cellular chlorophyll content dropped immediately as a consequence of the initial cell division (Figure I.2) and remained stable around 0.4 pg cell^{-1}.

Furthermore, the antenna size was approached through the proxy of chlorophyll *a* and *b* ratio (Chla/b) as proposed by Friedland et al. (Friedland et al., 2019). The Chla/b ratio was about 4 at 0 h for every induction method (Figure I.6.B). Subsequently, the Chla/b ratio progressively increased for N+ and RL cultures (i.e. associated with a decrease of antenna size), while it progressively decreased for N- and HT cultures (i.e. increasing antenna size). In theory, antenna size of microalgae should increase as the culture becomes denser and light availability decreases. However, the opposite phenomenon intriguingly occurred for the control N+ and under red-light illumination. In the case of N- and HT, the decrease of Chla/b is also surprising. The

reaction centers of photosystems (Chl*a*-containing) likely degraded faster than the light harvesting complex (Chl*a*- and Chl*b*- containing).

On the one hand, N- and HT exhibited a similar decrease in their photosynthetic capacities, as evidenced by the simultaneous decrease of QY_{max}. The NPQ was strongly activated in N- and under-activated in HT, while N- and HT cultures had distinct cellular chlorophyll content due to differences in cell division. Overall, these results illustrate that the photosynthetic apparatus reacted negatively, albeit differently, to both nitrogen starvation and supra-optimal temperature.

On the other hand, the RL condition completely preserved the photosynthetic and light-harvesting capacities. Parameters such as QY_{max}, energy distribution at steady state, antenna size and cellular chlorophyll were very similar to the control N+. In conclusion, red-light illumination did not induce any visible damage to the photosynthetic apparatus of microalgae over 7 days.

I.2.5 Cell wall thickness and cell rupture

Chlorella vulgaris is known for its tough and thick cell wall, largely constituted of chitin, a polymer of glucosamine (Latil de Ros, 2017; Takeda, 1991). This robustness makes the extraction of an intracellular compound like starch challenging. *Chlorella vulgaris* cells can be efficiently broken by high-energy input devices such as high-pressure homogenizer (HPH). Moreover, the mechanical strength of microbial cells and the thickness of their cell walls have been linked to the ability to withstand mechanical rupture, including HPH (Middelberg, 1995; Yap et al., 2016). Therefore, we investigated the effect of the three starch induction methods on the cell wall thickness and cell rupture.

TEM images of cell walls are shown in Figure S1. Although the outer layer of the cell wall was also measured (Figure A.5), only the inner layer was used for cell wall thickness measurement as most of the thickness variation was attributed to this layer. At 0 h, violin plots of cell wall thickness were similar for all conditions, with a mean thickness of approximately 60 nm (Figure I.8). After 2 days (40 h), the cell walls slightly thickened in HT and RL cultures (92 ± 2 nm and 79 ± 16 nm, respectively). After 4 days (88 h), the differences in cell wall thickness increased. The N+ cell wall thickness remained stable (59 ± 15 nm). Conversely, N-, HT, and RL cells exhibited wall thickening (96 ± 27 nm, 127 ± 30 nm, and 84 ± 20 nm, respectively). Therefore, every starch induction method, with HT in particular, caused a significant increase in cell wall thickness compared to control after 4 days.

Interestingly, the cell wall thickening seemed to correlate with the cell division rate (Table A.S4). As mentioned in section 3.1, over the first 4 days, the cell concentration regularly increased for N+ and RL, while it increased during one day and then stagnated for N-, and never increased for HT. In parallel, the cell wall thickness of N+ remained low over the 4 days, while it increased from day 2 for N- and from day 0 for HT. Therefore, cell walls tended to thicken when the cellular growth rate was low for N- and HT, as shown in Figure I.2.B and illustrated in Table A.S4. Intriguingly, RL cell walls thickened despite having a cellular growth rate similar to that of N+.

In the literature, cell wall thickening is often associated with stationary phase culture, in which cell division is reduced (Canelli et al., 2021b; Spain and Funk, 2022). Furthermore, previous studies have established a relationship between cell division and the reduction of cell wall thickness (Yamamoto et al., 2004). Therefore, the cessation of cell division would result in an average increase in cell wall thickness in the culture. In our work, the microalga cells exhibited thicker cell walls when exposed to cell division inhibitors such as supra-optimal temperature and nitrogen starvation. However, it is noteworthy that red light appeared to induce cell wall thickening independently of the cellular growth rate.

To investigate whether cell wall thickness influenced the cell resistance to mechanical disruption, the biomass was disrupted by five subsequent cycles of HPH at 250 MPa (Figure I.8). At 0 h, the cell rupture by HPH showed two distinct efficiencies. For N+, N-, and HT biomass, the cells were rapidly disrupted, with approximately 80 % of cell rupture after the first HPH cycle and approximately 98 % after 3 cycles. For RL cells, the breakage occurred at a slower rate, with approximately 62 ± 3 % after one cycle and 95 ± 0 % after three cycles. This distinction underscores the slight biological differences between RL inoculum and the inocula used for other conditions, although these differences are not emphasized by the other characterizations. After 2 days (40 h), cell rupture remained unchanged, except for a reduction in the rate of HT cell rupture that appeared similar to RL cells. After 4 days (88 h), cell rupture after one cycle of HPH became 64 ± 2 % for HT, 70 ± 1 % for N-, 74 ± 1 % for N+ and 78 ± 1 % for RL cells. On the 3rd cycle, the cell rupture efficiencies were similar for all conditions, ranging between 95 and 97 %. In conclusion, cell disruption efficiencies differed slightly between conditions, but no clear pattern emerged over the three time points analyzed. Therefore, no consistent relation was identified between, on the one hand, the degree of cell mechanical resistance, and, on the other hand, the three starch-inducing conditions and the induced differences in cell wall thicknesses. In conclusion, the three starch induction methods did not cause any extra-difficulty for mechanical cell disruption by HPH, and thus ensured the same ease of recovery for the accumulated starch.

Yap et al. observed that differences in cell wall thickness between replete and N-starved *Chlorella vulgaris* did not impact cell rupture efficiency with HPH (Yap et al., 2016). In the present work, we extend the validity of this result to two novel starch induction methods, namely supra-optimal temperature and red light, which increase the cell wall thickness up to 2-fold higher than control.

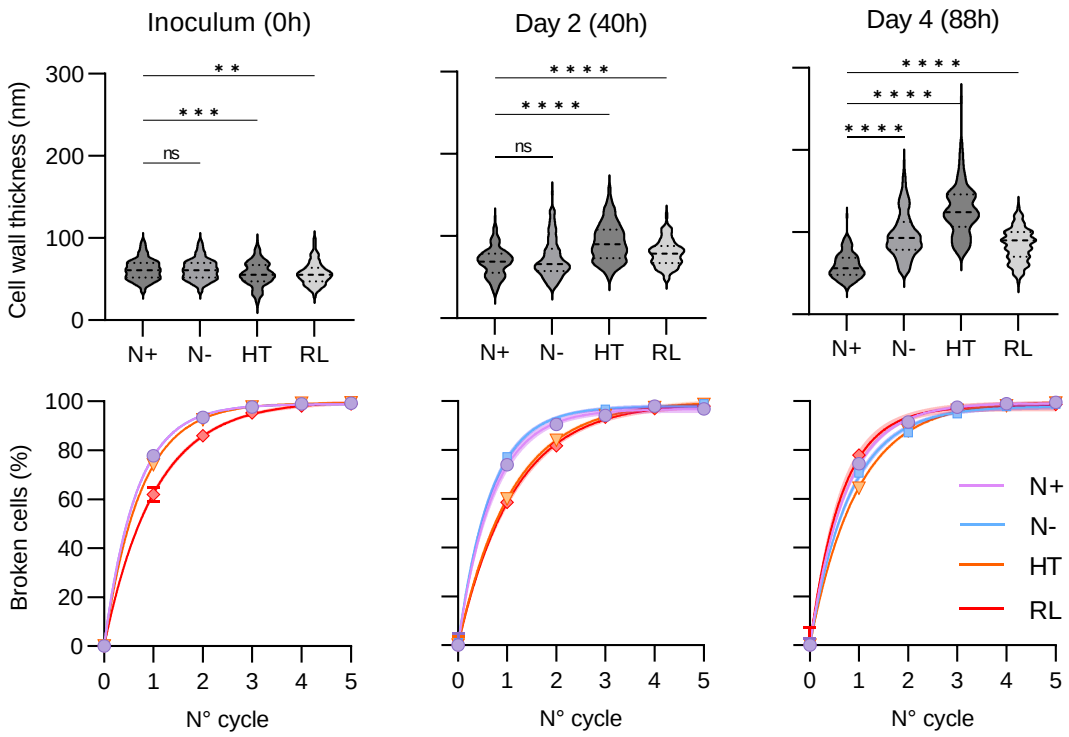

Figure I.8: Variations of cell wall thickening over time and corresponding effects on cell rupture. (A) Thickness of cell wall, measured on three regions for at least 60 cells per condition. (B) Cell rupture efficiency according to number of HPH cycles. The p-values for the comparisons indicated in the graph are calculated with Prism 9 (Graphpad Software, LLC) and based on ANOVA Dunnett's multiple comparisons test (**, P<0.0021; ***, P < 0.0005;****, P < 0.0001, n>160).

I.2.6 Application perspectives

Advantages and drawbacks of the three tested strategies

In this study, we evaluated the response of the microalga *Chlorella vulgaris* CCALA924 to three starch inducers: nitrogen starvation, supra-optimal temperature, and red-light illumination. The outcome provided valuable insights into the applicability of these starch-inducing methods. A supra-optimal temperature of 39 °C induced important starch accumulation, up to 64.3 wt% carbohydrate content, and starch-equivalent productivity of 0.37 g L^{-1} d^{-1} (i.e. 0.41 g L^{-1} d^{-1} carbohydrates) in 4 days. Notably, starch accumulation was initially higher than in nitrogen deprivation during the first two days, but considerably decreased afterward. The extensive stress caused by the high temperature was mainly visible through the complete stop in cell division, together with the sharp decrease in maximal quantum yield (QY_{max}) and highly reduced protein and chlorophyll productivities. Reducing the temperature could potentially mitigate this stress and thereby improve the stability of starch synthesis. Therefore, the supra-optimal temperature has the potential to be a highly efficient starch induction method for short-term accumulation but requires further optimization of the target temperature.

Nitrogen deprivation triggered the highest and fastest carbohydrate accumulation, with a starch-equivalent productivity of 0.58 g L^{-1} d^{-1} over the first 4 days (88 h) (i.e. 0.64 g L^{-1} d^{-1} carbohydrates), representing a 5-fold increase compared to the control. The maximal carbohydrates content reached 69.7 wt%. During this period, more than 80 % of the biomass produced was only carbohydrates, while the production of proteins, lipids and chlorophylls concomitantly decreased. Yet, the carbohydrate synthesis rapidly decelerated the decreasing photosynthetic capacity of the culture, reaching a maximal quantum yield (QY_{max}) below 0.2 after 7 days. In conclusion, the nitrogen starvation method should be considered for short-term starch accumulation strategies.

Red-light illumination induced a 3-fold improvement in starch-equivalent productivity, which notably persisted for 7 days without decrease. During the first 4 days, the starch-equivalent productivity reached 0.33 g L^{-1} d^{-1} (i.e. 0.36 mg L^{-1} d^{-1} carbohydrates), and the maximal carbohydrates content reached 46.8 wt%. Meanwhile, the protein synthesis slightly increased compared to the control, while lipid productivity decreased by 5-fold. Interestingly, the amylose content in the produced starch was low, contrary to the expected storage-type starch. Most notably, the dynamics of biomass growth under red-light were similar to the control with continuous and regular cell division. In addition, the photosynthetic capacities were fully sustained over 7 days, with no decrease in quantum yield or NPQ mechanisms implementation. Therefore, red-light illumination induced a significant starch accumulation without causing stress to the culture. To our knowledge, this is the first report on a significant starch accumulation concurrent with sustained cell health. In this view, red-light illumination appears to be a novel and gentle way to induce starch accumulation in the microalgae *Chlorella vulgaris*, with interesting characteristics for long-term accumulation.

Technical challenges for culture scale-up

The present work opens intriguing perspectives for the large-scale production of starch from microalgae. On the one hand, a continuous culture system illuminated with red LEDs could achieve high starch and protein productivities simultaneously. On the other hand, the nitrogen-deprivation induction can be easily implemented in batch cultivation by controlling the initial amount of nitrogen to start the deprivation at a targeted dry weight. Moreover, as suggested by Cheng et al. (Cheng et al., 2017), a two-reactor system could be used, with one reactor in replete conditions regularly supplying biomass to the second one operating in several-day batches under nitrogen deprivation.

Additionally, the present work raises a compelling scientific and technological interest in exploring the pathways responsible for induction of starch accumulation in response to red-light. A novel kinase signaling cascade has been recently described in *Chlamydomonas reinhardtii* where blue-light perception mediated by the serine/threonine kinase phototropin is transduced via the Phototropin-Mediated Signalling Kinase 1 to activate gene expression of GAP1, acting as enhancer of starch accumulation (Yuan et al., 2023). Validating and gaining a profound understanding of these pathways in *Chlorella vulgaris* could potentially result in engineering strains capable of simultaneously sustaining their growth while tripling their starch productivity under solar spectrum.

I.3 Conclusion

In this work, three abiotic starch-inducing methods were compared in terms of carbohydrate productivities, biomass composition, starch structure, photosynthetic capacities and cell rupture. *Chlorella vulgaris* CCALA924 was confirmed to be a high-starch-producing strain, while its lipid production appeared to be low. All three factors induced cell wall thickening without any impact on mechanical cell disruption performed with high-pressure homogenization at 250 MPa, ensuring similar ease of starch recovery. Overall, nitrogen deprivation and supra-optimal temperature induced fast but non-sustained starch accumulation, and should be preferred for short-term accumulation strategies in batch culture. Despite achieving a lower starch content, red-light illumination induced an enhanced and steady starch production suitable for continuous culture systems. This work opens up novel prospects for the production of microalgal starch, especially for large-scale applications such as bioplastics.

Paper II - Optimization of the light supply for fast starch accumulation in *Chlorella vulgaris* outdoor culture

This Paper is under preparation for submission to Algal Research (February, 2024).

II.1 Motivation & research objectives

One promising application of microalgae is to serve as feedstock for the starch industry. Nutrient deprivation is often used to stress the microalgae and induce the production of starch at the expense of cell division. To tackle with the growth impairment under nutrient stress, a two-stage culture process have been proposed where cells are first grown in optimal conditions and then diluted to reach depleted conditions (Brányiková et al., 2011; Cheng et al., 2017). This dilution modify the cell density and therefore allow to change the light availability in the culture.

Producing low carbon-footprint microalgal biomass requires efficient use of the incident solar energy. However, the efficiency of solar energy conversion into biomass can be significantly reduced depending on the degree of photon availability for the microalgae cells. Photon availability in culture is determined by the cell density as well as the incident light intensity, which are therefore two major parameters for optimizing microalgae cultivation.

With this in mind, this study aims to determine the optimal balance between cell density and light intensity at the beginning of the nutrient-deprived phase, the second stage of the starch accumulation process. Firstly, we investigated the behavior of cultures during the nutrient-deprived phase and their response to extended periods of dark. Subsequently, we established the relationship between a light-per-biomass criterion and starch accumulation outcomes (carbohydrate content, carbohydrate relative productivity, and photosynthesis efficiency) in small-scale, outdoor conditions. Finally, we assessed the transferability of these relationships at the pilot-scale using a distinct culture system and reactor geometry.

Contributions

The pilot scale culture (180 L) was performed with the help of Pablo Alvarez and Sophie Fon-Sing. The 3D figures and the associated code were conceptualized in collaboration with and developed by Paul Chambonnière. The small scale culture set-up (1 L) was developed by Gatien Fleury. The design of experiments was also supervised by Gatien Fleury. Organizational support and critical review were provided by Jean-François Sassi and Yonghua Li-Beisson.

II.2 Results

II.2.1 Sudden nitrogen deprivation under laboratory conditions under long night

Prior to perform outdoor cultures, we studied the behavior of cultures under nutrient starvation and their response to extended periods of dark at laboratory scale. The photoperiod was set to 11 h of light and 13 h of dark, corresponding to the sunlight photoperiod for the months of March/October.

Chlorella vulgaris cultures were cultivated under incubator conditions 9 days prior to the experiment start (25 °C, 2 % CO_2, 184 $\mu mol_{photon}/m^2/s$). Then, cultures were centrifuged and medium was replaced with fresh medium depleted in nitrogen to induce the starch accumulation. Three identical culture triplicates (nine flasks) were prepared from the same inoculum culture and grow under the same conditions. To avoid volume shortage in the 200 mL-filled Erlenmeyer, each triplicate was then dedicated to one day of experiment.

As presented in Figure II.1, the sudden nitrogen deprivation efficiently triggered starch accumulation. Indeed, total carbohydrates content increased from 20.9 ± 0.6 to 82.0 ± 4.0 $\%_{wt}$ in three days. Simultaneously, biomass concentration increased from 1.0 ± 0.0 to 2.6 ± 0.1 $g.L^{-1}$ and cell concentration approximately doubled. Interestingly, the mean cell volume did not increase over 3 days, probably due to the compensation of starch accumulation and cell division events. Despite the fact that total chlorophyll content in the biomass sharply decreased, the chlorophyll concentration remained stable, showing that chlorophyll was neither synthetized or degraded.

The long night periods of 13 h induced a visible loss of dry weight biomass and carbohydrates (Figure II.1). Indeed, mean carbohydrate productivity was 82.8 $mg.L^{-1}.h^{-1}$ during day periods and -13.8 $mg.L^{-1}.h^{-1}$ during night periods. Overall, mean carbohydrate productivity was 35.0 $mg.L^{-1}.h^{-1}$ during 56h, with a photoperiod sum of 30 h light, 26 h dark.

Here, sudden nitrogen deprivation was proved to be an efficient strategy for starch accumulation in laboratory incubator. The 13 h night period revealed high impact of long night, thereby raising the need to design short and optimized starch accumulation enabling to reduce the night time as much as possible. Indeed, long night could affect starch productivity in two ways: they not only resulted in starch degradation, but also considerably could reduce the available time for accumulation.

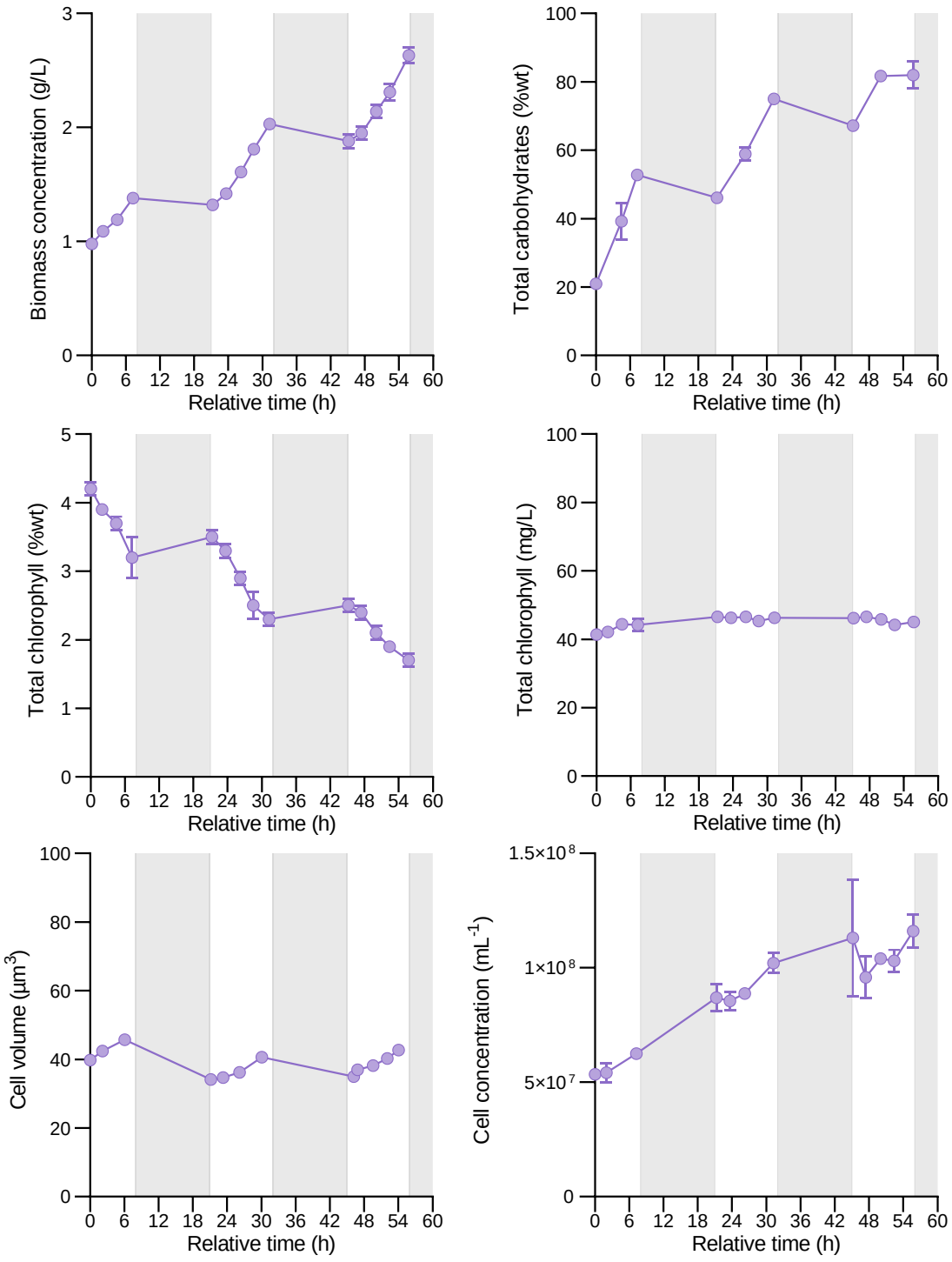

Figure II.1: Effect of long night on biomass growth after sudden nitrogen deprivation. Dark areas represent the 13h night periods.

II.2.2 Impact of biomass concentration for starch accumulation under sunlight

In this part, we aimed to determine the initial biomass concentration that would maximize the carbohydrates production of a culture. For this, the light actually available for the culture is of primary importance. Therefore, we studied the dynamics of carbohydrate accumulation with regards to both biomass concentration and received light.

Outdoor starch accumulation under a range of incident light

Our first goal was to study the evolution of carbohydrate accumulation under different level of received light per quantity of biomass. To do so, we designed an array of nine light-per-biomass levels by combining several biomass concentrations and light filters. Three initial biomass concentrations of 1.25 g/L, 0.2 g/L and 0.15 g/L were grown with three light filtration levels providing a transmittance of 100%, 50% and 25%. Each condition was tested in one replicate, resulting in nine different cultures. The nine cultures were deprived in nitrogen at experiment start and grown in 1L glass bottles placed within a controlled set-up in outdoor conditions (Figure II.2). The inoculum culture had previously grown in the same set-up for a week, with regular dilution to maintain exponential phase cultures.

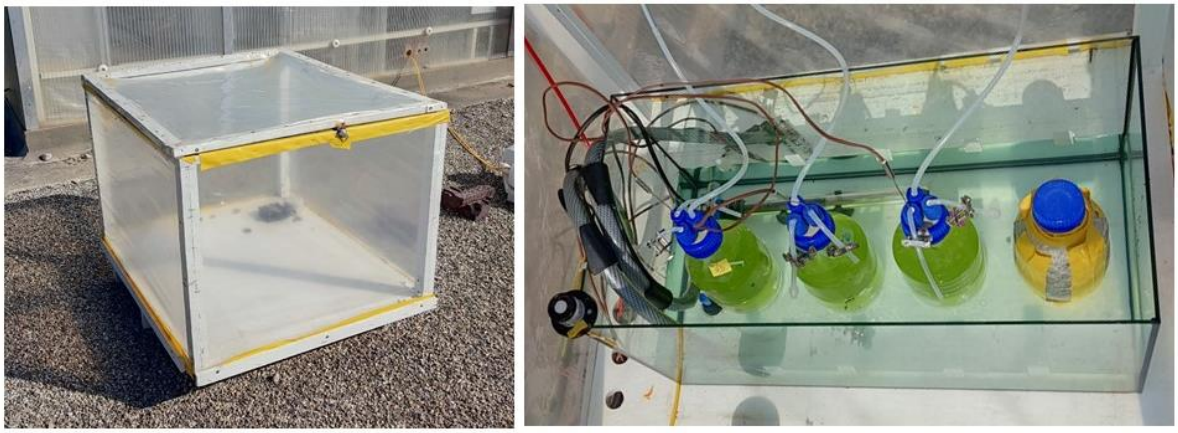

Figure II.2: Experimental set-up for outdoor culture cultivation under controlled conditions of temperature, injection of air-CO_2 mix and horizontal measurement of light.

Figure II.3 reports the biomass growth in nitrogen-depleted conditions for three cultures of the light-per-biomass range, namely X1.25_T25, X0.20_T50 and X0.15_T100 (X representing the biomass concentration in g/L and T the transmittance in %). X1.25_T25 and X0.15_T100 are the lowest and highest light-per-biomass, respectively, while X0.20_T50 is an intermediate light-per-biomass. For these three cultures, the biomass concentration regularly increased along the 7 days of the experiment (Figure II.3.A). Meanwhile, the carbohydrates content increased rapidly for the high light-per-biomass cultures X0.20_T50 and X0.15_T100, with an increase from 23.1 ± 0.9 % to 57.5 ± 0.7 and 60.0 ± 1.6 %, respectively, after 5h of culture (Figure II.3.B). On the other hand, the increase in carbohydrates content was significantly slower for the lowest light-per-biomass culture X1.25_T25.

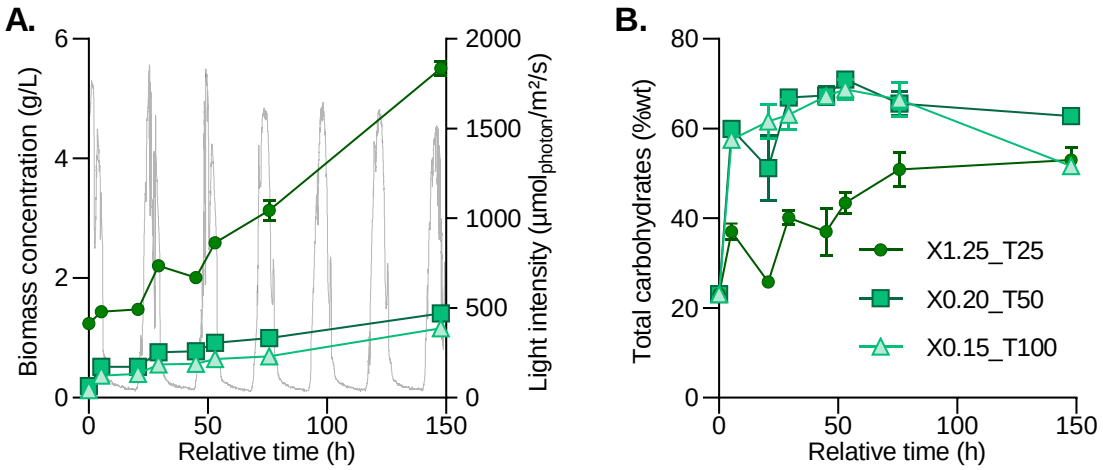

Figure II.3: Biomass growth of nitrogen-deprived cultures in 1L bottles and under natural light. (A) Dry-weight biomass concentration and horizontal light intensity received (grey line). (B) Carbohydrate content. The three cultures have an initial biomass concentration X of 1.25, 0.2, 0.15 g/L and light transmission T of 25%, 50% and 100%, respectively.

The starch accumulation in *Chlorella vulgaris* cells was clearly attested by electron microscopy (Figure II.4). After three days of nitrogen deprivation, starch granules were occupying most of the intracellular space for X1.25_T25, X0.20_T50 and X0.15_T100 cultures. Moreover, the presence of lipid bodies is particularly noticeable within the cells of the highest light-per-biomass culture X0.15_T100 (Figure II.4.E).

The model of light quantification described by Slegers and coworkers (Slegers et al., 2013, 2011) was adapted to translate the horizontal light measurements GHI presented in Figure II.3.A into the light flux received the culture in every bottle (see Appendix B). The light-per-biomass was then determined as photon flux per biomass ($PFPB$) by dividing the light received in a culture to its active biomass Xa. Here, the active biomass is defined as the fraction of biomass that plays a functional role for the production of carbohydrate and lipid reserve. We considered the active biomass Xa to be equivalent to the initial dry weight biomass X_0 during the whole experiment. Indeed, Kandilian et al. have shown that active biomass Xa was almost equivalent to X_0 when cultures of *Parachlorella kessleri* were grown under nutrient-replete conditions (Kandilian et al., 2019). Moreover, the concentration of non-reserve biomass is not expected to change along the few days of nitrogen starvation as nitrogen is an essential building block for active biomass.

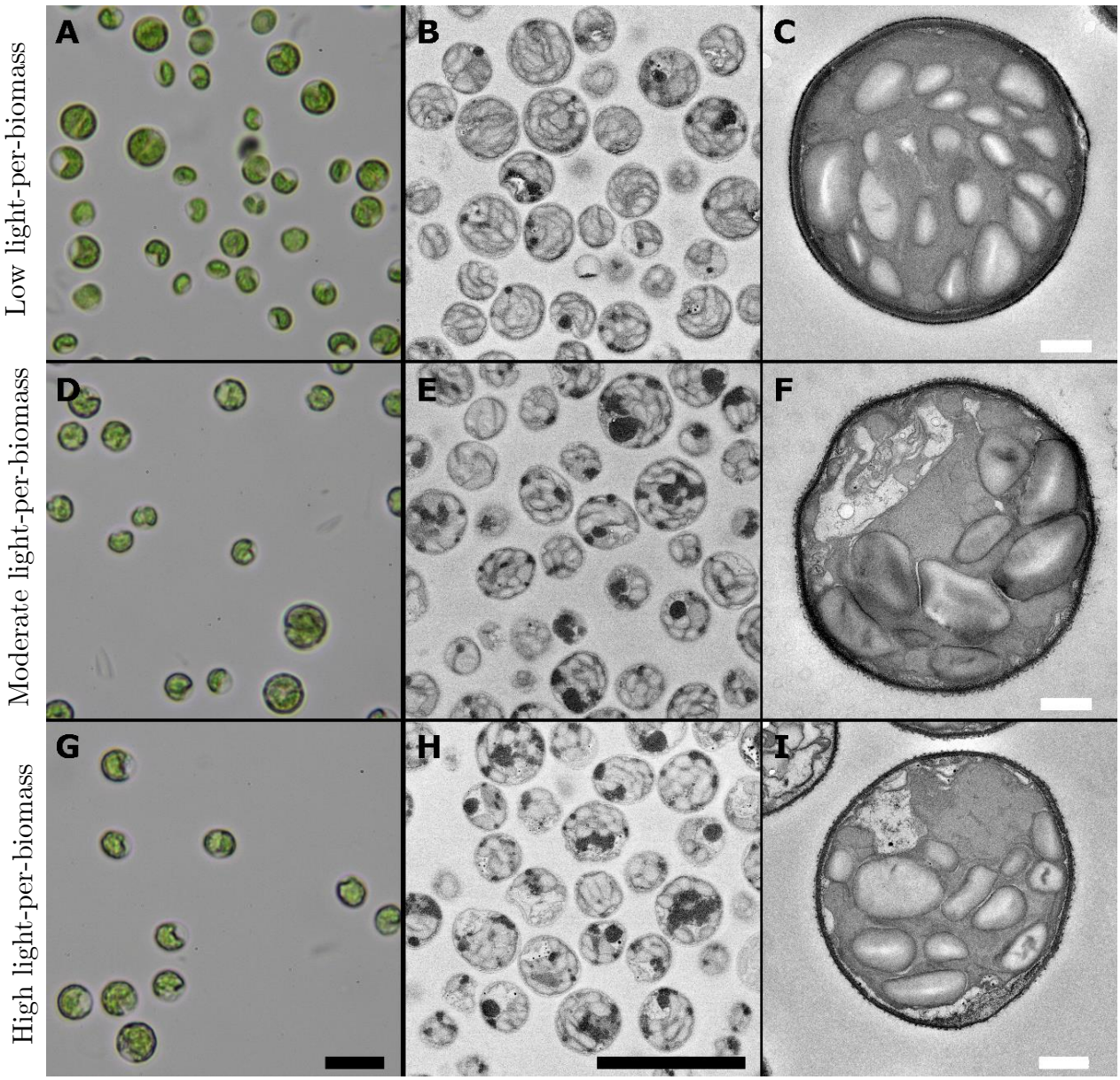

Figure II.4: Optical and electron microscopy pictures of *Chlorella vulgaris* cells on the 4th day of nitrogen starvation. (A-C) X1.25_T25 culture (i.e. high concentration and 25% transmittance), (D-F) X0.20_T50 (i.e. low concentration and 50% transmittance) and (G-I) X0.15_T100 (i.e. very low concentration and 100% transmittance). (A),(C),(G) Optical microscopy (B),(E),(H) Negative retrodiffuse of scanning electron microscopy. Black bodies are lipid droplets, white bodies are starch granules. (C),(F),(I) Transmission electron microscopy. Here, lipid droplets are light-grey. Black bars correspond to 10 µm and white bar to 1 µm.

Figure II.5 reports the evolution of carbohydrate accumulation according to the PFPB for every culture during the first three days. Carbohydrates content immediately increased with increasing PFPB and rapidly reach a plateau (Figure II.5.A). Oppositely, the conversion efficiency of light to carbohydrates instantaneously dropped with increasing PFPB, but tended to stabilize around the same light-per-biomass than for carbohydrate content (Figure II.5.C). On the other hand, the relative productivity of carbohydrates did not show this plateau effect; instead, it reached a maximum value before decreasing (Figure II.5.B).

Interestingly, the response of carbohydrates content and relative carbohydrate productivity to PFPB follow the shape of the light response curve (Tredici, 2010). When PFPB was near zero, the culture were photolimited and each impinging photon was used with high efficiency to produce carbohydrates, thus resulting in high photosynthetic efficiency (Figure II.5.C) and linear increase of relative productivity (Figure II.5.B) and carbohydrates content (Figure II.5.A). Then, as light-per-active biomass increased in the cultures, photosaturation happened and conversion efficiency sharply decreased while relative productivity and carbohydrate content stopped increasing linearly. Moreover, high PFPB induced immediate photoinhibition of the cultures, as relative productivity of carbohydrate notably decreases once the PFPB reached a certain value (approximately 200 $\mu mol_{photon}/g_{Xa}/s$ on day 1 and 100 $\mu mol_{photon}/g_{Xa}/s$ on day 2 and day 3). In addition, the photoinhibition also had a lag effect, visible from one day to another. Indeed, between day 1 to day 2, the relative productivity of carbohydrate sharply decreased for an important part of cultures in the high range of photon flux per biomass. In this case, the photosaturation and photoinhibition zones seemed to overlap. Overall, Figure II.5 clearly illustrates that there is no benefit to increase the light-per-biomass above a PFPB of 200 $\mu mol_{photon}/g_{Xa}/s$ on day 1 and 100 $\mu mol_{photon}/g_{Xa}/s$ on day 2 and day 3, as it would only lead to a loss of photons together with reduced relative carbohydrate productivity and photosynthesis efficiency.

Moreover, the curves of carbohydrates content, relative carbohydrate productivity, and photosynthetic efficiency provide general insights on the response of carbohydrates accumulation to the light-per-biomass for nitrogen-deprived cultures.

First, the carbohydrates content was shown to increase for any level of light-per-biomass, contrary to what is usually observed for lipid accumulation. Indeed, Kandilian et al. reported a necessary threshold value of 13 $\mu mol_{photon}/g_{Xa}/s$ (measured as mean volumetric rate of energy absorption) for inducing the lipid accumulation in N-starved *Nannochloropsis oculata* (Kandilian et al., 2014). Here, the carbohydrate accumulation happens without the need of reaching any light stress level.

Secondly, the photoinhibition effect on the relative carbohydrate productivity at high PFPB was intense. This harsh photoinhibition may have been enhanced by the nitrogen-deprivation of microalgae (Levasseur, 2021). Indeed, microalgae need to constantly repair the core proteins of photosystems II to cope with their regular destruction by incoming photons. Under nitrogen starvation, this reparation is impaired and the photosynthesis capacities of the culture constantly degrade (see Chapter 1).

Lastly, the observed photosynthesis efficiencies were low comparing to the theoretical maximum, with a highest photosynthesis efficiency of 11.1 % on day 1. This photosynthesis efficiencies represents the fraction of received light energy stored as chemical energy in the form of sugar considering only PAR photon with an energy level narrowed down to 680 nm photon. Based on the theoretical assumption that 10 photons are fixing 1-carbon equivalent of sugar (Janssen, 2016), the theoretical maximal value of photosynthesis efficiency is 26.2 %, which is twice higher than our maximal PE of 11.1 %. In the case where not only PAR photons but the whole spectrum of solar radiations are considered, the maximal photosynthesis efficiency on day 1 would

decrease from 11.1 to 3.8 % and the theoretical maximal from 26.2 to 9.0 % (Janssen, 2016).

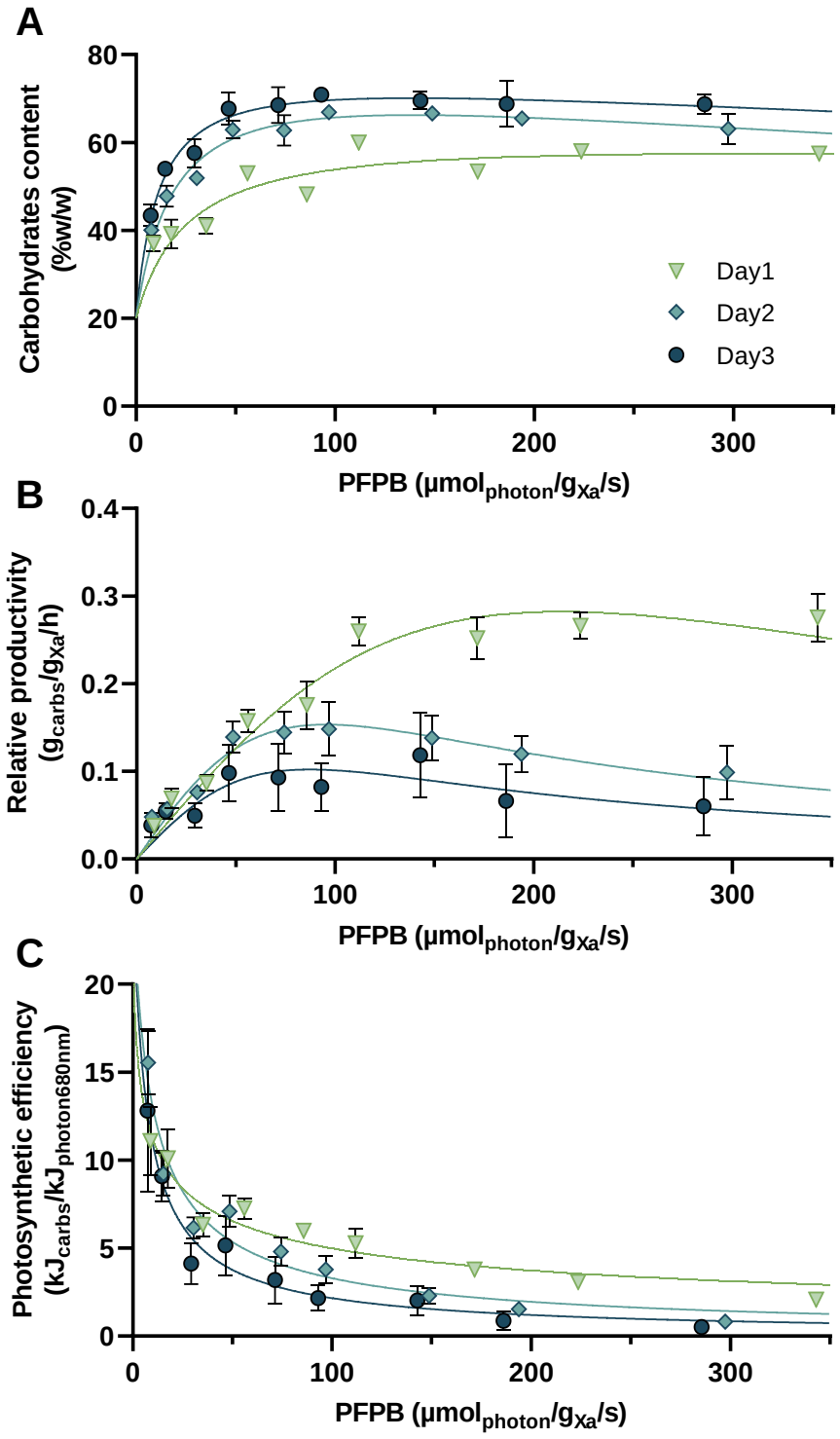

Figure II.5: Evolution of carbohydrates accumulation over the range of photon flux per biomass. (A) Carbohydrate content at the end of day, (B) Productivity of carbohydrates relative to active biomass X_a, (C) Photosynthetic efficiency. Triangle, diamond and round points represent the measured values for the first, second and third day of the 1L-bottle experiment, respectively. The lines are the fitting curves associated to these measured values. PFPB: photon flux per biomass.

Outdoor starch accumulation in pilot scale _ at panel PBRs

In the previous section, we evaluated how the carbohydrate accumulation in nitrogen-deprived cultures is affected by the light received per biomass. However, the curves describing these relationship should not be used directly as such to predict the starch accumulation. Indeed, these empirical models integrate many other parameters than light, such as temperature, pH or initial state of culture, and any variation of these conditions is likely to change the carbohydrate accumulation outcome. Nonetheless, cultivation in photobioreactors enable to control most of these conditions, and the empirical model could still give valuable, if not exact, insights on the carbohydrates productivity at a given light-per-biomass. Therefore, we confronted our small scale empirical models to a validation experiment of carbohydrates accumulation in a 180L air lift flat panel PBR, presented in Figure II.6.



Figure II.6: *Chlorella vulgaris* culture after 3 days of nitrogen-starvation (right panel). The air-lift flat panel photobioreactor of 180L is installed in a greenhouse near Saint-Paul-les-Durance, France, and offers regulation of temperature by water spray and pH by CO_2 injection.

Figure II.7 shows the biomass growth and carbohydrate content evolution along the nitrogen starvation in the flat panel PBR. Biomass growth continuously increased during each day period (Figure II.7.A). On the other hand, the carbohydrate content intriguingly stopped increasing from the end of day 2 (Figure II.7.B). Microalgae may have switched from starch to lipid storage, following the classic mechanism of carbon storage under nitrogen deprivation for *Chlorella vulgaris* (Nordin et al., 2020). However, no switch from starch to lipid accumulation was previously noticed for this particular strain, at laboratory scale (see Paper I) as well as in the 1L bottle experiment, despite similar conditions of light-per-biomass. It is worth to investigate further through a whole genome resequencing or transcriptomic experiment to figure out the underlying genetic reasons for this observed discrepancy. Alternatively, this lack of increase in carbohydrate content during day 3 could have been artificially caused by a underestimation of the carbohydrates content on the end of day 3, as the increase of carbohydrates content on the night from day 3 to day 4 seem questionably high (Figure II.7.B).

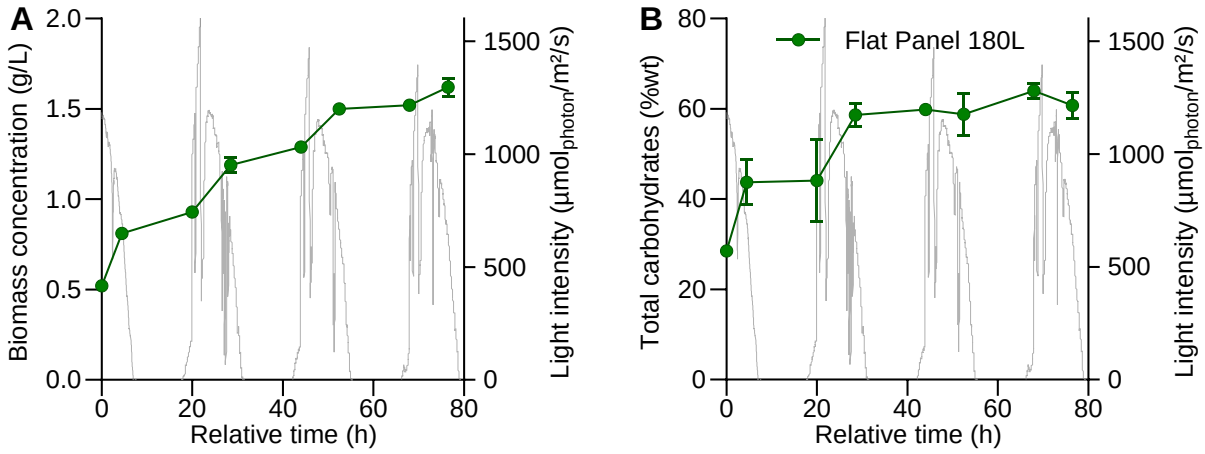

Figure II.7: Biomass growth of nitrogen-deprived culture in 180L flat panel PBR and under natural light. (A) Dry-weight biomass concentration and horizontal light intensity (grey line). (B) Carbohydrates content.

Here, the light model developed by Slegers was applied to the horizontal light measurement GHI (Figure II.7.A) in order to calculate the light received by the culture (Slegers et al., 2011). The photon flux per biomass PFPB was subsequently calculated and used to plot the carbohydrates accumulation according to the light-per-biomass (Figure II.8.A, Figure II.8.B, Figure II.8.C). Remarkably, the relationships between carbohydrate accumulation and PFPB in the flat panel PBR were very close to the curves modelling the 1L-bottle experiment. Only day 3 was far from the corresponding model curves of carbohydrate accumulation, most probably because of the surprising cessation of carbohydrates accumulation on day 3 (Figure II.7.B). Therefore, our empirical model developed in 1L bottles seemed able to return close prediction of the starch accumulation from the light-per-biomass, even for a very different photobioreactor such as the 180L flat panel PBR, in a different greenhouse configuration.

On the other hand, the 180L flat panel PBR and the 1L bottles also had similarities, such as surprisingly close surface-per-volume ratio (49.3 and 48.5 m^{-1}, respectively). In order to confront the model to a very different situation, we also analyzed the starch accumulation in the study of Brányiková and coworkers (Brányiková et al., 2011). In her study, Brányiková used the same Chlorella strain, *Chlorella vulgaris* CCALA924, exposed to sulphur starvation and grown within a thin-layer photobioreactor of 250 L. This PBR offered a high surface-per-volume ratio a of 96 m^{-1}, including 37% of dark volume (24 m^2 and 6.5 mm culture thickness against 250 L of total volume) and was exposed to a daily mean received light Im of 2300 $\mu mol_{photon}/m^2/s$. Unexpectedly, the starch accumulation according to the light-per-biomass was notably lower for the thin-layer PBR experiment than the predictions from the 1L bottle model (Figure II.8.D, Figure II.8.E), except for the carbohydrate content (Figure II.8.F). Here, the light intensity might be overestimated considering that the data provided in the article did not allowed a precise quantification of the light received by the culture. Moreover, the particularity of the thin-layer PBR, where

microalgae alternate between dark zones and intense light, could also explain this behavior difference. Overall, the model seemed to offer fairly good predictions of the starch accumulation for a PBR with similar surface-per-biomass ratio, but was not directly transposable to a different situation.

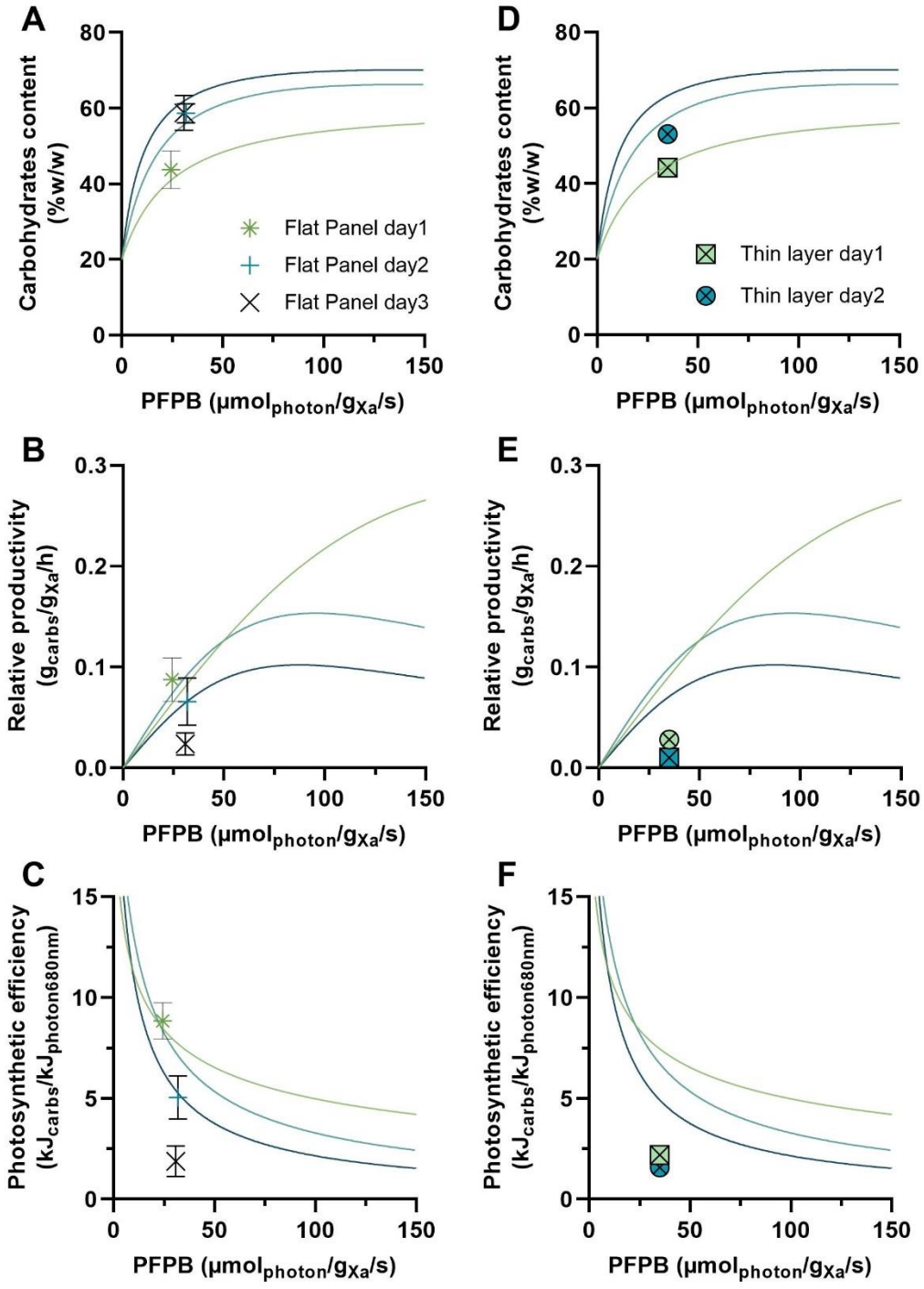

Figure II.8: Carbohydrates accumulation according to the photon flux per biomass. (A), (B), (C) Values measured during the experience conducted in the 180L flat panel PBR. (D), (E), (F) Values calculated from the data of Brányiková et al. 2011 for a sulfur starvation conducted in a thin-layer PBR of 250L. The lines correspond to the modelling lines issued from the small scale experiment.

II.2.3 Determination of the initial biomass concentration for optimal starch accumulation

As pointed out in previous sections, the initial light-per-biomass of a culture highly influences the outcomes of carbohydrate accumulation (Figure II.5). In practice, the solar incident light cannot be controlled, and the light-per-biomass can only be modified through the active biomass concentration Xa, which in our case is considered equivalent to the initial biomass concentration X_0.

First, we tried to understand how the initial biomass concentration would influence the carbohydrate accumulation. To do so, we fixed the illumination conditions to those encountered by the flat panel PBR of 180L (received light Im=330 µmolphoton/m^2/s and surface-per-volume a=49.3 m^{-1}). Then, we simulated how several photon flux per biomass would impact the initial biomass concentration and the carbohydrate outcome (Table II.1) accordingly to the model developed during the 1L bottle experiment. Visibly, the most interesting range of photon flux per biomass correspond to the photolimitation zone, as both carbohydrate volumetric productivity and photosynthetic efficiency are at the highest level even after three days, while carbohydrate content is still enhanced. However, Table II.1 also highlights the inverse relationship existing between final carbohydrate content in one hand, and volumetric productivity or photosynthetic efficiency on the other hand.

Initial parameters			Outcome estimation (end of day1 – end of day3)			
PFPB ($\mu mol_{photon}/g_{Xa}/s$)		X_a (g/L)	PE_{CHO} (energy%)	C_{CHO} (wt%)	P_{CHO}^{rel} ($g_{CHO}/g_{Xa}/h$)	P_{CHO}^{vol} ($g_{CHO}/L/h$)
Photo-limitation	5	3,3	13,5% - 15,0%	27% - 38%	0,01 - 0,01	0,04 - 0,04
	10	1,6	11,2% - 10,9%	32% - 47%	0,03 - 0,02	0,04 - 0,04
Photo-saturation	100	0,2	5,0% - 2,2%	54% - 70%	0,22 - 0,10	0,04 - 0,02
	200	0,1	3,6% - 1,1%	57% - 70%	0,28 - 0,08	0,02 - 0,01

PFPB: photon flux per biomass; X_a: active biomass concentration, equivalent to initial biomass concentration; g_{Xa}: gram of dry weight active biomass, equivalent to initial biomass; PE_{CHO}: photosynthetic efficiency of energy conversion into carbohydrates; C_{CHO}: carbohydrates content; P_{CHO}^{rel}: relative carbohydrate productivity; P_{CHO}^{vol}: volumetric carbohydrate productivity.

Table II.1: Estimation of the carbohydrate accumulation outcomes simulated from different photon flux per biomass. This simulation is calculated from the 1L-bottles model. The mean received light flux I_m was fixed to 329.7 $\mu mol/m^2/s$, which was the mean daily value for two typical sunny days on the flat panel PBR of 180L. Initial and active biomass concentrations are considered equivalent.

In the end, the choice of initial biomass concentration allows us to find the best trade-off between the different starch accumulation results. To better apprehend these compromises, it was necessary to extend the Table II.1 to the general case. Therefore, the model developed from the 1L-bottle experiment (see previous section) was extrapolated to make the relationships explicit between light-per-biomass and starch accumulation for a wide variety of light-per-biomass conditions (Figure II.9).

On the one hand, Figure II.9 illustrates the general response of final carbohydrate content, volumetric productivity, and photosynthetic efficiency to the active biomass concentration Xa and photon flux per biomass $PFPB$. Primarily, the final carbohydrate content and the mean photosynthetic efficiency are oppositely depending on the $PFPB$ (Figure II.9.A and Figure II.9.B). On the other hand, the mean volumetric productivity is depending on both $PFPB$ and active biomass Xa (Figure II.9.C). Supposedly, these relationships are generally valid for any photobioreactor geometry, as long as the received light is precisely quantified.

On the other hand, Figure II.9 also describes the practical response of carbohydrate accumulation for a specific PBR geometry, here illustrated with the 180L flat panel PBR. In practice, a photobioreactor illuminated with natural light is restrained to a certain range of received light during the day depending on the available light and its surface-per-volume ratio a (see equation (3)). Here, we defined the illumination conditions to match those of our flat panel PBR of 180 L, where a was equal to 49.3 m^{-1} and the mean daily photon flux density Im received on the PBR surface was fixed to 330 $\mu mol_{photon}/m^2/s$ (mean of two Im measured during typical sunny days of the

season). In these conditions, the PFPB is constrained to evolve only depending on Xa, which is illustrated by the dotted lines in Figure II.9. For these given conditions of 180L flat panel PBR, the Xa corresponding to the optimal trade-off between carbohydrate content, photosynthetic efficiency and volumetric productivity has to be found along this line.

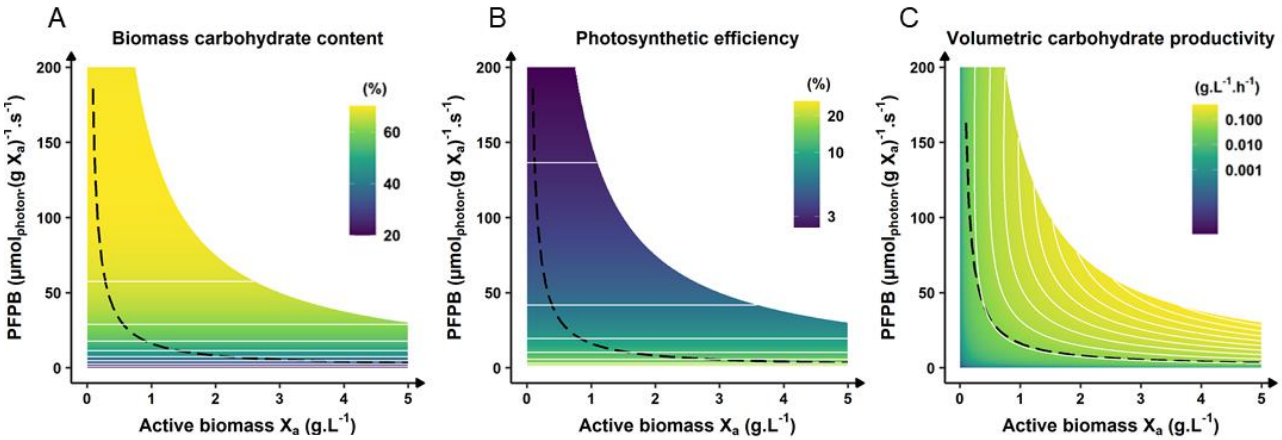

Figure II.9 Starch accumulation according to photon flux per biomass PFPB and to active biomass concentration Xa. The results are calculated from the 1L bottle model on a 3-day period. The dotted line represent the light conditions in the flat panel PBR for a typical sunny day (Im=329.7µmolphoton/m^2/s and a=49.3 m^{-1}). (A) Predictions of carbohydrate content reached after three days of starvation. (B) Predictions of daily mean carbohydrate photosynthetic efficiency, calculated as the mean of the three first days. (C) Predictions of daily mean volumetric carbohydrate productivity, calculated as the mean of the three days and based on Xa and relative productivity.

The previous approach allowed to predict the outcomes of carbohydrate accumulation for any Xa and the resulting $PFPB$, when the received light Im and the reactor surface-per-volume a were known. However, the mean daily received light Im is variating with the weather and the season. In order to better apprehend the effect of Im variability, we fixed the surface-per-volume a to 49.3 m^{-1} (flat panel PBR of 180 L) and represented the impact of Im and Xa on the starch accumulation in this configuration (Figure II.10).

In Figure II.10, the typical Im measured on our flat panel surface (Im = 330 $\mu mol_{photon}/m^2/s$) is represented by the horizontal dotted lines. From this fixed Im, several guidelines for the choice of the optimal initial biomass concentration Xa can be drawn. Overall, there is three different targets to maximize: the final carbohydrate content, the mean photosynthetic efficiency or the mean volumetric productivity. As observed in both Figure II.9 and Figure II.10, aiming for the highest carbohydrate content will globally lead to the minimal photosynthetic efficiency, and vice versa.

On the other hand, aiming for the highest volumetric productivity is visibly an interesting trade-off between carbohydrate content and photosynthesis efficiency. In the typical case where $Im = 330 \mu mol_{photon}/m^2/s$, the volumetric carbohydrate productivity is near its maximum value for $Xa = 0.8\, g/L$, with 0.130 g/L/h ; if Xa further increases, the volumetric carbohydrate productivity is only slightly improved

(0.130 g/L/h for $Xa = 0{,}8 g/L$, 0.135 g/L/h for $Xa = 3\ g/L$, and 0.135 g/L/h for $Xa = 50\ g/L$). At this limit value of $Xa = 0.8\ g/L$, the final carbohydrate content and the mean photosynthetic efficiency correspond to 56.9 % and 8.5 %, respectively. Therefore, aiming for high volumetric productivity appears as an interesting trade-off leading to both satisfying carbohydrate content and photosynthesis efficiency.

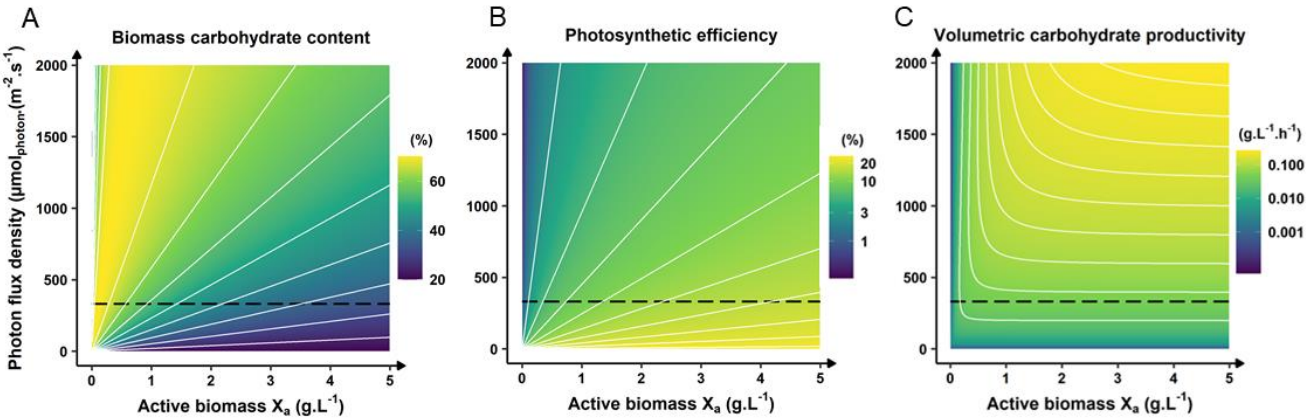

Figure II.10: Starch accumulation according to mean daily photon flux density I_m and to active biomass concentration Xa. The results are calculated from the 1L bottle model on a 3-day period. The surface-per-volume ratio a was fixed to 49.3 m^{-1}, corresponding to the flat panel PBR of 180L. (A) Predictions of carbohydrate content reached after three days of starvation. (B) Predictions of daily mean carbohydrate photosynthetic efficiency, calculated as the mean of the three first days. (C) Predictions of daily mean volumetric carbohydrate productivity, calculated as the mean of the three days and based on Xa and relative productivity.

II.2.4 Discussion: Model limitations and its implication for the two-stage process

In this work, we developed a model describing the response of starch accumulation to light-per-biomass. This model is empirical and is based on an experiment conducted in 1L bottles. However, its predictions were closed to the starch accumulation observed during the experiment performed in a 180L PBR. Despite this promising result, the model has several limitations regarding the light and the biological variations.

First, the light repartition within the culture vessel is not directly considered, despite its known effect biomass growth. Indeed, Artu showed that similar light-per-biomass can result in up to 3-fold higher photon-to-biomass conversion efficiencies, depending on the light repartition within the culture vessel (Artu, 2016). In our case, the light repartition is partly included through the incorporation of the surface-per-volume ratio a (m^{-1}), used as a factor in the $PFPB$ calculations. Nevertheless, our understanding of the significance of a on the model remains limited, as both the 1L bottles and 180L flat panel PBR used in the starch accumulation experiments exhibit similar surface-per-volume (48.5 and 49.3 m^{-1}, respectively). Intriguingly, the starch accumulation obtained with the high surface-per-volume thin-layer PBR (Brányiková et al., 2011) was not similar to our results. In addition, our model also assume a total absorption by the microalgae of the light received at the PBR surface. While light loss by transmittance was estimated negligeable in our case (Appendix B), enhancing the precision of the model for low biomass concentration could be achieved by integrating

the radiative properties of the cells, such as in the two-flux model developed by Cornet et al. (Cornet et al., 1995, 1992).

In the other hand, the starch accumulation is also dependent of the biological state of the microalgae. This biological state is modified by a variety of uncontrolled parameters, before, starting, or during the nitrogen depletion. Before the induction of starch accumulation, a few days of photoacclimation changes the response of photosynthesis to the incoming light intensity, and therefore may influence the resulting starch accumulation under nutrient starvation. When launching the starvation, the choice between sudden medium replacement (as done here) or natural depletion (as done in (Brányiková et al., 2011)) may also change the response of starch accumulation, as the low-nutrient phase preceding the total deprivation was shown to lead to a less efficient but more prolonged starch accumulation in other microalgae species (Yao et al., 2012). Finally, during the nutrient depletion, the response of microalgae to environmental factors variations in temperature or pH could greatly impact the response of starch accumulation for a same light-per-biomass.

Here, for our 180L flat panel PBR and considering a typical sunny day, an initial biomass concentration around 0.8 g/L was found to be the best trade-off for optimal starch accumulation in terms of volumetric productivity (0.130 $g_{carbohydrates}/L/h$), photosynthesis efficiency (8.5 %), and content (57 $\%_{carbohydrates}$). As a reminder, the photosynthesis efficiency is here expressed considering only PAR photons with energy level of 680nm photon; if complete sunlight radiations are accounted for, the photosynthesis efficiency would be of 2.9% instead of 8.5%. Considering that our 180L flat panel PBR occupies 3.7 m^2 (Derwenskus, 2020) and that mean volumetric productivity is maintained during 6h per day, the areal productivity would correspond to approximately 38 $g_{CHO}/m^2/d$. Altogether, these productivity figures are comparable with the typically 20-50 $g_{DW}/m^2/d$ and PE of 2-4% (total sunlight) achieved in short-term experiments with plants crops (Coombs, 1985).

In literature, a two-stage culture process is commonly proposed for the high-scale production of starch with nutrient-starved microalgae (Bakku et al., 2023; Cheng et al., 2017; Vitova et al., 2015). In this work, we provided a method to empirically determine the optimal concentration to start this second stage, in regard to the received light intensity. As expected, the final carbohydrate content was found to directly increase with increasing light-per-biomass, rather than with the initial biomass concentration alone. Notably, the photosynthesis efficiency evolved oppositely to the final carbohydrate content. Finally, the volumetric carbohydrate productivity was depending on both light-per-biomass and initial biomass concentration. Yet, further tests are needed to validate the transposition of this empirical model to photobioreactors with different surface-per-volume and operating conditions.

In general, our work demonstrated that achieving high carbohydrates content in an outdoor context and within a few days requires to start the second stage of the starch accumulation process at low concentration. Obtaining high starch content in the culture is interesting for the downstream processes of the culture, including the starch extraction. However, working with low biomass concentration is a major drawback, as it would further increase the energy demand of the critical harvesting step. One way

to maintain the high starch content while increasing the biomass concentration would be to increase the received light, either by increasing the surface-per-volume of the PBR or adding artificial light illumination.

II.3 Conclusion

In this work, the two-stage culture with sudden nitrogen deprivation was proven to be an efficient strategy for rapid starch accumulation, with consistent results from the laboratory to the pilot-scale. The empirical relationships between the starch accumulation and the light-per-biomass were identified under natural solar light conditions in 1L bottles, and then confirmed by one pilot-scale experiment in a 180L PBR. These relationships allowed to deduce general guidelines for the optimization of starch accumulation depending on the initial biomass concentration and the incident light-per-biomass. In the case of our flat panel PBR of 180 L, an initial concentration of 0.8 g/L was shown to theoretically optimize the outcomes of starch accumulation in terms of volumetric productivity, carbohydrate content and photosynthesis efficiency.

Paper III - Microalgal starch extraction, characterization and plasticization

III.1 Motivation & research objectives

The worldwide demand for plastic is expected to triple by 2060 (OECD, 2022). In response to the escalating pollution concerns, policymakers and industries are pushing towards the use of biobased-biodegradable plastics in different application sectors such as packaging. In this regard, starch emerges as an interesting source for these materials. Starch can be depolymerized into its glucose sub-units to serve as feedstock in fermentation processes to produce biopolyester (e.g. PLA, PHAs), or directly plasticized into thermoplastic starch (TPS) with the addition of a plasticizer. Yet, the current production of starch from traditional plant crops is likely not sufficient to supply the growing needs of the bioplastic industry, considering that starch is mainly dedicated to alimentary use. Microalgae could be a solution to increase the global production of starch, as their starch productivity may be similar to plant crops under field conditions (Brányiková et al., 2011). However, one particularity of microalgae comparing to plants is the difficulty to access the produced starch, as it is trapped into individual, small, and resilient cells. In addition, microalgal starch was never plasticized above the gram scale (Di Caprio et al., 2023; Mathiot et al., 2019).

Taking this into consideration, this study aims to develop an extraction process of microalgal starch, and to demonstrate the feasibility of microalgal starch plasticization into TPS. The secondary objective is to design up-scalable processes and test them with significant quantities of materials. Firstly, we adapted and simplified the extraction process of microalgal starch from laboratory to pilot scale. Then, we conducted the extraction, purification, and characterization of microalgal starch. Finally, we validated the processability of microalgal starch into TPS by extrusion and injection molding processes, and assessed its mechanical properties in comparison with commercial and potato-based TPS.

Contributions

Starch-enriched microalgae biomass was produced by Ana Compadre and Carole Dubreuil from CEA, France. Potato starch was kindly provided by Alejandro Aragon from ITENE, Spain. The microalgal starch characterization with laser granulometry, SEM observations, SAXS and DRX were performed by Jean-Luc Putaux and Christine Lancelon-Pin from CERMAV, Grenoble, France. David Dauvillée from Université de Lille, UGSF, Lille, France, presented the original laboratory-scale starch extraction process and performed the amylose quantification in the microalgal and potato starch. The plasticization trials, microstructural and mechanical characterization of TPS were performed under the supervision of Nicolas Le Moigne in the facilities of IMT Mines Alès, Alès, France. The overall work was supervised by Gatien Fleury. Organizational support and critical review were provided by Jean-François Sassi and Yonghua Li-Beisson.

III.2 Results

III.2.1 Extraction of the starch-enriched microalgae

In the literature, the extraction of starch from microalgae cells is typically conducted at laboratory scale and involves three successive steps: cell disruption, starch separation, and purification. Disruption of resistant microalgae cells such as *Chlorella vulgaris* is commonly achieved through chemical hydrolysis, enzymatic treatment, or mechanical stress. In contrast, the separation phase relies exclusively on centrifugation to isolate dense starch granules from other compounds present in the cell lysate. As final step, the purification of the separated starch is typically conducted using centrifugation with a Percoll gradient, following the protocol originally developed by Delrue and coworkers (Delrue et al., 1992). While highly efficient, this technique has limited applicability beyond the laboratory scale. Alternatively, liquid -liquid extraction processes as the aqueous two-phase systems have shown interesting starch separation capacities, but result in starch purity and extraction yield below 50 and 70%, respectively (Di Caprio et al., 2023; Suarez Ruiz et al., 2020a). Ethanol extraction at 75 °C enabled higher starch recovery and efficiently removal of pigments (Di Caprio et al., 2023; Gifuni, 2017b). However, it is likely that biomass components other than pigments are little affected by the ethanol extraction and no much is known about their actual removal. Overall, the upscaling of the starch extraction is still challenging, especially regarding the disruption and purification steps.

In this work, the high pressure homogenization was selected as the cell disruption method due to its demonstrated efficiency in disrupting *Chlorella vulgaris* (Yap et al., 2015) and its capacity to treat important volume. Additionally, our goal was to purify the microalgal starch without using any organic solvent, with the final objective of recovering more than 200 g of purified microalgal starch.

Adaptation of the extraction protocol

The starch extraction process was adapted and optimized from the protocol of Vonlanthen et al. (Vonlanthen et al., 2015). First, the disruption technique was modified to use the HPH instead of the French press. Indeed, cell disruption was confirmed to occur similarly with French press or HPH at the same pressure (Figure III.1.A). Then, the biomass concentration was attested to have no effect on the cell disruption efficiency with HPH, up to a concentration of 15% DW (Figure III.1.B). This result was also demonstrated by Yap et al. which argued for a limit concentration of 25% DW for another strain of *Chlorella vulgaris* (Yap et al., 2015). The release of starch granules and cell wall fragments in the suspension was confirmed with optical microscopy (Figure III.1.C) as well as with particle counting (Figure III.3). Finally, more than 99 % of the cells were disrupted after 5 cycles of HPH at 250 MPa.

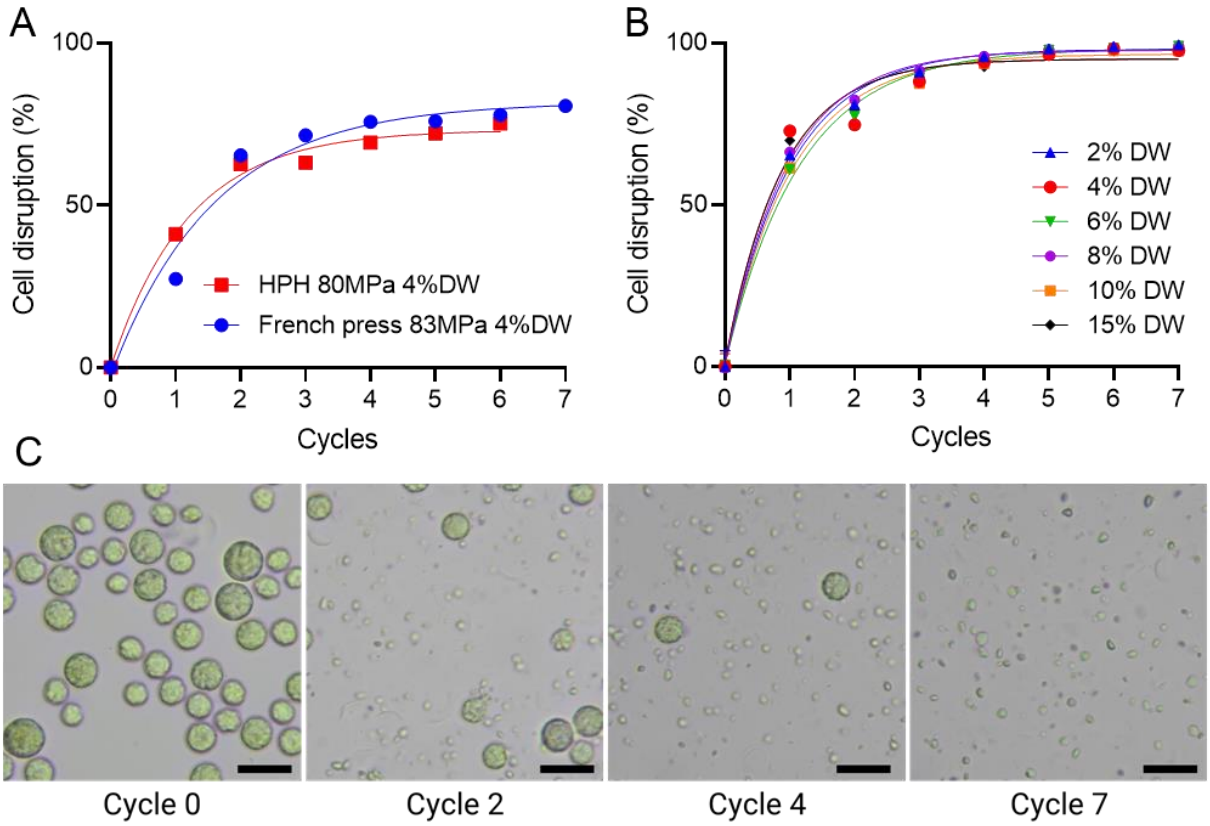

Figure III.1: Disruption of microalgae cells along the pressure cycles. (A) Comparison of high pressure homogenization and French press for similar pressure and concentration. (B) Efficiency of high pressure homogenization at 250 MPa for different biomass concentration. (C) Disruption of the microalgae cells along the HPH cycles for a 4% DW biomass. Scale bars correspond to 10 µm. Cell disruption was analyzed in technical triplicates.

Then, we attempted to improve the separation of starch by diluting the 15% DW cell lysate with water. After centrifugation, the final weight of the separated starch pellet was similar for all dilutions (Figure III.2). Therefore, the dilution of the cell lysate had no effect on the starch separation, with constant centrifugation at 5250 *g*.

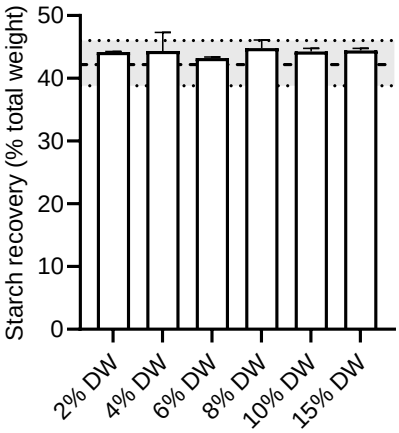

Figure III.2: Proportion of starch recovery from the initial cell lysate for several dilution. The dashed line corresponds to the starch content in cell broth, with the incertitude represented as dotted lines. The cell lysate was obtained after 5 HPH cycles of 15% DW biomass, and diluted in water before centrifugation at 5250 g for 10 min. The starch was then purified with Percoll and one water rinsing, freeze-dried and weighted.

Finally, we aimed at replacing the traditional Percoll purification of the starch pellet with water rinsing. First, we tried to identify the size range of the particles removed by the Percoll by analyzing the particle profile of cell lysate and Percoll purified starch (Figure III.3A). Interestingly, the removal of cell debris is not clearly visible from the particle profiles. Then, the starch purification was conducted by replacing the Percoll purification step by three successive water rinsing. Removing the Percoll addition still allowed visible removal of cell debris from the starch, as attested after each round of centrifugation (Figure III.3B).

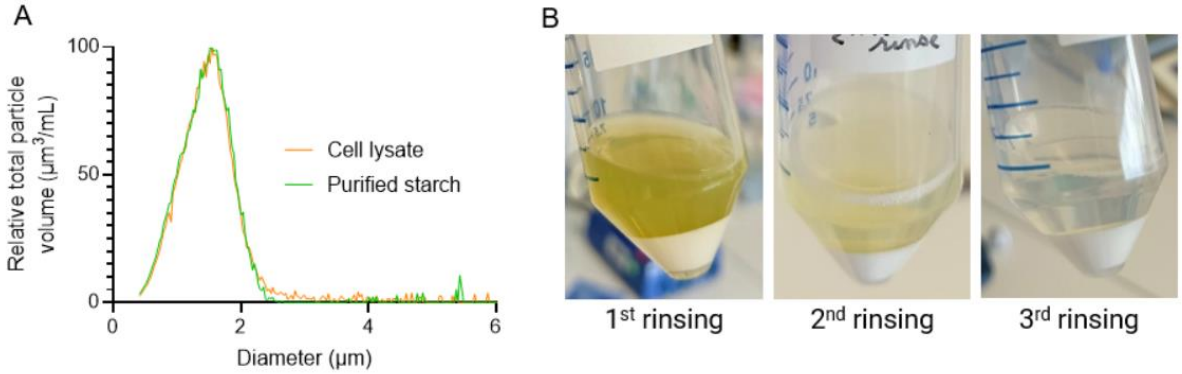

Figure III.3: Purification of the crude starch pellet with water rinsing. (A) Particle size repartition for the cell lysate (4% DW, 7 cycles at 250 MPa) and the corresponding Percoll-purified starch. The particle size repartition was determined by the cell counter device equipped with 20 µm probe (n=1, Multisizer 4e, Beckman Coulter, USA). (B) Removal of cell debris in supernatant along the successive water rinsing, without the use of Percoll.

Pilot scale starch extraction

After the development of the starch extraction protocol adapted from Delrue et al. (Delrue et al., 1992), we aimed to recover an important quantity of starch from a starch-enriched microalgae culture. The culture was grown outdoor in a flat panel PBR

and enriched in starch by triggering a nitrogen stress (Figure III.4), as described in the Materials & Methods section.

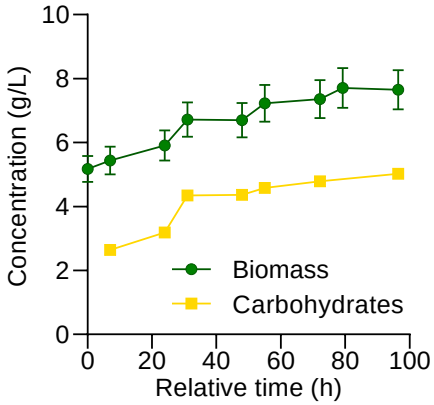

Figure III.4: Growth of the microalgae biomass after induction of starch accumulation by nitrogen deprivation. Biomass: n=1, Carbohydrates: n=3.

After growing and harvesting the starch-enriched biomass, starch was extracted from the microalgae cells following the starch extraction protocol as presented in Figure III.5.

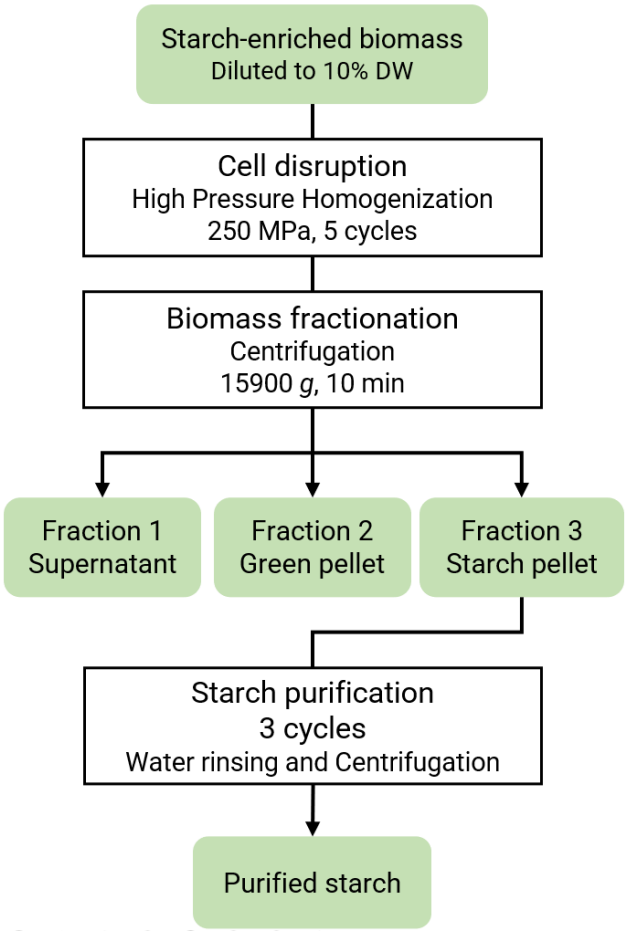

Figure III.5: Flowchart of the starch extraction protocol.

First, the microalgae cells were diluted to 10% DW in water and then disrupted by high pressure homogenization at 250 MPa for 5 cycles. Following the disruption, the centrifugation of the cell lysate resulted in the separation of three fractions: a supernatant and a pellet divided in two parts. The upper part of the pellet was green and doughy, and the bottom part was white and dense. At this stage, the dry weight content of supernatant, green pellet and starch pellet were of 4.2, 13.1 and 55.8 % of wet weight, respectively. The composition of these three fractions is reported in Table III.1. Next, the starch fraction was manually recovered from the other two fractions, and subsequently purified by three cycles of successive water addition, starch resuspension, centrifugation and supernatant removal. The rinsing supernatants decreased in turbidity and coloration along the rinsing cycles, until no chlorophyll absorption peak was noticed in the last rinsing supernatant (Figure III.6.B). The purification with water rinsing reduced the non-glucose carbohydrates and lipid content, while the starch content slightly increased (Table III.1).

The final composition of the purified starch was close to the traditional composition reported for granular starch (2% lipids, 0.6% protein, and 0.4% minerals)(Y. Zhang et al., 2014). Finally, from 430.3 ± 0.5 g_{DW} of microalgae biomass containing 42.2 ± 3.4 % of starch, we extracted 205.8 ± 1.2 g_{DW} of purified starch extract containing 86.9 ± 3.0 % of starch. At the end of the process, we obtained 178.8 g of starch from the 181.5 g of starch sheathed in the microalgae cells, for a final recovery yield of 98.5%.

Another starch extraction was conducted on the microalgae biomass issued from the same culture and led to similar starch recovery yield (data not shown), with a final extraction of approximately 80 g pure-starch.

Furthermore, our starch extraction process not only offered efficient starch recovery, but it also opened interesting biorefinery perspectives. Indeed, valuable microalgae compounds such as proteins and lipids were also sorted out during the separation phase. The supernatant was rich in lipids and proteins (19.0 ± 0.4 %DW lipids, 19.9 ± 0.7 %DW proteins), while the green pellet contained similar proteins but less lipids (7.3 ± 0.0 %DW lipids, 22.0 ± 1.6 %DW proteins)(Table III.1). Interestingly, the supernatant was the fraction recovering most of the lipids and proteins initially present in the cell lysate, with 79.5 ± 1.5 % and 61.1 ± 7.9 % recovery, respectively (Table III.2). Moreover, the lipid profile of *Chlorella vulgaris* CCALA924 was shown in Paper I to typically contain a majority of polyunsaturated fatty acids and only around 20% of saturated fatty acid, making the lipid fraction attractive for feed or food applications. However, supernatant and green pellet were ultimately mainly composed of water, with dry mass representing only 4.2 and 13.1%, respectively. Moreover, the recoverability of lipids and proteins from these fractions containing a lot of micronized cell debris is still an open question. In addition to creating micronized debris (Harrison, 1991), the multiple passes in HPH might be accompanied by the emulsion of lipid which may further hinder their downstream processing.

	Cell lysate	Fraction 1 Super-natant	Fraction 2 Green pellet	Fraction 3 Starch pellet	Puri⁒ed starch extract
Starch	42.2 ± 3.4 %	5.0 ± 0.6 %	5.2 ± 1.5 %	85.3 ± 4.7 %	86.9 ± 3.0 %
Non-glucose carbohydrates	24.7 ± 5.2 %	28.4 ± 1.1 %	41.4 ± 1.0 %	7.1 ± 2.3 %	1.8 ± 0.6 %
Lipids	7.9 ± 0.0 %	19.0 ± 0.4 %	7.3 ± 0.0 %	0.6 ± 0.1 %	0.2 ± 0.0 %
Protein	10.4 ± 1.3 %	19.9 ± 0.7 %	22.0 ± 1.6 %	0.6 ± 0.2 %	0.8 ± 1.3 %
Ashes	3.6 ± 0.2 %	9.1 ± 0.2 %	5.1 ± 0.1 %	0.5 ± 0.0 %	0.2 ± 0.0 %
Total chlorophyll	0.29 ± 0.00%	0.74 ± 0.01%	0.25 ± 0.00%	0.03 ± 0.00%	0.00 ± 0.00%
Other	11.2 %	18.6 %	19.0 %	5.9 %	10.1 %

Table III.1: Content in class of compounds for initial cell lysate, separated fractions, and purified starch. The composition of non-disrupted biomass was very similar to the cell lysate.

Finally, the energy cost of the cell disruption method used in our process is still prohibitive for industrial application. Indeed, Yap et al. 2015 evaluated that if a *Chlorella vulgaris* culture at 10 % DW and containing 30 % of lipids was disrupted with one pass of HPH at 150 MPa, the energy consumption of HPH would be equivalent to 37 % of the energy effectively accessible in the extracted lipids (Yap et al., 2015). In this work, we concluded on the necessity to run 5 cycles of HPH at 250 MPa to extract the totality of the starch. Therefore, the HPH disruption appears as highly inefficient regarding the required energy. Other disruption techniques could reduce the energy-footprint of the extraction process, such as enzymatic cell wall disruption.

	Dry weight	Starch	Non-glucose carbohydrates	Lipids	Proteins	Ashes
Fraction 1 Supernatant	32,3 ± 0,1 %	3.5 ± 0.5 %	46.1 ± 9.9 %	79.5 ± 1.5 %	61.1 ± 7.9 %	72.7 ± 4.4 %
Fraction 2 Green pellet	17,2 ± 0,1 %	2.0 ± 0.6 %	35.8 ± 7.5 %	16.3 ± 0.1 %	36.1 ± 5.2 %	21.5 ± 1.3 %
Fraction 3 Starch pellet	50,5 ± 1,5 %	94.5 ± 9.7 %	18.1 ± 7.0 %	4.2 ± 0.4 %	2.7 ± 1.2 %	5.9 ± 0.5 %
Normalization factor η	1,01	0.93	1.25	1.03	1.00	0.90
Total	100 %	100 %	100 %	100 %	100 %	100 %

Table III.2: Recovery of the class of compounds in the different fractions after the separation step. The reported values correspond to the ratio of fraction and cell lysate contents. The values were normalized to reach a sum of 100%, as indicated by the factor η.

On the other hand, the water-footprint of the process is more advantageous. Here, the three rinsing steps used in total approximately 13 L of water per kg of dry biomass, equivalent to 26 L of water per kg of dry-pure-starch. Tran et al. 2015 have shown that cassava starch extraction requires from 9.8 to 20.8 m^3_{water}/t_{starch} depending on the presence of water recycling in the process (Tran et al., 2015). Therefore, the water-footprint of our microalgal starch extraction at pilot-scale looks similar to the water-footprint of industrial-scale extraction of plant-starch.

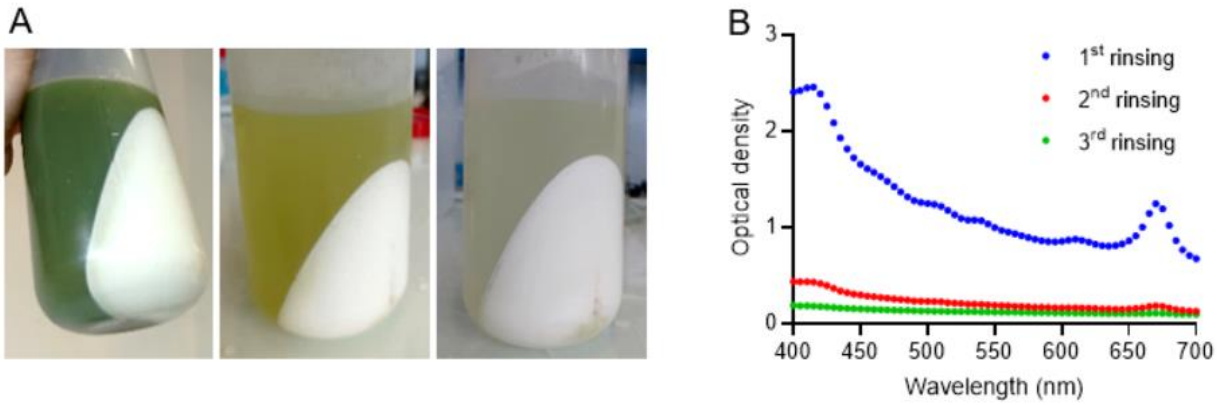

Figure III.6: Starch purification with successive water rinsing. (A) Pictures of pellet and supernatant after each rinsing step. (B) Absorbance profile of supernatants after each water rinsing step.

III.2.2 Characterization of microalgal starch

After starch extraction, we conducted a thorough analysis of the structure and characteristics of microalgal starch. First, SEM analysis indicated that the starch integrity was preserved throughout the extraction process, as attested by the presence of intact starch granules (Figure III.7).

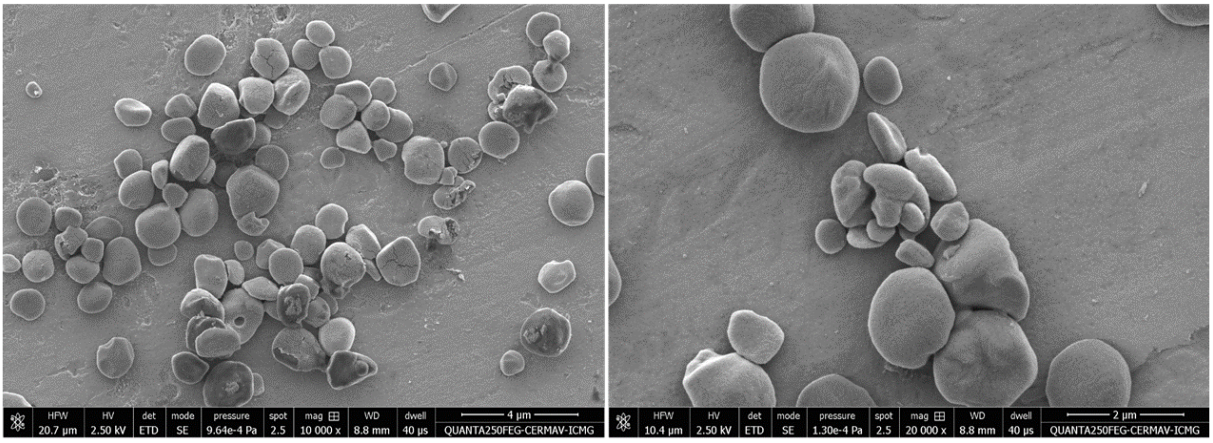

Figure III.7: Microalgal starch granules observed with scanning electron microscopy (magnifications 10 000 X and 20 000 X). Their angular shape is attributed to the tight packing of starch granules in the chloroplast during their accumulation.

The starch granules exhibited a mean diameter of 1.5 µm, as determined by laser granulometry (Figure III.8.A). Although this size range is relatively small compared to plant starch, it is typical for green microalgae (Di Caprio et al., 2023). Interestingly, the microalgal starch comprised 13.0% amylose (n=1, Figure III.8B), a relatively low

percentage for storage-type starch usually obtained under nitrogen-deprived conditions (Findinier et al., 2019). Furthermore, the structural analysis of the microalgal starch revealed a type A crystal structure, as shown by the DRX profile (Figure III.8C), along with a distance between crystalline lamella of 9.5 nm (Figure III.8D). Overall, the characteristics of the extracted starch fall within the typical range observed for Chlorella starch (Gifuni, 2017a).

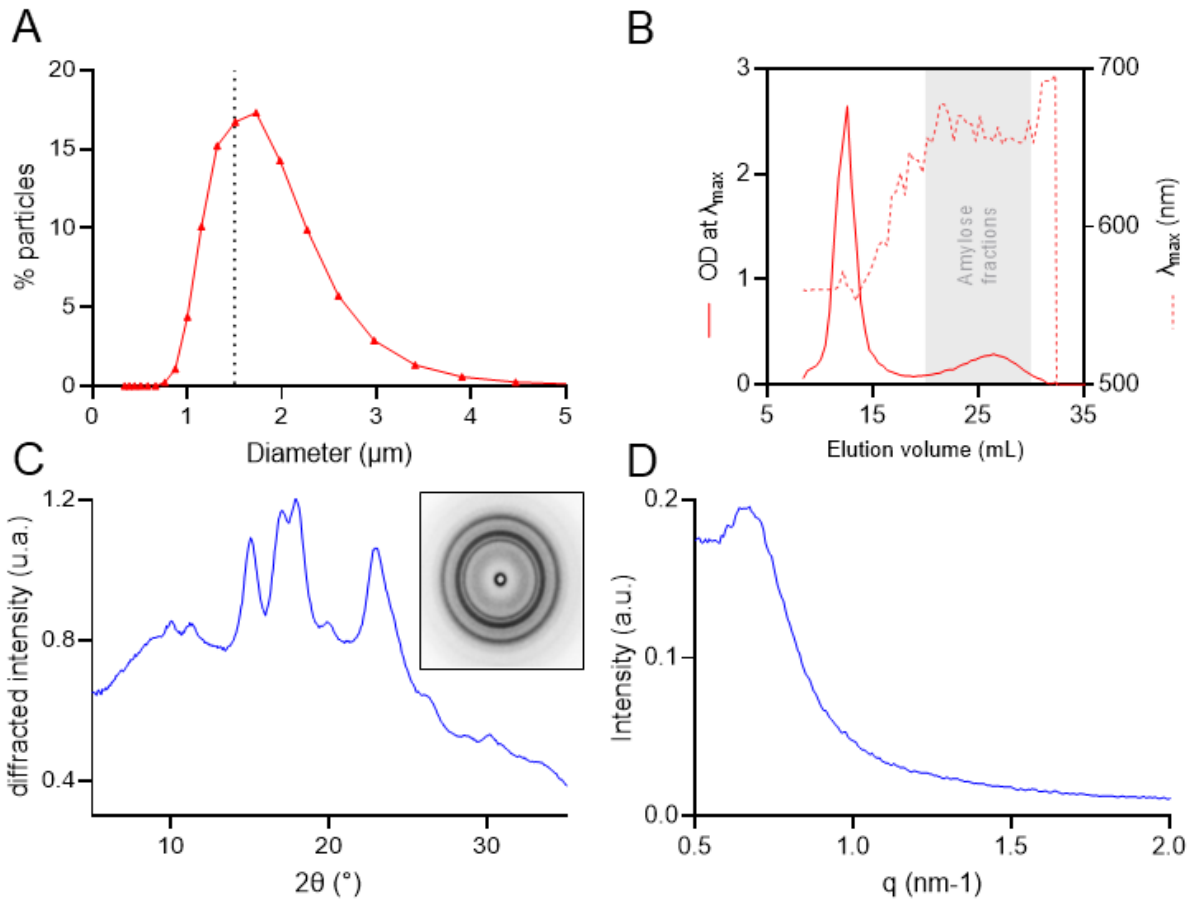

Figure III.8: Structural characterization of the extracted microalgal starch. (A) Size repartition of starch granules analyzed with laser granulometry. (B) Separation of amylopectin and amylose on CL-2B chromatography. Maximal absorbance of the polysaccharide/iodine complex (full line) was measured between 500 and 700 nm for each fraction and the wavelength at maximal absorbance determined (λ_{max} in nm, dotted line). The gel permeation chromatography excluded the high molecular weight amylopectin (1st peak; between 8 and 15 mL of elution); while lower molecular weight amylose was eluted later (2nd peak, after 18 mL of elution, grey area). (C) X-Ray diffraction (DRX) pattern of microalgal starch. (D) Small-angle x-ray scattering (SAXS) profile of microalgal starch granules.

Finally, we investigated how physical properties of the microalgal starch changes along with temperature. This analysis was performed by differential scanning calorimetry (DSC) as shown in Figure III.9. The first peak of heat flow decrease observed during the first temperature increase occurred around 65 °C. This change of heat flow corresponds to the gelatinization of the microalgal starch. An unexpected peak appeared around 100°C, probably due to the occurrence of a bubble. During the

temperature decrease, a slight exothermic peak is noticed at 75 °C. This could be due to crystallization of amylose with residual lipids. On the second heating, a long and very low endothermic peak can be noticed from 100 °C. This could be attributed to the fusion of the amylose-lipid complex. Standard maize starch, which is also of type A and contains lipids, usually display the same kind of trends in DSC.

Overall, the DSC of microalgal starch revealed normal starch behavior along the temperature. The gelatinization temperature of 65 °C falls in the range of expected values, as it was shown that microalgal starch gelatinization temperature varies from 65°C to 75°C (Izumo et al., 2007).

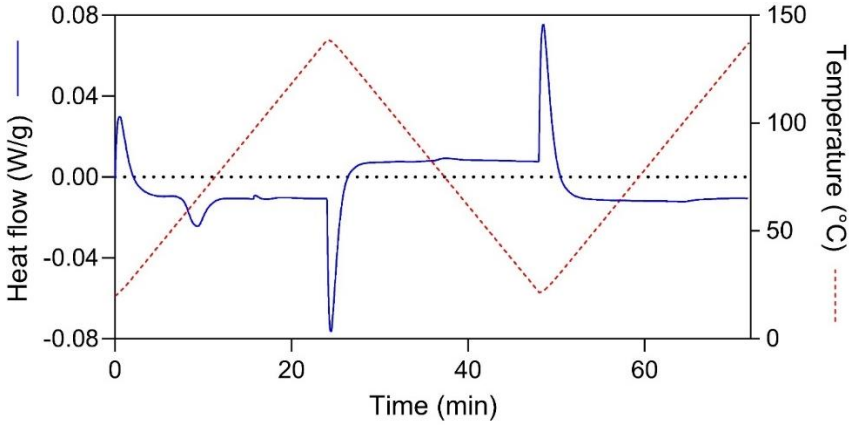

Figure III.9: Differential scanning calorimetry of the microalgal starch. The phase transitions are revealed by the changes of heat flow during the temperature evolution.

III.2.3 Plasticization of microalgal starch and characterization

Plasticization by temperature-controlled optical microscopy

The plasticization capacity of the extracted microalgal starch was compared with two control starches. The first control was a commercial grade of potato starch, widely employed in industrial thermoplastic-starch production. In contrast, the second control consisted of our freeze-dried raw microalgae biomass, containing intact starch-enriched cells. Although it has been shown that the use of entire cells can result in incomplete plasticization (Mathiot et al., 2019), comparison with extracted microalgal starch should provide insights into the relevance of the extraction and purification process with regard to plasticization. Furthermore, the direct plasticization of entire cells might be an interesting alternative route to limit processing steps for the production of microalgae-based TPS.

Initially, the plasticization capacity of the three materials was investigated in the presence of excess plasticizer (i.e. glycerol) and without the application of shear stress. A small quantity of dry material was introduced between two glass plates into a large volume of glycerol and heated gradually to 160 °C. The behavior of starch granules to the rising temperature was observed in-situ by optical microscopy with and without polarizers for the observation of birefringence. The microscopic observations at 50 and 160 °C with and without polarizers are reported in Figure III.10 and Figure III.11, respectively.

As the temperature increases, potato starch granules swell considerably at temperatures between 120 and 140 °C, along with a loss of crystallinity, as evidenced by the loss of birefringence. At 160°C, starch granule ghosts were still visible. Conversely, the swelling of individual microalgal starch granules was hardly visible due to their small size. Nevertheless, agglomerates of starch granules dispersed around 90 °C, and completely vanished between 120 and 140 °C, forming a homogeneous mixture with no birefringence. On the other hand, starch-rich microalgal cells remained agglomerated even at elevated temperatures up to 160 °C, but significant swelling was observed at both the cell and agglomerate levels. However, the cell walls prevented the observation of the birefringence evolution of starch granules; therefore, it remains unclear whether the observed cell and agglomerate swelling is attributable to thermal expansion or internal pressure resulting from the swelling and plasticization of starch granules within the cells. In any case, it clearly appears that the actions of plasticizer and temperature are not sufficient to trigger the plasticization of entire cells. This supports the need to break down microalgae cell walls beforehand using cell disruption pre-treatments (Günerken et al., 2015), or to break them down directly under the shear forces generated by thermoplastic processing, in order to achieve efficient starch plasticization. In this regard, the starch pre-extraction process developed in this work (section III.2.1) appears as an interesting and efficient route for the further plasticization of microalgae starch.

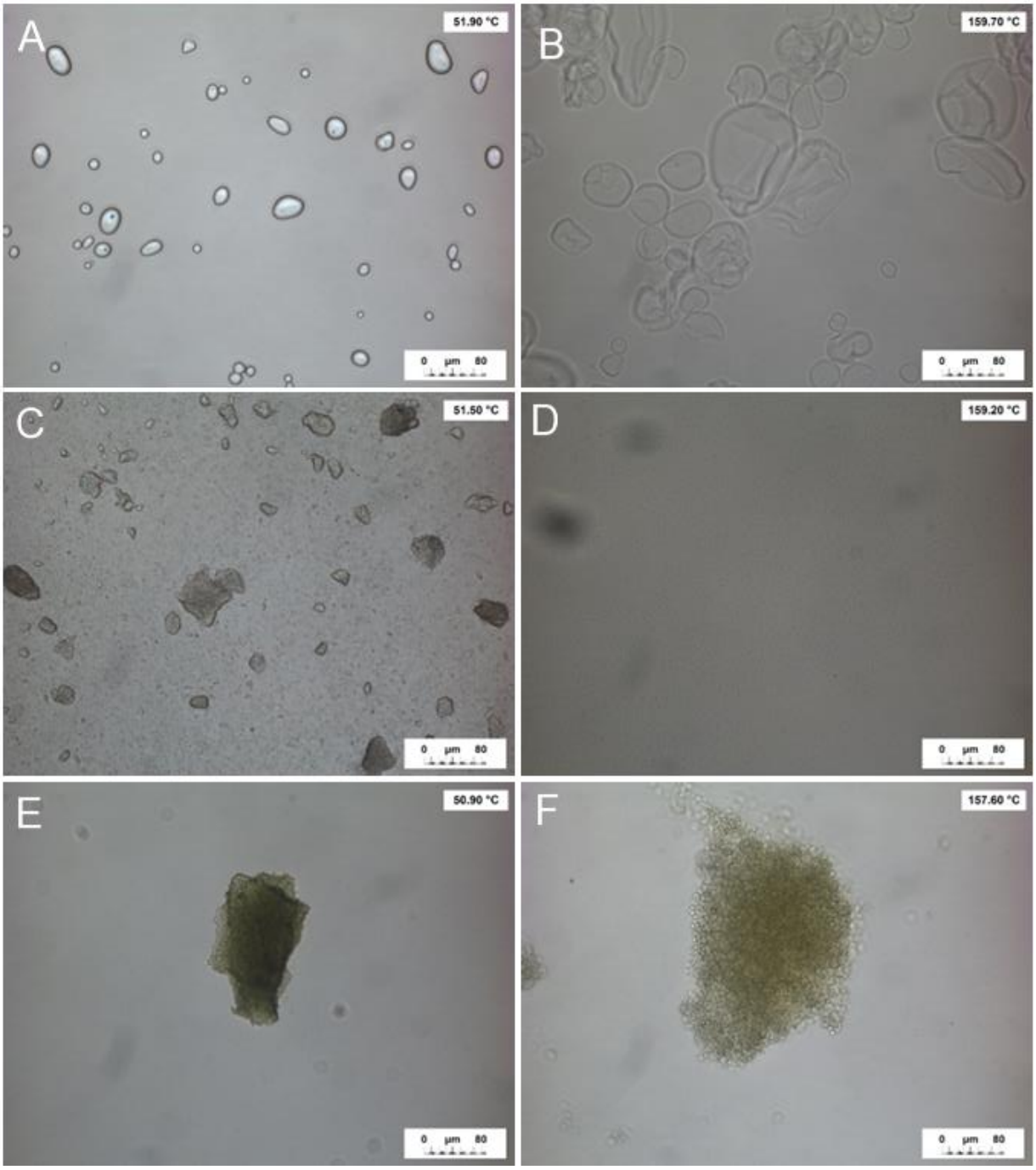

Figure III.10: Optical microscopy observations of starch plasticization in glycerol with increasing temperatures, without polarizer. (A, B) Potato starch, (C, D) microalgal starch, and (E, F) starch-rich microalgal cells, before (A, C, E) and after heating (B, D, F).

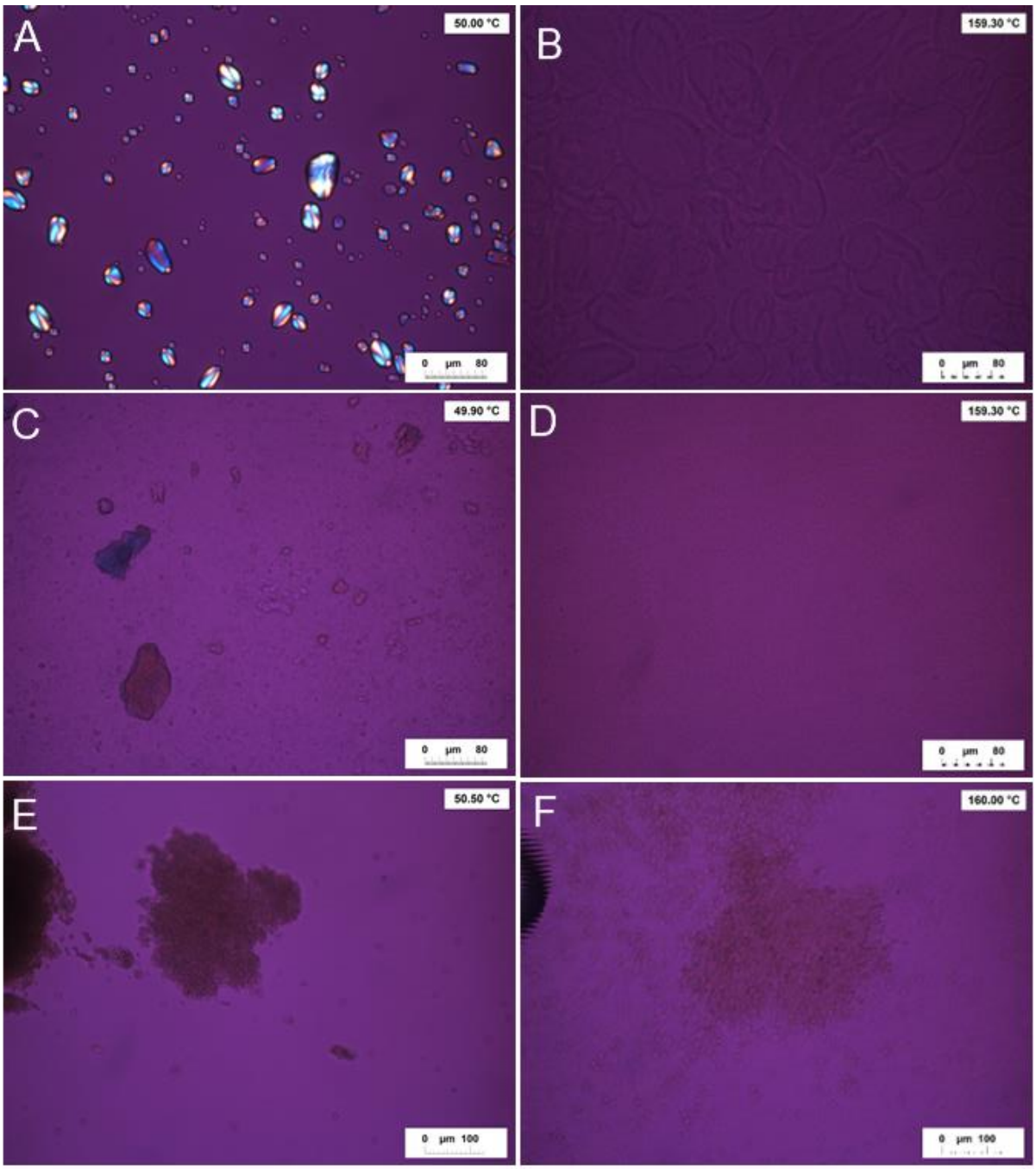

Figure III.11: Starch plasticization in glycerol with increasing temperatures, observed by optical microscopy equipped with polarizer. (A, B) Potato starch, (C, D) microalgal starch, and (E, F) starch-rich microalgal cells, before (A, C, E) and after heating (B, D, F).

Plasticization and shaping by extrusion and injection molding

Based on these observations, the plasticization ability of the three starch material was evaluated in practical conditions using a twin-screw extruder. The starch/glycerol batches (70/30 % w/w) were extruded at temperatures of 120 or 140 °C. Interestingly, a green color immediately appeared at the addition of glycerol in the white microalgal starch powder, meaning that microalgal starch was not extensively purified from its chlorophyll. During the extrusion process, microalgal starch did not plasticized properly, leaving a large proportion of the starch in powder form. As the microalgal

starch was drier than potato starch, and considering that water is known to aid in starch plasticization, we introduced 10 % water to the microalgal starch before adding glycerol. The final water content for microalgal starch, potato starch and raw biomass was then of 18.4 ± 0.4, 15.7 ± 0.1, and 8.5 ± 0.2 %, respectively. This increased moisture content facilitated proper plasticization of microalgal starch.

The extrudates from the three plasticized starch materials were recovered and subsequently injected into dogbones. At this stage, a commercial formulation of TPS was introduced as an additional control. Microalgal, potato, and commercial TPS all exhibited proper injection, with important shrinking immediately after unmolding (Figure III.12). Indeed, the chains of the polymer initially align in the injection direction, but immediately recover their helix configuration when injection is stopped (de Graaf et al., 2003). Interestingly, the shrinkage in microalgal and potato TPS was more pronounced for extrusion temperature of 140 °C than 120 °C. In addition, microalgal TPS displayed a sticky texture after injection and required careful unmolding, unlike the other two TPS. The extrudates produced at 120 and 140 °C from raw microalgae cells were easily injected but did not exhibit the shrinkage behavior typical of TPS.



Figure III.12: Injected dogbone specimens of potato TPS, microalgal TPS, plasticized raw biomass, and commercial TPS. The dogbone mold measures 7.5 cm in length, but TPS specimens showed immediate shrinkage after unmolding. The temperatures displayed on the right are extrusion temperatures, all the injection being performed at the same temperature of 140 °C.

The injected dogbones underwent cryo-fracturation in liquid nitrogen and were subsequently observed by scanning electron microscopy to study the material's aspect (Figure III.13). Microalgal TPS exhibited proper plasticization from an extrusion temperature of 120 °C, as attested by the homogeneous matrix observed (Figure III.13B,C). In contrast, the potato TPS displayed good plasticization when extruded at 140°C, but poor plasticization at 120 °C, characterized by a heterogeneous matrix containing entire starch granules (Figure III.13E). The specimens from entire microalgae cells presented a heterogeneous and granular texture at both extrusion temperatures (Figure III.13H,I). Closer inspection at higher magnification clearly distinguishes the entire cells, with the starch granules still mostly intact and hence unplasticized (Figure III.14). In addition, the dogbones of microalgae cells exhibited important fragility under traction, highlighting the weakness of intercellular binding. In summary, the plasticization of microalgae starch into TPS and its shaping by injection molding correctly occurred, except for the entire microalgae cells and for the potato starch at an extrusion temperature of 120 °C. For these reasons, the latter could not be used for tensile tests.

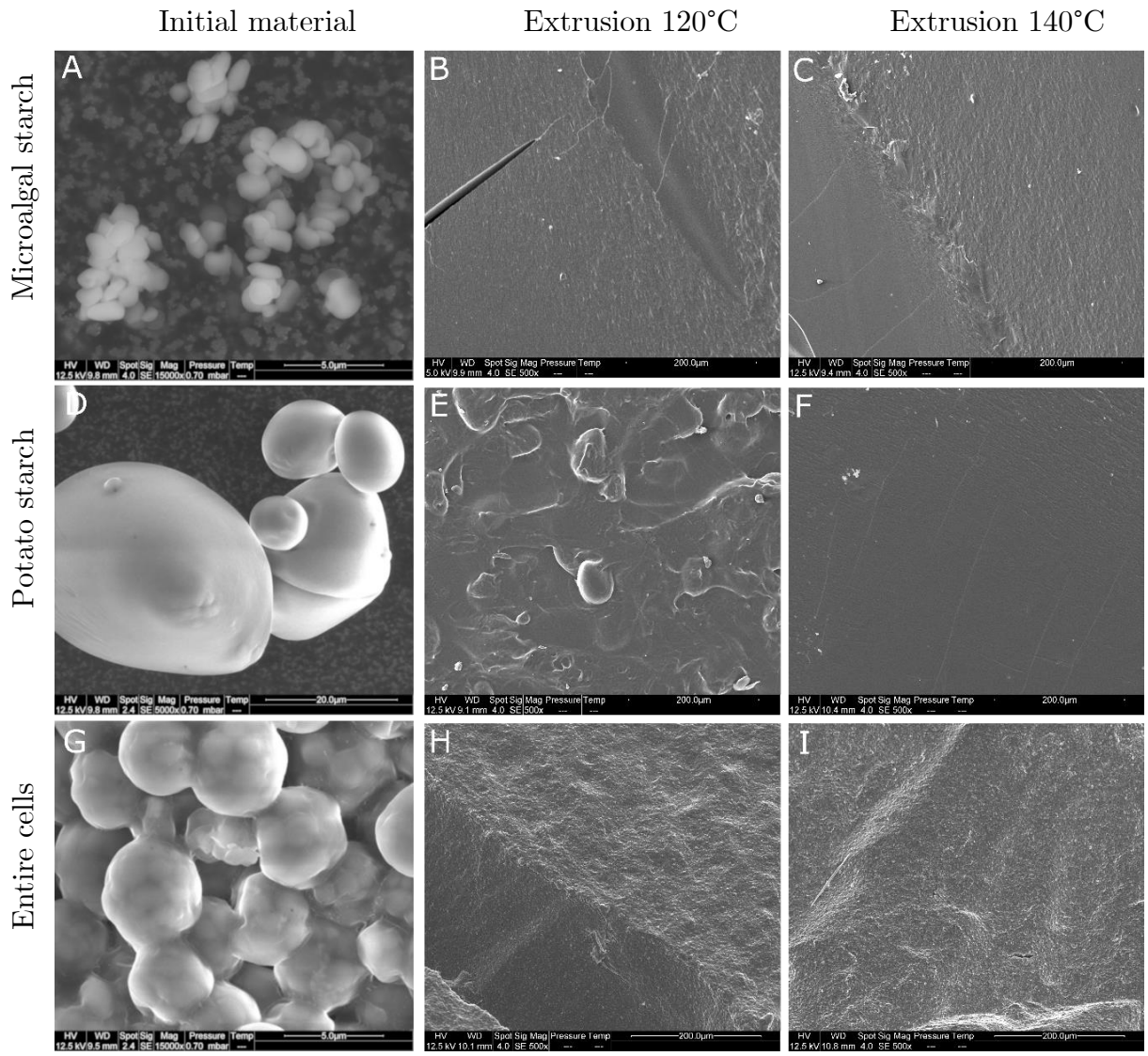

Figure III.13 : Scanning electron microscopy images of the materials in their initial and plasticized forms. (A-C) Microalgal starch, (D-F) potato starch, and (G-I) entire microalgae cells. The materials are presented in their (A,D,G) initial form, (B,E,H) extruded at 120 °C, and (C,F,I) extruded at 140 °C. (B,C,E,F,H,I) are cross-sections of the cryo-fractured dogbones. Dogbones were obtained after addition of 30 %w/w glycerol , extrusion and injection.

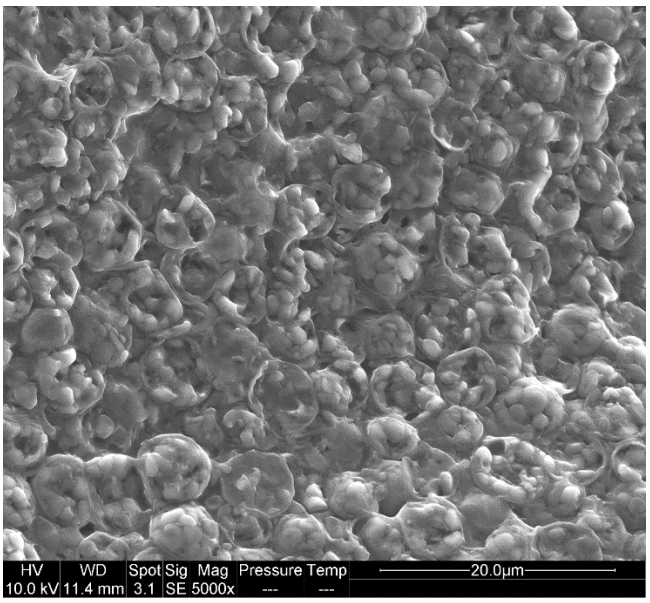

Figure III.14: Cross-section of cryo-fracturated raw biomass injected specimen. The dogbone specimen was obtained by extrusion and injection of a mix of 70%w/w entire microalgae cells and 30%w/w glycerol. Starch granules still largely intact and therefore unplasticized can be observed inside broken microalgae cells.

Tensile mechanical properties

Mechanical properties of injected TPS were investigated through tensile tests. In the light of SEM observations, the extrusion temperature of 140 °C was validated and used to produce additional batches of microalgal and potato TPS dogbones. After injection and a 3-day resting period, the stiffness, strain at break and strength were analyzed and compared for microalgal, potato, and commercial TPS dogbones. The resulting stress-strain curves are shown in Figure III.15. First of all, the reproducibility of the results is very satisfactory with well-grouped stress-strain curve clusters for each material. This supports the fact that the successive processing steps to obtain the TPS specimens, from starch extraction to plasticization by extrusion and injection, have been well mastered. Secondly, contrasted mechanical behavior can be observed between the different TPS materials. Commercial TPS is more rigid and less ductile, whereas potato and especially microalgal TPS show much softer and ductile behavior, with significantly higher elongation but lower strength.

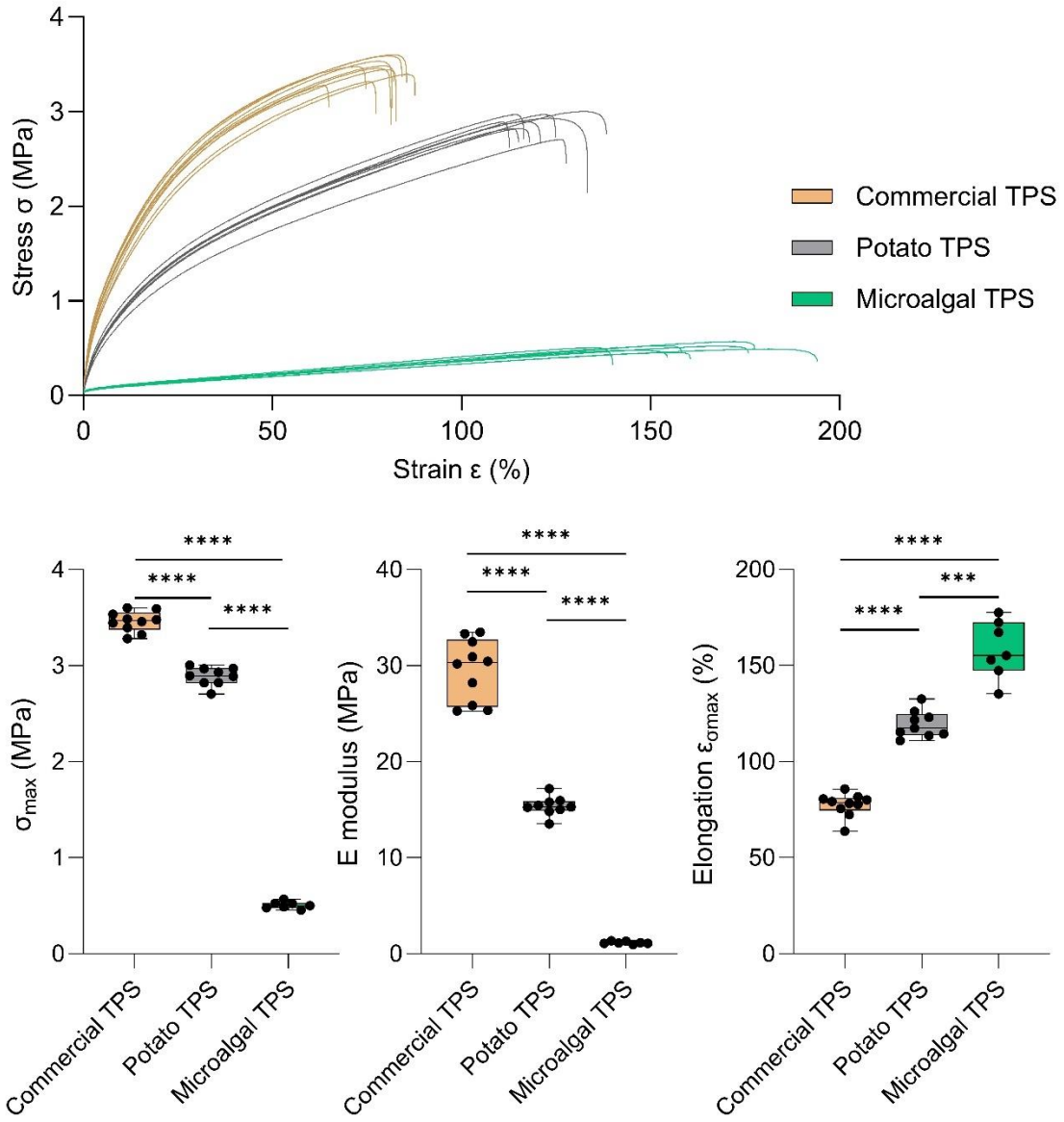

Figure III.15: Tensile mechanical properties of commercial, potato and microalgal TPS evaluated by tensile test. The p-values for the comparisons indicated in the graph are calculated with Prism 9 (Graphpad Software, LLC) and based on ANOVA Tukey's multiple comparisons test (***, P = 0.0007; ****, P < 0.0001; 7⩽n⩽10).

The values of maximal stress σ_{max} and Young's modulus E of potato and commercial TPS are in agreement with the literature (Thunwall et al., 2006; Y. Zhang et al., 2014), and the datasheet provided by the manufacturer, respectively. As pointed out, microalgal TPS is softer and demonstrated much greater elongation compared to potato and commercial TPS, with a mean elongation at maximal stress σ_{max} of 158 % against 120 and 78 %, respectively. Nevertheless, microalgal TPS exhibited maximal stress σ_{max} and E modulus of 0.5 and 1.2 MPa, respectively, which is significantly lower than potato (2.9 and 15.4 MPa, respectively) and commercial TPS (3.5 and 30 MPa, respectively). The differences in mechanical properties between microalgal and potato TPS could originate from differences in terms of plasticization efficiency, as well as

microstructural and molecular organization within the TPS composed of starch, glycerol and water.

The first hypothesis involves the presence of additional plasticizers in microalgal starch. It is known that an increase in plasticizer content in TPS can reduce tensile strength and Young's modulus while enhancing elongation (Y. Zhang et al., 2014). In our case, water content was slightly higher in microalgal starch than in potato starch after water addition (18.4 vs. 15.7 %, respectively). Therefore, we reduced the water addition to 7.5 instead of 10 % in microalgal starch (final water content 16.5 %), and produced dogbones for tensile test (Figure III.16). The mechanical properties were indeed changed, with a slightly increase in stiffness and strength, but they did not retrieve the level of potato TPS.

Furthermore, in addition to water and glycerol, various small bounded and non-bounded molecules could act as starch plasticizers, such as mono-hexose (mannose, fructose, glucose), sorbitol, urea or amino-acids (Y. Zhang et al., 2014). Carbohydrates and proteins were present in the initial microalgae biomass (Table III.1). Possibly, small quantities of small, organic molecules are still present in the extracted starch, contributing to additional plasticizing effect. However, the water rinsing steps during starch purification removed most of the soluble molecules non bounded to starch granules. If present, these plasticizing molecules should be in small quantities, as attested by the final mass balance of purified starch (Table III.1) and DRX profile (Figure III.8C). Therefore, any plasticizer effect induced by these contaminants shall be limited, as significant changes in mechanical properties typically require to increase the plasticizer content by about 50% (Zhang and Han, 2006).

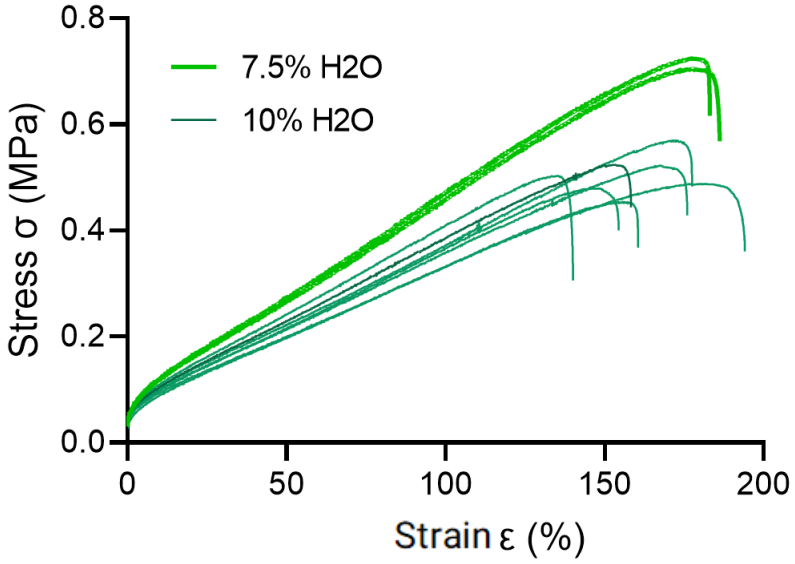

Figure III.16: Tensile mechanical properties of microalgal TPS with 7.5 or 10 % additional water, evaluated by tensile test.

The second hypothesis involves the potential difference in molecular weight between the microalgal and potato starch. Molecular weight was reported to significantly influence the mechanical properties of TPS films (Domene-López et al.,

2019; Y. Zhang et al., 2014). The molecular weight of starch is related to its molecular composition. Indeed, the two macromolecular constituents of starch, amylose and amylopectin, exhibit highly different average molecular sizes of 10^5 g/mol and 10^6-10^7 g/mol, respectively. For this reason, starches with high amylose content typically have lower molecular weight. This was studied by Domene-López and coworkers, showing that rice, potato, wheat, and corn starches with amylose content of 16.9, 20.5, 24.5, and 24.8 %, respectively, had average molecular weight of 83.2, 69.5, 51, and 51 MDa, respectively (Domene-López et al., 2019).

In the present study, microalgal starch contained 13% amylose (Figure III.8B). Potato starch is reported to have a typical amylose content of 20% (Domene-López et al., 2019; Kim, 1996; Malmir et al., 2018). Using the same analytical method as for microalgal starch, the potato starch showed an amylose content of 41%. Therefore, the difference in amylose content is approximately 28%. As shown in Figure III.15, the potato TPS exhibited higher tensile strength and Young's modulus, but lower elongation. Domene-López et al. showed that an amylose content higher of 8% (16.9 % for rice starch vs. 24.8 % for corn starch) resulted in TPS films with approximately two-fold higher tensile strength and Young's modulus, and three-fold lower elongation (Domene-López et al., 2019). In addition, the impact of amylose content on the mechanical properties of plasticized TPS is linearly valid within the range of 0-30% amylose (Lourdin et al., 1995). Therefore, the difference in amylose content between the microalgal and potato starches, and probably the underlying difference in molecular weight, may have contributed, at least partly, to the observed differences of mechanical properties.

Finally, the impact of crystallinity also needs to be addressed. On the one hand, the difference in crystal type between microalgal and potato starches (A and B, respectively) is not expected to result in variations in mechanical properties. Indeed, the initial differences in crystalline patterns are smoothed after extrusion and plasticization. Domene-López et al. showed that, after plasticization, the crystalline profile of potato TPS was similar to that of rice, wheat and corn TPS, with no discernible impact on mechanical properties (Domene-López et al., 2019). On the other hand, it could be interesting to monitor the evolution of the mechanical properties over time for microalgal TPS. Typically, the amorphous starch molecules in TPS undergo retrogradation to their crystalline forms during storage (Y. Zhang et al., 2014), especially in humid conditions. This increase in crystallinity leads to changes in mechanical properties, resulting in higher tensile strength and Young's modulus, and lower elongation. Therefore, microalgal starch may regain crystallinity overtime.

III.3 Conclusion

In this work, we developed a novel, simple and up-scalable downstream process for the extraction, purification, and plasticization of microalgal starch. The biorefinery of microalgae biomass was also proved by the parallel recovery of valuable fractions, such as lipids and proteins.

Firstly, the starch extraction process showed an extraction and purity yields of 98 and 87 %, respectively. The small sized starch granules were intact, and exhibited the

usual properties of native starches in terms of amylose content, diffraction profile, and shape. Secondly, the microalgal starch was successfully plasticized into thermoplastic starch and shaped by injection molding for the further analysis of its mechanical behavior. The measured tensile properties fall within the range expected for TPS, with much softer, ductile behavior, characterized by lower stiffness and strength, but higher elongation.

Remarkably, all the developed processing steps are transposable to an industrial scale. Here, the conversion of raw microalgae into thermoplastic starch at the pilot-scale demonstrates the relevance of microalgae for the industrial production of bioplastics.

Chapter 4 - General discussion and perspectives

4.1 Technical limitations of this work

Starch quantification

Throughout this study, we approached starch content by assessing total carbohydrate content, which poses significant limitations. Firstly, the Dubois method employed in our study measures the response of every carbohydrate, but quantifies them only relatively to a glucose calibration curve. In addition, the absorbance is measured at the wavelength adapted to glucose. Therefore, carbohydrates other than glucose are not precisely accounted for. Secondly, even if precisely quantified, total carbohydrates cannot be directly equated to starch. Functional carbohydrates, especially those contained in cell walls like galactose, rhamnose, arabinose, and glucosamine, represent an important part of the biomass.

Nevertheless, the Dubois method remains a valid tool for evaluating starch gain. Our observations indicate that an increase in carbohydrate content correlates with an increase in starch granules within cells. Additionally, this method (or equivalent acid lysis methods) is commonly used to quantify sugars in Chlorella (Brányiková et al., 2011). Although enzymatic kits are typically the preferred method for starch quantification, the robust cell wall of Chlorella prevent the access of enzymes to the starch and leads to underestimation when using enzymatic kits if the cell walls are not properly destroyed (Mathiot et al., 2019).

Overall, the Dubois method appears relevant for quantifying starch content in Chlorella. It would have been insightful to investigate more closely the real starch dosage performed by the Dubois method. While we intended to precisely quantify the initial functional pool of carbohydrates and also to compare the Dubois protocol against enzymatical kits on mechanically disrupted cells, time constraints prevented us from producing conclusive results on this matter.

Estimation of the protein content

The protein content within the biomass was derived from the total nitrogen (TN). TN was then multiplied by a nitrogen-to-protein ratio of 5.04, as documented for *Chlorella vulgaris* during the late lifecycle stage (Templeton and Laurens, 2015). This ratio was established based on the amino acid composition, which may fluctuate between 4.84 to 5.08 across different Chlorella strains and lifecycle stages. Although a nitrogen-to-protein ratio of 5.04 appears pertinent, achieving greater precision would necessitate a fresh correlation between amino acid content and TN in our specific strain and environmental conditions.

Balance of biomass composition

In both Paper I and Paper III, the total biomass composition did not reach 100%, despite the quantification of most biomass compounds. There are several potential reasons for this discrepancy. Firstly, certain compounds such as nucleic acids may not have been analyzed, contributing to the unaccounted portion of the biomass composition. Similarly, glycerol molecules were not considered during lipid

quantification, as they are removed from phospholipids or triacylglycerols after transmethylation; however glycerol is a minor fraction (in triacylglycerol containing 48C of fatty acids, the glycerol represents only 6% of total carbon).

Secondly, it is possible that the main analyzed compounds were under-quantified. For example, the quantification of total carbohydrates might not correctly quantify other carbohydrates than glucose, as developed previously. Additionally, the presence of water in rehydrated freeze-dried samples could have globally reduce lipid and protein quantification, where samples were weighed. Although efforts were made to carefully manage biomass samples to prevent rehydration, it would have been insightful to investigate the capacity of freeze-dried biomass to regain water.

In summary, the 10-20% of unquantified mass in the balance of biomass composition could be attributed to unquantified material, like nucleic acids or glycerol, and under-quantification of main compounds like carbohydrates, lipids, and proteins.

Limitations of light quantification model

In Paper II, a model was used to convert the horizontal light measurements GHI into values of light flux penetrating into the PBRs and made available to the cultures. For this approach, we adapted a model previously developed by Slegers (Slegers et al., 2013, 2011). The validity of the model was attested after comparing it with two other models, the direct equivalent model and an adapted version of Cornet's model (Appendix B). However, these two models rely on strong hypothesis, with notably strong assumption on the diffuse/collimated nature of the light. Even though this comparison of the Slegers model seems to provide a reliable quantification of the light, it would have been interesting to compare it to direct light measurement techniques adapted for complex geometry, such as chemical actinometry. However, implementing chemical actinometry in large, complex PBR is not straightforward, especially in the case of the intense solar light.

Control starch for thermoplastic starch plasticization

In Paper III, the plasticization of microalgal starch was compared to a control. This control, the potato starch, was selected for its industrial relevance. However, it did not accurately correspond to our microalgal starch, and tensile mechanical properties of potato and microalgal TPS were significantly different.

A more appropriate control would have been a plant starch with similar low amylose content and formulation. Specifically, starch formulation varied significantly depending on starch origin, probably due to the drying method. Microalgal starch exhibited small agglomerates after freeze drying, while commercial potato starch resulted in a thin, fluid powder due to spray drying. To obtain more comparable starch formulation, the microalgal starch should have been spray-dried, or maybe thinned with bead milling. Additionally, the amylose content lead to think that potato and microalgal starch have different molecular weight, which should be properly analyzed for more precision. Also, the crystallinity type of potato starch differs from microalgal starch, which may have an impact on plasticization.

4.2 Future experimental perspectives

Starch inducers and *Chlorella vulgaris* CCALA924 (Paper I)

In Paper I, it was demonstrated that different starch inducers could yield various outcomes. Further investigation into the cumulative effects of starch inducers, particularly red light illumination and nitrogen deprivation, would be insightful to determine if both accumulation pathways can occur simultaneously. Furthermore, it could be relevant to study the sequential coupling of natural light for inoculum growth, red light illumination for pre-starch accumulation (e.g. during night), and final starch accumulation with deprivation in complete light.

Additionally, exploring the distinction between a deficiency in a single nutrient like nitrogen versus deprivation of multiple macronutrients could eventually conclude on the unnecessity to use nutritive media during the deprivation step. Indeed, a test with one replicate showed that starch accumulation occurs similarly in softened water than in nitrogen-deprived medium for 2 days. Conversely, a test conducted in triplicate clearly showed that osmotic water kill the microalgae before they can accumulate starch.

Moreover, temperature effects were studied at only one temperature; conducting experiments across a range of temperatures could reveal an optimal temperature for starch accumulation, clarifying the competitive potential of temperature stress compared to nutrient deprivation.

Furthermore, our strain, *Chlorella vulgaris* CCALA924, did not exhibit lipid accumulation even after two weeks of starvation, contrary to typical expectations for Chlorella species. It would be insightful to evaluate more closely the lipid accumulation capacity of this strain and understand why lipid accumulation does not occur and how it might influence starch accumulation.

Light modelling (Paper II)

Following the results of Paper II, the light modeling approach was validated as an efficient method to optimize carbohydrate productivity. However, the light-to-carbohydrates model developed requires better validation. It would have been beneficial to generate additional experimental data to refine the model and broaden its applicability. Notably, future experiments in open systems relevant for industrial cultivation, such as raceways, would provide valuable insights into the real production capacity of starch with *Chlorella vulgaris*.

Moreover, assessing and incorporating the influence of other variables such as temperature or pH into the model would have enhanced its accuracy and utility. By considering these additional factors, the model could better simulate real-world conditions and provide more precise predictions for optimizing carbohydrate productivity in microalgae cultivation systems.

Starch extraction for biore%nery and plasticization (Paper III)

The extraction process developed in Paper III proved highly efficient for starch extraction and recovery. However, the other biomass fractions such as non-glucose carbohydrates, lipids, or proteins are not individually separated, conversely to what has been achieved in plant starch extraction processes. The entire extraction process should be directed towards full valorization of the biomass, encompassing more than just starch. Further experimental work is needed to efficiently separate each fraction, possibly by rethinking some steps like cell disruption. Additionally, a more sustainable and scalable cell disruption method than a high-pressure homogenizer needs to be explored, perhaps involving a combination of less energy-consuming disruption techniques and the addition of a steeping step with enzymes or chemical agents.

Moreover, the purified starch retains a green hue which is barely visible in starch powder but more apparent in plasticized starch. Complete removal of the green color should be achieved, while still avoiding the use of solvents. Overall, the extraction process should be further developed to increase its technology readiness level and further demonstrates its industrial applicability.

4.3 General discussion

Starch accumulation: two-stage culture process versus continuous starch induction

Harsh inducers, particularly nutrient deprivation, are commonly utilized in a two-stage outdoor cultivation process. Our findings in Paper I confirm that nitrogen starvation results in the highest starch-equivalent productivity within a short timeframe, reaching 0.58 g/L/day during 4 days. However, achieving the actual attainable productivity requires consideration of several hidden factors.

Firstly, in a production period of 4 days (88 hours), the time allocated for harvest, reactor cleaning, and inoculation is non-negligible, constituting roughly 5% of the cultivation duration. Additionally, maintaining a healthy culture for constant growth (first cultivation step) to support the starved culture (second cultivation step) is essential. Based on data from Paper I, with cultures grown in the same controlled conditions of culture vessel and artificial lightning, we can consider that the second cultivation step requires an initial concentration of 1 g/L. To produce 1 g/L from an initial concentration of 1 g/L, the replete culture takes approximately 40 hours. In the other hand, the second cultivation step last 88 hours for an initial concentration of 1 g/L. Therefore, the time required to grow the biomass for starting the starved culture represents 45% of starvation duration. Considering that microalgae growth is linear according to time, as it seems to be the case in Paper I, we can approximate that the synchronization of the first and second cultivation steps in a 88 hours basis would require to reduce the inoculum volume to 45% of the volume of second cultivation (Figure 4.1). Thus, based on the above hypotheses and on our laboratory conditions, the overall starch productivity of the second phase could be reduced by approximately 30% for inoculum preparation (due to overall volume increase) and 5% for preparation steps (due to time increase).

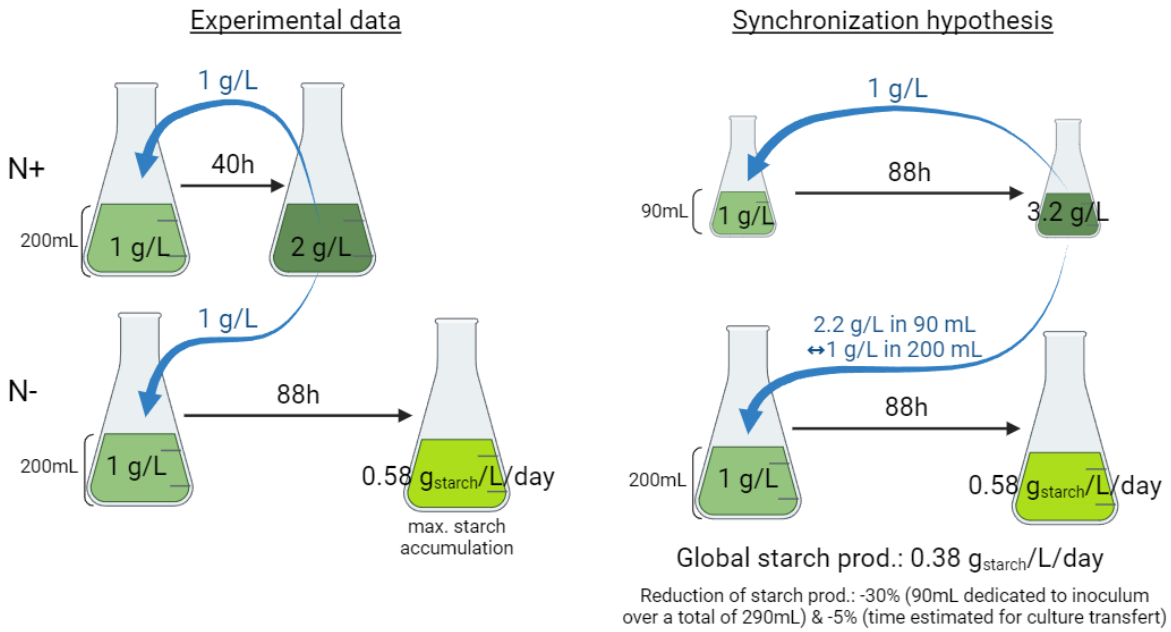

Figure 4.1: Inoculum preparation leads to reduced starch productivity. The synchronization hypothesis helps to illustrate the volume required for inoculum preparation, which represents 45% of N- volume. Calculations are based on a linear projection of N+ productivity.

Consequently, the final starch productivity would decrease from 0.58 g/L/day for starvation alone to around 0.38 g/L/day for the complete two-stage culture system. Interestingly, this figure closely resembles the 0.33 g/L/day obtained for starch induction under red-light illumination, where the cultures could be grown in semi-continuous mode without the need to prepare an inoculum. Moreover, starch accumulation under red light is concurrent with high levels of proteins and highly efficient photosynthesis. Therefore, red-light illumination appears to offer numerous advantages over nutrient deprivation and starch induction.

However, the investment and operational costs associated with red LED illumination are currently prohibitive for low-cost applications such as starch production. As indicated in the literature, the impact of red light lies not in the light itself, but rather in the absence of blue-photon stimulation. Consequently, there is significant interest in developing a mutant insensitive to blue photons that would continuously produce starch to high basal level with sustained photosynthetic capacity under any light wavelength.

Nevertheless, developing such an efficient mutant may not be straightforward. Sensitivity to blue light is associated with regulatory pathways beyond starch. For example, a *Chlamydomonas reinhardtii* mutant lacking phototropin, the blue-light-sensitive signaling protein, exhibited reduced resistance to high light intensities (Petroutsos et al., 2016). Therefore, further understanding of blue-light regulatory pathways, particularly in Chlorella, is necessary before considering the creation of a mutant capable of theoretically accumulating starch in a continuous process under full sunlight.

High carbohydrate content or high photosynthesis e ciency: challenges in light supply during starch accumulation

The ultimate aim of starch cultivation with microalgae is to achieve both high carbohydrate content and high areal carbohydrate productivity. In an outdoor culture, areal productivity is linked to the photosynthetic efficiency, as light is the limiting resource and that its efficient conversion is necessary to reach high areal productivity. However, our experimental study revealed a trade-off between the carbohydrate content and the photosynthetic efficiency. We found that achieving high carbohydrate content often occurs under photosaturation conditions, which typically result in low photosynthetic efficiency. In general, mass cultivation of microalgae should minimize photosaturation as much as possible, as it correlates with significant loss of available energy. Consequently, it seems difficult or undesirable to achieve very high carbohydrate content under practical growing conditions. On the other hand, a compromise on lighting conditions may enable intermediate carbohydrate content and photosynthetic efficiency to be achieved.

In practice, the most relevant criterion for designing efficient starch cultivation with microalgae is the targeted starch content. The targeted starch content determines the concentration at which a culture should be run, thus influencing its light energy conversion efficiency. Pursuing very high carbohydrate content requires high light availability, which means low microalgae concentration and low photosynthesis efficiency. Conversely, lower starch content requirements allow for higher microalgae concentration, leading to easier harvest and higher energy conversion efficiency. Nevertheless, the starch content should still be sufficient for the extraction process to be efficient. As proposed in Paper II, targeting a carbohydrate content of 57% (approximately 50% starch) would result in our flat panel photobioreactor having an initial biomass concentration of 0.8 g_{DW}/L, a photosynthesis efficiency of 2.9% (considering full sunlight spectrum), a volumetric productivity of 0.13 $g_{CHO}/L/h$, and an aerial productivity of approximately 38 $g_{CHO}/m^2/d$. These figures are comparable to those obtained in short-term experiments for plant crops (Coombs, 1985).

Chlorella vulgaris as a biomass source for the bioplastic industry: are microalgae from open systems competitive with plants?

The production of starch, a product with relative low value, necessitates large-scale and low-cost cultivation, especially for high-volume applications like bioplastics. In microalgae cultivation, this translates to production in open culture systems such as raceways, as opposed to photobioreactors used in this study (Paper II). Open culture systems, comparable to crop fields in size and functionality, require more complex infrastructure and higher water and energy inputs. Regardless of the system's location, investment in microalgae cultivation would only be justified if the productivity of open ponds surpasses that of plant crops.

Bakku et al. achieved 10-15 $g/m^2/d$ for 16 consecutive weeks in raceways with *Euglena gracilis* containing 40-60% paramylon, a polysaccharide similar to starch (Bakku et al., 2023). Considering a 45% productivity reduction for inoculum preparation (as described previously), the productivity output would be approximately

2 to 4 g/m²/d of paramylon. Brányiková et al. achieved a starch productivity of around 9 g/m²/d with *Chlorella vulgaris* cultivated in batch with a thin-layer cascade reactor for 7 days (Brányiková et al., 2011). Compared to practical productivities in crop fields in the USA, these paramylon and starch productivities are average. A corn field typically produces the equivalent of 1 to 2 g/m²/d of starch, while a wheat field yields around 4 to 7 g/m²/d (Table 4.1).

	Wheat	Cassava	Potatoes	Maize	Beet	Cane
Fresh crop yield in the USA (t_{FW}/ha/year)	27-35	40-49 (Guyana)	40-51	8-11	50-74	50-86
Product	Starch	Starch	Starch	Starch	Sucrose	Sucrose
Typical content in product (%FW)	55-70% (Maningat et al., 2009)	32-35% (Bantadjan et al., 2020)	15-20% (Robertson et al., 2018)	53-78% (Eckhoff and Watson, 2009)	21-22% (Gruska et al., 2022)	13-16% (Wu and Birch, 2007)
Yield in product (t_{DW}/ha/year)	15-25	13-17	6-10	4-7	11-16	7-14
Yield in product (g_{DW}/m²/d)	4-7	4-5	2-3	1-2	3-4	2-4

Table 4.1: Yield in starch or sucrose from the main crops solicited for starch or bioethanol production. FW: Fresh Weight. DW: Dry weight. The fresh crop yield data is issued from FAO statistic for the USA in the years 2000-2020, except for cassava where data is from Guyana. Fresh crop yield is expressed omitting the productivity of secondary plant material like stems or leaves.

There is limited data on long-term production of polysaccharides with microalgae in open systems. As of today, it is likely that microalgae starch production in large open systems would not significantly surpass the productivity of plant crops in the field. However, the unique feature of microalgae, i.e. growth in suspension in water, offers leverage to regulate and optimize productivity, a capability absent in plants. Biomass concentration can be carefully adjusted to light conditions to enhance productivity, as proposed in this work for cultivation in photobioreactors. This approach allows for selection of the optimal biomass concentration corresponding to the optimal carbohydrate output.

Processing microalgae biomass for starch recovery: parallels with the current starch industry

Starch recovery from *Chlorella vulgaris* remains a challenge. In this work, we established an extraction process based on starch release through cell disruption by high-pressure homogenization, starch separation by centrifugation, and starch purification by water rinses and centrifugation. As described in Paper II, the overall process is energy-intensive and has a significant water footprint. While assessing the absolute footprint of the process is crucial, it is equally important to compare it to the current alternative of plant-starch production industry.

The starch extraction industry has been evolving for over 150 years and achieves massive production, with more than 60 million tons of starch annually (Grommers and van der Krogt, 2009). This highly specialized industry tailors extraction processes to specific crops (corn, potato, cassava, wheat, rice). While all extraction processes rely on a similar set of techniques, each is adapted to its respective crop. Plant starch extraction processes share common techniques with our laboratory-scale protocol for microalgae, such as starch release from grains or tubers through dry or wet milling, followed by separation and purification mainly through centrifugation and water rinses.

Starch release by milling or grinding in plant crops is comparatively simpler than the cell disruption required in microalgae like *Chlorella vulgaris*. However, some plants, like corn, require a complex steeping step to soften their grain before milling. Corn steeping involves 1.5 m^3/t_{corn}, water heated at 50°C, lactic bacterial fermentation, and SO_2 injection (a high air pollutant), which in total accounts for around 20% of the overall plant's energy and capital costs (Eckhoff and Watson, 2009; Yu and Moon, 2021). Corn starch extraction is highly efficient and allows for recovery of proteins, oil, or fibers in different fractions. However, it is complex, energy-intensive, water-consuming, and polluting. Despite these drawbacks, corn starch dominates the market with a 71% share (Adewale et al., 2022). The scale of facilities in the corn starch industry, with tanks holding 250-600 tons of corn in newer US plants (Eckhoff and Watson, 2009), plays a significant role in cost reduction. Ultimately, process complexity matters less than final cost, which can be minimized by large-scale operations and abundant raw materials.

Based on the protocols complexity in the starch industry, scaling up microalgal starch extraction could be economically viable. However, the primary obstacles to industrial-scale microalgal starch extraction would be competition with established industries and, most importantly, access to storable and readily available raw material.

Developing the microalgae production of polysaccharides: a supplementary source for biobased applications

One advantage of microalgae is their capacity to produce the same compounds as plants but in a different context. Whether sourced from plants or microalgae, polysaccharides should seamlessly integrate into various applications. Indeed, our work in Paper III demonstrated that microalgal starch was suitable for plasticizing thermoplastic starch. We also illustrated that releasing starch from microalgae cells was essential for achieving a homogeneous plasticized matrix.

Beyond direct plasticization, microalgal starch can serve a wide array of applications. Depolymerized starch can be used in fermentation processes to produce various products. For example, microalgal starch from *Chlorella vulgaris* was depolymerized and fed to bacteria to produce PHA, another bioplastic, as part of the European project Nenu2PHAr. Alternatively, depolymerized starch could be utilized to produce bioethanol, as currently done from maize starch.

Overall, there is a compelling interest in developing carbohydrate production by microalgae, as it could integrate all existing processes based on carbohydrates in the biomaterial industry and beyond.

The primary challenge remaining is scaling up microalgae mass production. Presently, microalgae cultivation for low-value products is not economically viable. Three solutions are envisaged to address the main drawbacks of microalgae cultivation. First, increasing the efficiency of energy conversion towards the targeted product by developing mutants with lower pigmentation to reduce photo-saturation and upregulated pathways to overproduce the targeted compound. Second, reducing the cost of culture and harvest by utilizing strains associated with low-energy harvest, such as spirulina, and sourcing nutrients from wastewater. Lastly, fully valorizing the entire microalgae organism by developing solvent-free and low-energy extraction processes. Currently, the potential of microalgae lies in their specific applications, such as wastewater treatment or CO_2 mitigation from industrial gases.

Conclusion

This work aimed to evaluate the efficiency of microalgae as starch producers for bioplastic applications. To do so, we focused on the induction of starch accumulation, on the optimal light management of starch-accumulating culture under natural light, and on the extraction and plasticization of microalgal starch.

The investigation of scientific literature revealed that a major bottleneck of microalgae cultivation is the photosaturation and photoinhibition occurring in the first layers of the culture. The photosynthesis-relative-to-irradiance curve (PI-curve) reveals three states of light utilization: photolimitation, photosaturation, and photoinhibition. Photolimitation is favored in outdoor culture systems to maximize photon utilization without harming the culture. Nevertheless, the optimal light supply for starch-accumulating culture had not been investigated so far.

In practice, industrial cultivation of microalgae should be preferred over plants for other reasons than aerial yield or solar energy conversion. One compelling capacity of green microalgae like *Chlorella vulgaris* is their ability to completely redirect their metabolism towards starch accumulation in case of stress. Although various starch induction methods are described in the literature, they lacked comprehensive comparison in a similar context.

Starch is both an energy reserve molecule and a polymer with interesting properties, making it suitable for bioplastics production. However, current starch extraction in microalgae processes are complex and lack of efficiency. Similarly, plasticization of microalgal starch into thermoplastic starch has only been conducted at very low scale.

Three major results issued from this study are:

Firstly, we compared three abiotic starch-inducing methods in terms of carbohydrate productivities, biomass composition, starch structure, photosynthetic capacities and cell rupture. Nitrogen deprivation and supra-optimal temperature induced rapid but unsustainable starch accumulation, suitable for short-term batch culture strategies. Conversely, red-light illumination facilitated enhanced and steady starch production, ideal for continuous culture systems. Overall, *Chlorella vulgaris* CCALA924 was confirmed to be a high-starch-producing strain, albeit with low lipid production.

Secondly, we investigated light management in outdoor starch-accumulating cultures, establishing empirical relationships between starch accumulation and light-per-biomass ratio under natural solar light conditions. These relationships provided general guidelines for optimizing starch accumulation based on the initial biomass concentration and incident light-per-biomass.

Finally, we developed a novel and simplified downstream process for extracting, purifying, and plasticizing microalgal starch. The extraction process yielded extraction and purity rates of 98% and 87%, respectively, with intact starch granules exhibiting typical properties of native starches. Successful plasticization of microalgal starch into

thermoplastic starch at the pilot scale underscores the industrial potential of microalgae for bioplastic production.

Future endeavors could explore strategies to enhance the profitability of microalgae mass culture. For instance, blue-light signalization pathways should be investigated to potentially generate mutants with continuous high-level starch production. Efforts to maximize energy conversion efficiency in outdoor culture should also be extended to open culture systems. Moreover, scaling up the starch extraction process to industrial levels could make microalgal starch processing competitive with plant starch extraction, provided sufficient volumes of microalgae are supplied.

In conclusion, this research provides practical insights into starch accumulation, outdoor cultivation, and conversion processes of microalgae into bioplastics. The development of carbohydrate production with microalgae holds promise for the broader biobased industry. Overall, this work represents a new step toward bringing the gap in industrial bioplastic production from microalgae starch.

Appendices

Appendix A. Supplementary materials of Paper I

Table A.S1: Nutrient availability in culture media of control N+ and red light illumination RL. N.D.: not determined.

	Control N+			Red light RL		
	Day 3 (64h)	Day 4 (88 h)	Day 7 (160 h)	Day 3 (64 h)	Day 4 (88 h)	Day 7 (160 h)
NO_3^- (mg/L)	951.4	671.3	420.0	799.4	795.9	434.5
PO_4^{2-} (mg/L)	42.8	19.1	N.D.	35.3	24.8	N.D.
SO_4^{2-}(mg/L)	13.7	N.D.	N.D.	Present, not quantified	N.D.	N.D.

Table A.S2: Table characterization of biomass and compound evolution during the starch induction experiments ; ND: note determined due to analytical problems.

	Control N+				Nitrogen deprivation N-				Supra-optimal temperature HT				Red light RL			
	0 h	40 h	88 h	160 h	0 h	40 h	88 h	160 h	0 h	40 h	88 h	160 h	0 h	40 h	88 h	160 h
TC/TN	4.73 ± 0.09	6.01 ± 0.15	6.37 ± 0.23	8.35 ± 0.12	4.73 ± 0.09	12.78 ± 0.38	21.74 ± 0.80	25.29 ± 0.28	6.18 ± 0.33	11.66 ± 0.47	15.17 ± 1.19	11.87 ± 0.13	4.97 ± 0.15	7.96 ± 0.17	6.78 ± 0.21	9.95 ± 0.21
Biomass (g L^{-1})	0.90 ± 0.01	1.93 ± 0.01	3.05 ± 0.00	5.92 ± 0.04	0.91 ± 0.02	2.25 ± 0.00	3.56 ± 0.04	4.58 ± 0.01	0.85 ± 0.03	1.98 ± 0.01	2.66 ± 0.02	2.12 ± 0.03	0.83 ± 0.01	2.08 ± 0.02	3.28 ± 0.01	5.93 ± 0.07
Carbohydrates (wt%)	14.67 ± 3.68	25.80 ± 2.01	19.13 ± 0.50	42.80 ± 4.10	14.67 ± 3.68	54.99 ± 3.22	69.74 ± 1.77	67.00 ± 6.20	25.80 ± 0.73	60.50 ± 1.87	64.30 ± 3.32	49.30 ± 1.08	24.22 ± 0.62	38.24 ± 3.96	46.80 ± 0.00	44.44 ± 8.55
Proteins (wt%)	52.44 ± 0.89	41.32 ± 1.03	37.66 ± 1.24	27.14 ± 0.37	52.44 ± 0.89	16.64 ± 0.45	10.43 ± 0.36	7.80 ± 0.08	ND ; 50.00	18.51 ± 0.74	14.27 ± 1.01	18.74 ± 0.21	50.00 ± 1.48	28.58 ± 0.60	35.00 ± 1.03	21.62 ± 0.44
Lipids (wt%)	10.40 ± 0.33	8.49 ± 0.29	9.48 ± 0.59	8.20 ± 0.04	10.40 ± 0.33	6.41 ± 0.10	7.12 ± 0.70	8.27 ± 0.20	8.73 ± 0.52	5.76 ± 0.64	6.98 ± 0.44	9.26 ± 0.09	10.27 ± 0.49	1.14 ± 0.04	3.72 ± 0.47	6.37 ± 0.06
Total chlorophyll (wt%)	4.40 ± 0.14	4.40 ± 0.01	4.70 ± 0.01	3.00 ± 0.05	4.40 ± 0.14	1.90 ± 0.02	1.10 ± 0.02	0.80 ± 0.01	5.40 ± 0.17	2.50 ± 0.17	1.70 ± 0.06	1.60 ± 0.08	3.80 ± 0.27	3.10 ± 0.15	3.00 ± 0.05	2.30 ± 0.05
Carotenoids (wt%)	0.62 ± 0.03	0.66 ± 0.00	0.69 ± 0.00	0.46 ± 0.01	0.62 ± 0.03	0.35 ± 0.01	0.25 ± 0.00	0.22 ± 0.01	0.76 ± 0.01	0.45 ± 0.03	0.39 ± 0.01	0.42 ± 0.01	0.57 ± 0.03	0.44 ± 0.01	0.46 ± 0.01	0.37 ± 0.02

Table A.S3: Biomass growth parameters and productivities of compounds during the starch induction experiments.

	Control N+			Nitrogen deprivation N-			Supra-optimal temperature HT			Red light RL		
	0 to 40 h	40 to 88 h	88 to 160 h	0 to 40 h	40 to 88 h	88 to 160 h	0 to 40 h	40 to 88 h	88 to 160 h	0 to 40 h	40 to 88 h	88 to 160 h
Cellular growth rate μ (d^{-1})	0.61 ± 0.03	0.20 ± 0.00	0.07 ± 0.00	0.71 ± 0.03	-0.03 ± 0.00	0.02 ± 0.00	0.04 ± 0.00	0.02 ± 0.00	0.06 ± 0.00	0.59 ± 0.01	0.26 ± 0.01	0.07 ± 0.00
Biomass (mg L^{-1} d^{-1})	615.0 ± 8.6	558.8 ± 6.7	959.4 ± 12.8	804.0 ± 13.1	655.4 ± 19.6	340.3 ± 13.8	678.5 ± 19.4	339.2 ± 9.7	-178.9 ± 10.7	752.4 ± 14.7	601.7 ± 13.1	883.6 ± 24.0
Carbohydrates (mg L^{-1} d^{-1})	219.0 ± 23.6	42.5 ± 20.9	650.1 ± 80.6	662.3 ± 45.4	622.9 ± 49.9	195.5 ± 97.5	587.8 ± 29.3	254.9 ± 48.3	-220.6 ± 31.0	357.2 ± 49.9	370.6 ± 41.5	366.9 ± 169.5
Proteins (mg L^{-1} d^{-1})	193.9 ± 12.3	175.3 ± 21.4	207.8 ± 15.4	-61.6 ± 6.1	-1.5 ± 8.4	10.0 ± 4.7	-34.9 ± 13.8	6.4 ± 15.3	21.8 ± 9.3	108.9 ± 8.4	277.2 ± 18.5	52.9 ± 15.4
Lipids (mg L^{-1} d^{-1})	41.9 ± 3.4	62.6 ± 9.4	65.5 ± 6.1	29.7 ± 1.4	54.7 ± 12.6	41.8 ± 8.9	23.9 ± 7.6	35.7 ± 8.6	-31.5 ± 4.0	-36.7 ± 0.5	49.2 ± 7.7	85.2 ± 5.5
Total chlorophyll (mg L^{-1} d^{-1})	27.3 ± 0.9	28.8 ± 0.3	12.0 ± 1.0	2.2 ± 1.0	-2.4 ± 0.5	-1.3 ± 0.3	2.7 ± 2.5	-2.2 ± 1.9	-4.2 ± 0.8	20.3 ± 2.4	15.8 ± 1.8	13.8 ± 1.2
Carotenoids (mg L^{-1} d^{-1})	4.3 ± 0.2	4.1 ± 0.1	2.2 ± 0.2	0.7 ± 0.2	0.5 ± 0.1	0.3 ± 0.1	1.4 ± 0.4	0.8 ± 0.3	-0.5 ± 0.1	2.7 ± 0.2	3.0 ± 0.2	2.3 ± 0.4

Table A.S4: Mean cell wall thickness and cellular growth rate for every growth condition. The cell wall thickness refers to the inner cell wall, as described in figure S4.

		N+	N-	HT	RL
Mean cell wall thickness (nm)	0 h	61.7 ± 12.8	61.7 ± 12.8	56.19 ± 14.6	56.8 ± 13.6
	40 h	68.4 ± 17.5	72.7 ± 2.3	92.4 ± 2.3	79.0 ± 16.1
	88 h	59.2 ± 15.2	96.5 ± 27.5	126.5 ± 30.7	83,8 ± 19.7
Growth rate μ (day^{-1})	0-40 h	0.609 ± 0.062	0.712 ± 0.040	0.037 ± 0.040	0.586 ± 0.033
	40-88 h	0.205 ± 0.049	-0.023 ± 0.029	0.022 ± 0.026	0.263 ± 0.031

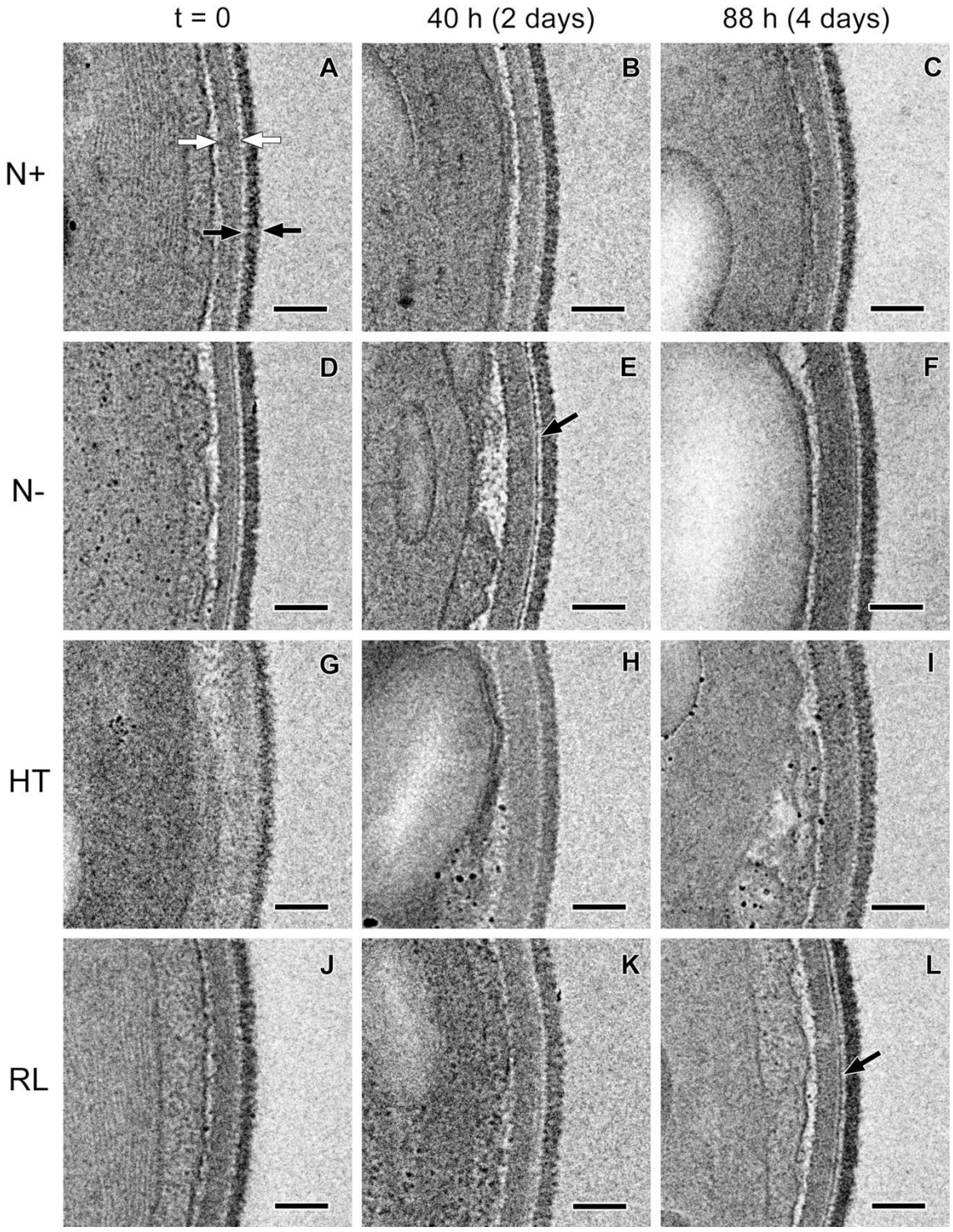

Figure A.1: TEM images of ultrathin sections of resin-embedded *Chlorella vulgaris* cells after 0, 44 and 88 h of starch induction. The cell walls are composed of two layers. The inner cell wall is the layer on the inside of the cell (white arrows in A), sometimes accompanied with an additional thin supplementary layer (black arrows in E and L). The outer cell wall presents a hairy-like and electron dense structure (black arrows in A). Scale bars correspond to 200 nm.

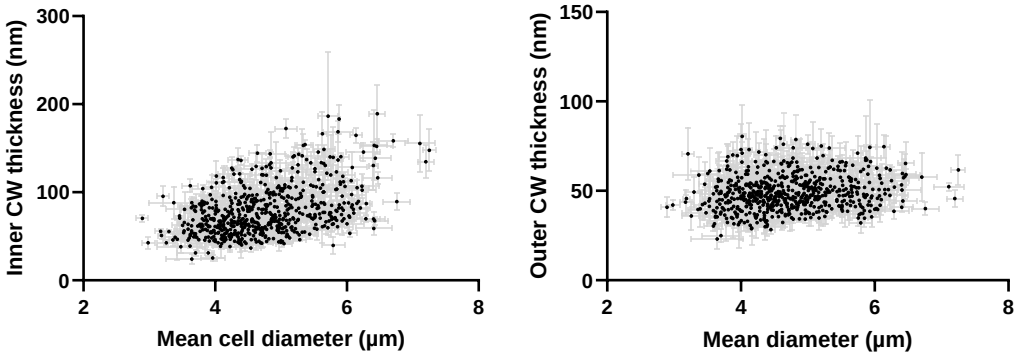

Figure A.2: Cell wall thickness compared to the mean diameter of the corresponding cell. The clouds correspond to the merging of data points from the four conditions at 0 h, 40 h and 88 h. For each cell, the inner cell wall, outer cell wall and cell thickness were measured from TEM images on three regions with the ImageJ software.

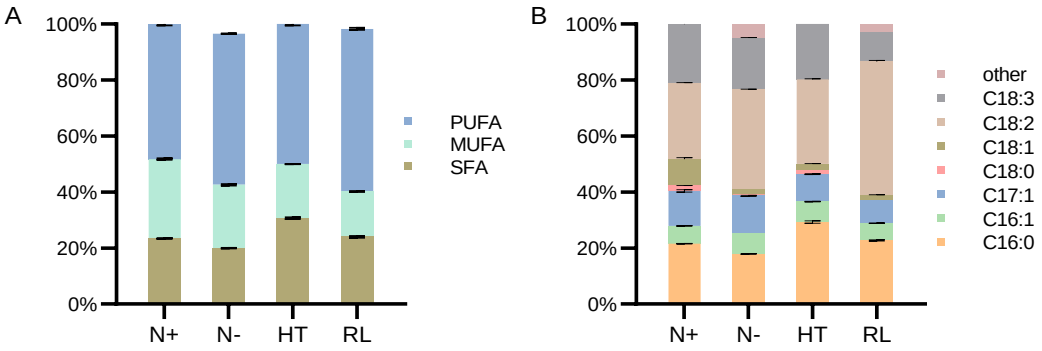

Figure A.3: FAME profile of *Chlorella vulgaris* CCALA924 according to four growth conditions, after 7 days (160 h).

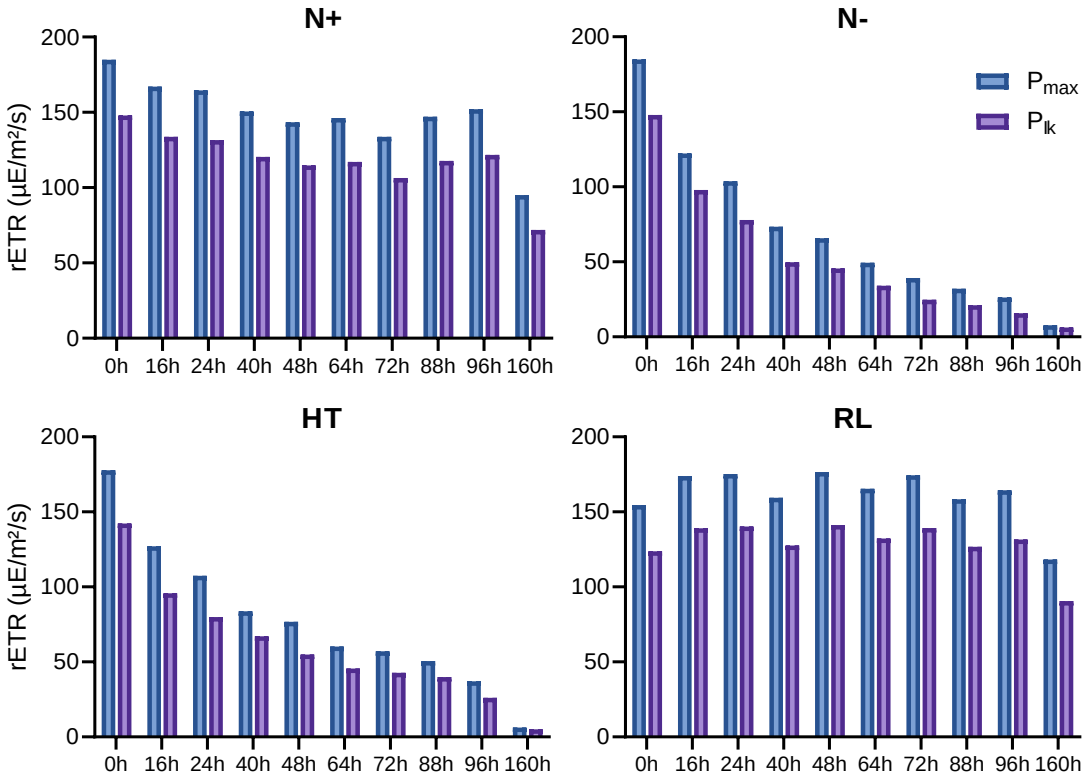

Figure A.4: Relative electron transport rate (rETR) over the starch induction time. rETR is the quantity of photons entering the PSII and can be assimilated to the photosynthetic rate, assuming that incident light is fully absorbed. For more details about P_{max} and P_{Ik}, please refer to Figure A.6. The reported results are issued from one measurement (n=1).

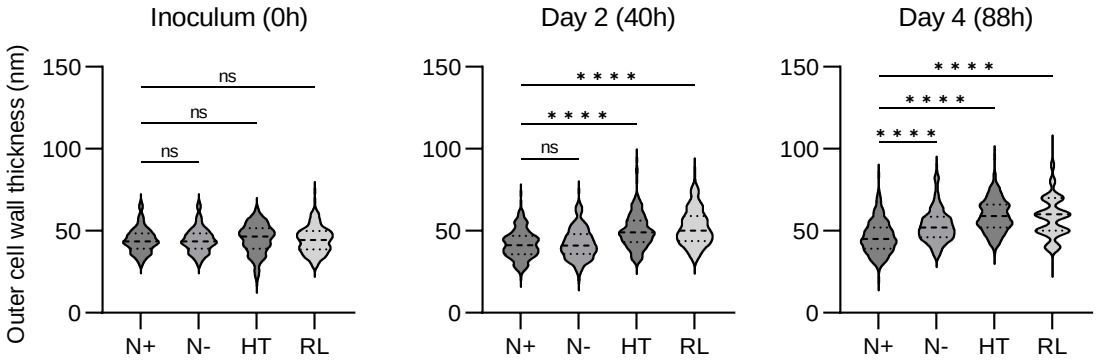

Figure A.5: Thickness of the outer cell wall, measured on three regions for at least 60 cells per condition. The p-values for the comparisons indicated in the graph were calculated with Prism 9 (Graphpad Software, LLC) and based on ANOVA Dunnett's multiple comparisons test (****, $P < 0.0001$, n>160).

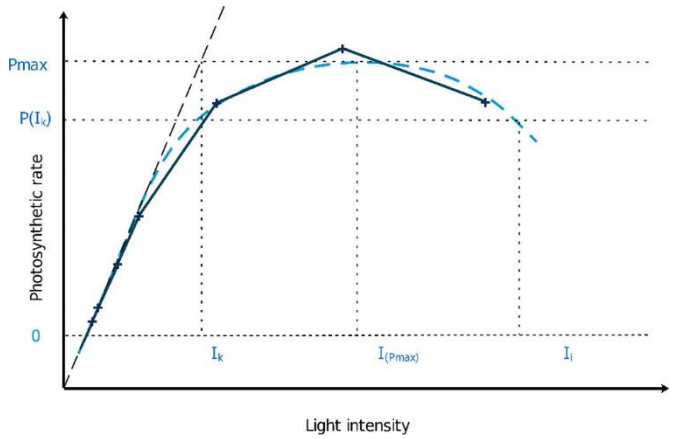

Figure A.6: Illustration of an instantaneous light curve obtained by fluorometric assay and the associated key values. P_{max} is the maximum rate of photosynthesis, often reached at high light intensities. P_{Ik} is the photosynthetic rate at the intensity I_k. I_k is the light intensity corresponding to the intersection point between the theoretical linear relationship and P_{max} (delimiting the end of the photolimitation zone). Reproduced by courtesy of (Levasseur et al., 2023).

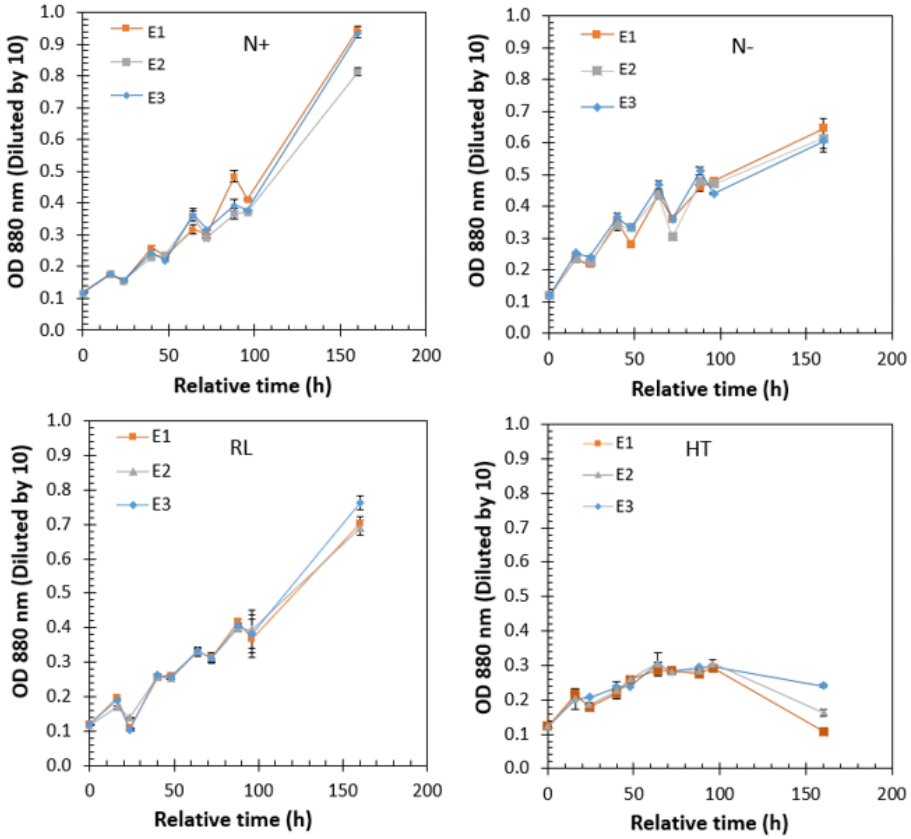

Figure A.7: Optical density of the biological triplicates in the 4 conditions; OD_{880nm} measures are obtained after a 10 fold dilution and substraction of the blank (cuvette filled up with medium).

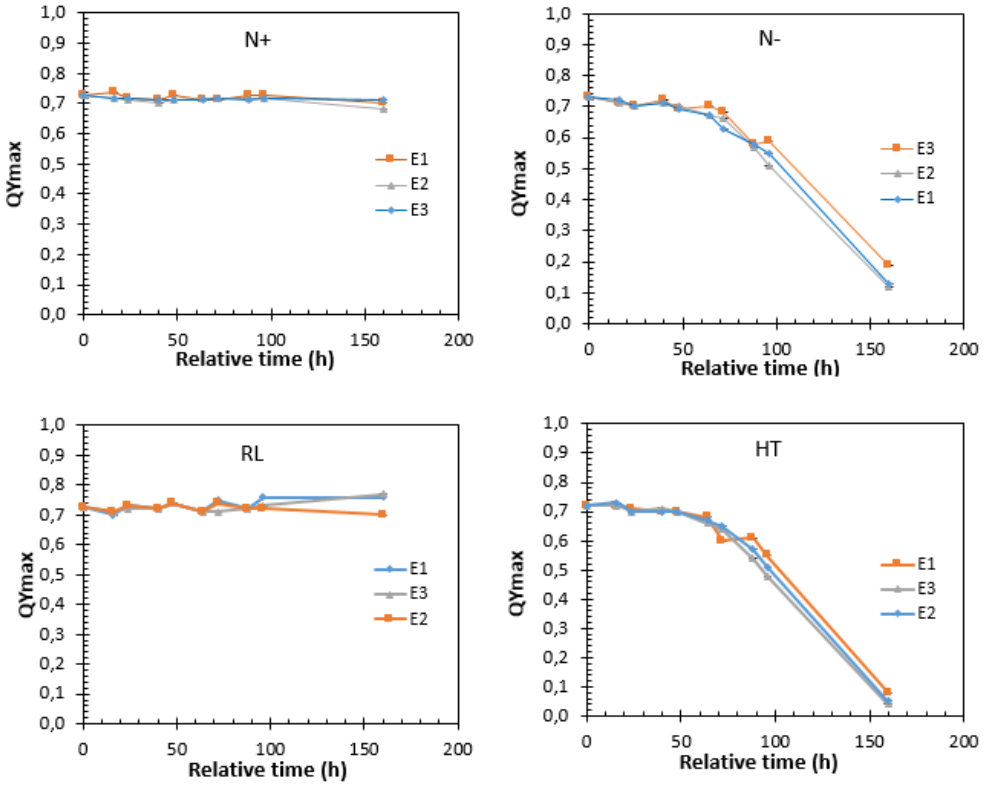

Figure A.8: Measurement of the maximal quantum yield (QYmax) of the biological triplicates in the 4 conditions, after dilution of the sample to 0.1 OD_{880nm} (no technical replicate performed).

Appendix B. Light input in vertical cylindrical bottle and ⁀ at panel PBR

This appendix focus on the quantification of light input in vertical cylindrical bottle by three different models. It also describes the light quantification in flat-panel PBR.

Context:

Light intensity is often measured by flat horizontal sensors as the global horizontal irradiance (GHI). One way to account for the total light incoming to the surface of the PBR is to directly transpose the horizontal measurement to the illuminated surface of the PBR. This approach of direct equivalence was tested as a first hypothesis.

However, the direct equivalent model is an extreme simplification of light behavior. Indeed, the amount of light reaching a surface is dependent of its orientation towards the sun. In practice, one needs to integrate the position, geometry and orientation of the PBRs to transpose the horizontal light measurement GHI into incident light. Moreover, the solar position along time, light reflection events, as well as the direct and diffuse light input should be considered. For this approach, we considered an adapted version of the model presented by Slegers for tubular and flat panel PBRs (Slegers et al., 2013, 2011).

Alternatively to modelling the incident light from horizontal data, one can directly measure the light within the PBRs, and transpose it to the total light received by the PBR. For this approach, we used spherical sensor integrating incoming photons 0°-360° around its top-bottom axis with an angle of 100° from the top of the sphere. Those measurements where then transposed to incident light on the cylindrical surface of the bottle by applying the view factor presented by Cornet et al., assuming completely diffuse or direct light, and a mix of both diffuse and direct light (Cornet et al., 2023).

Methodology of light measurement during biological experiment:

Here, PBRs were vertical cylindrical 1L bottles in borosilicate. During microalgae cultivation, three bottles were aligned in the south-north axis, with a fourth bottle on the south side to ensure similar shadowing in the three PBRs. PBRs were disposed in a temperature-regulated water tank in glass. Later, the effect of water and glass of the regulation tank were neglected. This set-up was protected by a small greenhouse wrapped with diffusing film, as presented in figure Figure II.2. GHI (global horizontal irradiance) were registered every 30 s on the top of the water tank with a flat sensor (MQS-B, Walz, Germany).

Methodology of light measurement independent from biological experiment:

To compare the data from flat light sensor, new measurements were conducted with a spherical sensor on the next year, with very close seasonality and identical sunny weather. Spherical measurements were done every 5 min directly in the water-filled bottles. Spherical sensors (US-SQS/L, Walz, Germany) were placed in the middle of

the cylindrical part of bottle and along the middle axis. The horizontal interface of bottles was covered with a black polymer to ensure that all incident light was coming from the cylindrical surface.

Similarly, both the horizontal and spherical diffuse-direct light proportions were measured every 1 h during an average sunny day of the same season. Diffuse light was measured by blocking the direct light with a 5 cm opaque disc, placed at close distance (roughly 15cm) from the horizontal flat or spherical sensor. From the actual measurements, proportion of direct and diffuse light was estimated to be constant during the day at 55% diffuse light. Despite the absence of clouds, this high proportion of diffuse light was explained by the presence of the diffusing film around the small greenhouse. The measured proportion of direct and diffuse light was then transposed to other days.

B.1. Direct equivalent model (⌒ at sensor)

Light measurement of horizontal sensor was directly transposed to the illuminated surface of the PBR. The surface considered is the addition of the horizontal surface and half the cylindrical surface.

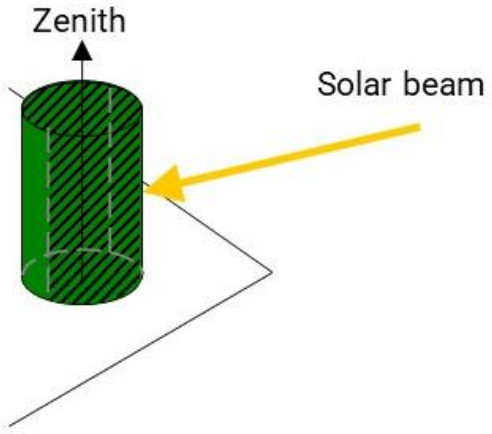

Figure B.1: Representation of surface considered for the direct equivalent model

B.2. Slegers-adapted model (⌒ at sensor)

Here, the cylindrical and horizontal surface of the PBR were treated separately but accordingly to the same model adapted from (Slegers et al., 2011).

B.2.1. Solar incidence angle

The direct light incoming on the cylindrical PBR surface varies with the solar position. Figure B.2 shows how the solar incidence angle ϑ depends on the solar hour angle ω and the orientation γ. The solar elevation α_v is shown. In-depth, the calculation of the solar incidence angle ϑ (°) involves considering several factors, such as the solar declination δ (°) representing the sun angular position at solar noon relative to the equator plane. Additionally, it takes into account the latitude of the reactor location φ (°), the slope angle of the reactor with the ground surface β (°), the surface azimuth

angle γ (°) between the normal of the reactor surface and the south direction, and the solar hour angle ω (°):

$$\cos(\vartheta(\gamma,t)) = \sin\delta\sin\varphi\cos\beta - \sin\delta\cos\varphi\sin\beta\cos\gamma + \cos\delta\cos\varphi\cos\beta\cos\omega + \cos\delta\sin\varphi\sin\beta\cos\gamma\cos\omega + \cos\delta\sin\beta\sin\gamma\sin\omega \quad (11)$$

The angles β and φ are fixed, the angle δ depends on the day of the year and the angle γ varies with ω. The solar hour angle ω depends on the solar hour and is the angle between the horizontal solar incidence and the north-south axis. The angles δ and ω were calculated accordingly to the method provided by NOAA and based on equations from (Meeus, 2009).

The zenith angle ϑ_z is complementary of the solar elevation α_v and is given by:

$$\vartheta_z = 90 - \alpha_v \quad (12)$$

$$\cos(\vartheta_z) = \sin\delta\sin\varphi + \cos\delta\cos\varphi\cos\omega \quad (13)$$

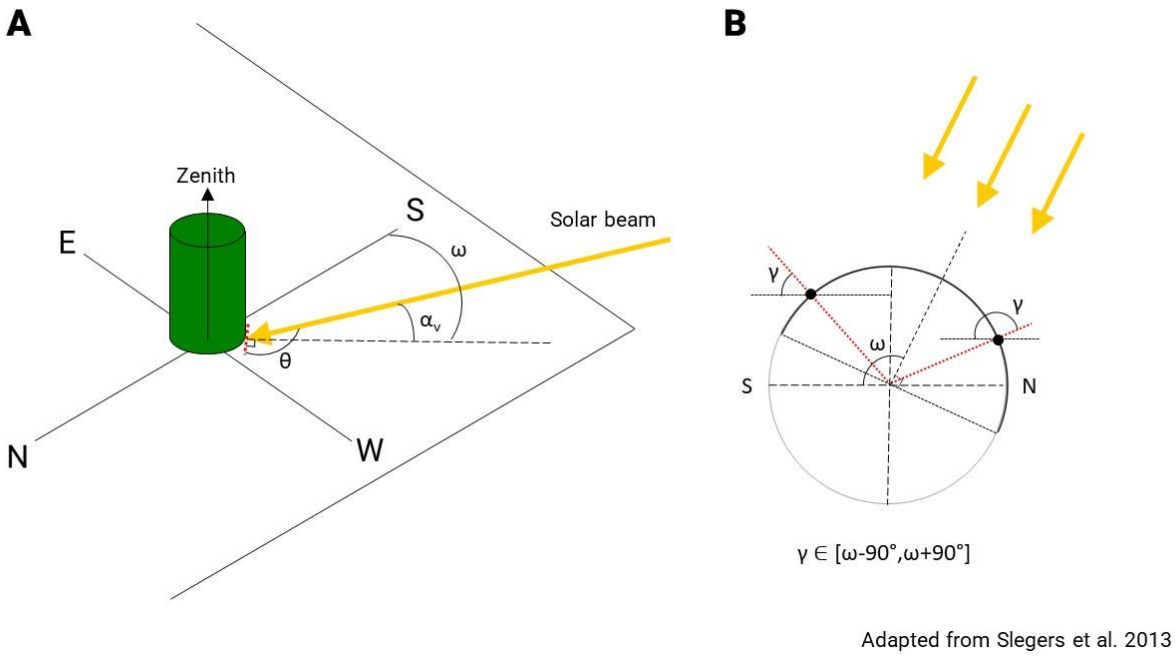

Figure B.2: Description of light beams incidence on the PBR surface.illustrates the main relevant angles ω, α_v and ϑ variating with time and (B) shows how the solar incidence angle ϑ varies with γ for every point of the cylindrical surface. Adapted from (Slegers et al., 2013).

B.2.2. Light input

Horizontal light measurements, or GHI, are converted into light on the PBR surface by geometric factors according to the method performed by Slegers et al. (Slegers et al., 2013, 2011). The PBR surface is divided between the cylindrical surface, called side surface, and the horizontal surface, called top surface. The geometric factors are different for direct and diffuse radiation:

$$G_{direct}(t) = \frac{\cos\theta(\gamma, t)}{\cos\theta_z(t)} \tag{14}$$

where ϑ the solar incidence angle and ϑ_z the solar zenith angle are varying accordingly to time and over the range of the surface azimuth angle γ (°), $\gamma \in [\omega\text{-}90°, \omega+90°]$. For the side surface, β is equal to 90°. In the case of the top surface, β=0° and $\cos\theta = \cos\theta_z$, resulting in $G_{direct,horizontal} = 1$.

$$G_{diffuse} = \frac{1 + \cos(\beta)}{2} \tag{15}$$

And therefore:

$$G_{diffuse,side} = 0.5 \text{ and } G_{diffuse,top} = 1 \tag{16)(17}$$

In addition, for side surface both diffuse and direct light are influenced by the ground reflected radiation and the ground reflectivity ρ such as:

$$G_{reflect,side} = \rho * \frac{1 + \cos(\beta)}{2} \tag{18}$$

with ρ=0.5 for white lining.

Therefore:

$$G_{reflect,side} = 0.25 \tag{19}$$

Ground reflection for top surface is assumed null.

Finally, the total light received on the top and side surface of the PBR is given by:

$$\begin{aligned} I_{0,side}(t) = \left(G_{direct,side}(t) + G_{reflect,side}\right) * I_{direct\ \text{measured}}(t) \\ * P_{g\ direct,side}(t) + \left(G_{diffuse,side}(t) + G_{reflect,side}\right) \\ * I_{diffuse\ \text{measured}}(t) * P_{g\ diffuse,side}(t) \end{aligned} \tag{20}$$

$$\begin{aligned} I_{0,top}(t) = G_{direct,top} * I_{direct\ \text{measured}}(t) * R_{g\ direct,top}(t) + G_{diffuse,top} \\ * I_{diffuse\ \text{measured}}(t) * R_{g\ diffuse,top}(t) \end{aligned} \tag{21}$$

Where P_g is the coefficient of passing light after loss by reflection at the PBR surface. Details about P_g calculations are described in the section below.

B.2.3. Light re_ection at and absorbance of the PBR wall

Figure B.3: Refraction and reflection of light at the different parts of the reactor wall. represents the succession of interfaces encountered by light. For the cylindrical face of the reactor, the interfaces occur between the water of the thermoregulated bath, the reactor wall in borosilicate and the water of the culture. For the horizontal face of the culture, the interfaces are between the air, the reactor wall, the air and the culture. The initial incidence angle of direct is the solar incidence angle, either corrected by the reactor wall slope ŝ. The angle of incidence for diffuse light is assumed to be 60° on any part of the reactor wall (Duffie and Beckman, 2013). Then, the succession of incidence and refraction angles is calculated from the Snell–Descartes equation (22).

$$\theta_r = \sin^{-1}\left(\frac{n_i}{n_r}\sin\theta_i\right) \tag{22}$$

Where ϑ_r and ϑ_i are the refraction and incidence angle respectively, and n_r and n_i are the refractive index of the material before and after the interface, respectively. Here, the refractive index were n_{Air}=1.00, $n_{Borosilicate}$=1.473 and n_{Water}=1.33.

The final extend of light loss due to reflection events is calculated from the Fresnel equations. The reflection of p-polarized and s-polarized light are formulated by (23) and (24), respectively.

$$R_p(\theta_i) = \left(\frac{\frac{n_r}{n_i}\cos\theta_i - \cos\theta_r}{\frac{n_r}{n_i}\cos\theta_i + \cos\theta_r}\right)^2 \tag{23}$$

$$R_s(\theta_i) = \left(\frac{\cos\theta_i - \frac{n_r}{n_i}\cos\theta_r}{\cos\theta_i + \frac{n_r}{n_i}\cos\theta_r}\right)^2 \tag{24}$$

As the sunlight is unpolarized, the global reflection equals to the mean of p- and s- polarized light. Therefore, the coefficient of light loss by reflection at the interface k is given by:

$$P_k = 1 - \left(\frac{R_p + R_s}{2}\right) \tag{25}$$

The global coefficient of passing light after reflection P_g is the product of the coefficients P_k corresponding to each interface crossed by light path.

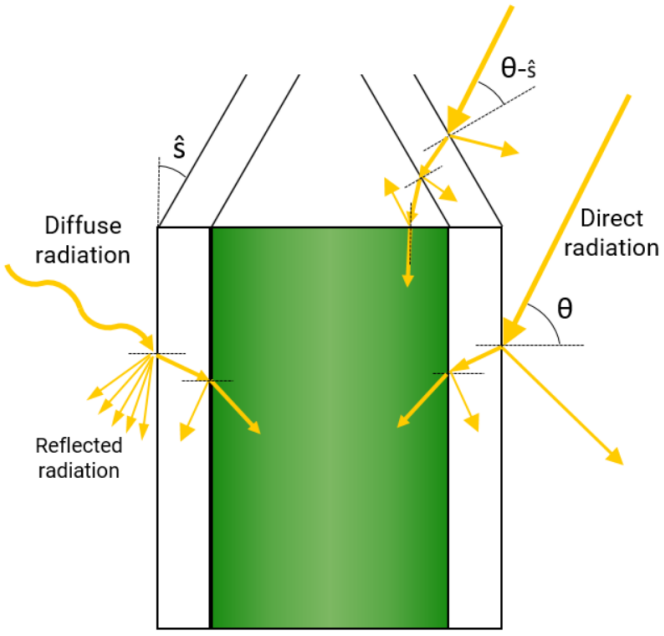

Figure B.3: Refraction and reflection of light at the different parts of the reactor wall. Light is partly lost due to reflection. The angle ŝ is the slope of the upper part of the bottle, with ŝ=30°. The incidence angle of diffuse light is considered constant at 60°. Adapted from (Slegers et al., 2011).

In addition, the absorbance of the material A_m lead to further light loss. Here, Duran bottles were made in borosilicate, with A_m=0.07 (constructor data, personal communication). Despite being high, this value was selected to ensure conservativeness over the different wavelength of the PAR.

The total incident light flux received by the culture at the time t is equal to (26):

$$L_0(t) = \left(I_{0,side}(t) * S_{side} + I_{0,top}(t) * S_{top}\right) * (1 - A_m) \quad (26)$$

where S_{side} and S_{top} are the area of cylindrical (side) and horizontal (top) surfaces, and $L_0(t)$ is in mol_{photon}/s.

Finally, the mean total incident light flux L_m (in mol_{photon}/s) is calculated by integration of I_0 over the period of interest:

$$L_m = \frac{\left(\sum_{t=t_1}^{t_n} L(t)\right) * \Delta d}{t_n - t_1} \quad (27)$$

where Δd is the duration between two measurements and t the time of measurement such as t_1 is the first and t_n is the last of the period of interest, so that t_n-t_1 represents the total duration of considered period. The mean total incident light

flux density I_m (in $mol_{photon}/m^2/s$) is calculated as the ratio of L_m and the total surface S.

B.2.4. Shading by neighboring bottles and light transmission are negligible

The shading between the bottles aligned in the south-north axis was neglected. Indeed, bottles self-shadowing at noon was estimated to less than 5% of incident light reduction on the cylindrical part of the PBR. This estimation was calculated from the method proposed by (Slegers et al., 2011) assuming the bottles to be flat panel reactors of height correspond to culture height in the bottles and separated by the distance between the middle of one bottle and the nearest extremity of the next.

The light transmission was also evaluated as negligible after Beer-Lambert estimation. Overall, only the highest light-per-biomass bottle shown an initial transmittance of 10%. Therefore, the light transmission was completely neglected over the nine bottles range. Briefly, Beer-Lambert law was used to calculate the proportion of transmitted light from the mean direct incident light on the cylindrical part. For this, the biomass absorption over the 400-700nm range for each bottle was calculated by applying a DW-to-absorbance conversion factor. This conversion factor was calculated from previous data on chlorophyll-rich biomass, and the dry weight measurements were those of the experiment start. Also, the round bottle was considered to be rectangle, with the length of its light-exposed face equal to bottle diameter D and the length of light-path L calculated to conserve the original surface A of bottle section (L=A/D). Despite relying on many hypothesis, these calculations are based on rather conservative assumptions that overestimate light transmission, such as the omission of incidence angle leading to shortened light path.

B.3. Cornet-adapted model (spherical sensor)

The spherical sensor light measurements are transposed to the light incidence on the cylindrical surface of the PBR by the view factors proposed by Cornet el al. (Cornet et al., 2023). This method was developed for cylindrical PBR radially illuminated with a surrounding light source device of known degree of collimation. To adapt this original model to the natural sunlight case, we considered the measured light to be either: fully diffuse (Lambertian case), fully collimated with normal incidence, or a mix of both diffuse and collimated in the proportion of the diffuse/direct ratio measured every hour on a typical sunny day. The photon flux density (PFD) on the cylinder surface q_0 is calculated from the measured fluence rate Ψ:

$$\text{Fully diffuse light: } q_o(t) = \frac{\Psi(t)\, R_s}{4\, R_c} \tag{28}$$

$$\text{Fully collimated light: } q_o(t) = \frac{\Psi(t)\sqrt{1+\left(\frac{R_c}{H}\right)^2}}{4} \tag{29}$$

$$\text{Mix diffuse-collimated light: } q_o(t) = \frac{\Psi_{diffuse}(t)\, R_s}{4\, R_c} + \frac{\Psi_{collimated}(t)\sqrt{1+\left(\frac{R_c}{H}\right)^2}}{4} \tag{30}$$

With:

$$\Psi_{diffuse}(t) = \Psi_{total}(t) * P_{diffuse} \tag{31}$$

$$\Psi_{collimated}(t) = \Psi_{total}(t) * P_{collimated} \tag{32}$$

Where R_s and R_c are the radius of the sensor and the cylinder, H is the height of the cylinder, and $P_{diffuse}$ and $P_{collimated}$ are the proportion of diffuse and collimated light.

The incident light entering the culture from the horizontal surface is calculated from the Slegers-adapted model. Then the total incident light is obtained by adding the horizontal and cylindrical incident light.

B.4. Model comparison

Table B.1 compares the light quantification performed by the three different models for three consecutive days. The days of measurement were chosen to be closely similar to the light conditions encounter by microalgae cultures during the experiment (complete sun with no cloud, similar date of the following year). Despite using different sources of measurement, equations and hypothesis, the three models (direct equivalent, Slegers-adapted and Cornet-adapted diffuse/direct mix) returned similar results.

Finally, the Slegers-adapted model was chosen to quantify the light in the bottles for the biomass experiment. Indeed, light measurement with flat sensor is more practical than spherical measurement. Moreover, our adaptation of the Slegers model is well adapted to our design, while the Cornet model was not primarily designed for solar light quantification.

Model used		Horizontal sensor		Spherical sensor		
		Direct equivalent model	Slegers-adapted model	Cornet-adapted model		
				Hypothesis 1: collimated light	Hypothesis 2: diffuse light	Hypothesis 3: mix diffuse/ collimated
Mean daily light flux L_m ($\mu mol_{phot}/s$)	10/10/2023	27,8	32,9	6,4	34,4	28,2
	11/10/2023	25,0	29,5	5,8	30,7	25,1
	12/10/2023	26,3	30,7	6,1	33,7	27,3

Table B.1: Light quantification according to the different light models. The models transform the light measured by horizontal or spherical sensors on three consecutive sunny days of October 2023 into the mean daily light flux L_m received in the culture vessel. The Cornet-adapted model is applied following three different hypotheses about light: completely collimated light of normal incidence, completely diffuse light, and a mix of diffuse and collimated light (based on measurements).

B.5. Light input in vertical ͡ at panel PBR

The incident light of the air lift flat panel PBR was quantified with the model of Slegers et al. 2011 without adaptation (Slegers et al., 2011). The light transmission Tm through the PBR material was estimated to be Tm=0.8 based on light transmission measurements. The PBR material is PVC, therefore we considered n_{PVC}=1.53 for reflection calculations. Diffuse/direct light ratio was estimated in a similar way to the bottle set-up, and considered constant at 55% diffuse light.

Alternatively, the incident light on the flat panel PBR was also quantified by direct equivalent approach. Two light sensors were placed on the top of the PBR, and directed towards the normal of the PBR surface, one on each face. Then, the total light received was approximated as the sum of the light measurements from both sensors. However, this method was found to overestimated the received light compared to the Slegers method by approximately 40%.

Appendix C. Supplementary material Paper II

Experimental data

Relative time (h)	Biomass concentration Cx (g/L) n=3	Total chlorophyll content (%) n=3	Carbohydrate content (%) n=3	Cell density (cell/mL) n=3
0.00	0.98 ± 0.01	4.2 ± 0.1 %	20.9 ± 0.6 %	5.3 ± 0.1 E+7
2.00	1.09 ± 0.01	3.9 ± 0.0 %	n.d.	5.4 ± 0.4 E+7
4.50	1.19 ± 0.03	3.7 ± 0.1 %	39.2 ± 5.4 %	n.d.
7.25	1.38 ± 0.04	3.2 ± 0.3 %	52.7 ± 1.5 %	6.3 ± 0.2 E+7
21.25	1.32 ± 0.02	3.5 ± 0.1 %	46.1 ± 0.7 %	8.7 ± 0.6 E+7
23.67	1.42 ± 0.03	3.3 ± 0.1 %	n.d.	8.5 ± 0.4 E+7
26.25	1.61 ± 0.05	2.9 ± 0.1 %	58.9 ± 1.9 %	8.9 ± 0.2 E+7
28.50	1.81 ± 0.04	2.5 ± 0.2 %	n.d.	n.d.
31.25	2.03 ± 0.05	2.3 ± 0.1 %	75.0 ± 1.6 %	10.2 ± 0.4 E+7
45.17	1.88 ± 0.06	2.5 ± 0.1 %	67.2 ± 1.7 %	11.3 ± 2.6 E+7
47.42	1.95 ± 0.06	2.4 ± 0.1 %	n.d.	9.6 ± 0.9 E+7
50.00	2.14 ± 0.06	2.1 ± 0.1 %	81.7 ± 0.5 %	10.4 ± 0.1 E+7
52.42	2.31 ± 0.07	1.9 ± 0.0 %	n.d.	10.3 ± 0.5 E+7
55.75	2.63 ± 0.07	1.7 ± 0.1 %	82.0 ± 4.0 %	11.6 ± 0.7 E+7

Table C.1: Data set of the laboratory experiment with long nights. The letter n indicates the number of analytical replicate and n.d. stands for no data. The reported error corresponds to the standard deviation.

	Relative time (h)	X1.25_ T100	X1.25_ T50	X1.25_ T25	X0.20_ T100	X0.20_ T50	X0.20_ T25	X0.15_ T100	X0.15_ T50	X0.15_ T25
Biomass concentration Cx (g/L) n=3	0.00	1.24 ± 0.02	1.24 ± 0.02	1.24 ± 0.02	0.20 ± 0.00	0.20 ± 0.00	0.20 ± 0.00	0.13 ± 0.00	0.13 ± 0.00	0.13 ± 0.00
	5.25	2.07 ± 0.10	1.88 ± 0.10	1.44 ± 0.08	0.55 ± 0.02	0.52 ± 0.02	0.39 ± 0.02	0.37 ± 0.03	0.37 ± 0.03	0.30 ± 0.04
	20.75	2.01 ± 0.05	1.84 ± 0.05	1.47 ± 0.05	0.57 ± 0.03	0.51 ± 0.03	0.40 ± 0.02	0.40 ± 0.02	0.38 ± 0.02	0.31 ± 0.02
	29.25	2.87 ± 0.10	2.44 ± 0.10	2.21 ± 0.10	0.79 ± 0.04	0.76 ± 0.04	0.65 ± 0.04	0.56 ± 0.03	0.55 ± 0.03	0.50 ± 0.03
	45.00	2.89 ± 0.10	2.67 ± 0.10	2.01 ± 0.10	0.81 ± 0.04	0.78 ± 0.04	0.65 ± 0.04	0.57 ± 0.03	0.56 ± 0.03	0.52 ± 0.03
	53.00	3.33 ± 0.11	3.31 ± 0.11	2.59 ± 0.10	0.94 ± 0.04	0.92 ± 0.04	0.86 ± 0.04	0.65 ± 0.03	0.68 ± 0.03	0.62 ± 0.03
	75.75	n.d.	n.d.	3.13 ± 0.17	n.d.	0.99 ± 0.06	n.d.	0.69 ± 0.04	n.d.	n.d.
	147.75	n.d.	n.d.	5.51 ± 0.11	n.d.	1.41 ± 0.07	n.d.	1.16 ± 0.06	n.d.	n.d.
Total chlorophyll content (%) n=2	0.00	3.6 ± 0.5%	3.6 ± 0.5%	3.6 ± 0.5%	3.6 ± 0.5%	3.6 ± 0.5%	3.6 ± 0.5%	3.6 ± 0.5%	3.6 ± 0.5%	3.6 ± 0.5%
	5.25	2.8 ± 0.5%	3.3 ± 0.5%	4.2 ± 0.7%	1.1 ± 0.2%	1.2 ± 0.2%	1.8 ± 0.2%	1.0 ± 0.2%	1.1 ± 0.2%	1.5 ± 0.2%
	20.75	2.9 ± 0.5%	3.4 ± 0.6%	3.8 ± 0.6%	1.2 ± 0.3%	1.4 ± 0.3%	2.2 ± 0.5%	1.1 ± 0.3%	1.2 ± 0.3%	1.7 ± 0.3%

	29.25	1.8 ± 0.3%	2.2 ± 0.3%	2.6 ± 0.4%	0.7 ± 0.2%	0.8 ± 0.2%	1.2 ± 0.2%	0.6 ± 0.2%	0.8 ± 0.2%	0.9 ± 0.2%
	45.00	2.0 ± 0.5%	2.5 ± 0.5%	3.1 ± 0.6%	0.7 ± 0.3%	0.8 ± 0.3%	1.2 ± 0.3%	0.7 ± 0.2%	0.8 ± 0.2%	1.0 ± 0.3%
	53.00	1.6 ± 0.3%	2.0 ± 0.3%	2.5 ± 0.3%	0.5 ± 0.2%	0.6 ± 0.1%	0.9 ± 0.1%	0.5 ± 0.2%	0.6 ± 0.1%	0.8 ± 0.1%
	75.75	n.d.	n.d.	1.6 ± 0.2%	n.d.	0.6 ± 0.2%	n.d.	0.5 ± 0.2%	n.d.	n.d.
	147.75	n.d.	n.d.	1.4 ± 0.2%	n.d.	0.5 ± 0.1%	n.d.	0.3 ± 0.1%	n.d.	n.d.
Carbohydrate content (%) n=3	0.00	23.1 ± 0.9%	23.1 ± 0.9%	23.1 ± 0.9%	23.1 ± 0.9%	23.1 ± 0.9%	23.1 ± 0.9%	23.1 ± 0.9%	23.1 ± 0.9%	23.1 ± 0.9%
	5.25	41.0 ± 1.8%	39.2 ± 3.2%	37.0 ± 1.8%	58.0 ± 0.8%	60.0 ± 1.6%	53.0 ± 0.5%	57.5 ± 0.7%	53.4 ± 1.5%	48.2 ± 1.7%
	20.75	34.3 ± 2.6%	30.9 ± 0.9%	25.8 ± 1.1%	56.3 ± 1.9%	51.2 ± 7.3%	44.9 ± 0.9%	61.6 ± 3.7%	57.6 ± 3.2%	50.9 ± 0.7%
	29.25	51.9 ± 0.3%	47.8 ± 2.4%	40.1 ± 1.6%	65.5 ± 0.1%	66.9 ± 1.4%	62.9 ± 1.9%	63.1 ± 3.4%	66.6 ± 0.5%	62.7 ± 3.5%
	45.00	49.4 ± 1.4%	46.7 ± 0.9%	37.0 ± 5.3%	66.8 ± 2.4%	67.4 ± 2.0%	66.0 ± 0.9%	67.2 ± 0.5%	63.3 ± 6.5%	64.7 ± 1.1%
	53.00	57.6 ± 3.2%	54.0 ± 1.1%	43.4 ± 2.5%	68.8 ± 5.2%	70.9 ± 0.6%	67.7 ± 3.8%	68.8 ± 2.2%	69.5 ± 2.0%	68.5 ± 4.0%
	75.75	n.d.	n.d.	50.9 ± 3.7%	n.d.	65.6 ± 2.6%	n.d.	66.5 ± 3.7%	n.d.	n.d.
	147.75	n.d.	n.d.	53.0 ± 2.8%	n.d.	62.8 ± 0.3%	n.d.	51.6 ± 0.5%	n.d.	n.d.
Cell density (cell/mL) n=1	0.00	4.2E+7	4.2E+7	4.2E+7	6.7E+6	6.7E+6	6.7E+6	4.4E+6	4.4E+6	4.4E+6
	5.25	4.6E+7	4.7E+7	4.6E+7	7.1E+6	7.0E+6	7.2E+6	4.6E+6	4.6E+6	4.3E+6
	20.75	1.4E+8	1.1E+8	7.1E+7	2.4E+7	2.4E+7	2.3E+7	1.6E+7	1.6E+7	1.6E+7
	29.25	1.6E+8	1.3E+8	9.7E+7	2.8E+7	2.6E+7	3.0E+7	2.1E+7	1.9E+7	1.9E+7
	45.00	1.6E+8	1.7E+8	1.2E+8	2.7E+7	2.5E+7	2.4E+7	1.7E+7	1.9E+7	1.6E+7
	53.00	1.7E+8	1.6E+8	1.3E+8	2.7E+7	2.4E+7	2.6E+7	1.8E+7	1.8E+7	1.8E+7
	75.75	n.d.	n.d.	n.d.	n.d.	n.d.	n.d.	n.d.	n.d.	n.d.
	147.75	n.d.	n.d.	n.d.	n.d.	n.d.	n.d.	n.d.	n.d.	n.d.
Chla/b ratio (-) n=2	0.00	3.17 ± 0.45	3.17 ± 0.45	3.17 ± 0.45	3.17 ± 0.45	3.17 ± 0.45	3.17 ± 0.45	3.17 ± 0.45	3.17 ± 0.45	3.17 ± 0.45
	5.25	3.18 ± 0.07	3.30 ± 0.09	3.37 ± 0.07	2.51 ± 0.17	2.57 ± 0.21	2.69 ± 0.23	2.37 ± 0.05	2.55 ± 0.00	2.68 ± 0.13
	20.75	3.22 ± 0.12	3.32 ± 0.19	3.32 ± 0.03	2.95 ± 0.00	3.00 ± 0.04	3.27 ± 0.20	2.97 ± 0.07	3.07 ± 0.15	3.09 ± 0.23
	29.25	2.82 ± 0.03	2.93 ± 0.04	2.93 ± 0.12	2.66 ± 0.08	2.60 ± 0.05	2.75 ± 0.05	2.75 ± 0.16	2.77 ± 0.05	2.69 ± 0.00
	45.00	3.13 ± 0.39	3.24 ± 0.08	3.29 ± 0.00	3.19 ± 0.09	3.11 ± 0.07	3.29 ± 0.06	3.07 ± 0.32	3.11 ± 0.00	3.26 ± 0.13
	53.00	2.89 ± 0.07	3.03 ± 0.06	2.98 ± 0.23	2.82 ± 0.20	2.80 ± 0.13	2.88 ± 0.09	2.85 ± 0.23	2.70 ± 0.05	2.71 ± 0.42
	75.75	n.d.	n.d.	2.96 ± 1.26	n.d.	2.73 ± 0.00	n.d.	2.97 ± 0.52	n.d.	n.d.
	147.75	n.d.	n.d.	2.94 ± 0.16	n.d.	2.34 ± 0.41	n.d.	3.02 ± 0.00	n.d.	n.d.
Maximum quantum yield (-) n=1	0.00	n.d.	n.d.	0.80	n.d.	0.80	n.d.	0.80	n.d.	n.d.
	5.25	n.d.	n.d.	0.75	n.d.	n.d.	n.d.	0.64	n.d.	n.d.
	20.75	n.d.	n.d.	n.d.	n.d.	n.d.	n.d.	n.d.	n.d.	n.d.
	29.25	n.d.	n.d.	0.79	n.d.	0.55	n.d.	0.35	n.d.	n.d.
	45.00	n.d.	n.d.	n.d.	n.d.	n.d.	n.d.	n.d.	n.d.	n.d.
	53.00	n.d.	n.d.	0.80	n.d.	0.49	n.d.	0.33	n.d.	n.d.

	75.75	n.d.	n.d.	n.d.	n.d.	n.d.	n.d.	n.d.	n.d.	n.d.
	147.75	n.d.	n.d.	n.d.	n.d.	n.d.	n.d.	n.d.	n.d.	n.d.

Table C.2: Data set of the 1L-bottle experiment for the nine bottles. X indicates the initial concentration (1.25, 0.2 or 0.15 g/L) and T the light transmittance on the bottle rear (100, 50 or 25 %). The letter n indicates the number of analytical replicate and n.d. stands for no data. The reported error corresponds to the standard deviation.

Relative time (h)	Biomass concentration Cx (g/L) n=3	Total chlorophyll content (%) n=3	Carbohydrate content (%) n=3	Cell density (cell/mL) n=3	Chla/b ratio (-) n=3	Maximal quantum yield (-) n=3
0	0.52 ± 0.00	3.8 ± 0.1%	28.5 ± 0.4%	1.79 ± 0.04 E+7	3.63 ± 0.32	0.68 ± 0.01
4.5	0.81 ± 0.01	2.5 ± 0.0%	43.8 ± 5.0%	1.63 ± 0.05 E+7	3.65 ± 0.19	0.72 ± 0.01
20	0.93 ± 0.02	2.0 ± 0.0%	44.1 ± 9.0%	3.15 ± 0.05 E+7	3.80 ± 0.21	0.69 ± 0.02
28.5	1.19 ± 0.04	1.4 ± 0.2%	58.7 ± 2.5%	3.28 ± 0.06 E+7	3.79 ± 1.78	0.63 ± 0.02
44	1.29 ± 0.01	1.3 ± 0.0%	59.9 ± 1.2%	3.34 ± 0.09 E+7	4.25 ± 0.15	0.65 ± 0.02
52.5	1.50 ± 0.01	1.1 ± 0.0%	58.8 ± 4.6%	3.28 ± 0.03 E+7	4.38 ± 0.00	0.57 ± 0.00
68	1.52 ± 0.01	1.1 ± 0.1%	64.0 ± 1.7%	3.41 ± 0.12 E+7	4.25 ± 1.10	0.59 ± 0.01
76.5	1.62 ± 0.05	1.0 ± 0.1%	60.8 ± 3.0%	3.20 ± 0.11 E+7	3.84 ± 0.71	0.49 ± 0.04

Table C.3: Data set of the 180L PBR experiment. The letter n indicates the number of analytical replicate. The reported error corresponds to the standard deviation.

	Carbohydrate content				Relative carbohydrate productivity			Photosynthesis efficiency		
	C_{CHO}^{min}	K_{C1}	K_{C2}	C_{CHO}^{max}	K_{P1}	K_{P2}	$P_{CHO}^{rel,ma}$	PE_{CHO}^{max}	K_1^{PE}	K_2^{PE}
Day 1	0.2	0.038	9.781E-06	0.436	1.458E-04	0.219E-04	18.400	26.2	0.421	0.502
Day 2	0.2	0.051	51.767E-06	0.592	2.534E-04	1.096E-04	12.822	26.2	0.148	0.836
Day 3	0.2	0.086	51.349E-06	0.584	3.044E-04	1.314E-04	7.786	26.2	0.175	0.902

Table C.4: Calculated values of the identification parameters used to draw the relationship between the photon flux per biomass and the starch accumulation.

Appendix D. Extended summary (French)

Introduction

Les plastiques sont une source majeure de pollution environnementale. En effet, l'absence de gestion adéquate des déchets plastiques entraîne leur relargage continu dans l'environnement, totalisant 22 Mt par an à l'échelle mondiale en 2019. Ces déchets plastiques s'accumulent dans les milieux aquatiques, atteignant 139 Mt en 2019, avec une projection stupéfiante de 493 Mt d'ici 2060.

Les impacts néfastes des déchets plastiques sur la santé humaine et des écosystèmes deviennent de plus en plus évidents. Une fois répandus dans l'environnement, les déchets plastiques se décomposent progressivement en micro- ou nano-plastiques qui peuvent entrer dans la chaîne alimentaire humaine *via* le transfert trophique, avec des risques probables pour la santé humaine. Les débris plastiques altèrent les habitats, mettent en danger la faune sauvage et perturbent le fonctionnement, les services et la productivité des écosystèmes (Beaumont et al., 2019 ; Secrétariat de la Convention sur la diversité biologique, 2012). La pollution plastique n'est pas seulement une catastrophe environnementale et un danger pour la santé publique ; elle est également un vaste gâchis économique, car la productivité des écosystèmes diminue et des milliards de dollars de valeur économique sont gaspillés par une utilisation unique et brève des plastiques.

La première et la plus évidente solution pour aborder le problème de la pollution plastique est de réduire de toute urgence notre utilisation des plastiques. Une solution secondaire et parallèle est d'augmenter l'utilisation des bioplastiques, un terme qui désigne les plastiques biodégradables ou biosourcés. Les plastiques biodégradables se décomposent spontanément lorsqu'ils sont rejetés dans l'environnement et préviennent ainsi la pollution à sa source. Les plastiques biosourcés sont dérivés d'une biomasse renouvelable et non d'une ressource fossile (pétrole), ce qui pourrait réduire les émissions mondiales de CO_2 de l'industrie plastique, à la condition qu'aucune augmentation de l'utilisation des terres ne soit nécessaire (OCDE, 2022).

Comme la production actuelle de biomasse est limitée, de nouvelles matières premières sont nécessaires pour augmenter la production de bioplastiques. Les microalgues ont un grand potentiel de production de biomasse : elles atteignent des rendements comparables aux plantes (Masojídek et al., 2013 ; Tredici, 2010) et ont la capacité de croître dans des eaux usées ou sur des terres non arables. De plus, les microalgues sont des producteurs compétitifs d'amidon (Brányiková et al., 2011), une molécule qui est à la fois une réserve d'énergie et un polymère, ce qui en fait un composant attrayant pour la fabrication de bioplastiques.

Cependant, la production industrielle de microalgues est encore limitée. Étant donné le fort potentiel des microalgues, il existe un réel intérêt à développer nos capacités de production et les procédés d'accumulation de composés spécifiques comme l'amidon.

Dans la littérature, plusieurs travaux ont ouvert la voie vers une production d'amidon par les microalgues pour des applications de bioplastiques. Brányiková et al. ont développé l'induction de l'accumulation d'amidon par carence nutritive et ont démontré qu'il est possible d'atteindre une productivité élevée en amidon en extérieur sous lumière naturelle (Brányiková et al., 2011). Cependant, les études sur les méthodes d'induction de l'amidon autres que la carence nutritive sont rares, et l'efficacité de l'accumulation d'amidon en ce qui concerne l'apport en lumière naturelle n'a jamais été étudiée. De plus, bien que l'extraction et la plastification de l'amidon aient été démontrées à l'échelle du laboratoire (Di Caprio et al., 2023 ; Gifuni, 2017a), les processus actuellement utilisés doivent être simplifiés et montés à l'échelle pilote pour envisager leur industrialisation.

Dans ce contexte, cette thèse de doctorat s'est concentrée sur la comparaison de différents facteurs d'induction de l'accumulation d'amidon, sur l'étude des conditions lumineuses optimales en conditions extérieures pour l'accumulation d'amidon, ainsi que sur le développement du processus d'extraction et de plastification de l'amidon.

Au-delà de l'application dans les bioplastiques, ce travail sur la production d'amidon ouvre également la voie à l'utilisation des microalgues comme producteurs hautement efficaces de polysaccharides, une importante bioressource renouvelable.

Etat de l art

Les microalgues sont un groupe d'organismes diversifiés présentant un haut potentiel biotechnologique. Le modèle *Chlorella vulgaris*, présenté en Figure D.1, a été sélectionné pour explorer la faisabilité de la production de bioplastiques avec les microalgues, à la fois pour sa pertinence industrielle et sa capacité à accumuler de grandes quantités d'amidon. Comme d'autres microalgues, *Chlorella vulgaris* convertit l'énergie lumineuse en biomasse grâce au processus de photosynthèse. Cependant, la machinerie photosynthétique est sensible aux fortes intensités lumineuses, ce qui implique la mise en place de mécanismes régulateurs de protection. En conséquence, les microalgues exposées à une lumière intense n'utilisent qu'une partie de la lumière tout en dissipant le reste, principalement sous forme de chaleur.

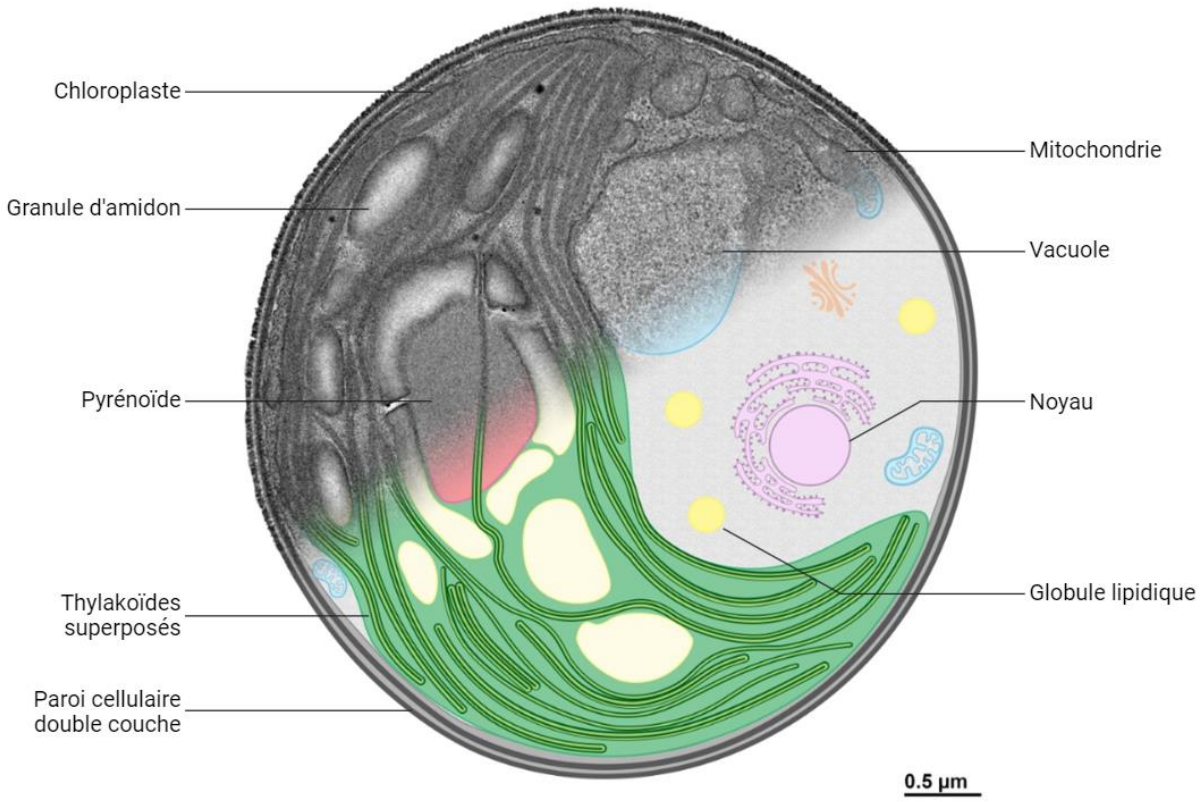

Figure D.1: Morphologie cellulaire de la microalgue *Chlorella vulgaris*. La moitié supérieure de l'image représente une image TEM réelle d'une cellule de *Chlorella vulgaris* CCALA924 cultivée dans des conditions normales. La moitié inférieure étend l'image par un schéma coloré afin de fournir une représentation plus visuelle de l'organisation subcellulaire.

L'étude de la littérature scientifique a révélé qu'un obstacle majeur à la culture des microalgues est la photosaturation et la photoinhibition qui se produisent notamment dans les couches supérieures des cultures. La courbe de photosynthèse relative à l'irradiance (courbe PI) révèle trois états d'utilisation de la lumière : la photolimitation, la photosaturation et la photoinhibition. La photolimitation est à privilégier dans les systèmes de culture en lumière solaire pour maximiser l'utilisation des photons sans nuire à la culture.

La gestion efficace de la lumière est d'une importance primordiale dans la culture des microalgues. Cependant, utiliser une lumière naturellement et aléatoirement fluctuante n'est pas simple. Par nature, les zones de photolimitation et de photoinhibition sont présentes de manière inhérente dans les cultures exposées à la lumière du soleil. Une approche pour augmenter l'efficacité de l'utilisation de la lumière est d'ajuster la concentration en biomasse pour minimiser les zones de photolimitation et de photoinhibition, tout en évitant l'apparition de zones sombres où la respiration prédomine comme illustré sur la Figure D.2. Néanmoins, l'approvisionnement optimal en lumière pour une culture accumulant de l'amidon n'a pas encore été étudié.

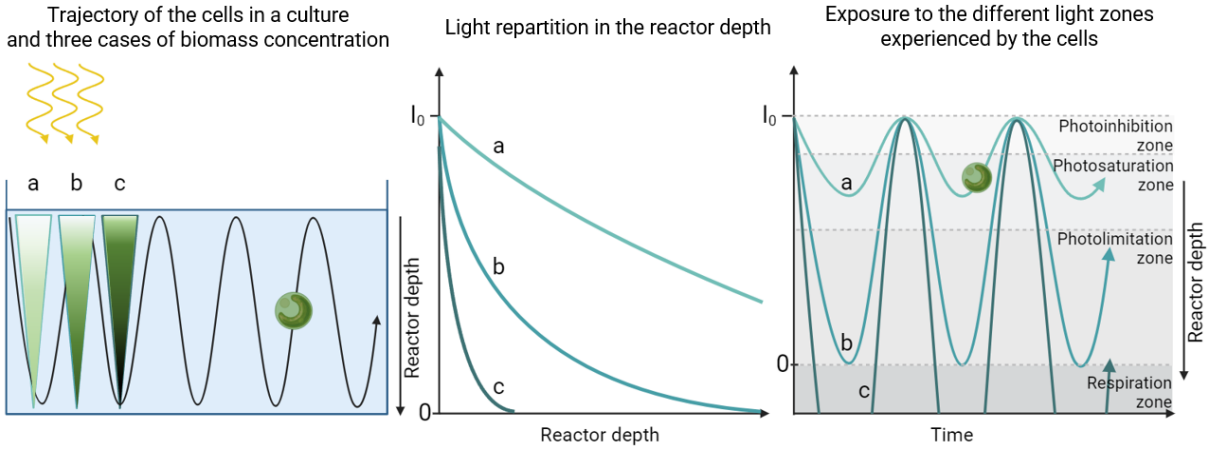

Figure D.2: Lumière perçue par les cellules de microalgues en fonction de la concentration en biomasse. Les trois concentrations en biomasse sont a (très diluée, la lumière atteint et traverse l'arrière du réacteur), b (intermédiaire, la lumière est totalement absorbée au niveau de l'arrière du réacteur), et c (très dense, la lumière est totalement absorbée et la partie inférieure de la culture est obscure). Comme les cellules se déplacent constamment en raison de l'agitation, elles rencontrent différentes zones de lumière, avec des proportions différentes selon la répartition de la lumière dans le réacteur, et donc selon la concentration en biomasse. Inspiré de (Tredici, 2010) et (Levasseur, 2021).

Les microalgues ont un avantage distinct par rapport aux plantes dans la production d'amidon, car elles peuvent rediriger rapidement leur métabolisme pour accumuler de l'amidon à haute concentration. Cette accumulation peut être induite par plusieurs facteurs, notamment la carence nutritive. Suite à l'induction, les microalgues stockent la majeure partie de l'énergie dérivée de la photosynthèse sous forme d'amidon. Bien que plusieurs méthodes d'induction de l'amidon soient décrites dans la littérature, il nous semblait qu'il manquait une comparaison fine réalisée dans des conditions similaires qui démontrerait les avantages et inconvénients de chaque méthode.

Après la culture et la récolte, la biomasse de microalgues doit être traitée pour séparer chaque composé et récupérer l'amidon. La double nature de l'amidon, à la fois réserve d'énergie et matériau polymère, le rend adapté à la production de divers bioplastiques avec différents procédés. Les procédés d'extraction de l'amidon ont déjà été abordés dans la littérature (Di Caprio et al., 2023 ; Gifuni, 2017a), mais doivent être encore simplifiés et transféré à plus grande échelle.

Résultats expérimentaux

Le travail expérimental a d'abord consisté à comparer les méthodes d'induction de l'accumulation d'amidon dans un même contexte. La carence en azote, la température supra-optimale, et l'absence de lumière bleue ont été testées à l'échelle laboratoire sur la souche *Chlorella vulgaris* CCALA924. Les trois méthodes abiotiques d'induction de l'amidon ont été comparées en termes de productivités en carbohydrates (directement comparable à l'amidon), composition de la biomasse, structure de l'amidon, capacités photosynthétiques et résistance mécanique de la cellule à la rupture.

Dans l'ensemble, les trois méthodes d'induction ont permis d'augmenter la production d'amidon (Figure D.3 et Figure D.4). La carence en azote et la température supra-optimale ont induit une accumulation rapide mais non soutenable de l'amidon (Figure D.4), et devraient être préférées pour les stratégies d'accumulation à court terme en batch. Malgré l'obtention d'une teneur en amidon plus faible, l'illumination en rouge a induit une production d'amidon accrue et constante (Figure D.4), qui semble adaptée à la culture continue. Ce travail ouvre de nouvelles perspectives pour la production d'amidon de microalgues, notamment pour des applications à grande échelle telles que les bioplastiques.

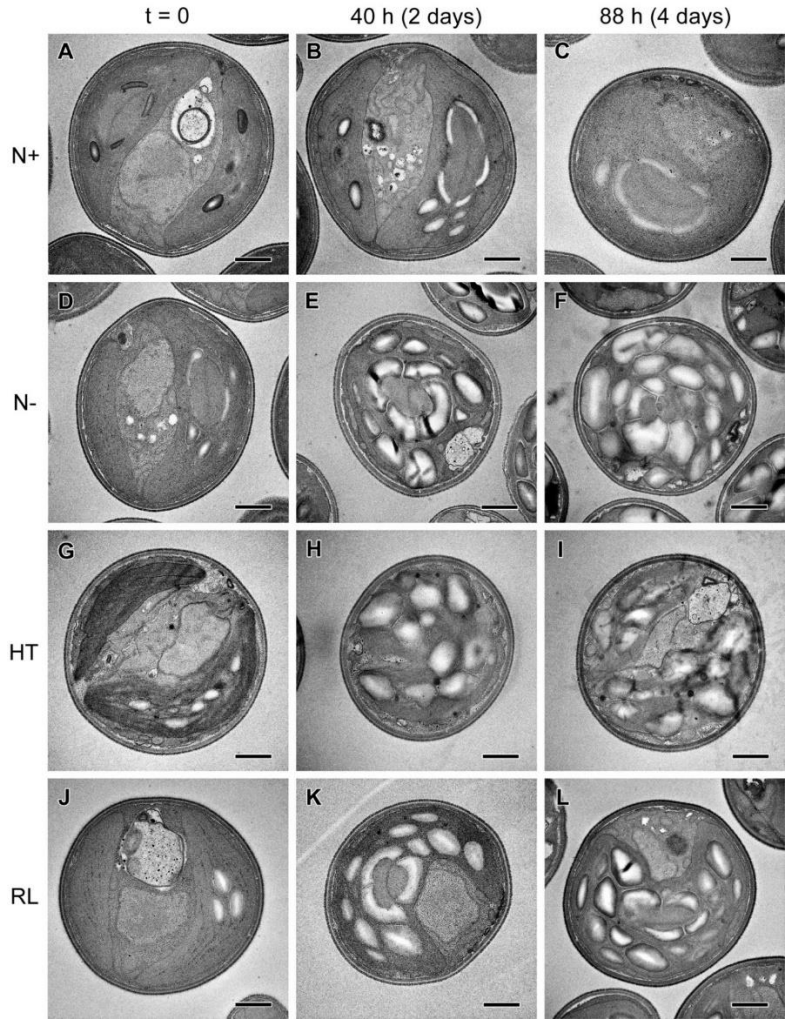

Figure D.3: Images TEM de coupes ultraminces de cellules de *Chlorella vulgaris* incluses dans de la résine après 0, 44 et 88 h d'induction de l'amidon. Les granules d'amidon (en blanc) sont visibles dans le chloroplaste et ont rapidement augmenté en nombre et en taille à partir de 44 h pour N-, HT et RL. Les barres d'échelle correspondent à 1 µm.

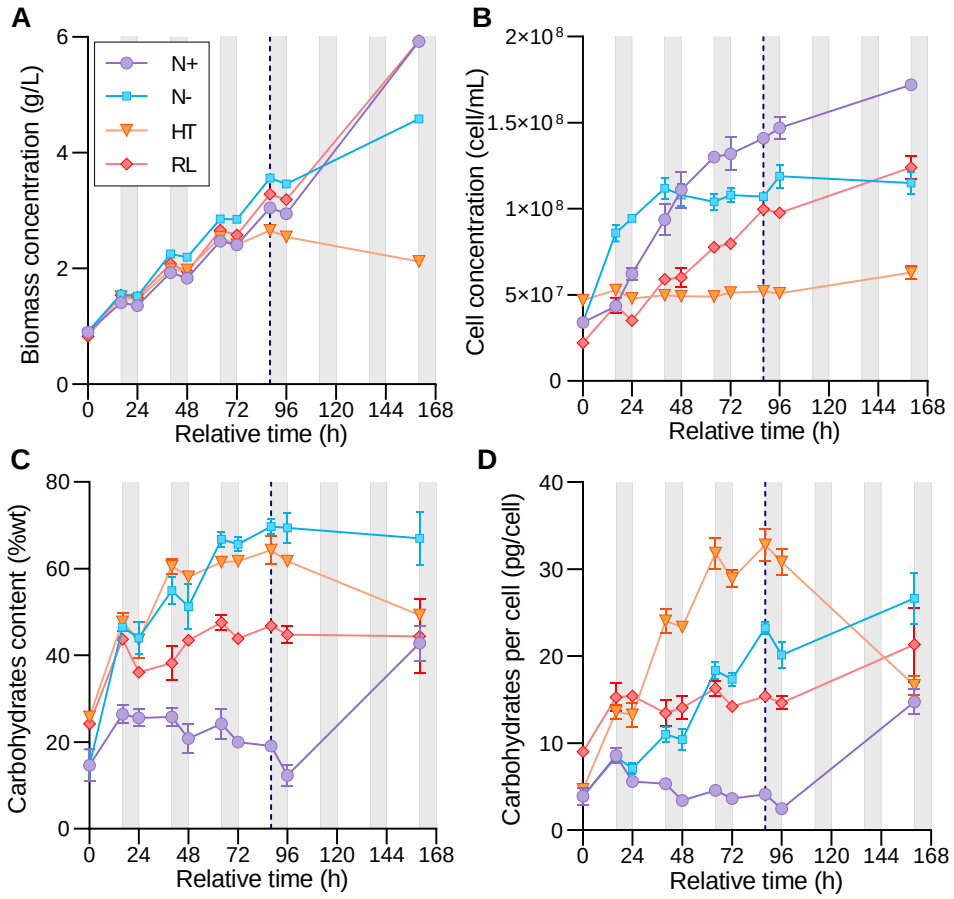

Figure D.4: Impact des facteurs abiotiques sur l'accumulation de biomasse et de carbohydrates chez *Chlorella vulgaris* CCALA924. (A) Matière sèche en suspension, (B) densité cellulaire, et (C) contenu en carbohydrates. Le contenu en carbohydrates par cellule (D) a été déterminé à partir des mesures de concentration cellulaire et de carbohydrates. Le soufre a été naturellement épuisé à 88 h dans la culture témoin N+ (ligne verticale en pointillés), ce qui explique la forte quantité d'amidon observée après 96 h de culture dans C et D. Les zones grisées représentent les périodes nocturnes de 8 heures.

La deuxième partie expérimentale a consisté à estimer la production d'amidon en fonction de l'apport en lumière solaire. Pour cela, une première expérience a consisté à mettre en parallèle la disponibilité de la lumière solaire (en quantité de photon par masse de microalgues par seconde) avec la productivité en carbohydrates (en contenu, productivité relative, et efficacité photosynthétique) lors d'une carence en azote. Cette expérience a été réalisée dans des bouteilles de 1L et a permis de tracer les courbes de la réponse de la productivité en carbohydrates en fonction de la lumière solaire (Figure D.5). Ce modèle empirique a ensuite été comparé avec une autre expérience, menée dans un réacteur plat de 180L. Les résultats de productivité en carbohydrates en fonction de la lumière solaire se sont révélés proches du modèle empirique développé à partir des mesures réalisées à l'échelle des bouteilles.

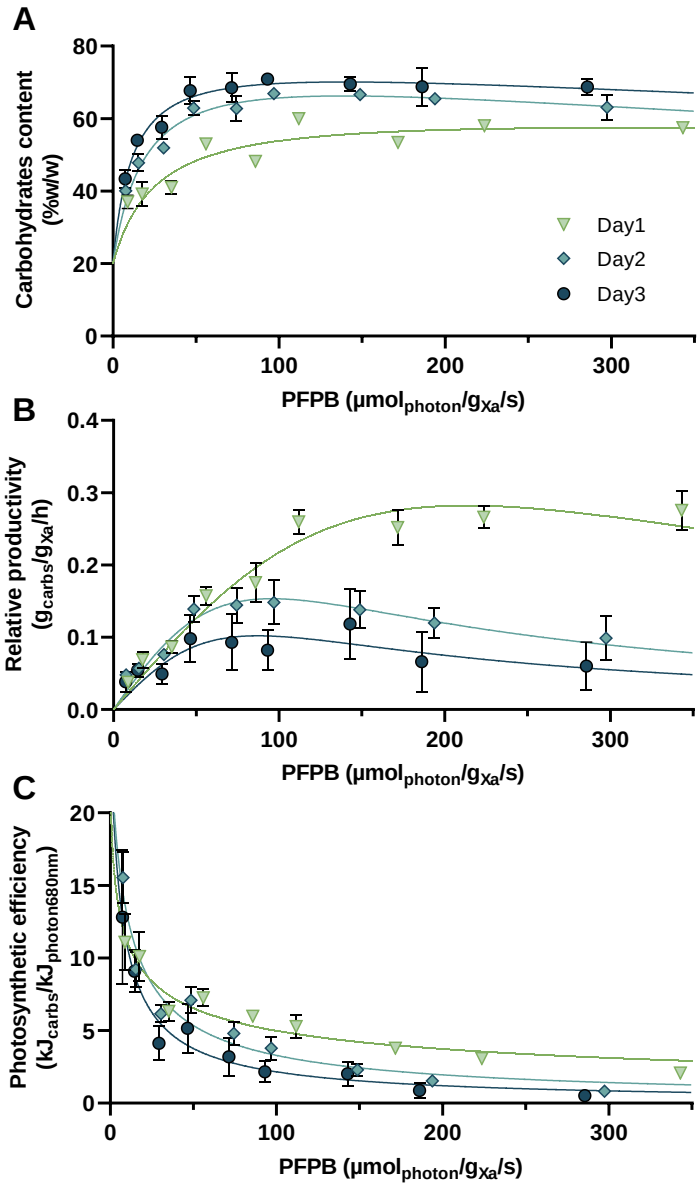

Figure D.5: Évolution de l'accumulation de carbohydrates en fonction du flux de photons par masse de matière sèche. (A) Contenu en carbohydrates à la fin de la journée, (B) Productivité des carbohydrates par rapport à la biomasse active Xa (Xa équivalent à X_0, la densité initiale en biomasse), (C) Efficacité photosynthétique. Les points triangulaires, en losange et ronds représentent les valeurs mesurées pour le premier, deuxième et troisième jour de l'expérience en bouteille de 1 litre, respectivement. Les lignes sont les courbes d'ajustement associées à ces valeurs mesurées. PFPB : flux de photons par biomasse.

Le modèle établi à l'échelle des bouteilles de 1L semble donc avoir été validé à l'échelle du réacteur de 180L. Par la suite, ce modèle a donc servi de base pour établir un calcul théorique de l'accumulation d'amidon en lumière naturelle. Cette approche propose une prédiction de la productivité d'amidon en fonction de la lumière incidente et de la quantité de biomasse dite active, qui correspond dans notre situation à la

biomasse initialement présente dans le réacteur au début de la carence nutritive (Figure D.6). Cette prédiction est théoriquement valide pour n'importe quel réacteur tant que la lumière incidente considérée correspond au flux moyen incident à la surface du réacteur.

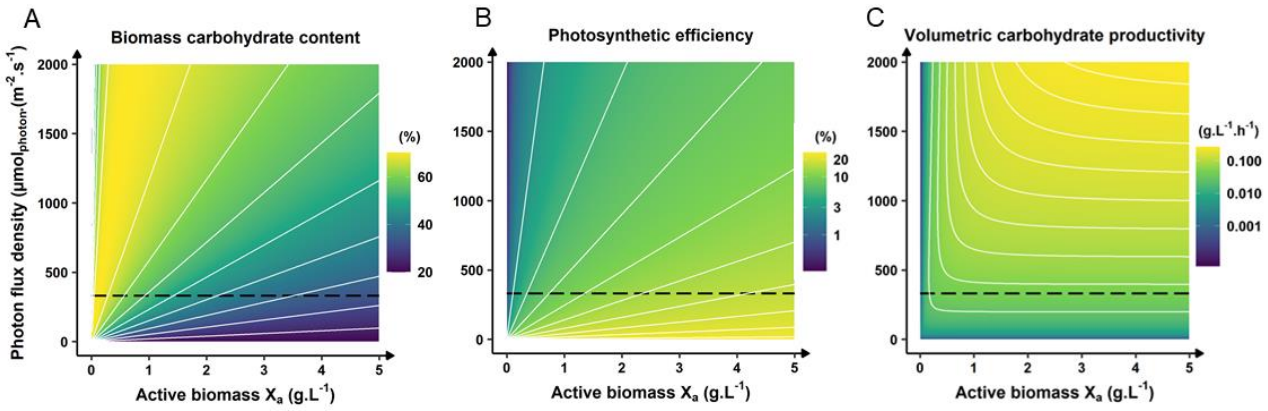

Figure D.6: Accumulation d'amidon selon la densité de flux de photons moyenne quotidienne Im et la concentration en biomasse active Xa. Les résultats sont calculés pour une période de 3 jours à partir du modèle de bouteille de 1 L. Le rapport surface-volume a été fixé à 49,3 m^{-1}, correspondant au photobioréacteur plat de 180 L. (A) Prédictions du contenu en carbohydrates atteint après trois jours de carence. (B) Prédictions de l'efficacité photosynthétique moyenne quotidienne en carbohydrates, calculée comme la moyenne des trois premiers jours. (C) Prédictions de la productivité volumétrique moyenne quotidienne en carbohydrates, calculée comme la moyenne des trois jours et basée sur Xa et la productivité relative.

Pour notre photobioréacteur plat de 180 L et en considérant une journée ensoleillée typique d'Octobre dans la région d'Aix-en-Provence, une concentration initiale en biomasse d'environ 0,8 g/L a été trouvée être le meilleur compromis pour une accumulation optimale d'amidon en termes de productivité volumétrique (0,130 $g_{carbohydrates}$/L/h), d'efficacité photosynthétique (2,9 % du rayonnement solaire total) et de teneur (57 $\%_{carbohydrates}$). En considérant que notre photobioréacteur de 180 L occupe une surface au sol de 3,7 m^2 (Derwenskus, 2020) et que la productivité volumétrique moyenne est maintenue pendant 6 heures par jour, la productivité surfacique correspondrait à environ 38 $g_{carbohydrates}/m^2$/jour. Dans l'ensemble, ces chiffres de productivité sont comparables aux 20-50 g de biomasse sèche/m^2/jour et aux 2-4 % d'efficacité photosynthétique (rayonnement solaire total) obtenus dans des expériences à court terme avec des cultures végétales (Coombs, 1985).

La troisième et dernière partie expérimentale a consisté à développer un procédé d'extraction de l'amidon à partir de cellules de microalgues à forte teneur en amidon, et à transformer cet amidon extrait en amidon thermoplastique (TPS pour thermoplastic starch). A la fin du procédé d'extraction présenté en Figure D.7, les rendements d'extraction et de pureté étaient respectivement de 98 et 87 %. Les granules d'amidon étaient de petite taille et présentaient les propriétés habituelles des amidons natifs en termes de contenu d'amylose, de profil de diffraction, et de forme.

A.

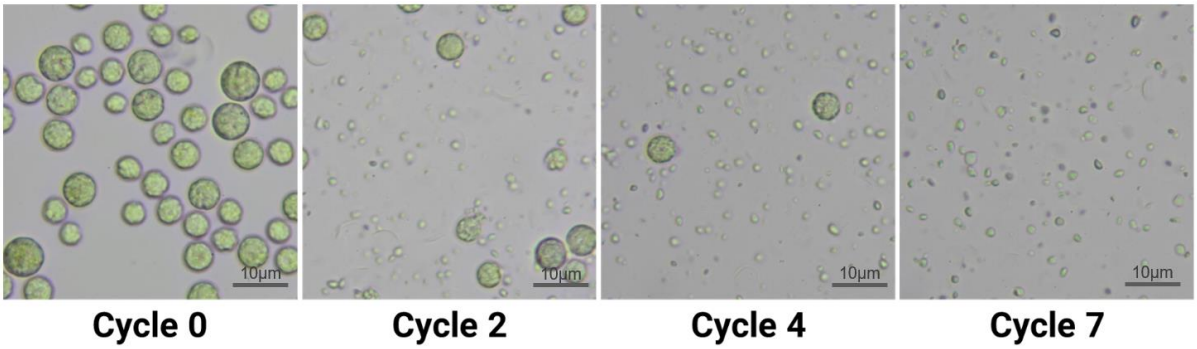

B.

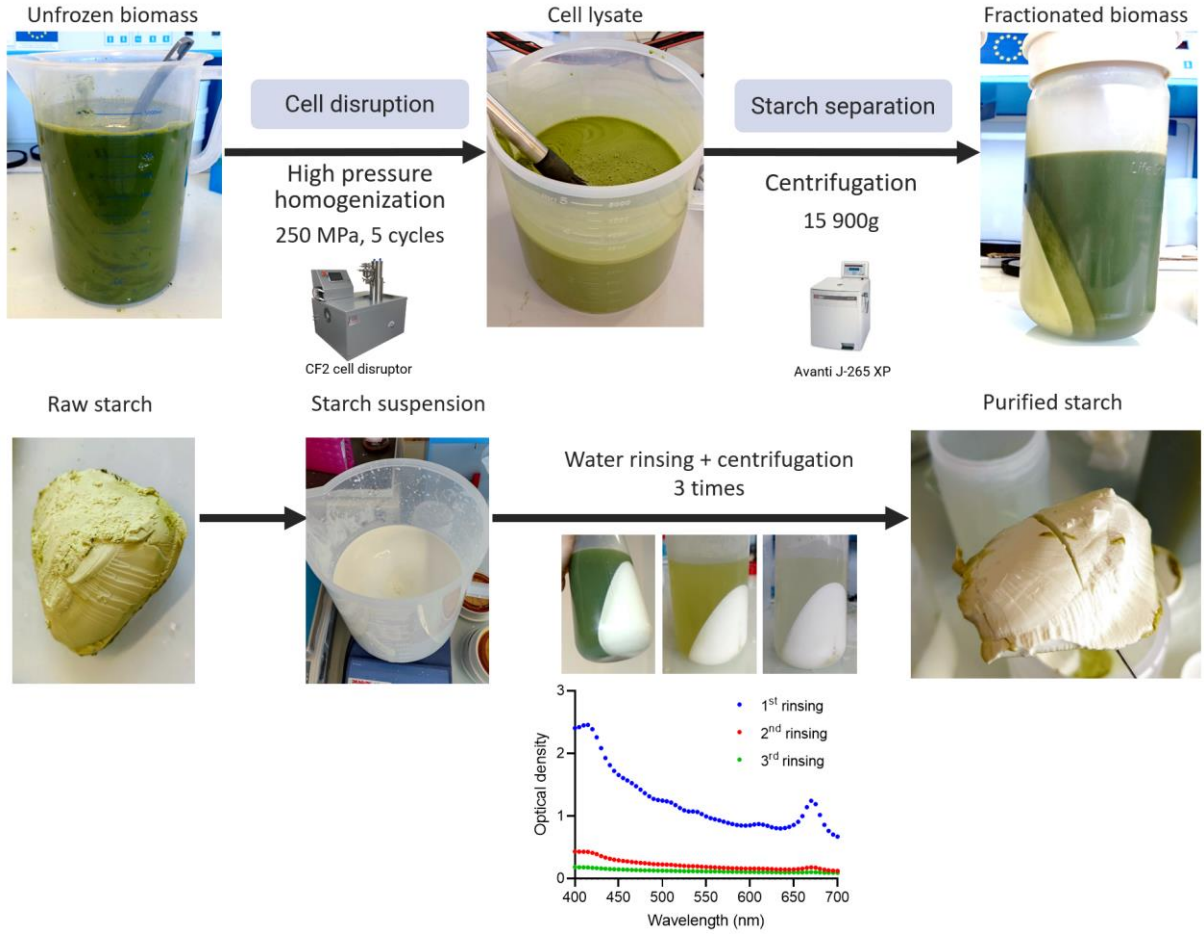

Figure D.7: Procédé d'extraction de l'amidon à partir de biomass de *Chlorella vulgaris* CCALA924. (A) Disruption des cellules de *Chlorella vulgaris* et relargage des grains d'amidon au fur et à mesure des cycles d'homogénéisateur haute pression (HPH). (B) Schéma du procédé d'extraction réalisé à l'échelle pilote.

Deuxièmement, l'amidon de microalgue a été plastifié avec succès en TPS, en utilisant des méthodes de production facilement transposables à l'échelle industrielle (Figure D.8A). L'étude des propriétés mécaniques de ce TPS de microalgues, en comparaison à d'autres TPS, a permis de montrer qu'il se situe dans la plage des caractéristiques attendues pour les TPS (Figure D.8B).

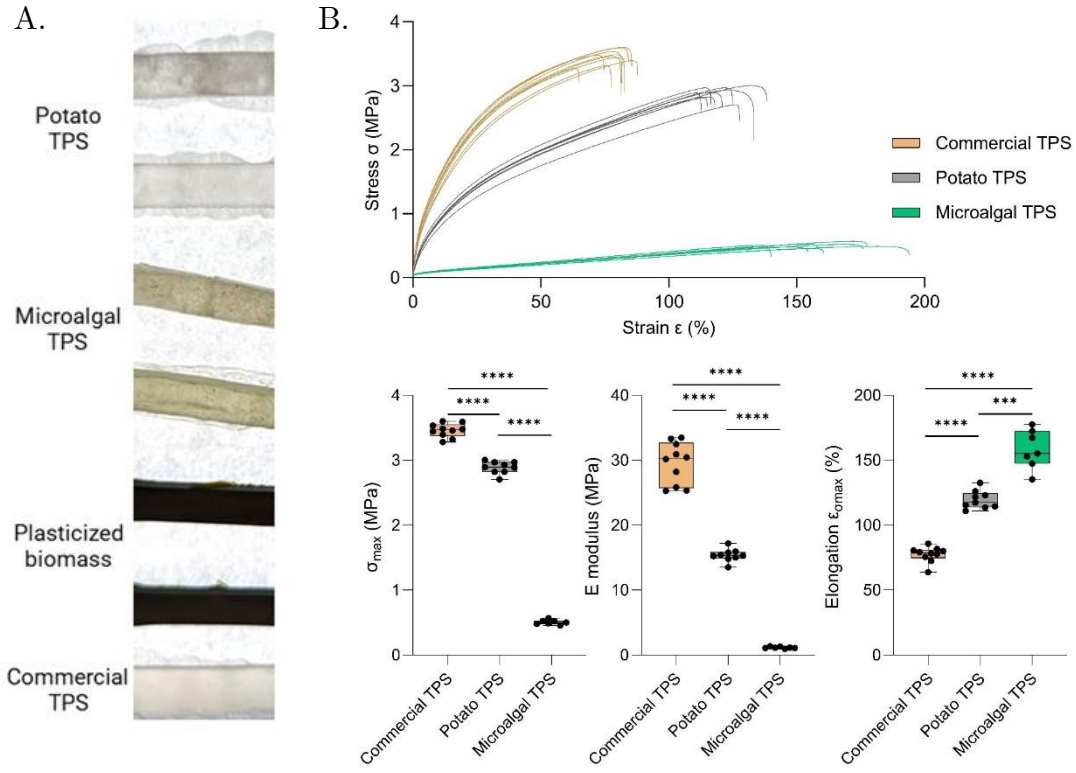

Figure D.8: Echantillons plastifiés et essais mécaniques de traction. (A) Echantillons de thermoplastic starch (TPS) obtenus en mélangeant du glycerol avec de l'amidon de pomme de terre, de l'amidon de microalgues, des microalgues, ou une formulation commerciale de TPS. (B) Propriétés mécaniques en traction (contrainte maximale, module de Young, élongation à la rupture) des différents échantillons.

Discussion et perspectives

Dans la première partie expérimentale, il a été démontré que différents inducteurs d'amidon pouvaient donner des résultats d'accumulation d'amidon variés. Une enquête plus approfondie sur les effets cumulatifs des inducteurs d'amidon, en particulier l'application de la combinaison d'une illumination en lumière rouge et d'une carence en azote, serait instructive pour déterminer si les effets des deux voies d'accumulation peuvent se cumuler. De plus, explorer la distinction entre une carence en un seul élément nutritif comme l'azote par rapport à la privation en plusieurs macronutriments pourrait éventuellement conclure qu'il est possible d'ajouter aucun nutriment pendant l'étape de d'accumulation.

Suite aux résultats de la deuxième partie expérimentale, l'approche utilisée pour modéliser la lumière incidente dans les réacteurs a été validée comme une méthode efficace pour optimiser la productivité en carbohydrates. Cependant, le modèle lumière-carbohydrates développé nécessite une meilleure validation. Il aurait été bénéfique de générer des données expérimentales supplémentaires pour affiner le modèle et élargir son applicabilité. Notamment, des expériences futures dans des systèmes ouverts pertinents pour la culture industrielle, tels que les bassins raceways, fourniraient des informations précieuses sur la capacité réelle de production d'amidon avec *Chlorella vulgaris* en contexte industriel.

Le processus d'extraction développé dans la troisième partie expérimentale s'est révélé très efficace pour l'extraction et la récupération de l'amidon. Cependant, les autres fractions de biomasse telles que les sucres libres, les lipides ou les protéines ne sont pas séparées individuellement, contrairement à ce qui est réalisé lors les processus d'extraction d'amidon végétal. Un travail expérimental supplémentaire est nécessaire pour séparer efficacement chaque fraction, éventuellement en repensant certaines étapes comme la rupture cellulaire. De plus, une méthode de rupture cellulaire moins énergivore qu'un homogénéisateur à haute pression doit être explorée.

La plastification de l'amidon de microalgues a été comparée à un témoin. Ce contrôle, l'amidon de pomme de terre, a été sélectionné pour sa pertinence industrielle. Cependant, il ne correspondait pas précisément à notre amidon de microalgue, et les propriétés mécaniques en traction du TPS d'amidon de pomme de terre et de microalgues étaient significativement différentes. Un contrôle plus approprié aurait été un amidon végétal avec une teneur en amylose et une méthode de séchage similaire à l'amidon de microalgue.

Conclusion

Les travaux expérimentaux de cette thèse de doctorat ont apporté trois résultats principaux.

Tout d'abord, nous avons comparé trois méthodes d'induction de l'amidon en termes de productivités en carbohydrates, composition de la biomasse, structure de l'amidon, capacités photosynthétiques et rupture cellulaire. La privation en azote et la température supra-optimale ont induit une accumulation rapide mais non durable de l'amidon, adaptée aux stratégies de culture à court terme. En revanche, l'illumination en lumière rouge a facilité une production régulière d'amidon, idéale pour les systèmes de culture continue. Dans l'ensemble, *Chlorella vulgaris* CCALA924 a été confirmée comme étant une souche à haute productivité d'amidon, et faible teneur en lipides.

Deuxièmement, nous avons étudié la gestion de la lumière dans les cultures de microalgues accumulant de l'amidon en lumière solaire, établissant des relations empiriques entre le rapport lumière par biomasse et l'accumulation d'amidon. Ces

relations ont fourni des lignes directrices pour optimiser l'accumulation d'amidon en fonction de la concentration initiale en biomasse et de la lumière incidente.

Enfin, nous avons développé un processus novateur et simplifié pour extraire, purifier et plastifier l'amidon de microalgues. Le processus d'extraction a donné des taux d'extraction et de pureté de 98 % et 87 % respectivement, avec des granules d'amidon intacts présentant des propriétés typiques des amidons natifs. La plastification réussie de l'amidon de microalgue en amidon thermoplastique à l'échelle pilote souligne le potentiel industriel des microalgues pour la production de bioplastiques.

Les futurs travaux pourraient explorer des stratégies visant à améliorer la rentabilité de la culture en masse de microalgues. Par exemple, les voies de signalisation de la lumière bleue devraient être étudiées pour potentiellement générer des mutants avec une production continue d'amidon jusqu'à des teneurs cellulaires élevées. Les efforts visant à maximiser l'efficacité de conversion de l'énergie solaire devraient également être étendus aux systèmes de culture ouverts. De plus, la montée en échelle du processus d'extraction de l'amidon à des volumes industriels pourrait rendre le traitement de l'amidon de microalgues compétitif face à celui de l'amidon végétal, à condition que des volumes suffisants de microalgues soient produits.

En conclusion, ce travail de thèse permet d'entrevoir des perspectives appliquées sur l'accumulation d'amidon, la culture de microalgues en lumière solaire et les processus de conversion des microalgues en bioplastiques. Il a notamment permis d'obtenir des données expérimentales qui pourront être extrapolées pour positionner cette nouvelle filière vis-à-vis des technologies matures utilisées dans les amidonneries industrielles actuelles. Le développement de la production de carbohydrates avec les microalgues offre des perspectives pour différentes filières industrielles utilisant des produits biosourcés. Dans l'ensemble, ce travail représente une avancée vers la production industrielle de bioplastiques à partir d'amidon de microalgues.

References

Abdulqader, G., Barsanti, L., Tredici, M.R., 2000. Harvest of Arthrospira platensis from Lake Kossorom (Chad) and its household usage among the Kanembu. Journal of Applied Phycology 12, 493–498. https://doi.org/10.1023/A:1008177925799

Adewale, P., Yancheshmeh, M.S., Lam, E., 2022. Starch modification for non-food, industrial applications: Market intelligence and critical review. Carbohydrate Polymers 291, 119590. https://doi.org/10.1016/j.carbpol.2022.119590

Aguirre, A.-M., Bassi, A., 2013. Investigation of biomass concentration, lipid production, and cellulose content in Chlorella vulgaris cultures using response surface methodology. Biotechnology and Bioengineering 110, 2114–2122. https://doi.org/10.1002/bit.24871

Alsema, E.A., 1998. Energy Requirements and CO2 Mitigation Potential of PV Systems.

Andersen, R.A., 2013. The Microalgal Cell, in: Handbook of Microalgal Culture. John Wiley & Sons, Ltd, pp. 1–20. https://doi.org/10.1002/9781118567166.ch1

Antal, T.K., Kovalenko, I.B., Rubin, A.B., Tyystjärvi, E., 2013. Photosynthesis-related quantities for education and modeling. Photosynth Res 117, 1–30. https://doi.org/10.1007/s11120-013-9945-8

Aro, E.-M., Virgin, I., Andersson, B., 1993. Photoinhibition of Photosystem II. Inactivation, protein damage and turnover. Biochimica et Biophysica Acta (BBA) - Bioenergetics 1143, 113–134. https://doi.org/10.1016/0005-2728(93)90134-2

Artu, A., 2016. Etude et optimisation de la culture de microalgues en photobioréacteurs solaires (These de doctorat). Nantes.

Avebe, 2017. General product information document - Potato starch food grade quality.

Baker, N.R., 2008. Chlorophyll Fluorescence: A Probe of Photosynthesis In Vivo. Annual Review of Plant Biology 59, 89–113. https://doi.org/10.1146/annurev.arplant.59.032607.092759

Bakku, R.K., Yamamoto, Y., Inaba, Y., Hiranuma, T., Gianino, E., Amarianto, L., Mahrous, W., Suzuki, H., Suzuki, K., 2023. New insights into raceway cultivation of Euglena gracilis under long-term semi-continuous nitrogen starvation. Sci Rep 13, 7123. https://doi.org/10.1038/s41598-023-34164-1

Bantadjan, Y., Rittiron, R., Malithong, K., Narongwongwattana, S., 2020. Rapid Starch Evaluation in Fresh Cassava Root Using a Developed Portable Visible and Near-Infrared Spectrometer. ACS Omega 5, 11210–11216. https://doi.org/10.1021/acsomega.0c01346

Bassi, R., Dall'Osto, L., 2021. Dissipation of Light Energy Absorbed in Excess: The Molecular Mechanisms. Annual Review of Plant Biology 72, 47–76. https://doi.org/10.1146/annurev-arplant-071720-015522

Baudelet, P.-H., Ricochon, G., Linder, M., Muniglia, L., 2017. A new insight into cell walls of Chlorophyta. Algal Research 25, 333–371. https://doi.org/10.1016/j.algal.2017.04.008

Beaumont, N.J., Aanesen, M., Austen, M.C., Börger, T., Clark, J.R., Cole, M., Hooper, T., Lindeque, P.K., Pascoe, C., Wyles, K.J., 2019. Global ecological, social and economic impacts of marine plastic. Marine Pollution Bulletin 142, 189–195. https://doi.org/10.1016/j.marpolbul.2019.03.022

Becker, E.W., 2013. Microalgae for Human and Animal Nutrition, in: Handbook of Microalgal Culture. John Wiley & Sons, Ltd, pp. 461–503. https://doi.org/10.1002/9781118567166.ch25

Benemann, J.R., 2023. Large-Scale Production of Microalgae Biomass, Oral presentation, AlgaEurope 2023.

Bergmann, P., Ripplinger, P., Beyer, L., Trösch, W., 2013. Disposable Flat Panel Airlift Photobioreactors. Chemie Ingenieur Technik 85, 202–205. https://doi.org/10.1002/cite.201200132

Blankenship, R.E., Chen, M., 2013. Spectral expansion and antenna reduction can enhance photosynthesis for energy production. Current Opinion in Chemical Biology, Next generation therapeutics • Energy 17, 457–461. https://doi.org/10.1016/j.cbpa.2013.03.031

Blankenship, R.E., Tiede, D.M., Barber, J., Brudvig, G.W., Fleming, G., Ghirardi, M., Gunner, M.R., Junge, W., Kramer, D.M., Melis, A., Moore, T.A., Moser, C.C., Nocera, D.G., Nozik, A.J., Ort, D.R., Parson, W.W., Prince, R.C., Sayre, R.T., 2011. Comparing Photosynthetic and Photovoltaic Efficiencies and Recognizing the Potential for Improvement. Science 332, 805–809. https://doi.org/10.1126/science.1200165

Boelee, E., Geerling, G., van der Zaan, B., Blauw, A., Vethaak, A.D., 2019. Water and health: From environmental pressures to integrated responses. Acta Tropica 193, 217–226. https://doi.org/10.1016/j.actatropica.2019.03.011

Brányiková, I., Maršálková, B., Doucha, J., Brányik, T., Bišová, K., Zachleder, V., Vítová, M., 2011. Microalgae-novel highly efficient starch producers. Biotechnol. Bioeng. 108, 766–776. https://doi.org/10.1002/bit.23016

Burlacot, A., Sawyer, A., Cuiné, S., Auroy-Tarrago, P., Blangy, S., Happe, T., Peltier, G., 2018. Flavodiiron-Mediated O $_2$ Photoreduction Links H $_2$ Production with CO $_2$ Fixation during the Anaerobic Induction of Photosynthesis. Plant Physiol. 177, 1639–1649. https://doi.org/10.1104/pp.18.00721

Busch, F.A., Sage, R.F., Farquhar, G.D., 2018. Plants increase CO2 uptake by assimilating nitrogen via the photorespiratory pathway. Nature Plants 4, 46–54. https://doi.org/10.1038/s41477-017-0065-x

Canelli, G., Murciano Martínez, P., Austin, S., Ambühl, M.E., Dionisi, F., Bolten, C.J., Carpine, R., Neutsch, L., Mathys, A., 2021a. Biochemical and Morphological Characterization of Heterotrophic Crypthecodinium cohnii and Chlorella

vulgaris Cell Walls. J. Agric. Food Chem. 69, 2226–2235. https://doi.org/10.1021/acs.jafc.0c05032

Canelli, G., Murciano Martínez, P., Maude Hauser, B., Kuster, I., Rohfritsch, Z., Dionisi, F., Bolten, C.J., Neutsch, L., Mathys, A., 2021b. Tailored enzymatic treatment of Chlorella vulgaris cell wall leads to effective disruption while preserving oxidative stability. LWT 111157. https://doi.org/10.1016/j.lwt.2021.111157

Carlsson, P.A.S., van Beilen, J.B., Möller, R., Clayton, D., Bowles, D., 2007. MICRO- AND MACRO-ALGAE: UTILITY FOR INDUSTRIAL APPLICATIONS.

Carmichael, W.W., Drapeau, C., Anderson, D.M., 2000. Harvesting of Aphanizomenon flos-aquae Ralfs ex Born. & Flah. var. flos-aquae (Cyanobacteria) from Klamath Lake for human dietary use. Journal of Applied Phycology 12, 585–595. https://doi.org/10.1023/A:1026506713560

Cazzaniga, S., Dall'Osto, L., Szaub, J., Scibilia, L., Ballottari, M., Purton, S., Bassi, R., 2014. Domestication of the green alga Chlorella sorokiniana: reduction of antenna size improves light-use efficiency in a photobioreactor. Biotechnol Biofuels 7, 157. https://doi.org/10.1186/s13068-014-0157-z

CERMAV, 2016. Amidothèque [WWW Document]. URL https://amidotheque.cermav.cnrs.fr/ (accessed 1.15.24).

Chambonniere, P., Ramírez-Romero, A., Dimitriades-Lemaire, A., Sassi, J.-F., Delrue, F., 2022. Photosynthetic Carbon Uptake Correlates with Cell Protein Content during Lipid Accumulation in the Microalga Chlorella vulgaris NIES 227. Fermentation 8, 614. https://doi.org/10.3390/fermentation8110614

Cheng, D., Li, D., Yuan, Y., Zhou, L., Li, X., Wu, T., Wang, L., Zhao, Q., Wei, W., Sun, Y., 2017. Improving carbohydrate and starch accumulation in Chlorella sp. AE10 by a novel two-stage process with cell dilution. Biotechnol Biofuels 10, 75. https://doi.org/10.1186/s13068-017-0753-9

Chiba, S., Saito, H., Fletcher, R., Yogi, T., Kayo, M., Miyagi, S., Ogido, M., Fujikura, K., 2018. Human footprint in the abyss: 30 year records of deep-sea plastic debris. Marine Policy 96, 204–212. https://doi.org/10.1016/j.marpol.2018.03.022

Converti, A., Casazza, A.A., Ortiz, E.Y., Perego, P., Del Borghi, M., 2009. Effect of temperature and nitrogen concentration on the growth and lipid content of Nannochloropsis oculata and Chlorella vulgaris for biodiesel production. Chemical Engineering and Processing: Process Intensification 48, 1146–1151. https://doi.org/10.1016/j.cep.2009.03.006

Coombs, J. (Ed.), 1985. Techniques in bioproductivity and photosynthesis, 2nd ed. ed, Pergamon international library of science, technology, engineering, and social studies. Pergamon Press, Oxford ; New York.

Cornet, J.-F., Dauchet, J., Vourc'h, T., Arnau, C., Garcia-Gragera, D., Gòdia, F., Gros, F., Peiro, E., 2023. A Simple and Reliable Method to Determine Mean Incident Light Flux Densities on Cylindrical Photoreactors and Photobioreactors from a

Unique Fluence Rate Measurement. Ind. Eng. Chem. Res. 62, 4875–4884. https://doi.org/10.1021/acs.iecr.2c04151

Cornet, J.F., Dussap, C.G., Dubertret, G., 1992. A structured model for simulation of cultures of the cyanobacterium Spirulina platensis in photobioreactors: I. Coupling between light transfer and growth kinetics. Biotechnology and Bioengineering 40, 817–825. https://doi.org/10.1002/bit.260400709

Cornet, J.-F., Dussap, C.G., Gros, J.-B., Binois, C., Lasseur, C., 1995. A simplified monodimensional approach for modeling coupling between radiant light transfer and growth kinetics in photobioreactors. Chemical Engineering Science 50, 1489–1500. https://doi.org/10.1016/0009-2509(95)00022-W

da Silva Ferreira, V., Sant'Anna, C., 2016. Impact of culture conditions on the chlorophyll content of microalgae for biotechnological applications. World J Microbiol Biotechnol 33, 20. https://doi.org/10.1007/s11274-016-2181-6

Dall'Osto, L., Cazzaniga, S., Guardini, Z., Barera, S., Benedetti, M., Mannino, G., Maffei, M.E., Bassi, R., 2019. Combined resistance to oxidative stress and reduced antenna size enhance light-to-biomass conversion efficiency in Chlorella vulgaris cultures. Biotechnol Biofuels 12, 221. https://doi.org/10.1186/s13068-019-1566-9

Dauvillée, D., 2001. Implication des enzymes de débranchement dans la biosynthèse de l'amylopectine (These de doctorat). Lille 1.

Dauvillée, D., Colleoni, C., Mouille, G., Buléon, A., Gallant, D.J., Bouchet, B., Morell, M.K., d'Hulst, C., Myers, A.M., Ball, S.G., 2001. Two Loci Control Phytoglycogen Production in the Monocellular Green Alga *Chlamydomonas reinhardtii*. Plant Physiology 125, 1710–1722. https://doi.org/10.1104/pp.125.4.1710

de Graaf, R.A., Karman, A.P., Janssen, L.P.B.M., 2003. Material Properties and Glass Transition Temperatures of Different Thermoplastic Starches After Extrusion Processing. Starch - Stärke 55, 80–86. https://doi.org/10.1002/star.200390020

De Troostembergh, J.-C., 2001. Starch-Based Raw Materials for Fermentation Applications, in: Biotechnology Set. John Wiley & Sons, Ltd, pp. 31–46. https://doi.org/10.1002/9783527620999.ch1bf

Delrue, B., Fontaine, T., Routier, F., Decq, A., Wieruszeski, J.M., Van Den Koornhuyse, N., Maddelein, M.L., Fournet, B., Ball, S., 1992. Waxy Chlamydomonas reinhardtii: monocellular algal mutants defective in amylose biosynthesis and granule-bound starch synthase activity accumulate a structurally modified amylopectin. Journal of Bacteriology 174, 3612–3620. https://doi.org/10.1128/jb.174.11.3612-3620.1992

Demir-Yilmaz, I., Schiavone, M., Esvan, J., Guiraud, P., Formosa-Dague, C., 2023. Combining AFM, XPS and chemical hydrolysis to understand the complexity and dynamics of C. vulgaris cell wall composition and architecture. Algal Research 103102. https://doi.org/10.1016/j.algal.2023.103102

Demory, D., Combe, C., Hartmann, P., Talec, A., Pruvost, E., Hamouda, R., Souillé, F., Lamare, P.-O., Bristeau, M.-O., Sainte-Marie, J., Rabouille, S., Mairet, F., Sciandra, A., Bernard, O., 2018. How do microalgae perceive light in a high-rate pond? Towards more realistic Lagrangian experiments. Royal Society Open Science 5, 180523. https://doi.org/10.1098/rsos.180523

Derwenskus, F., 2020. Entwicklung und Bewertung eines Verfahrens zur Herstellung von Fucoxanthin und Eicosapentaensäure mit Phaeodactylum tricornutum (doctoralThesis). https://doi.org/10.18419/opus-11183

Deschamps, P., Colleoni, C., Nakamura, Y., Suzuki, E., Putaux, J.-L., Buléon, A., Haebel, S., Ritte, G., Steup, M., Falcón, L.I., Moreira, D., Löffelhardt, W., Raj, J.N., Plancke, C., d'Hulst, C., Dauvillée, D., Ball, S., 2008. Metabolic Symbiosis and the Birth of the Plant Kingdom. Molecular Biology and Evolution 25, 536–548. https://doi.org/10.1093/molbev/msm280

Di Caprio, F., Amenta, S., Francolini, I., Altimari, P., Pagnanelli, F., 2023. Microalgae Biorefinery: Optimization of Starch Recovery for Bioplastic Production. ACS Sustainable Chem. Eng. https://doi.org/10.1021/acssuschemeng.3c04133

Domene-López, D., García-Quesada, J.C., Martin-Gullon, I., Montalbán, M.G., 2019. Influence of Starch Composition and Molecular Weight on Physicochemical Properties of Biodegradable Films. Polymers 11, 1084. https://doi.org/10.3390/polym11071084

DuBois, Michel., Gilles, K.A., Hamilton, J.K., Rebers, P.A., Smith, Fred., 1956. Colorimetric Method for Determination of Sugars and Related Substances. Anal. Chem. 28, 350–356. https://doi.org/10.1021/ac60111a017

Duffie, J.A., Beckman, W.A., 2013. Solar engineering of thermal processes. John Wiley & Sons.

Duval, J.F.L., Razafitianamaharavo, A., Bihannic, I., Offroy, M., Lesniewska, N., Sohm, B., Le Cordier, H., Mustin, C., Pagnout, C., Beaussart, A., 2023. New insights into the effects of growth phase and enzymatic treatment on the cell-wall properties of Chlorella vulgaris microalgae. Algal Research 69, 102955. https://doi.org/10.1016/j.algal.2022.102955

Eckhoff, S.R., Watson, S.A., 2009. Chapter 9 - Corn and Sorghum Starches: Production, in: BeMiller, J., Whistler, R. (Eds.), Starch (Third Edition), Food Science and Technology. Academic Press, San Diego, pp. 373–439. https://doi.org/10.1016/B978-0-12-746275-2.00009-4

Edmundson, S.J., Huesemann, M.H., 2015. The dark side of algae cultivation: Characterizing night biomass loss in three photosynthetic algae, Chlorella sorokiniana, Nannochloropsis salina and Picochlorum sp. Algal Research 12, 470–476. https://doi.org/10.1016/j.algal.2015.10.012

Erickson, E., Wakao, S., Niyogi, K.K., 2015. Light stress and photoprotection in *Chlamydomonas reinhardtii*. Plant J 82, 449–465. https://doi.org/10.1111/tpj.12825

Falkowski, P.G., Barber, R.T., Smetacek, V., 1998. Biogeochemical Controls and Feedbacks on Ocean Primary Production. Science 281, 200–206. https://doi.org/10.1126/science.281.5374.200

Falkowski, P.G., Knoll, A.H., 2007. Evolution of primary producers in the sea. Elsevier Academic Press, Amsterdam Boston.

Findinier, J., Laurent, S., Duchêne, T., Roussel, X., Lancelon-Pin, C., Cuiné, S., Putaux, J.-L., Li-Beisson, Y., D'Hulst, C., Wattebled, F., Dauvillée, D., 2019. Deletion of BSG1 in Chlamydomonas reinhardtii leads to abnormal starch granule size and morphology. Sci Rep 9, 1990. https://doi.org/10.1038/s41598-019-39506-6

Findinier, J., Tunçay, H., Schulz-Raffelt, M., Deschamps, P., Spriet, C., Lacroix, J.-M., Duchêne, T., Szydlowski, N., Li-Beisson, Y., Peltier, G., D'Hulst, C., Wattebled, F., Dauvillée, D., 2017. The Chlamydomonas mex1 mutant shows impaired starch mobilization without maltose accumulation. Journal of Experimental Botany 68, 5177–5189. https://doi.org/10.1093/jxb/erx343

Friedland, N., Negi, S., Vinogradova-Shah, T., Wu, G., Ma, L., Flynn, S., Kumssa, T., Lee, C.-H., Sayre, R.T., 2019. Fine-tuning the photosynthetic light harvesting apparatus for improved photosynthetic efficiency and biomass yield. Sci Rep 9, 13028. https://doi.org/10.1038/s41598-019-49545-8

García, J.L., de Vicente, M., Galán, B., 2017. Microalgae, old sustainable food and fashion nutraceuticals. Microb Biotechnol 10, 1017–1024. https://doi.org/10.1111/1751-7915.12800

Genty, B., Briantais, J.-M., Baker, N.R., 1989. The relationship between the quantum yield of photosynthetic electron transport and quenching of chlorophyll fluorescence. Biochimica et Biophysica Acta (BBA) - General Subjects 990, 87–92. https://doi.org/10.1016/S0304-4165(89)80016-9

Gerken, H.G., Donohoe, B., Knoshaug, E.P., 2013. Enzymatic cell wall degradation of Chlorellavulgaris and other microalgae for biofuels production. Planta 237, 239–253. https://doi.org/10.1007/s00425-012-1765-0

Gifuni, I., 2017a. GIFUNI, Imma. VALORISATION OF STARCH PRODUCTION IN MICROALGAE BIOREFINERY.

Gifuni, I., 2017b. Microalgae as New Sources of Starch: Isolation and Characterization of Microalgal Starch Granules.

Grommers, H.E., van der Krogt, D.A., 2009. Chapter 11 - Potato Starch: Production, Modifications and Uses, in: BeMiller, J., Whistler, R. (Eds.), Starch (Third Edition), Food Science and Technology. Academic Press, San Diego, pp. 511–539. https://doi.org/10.1016/B978-0-12-746275-2.00011-2

Gruska, R.M., Baryga, A., Kunicka-Styczyńska, A., Brzeziński, S., Rosicka-Kaczmarek, J., Miśkiewicz, K., Sumińska, T., 2022. Fresh and Stored Sugar Beet Roots as a Source of Various Types of Mono- and Oligosaccharides. Molecules 27, 5125. https://doi.org/10.3390/molecules27165125

Guiry, M.D., 2012. How Many Species of Algae Are There? Journal of Phycology 48, 1057–1063. https://doi.org/10.1111/j.1529-8817.2012.01222.x

Günerken, E., D'Hondt, E., Eppink, M.H.M., Garcia-Gonzalez, L., Elst, K., Wijffels, R.H., 2015. Cell disruption for microalgae biorefineries. Biotechnology Advances 33, 243–260. https://doi.org/10.1016/j.biotechadv.2015.01.008

Hagemann, M., Bauwe, H., 2016. Photorespiration and the potential to improve photosynthesis. Current Opinion in Chemical Biology, Energy Mechanistic Biology 35, 109–116. https://doi.org/10.1016/j.cbpa.2016.09.014

Hall, D.O., Rao, K.K., 1999. Photosynthesis, 6th ed. ed, Studies in biology. Cambridge University Press, Cambridge, UK ; New York.

Hamlaoui, S., Yéprémian, C., Duval, C., Marie, B., Djédiat, C., Piquet, B., Bernard, C., Duperron, S., 2022. The Culture Collection of Cyanobacteria and Microalgae at the French National Museum of Natural History: A Century Old But Still Alive and Kicking! Including in Memoriam: Professor Alain Couté. crya 43, 41–83. https://doi.org/10.5252/cryptogamie-algologie2022v43a3

Hann, E.C., Overa, S., Harland-Dunaway, M., Narvaez, A.F., Le, D.N., Orozco-Cárdenas, M.L., Jiao, F., Jinkerson, R.E., 2022. A hybrid inorganic–biological artificial photosynthesis system for energy-efficient food production. Nat Food 3, 461–471. https://doi.org/10.1038/s43016-022-00530-x

Harrison, S.T.L., 1991. Bacterial cell disruption: A key unit operation in the recovery of intracellular products. Biotechnology Advances 9, 217–240. https://doi.org/10.1016/0734-9750(91)90005-G

Harun, R., Singh, M., Forde, G.M., Danquah, M.K., 2010. Bioprocess engineering of microalgae to produce a variety of consumer products. Renewable and Sustainable Energy Reviews 14, 1037–1047. https://doi.org/10.1016/j.rser.2009.11.004

Heber, U., Walker, D., 1992. Concerning a dual function of coupled cyclic electron transport in leaves. Plant Physiol 100, 1621–1626. https://doi.org/10.1104/pp.100.4.1621

Hendrickson, L., Furbank, R.T., Chow, W.S., 2004. A Simple Alternative Approach to Assessing the Fate of Absorbed Light Energy Using Chlorophyll Fluorescence. Photosynthesis Research 82, 73–81. https://doi.org/10.1023/B:PRES.0000040446.87305.f4

Hu, Q., 2013. Environmental Effects on Cell Composition, in: Handbook of Microalgal Culture. John Wiley & Sons, Ltd, pp. 114–122. https://doi.org/10.1002/9781118567166.ch7

Huot, Y., Babin, M., 2010. Overview of Fluorescence Protocols: Theory, Basic Concepts, and Practice, in: Suggett, D.J., Prášil, O., Borowitzka, M.A. (Eds.), Chlorophyll a Fluorescence in Aquatic Sciences: Methods and Applications. Springer Netherlands, Dordrecht, pp. 31–74. https://doi.org/10.1007/978-90-481-9268-7_3

IPCC, 2023. Climate Change 2022 – Impacts, Adaptation and Vulnerability: Working Group II Contribution to the Sixth Assessment Report of the Intergovernmental Panel on Climate Change, 1st ed. Cambridge University Press. https://doi.org/10.1017/9781009325844

IPCC, Dasgupta, D., Krinner, G., Mukherji, A., Thorne, P.W., Trisos, C., Romero, J., Aldunce, P., Barrett, K., Blanco, G., Cheung, W.W.L., Connors, S., Denton, F., Diongue-Niang, A., Dodman, D., Garschagen, M., Geden, O., Hayward, B., Jones, C., Jotzo, F., Krug, T., Lasco, R., Lee, Y.-Y., Masson-Delmotte, V., Meinshausen, M., Mintenbeck, K., Mokssit, A., Otto, F.E.L., Pathak, M., Pirani, A., Poloczanska, E., Pörtner, H.-O., Revi, A., Roberts, D.C., Roy, J., Ruane, A.C., Skea, J., Shukla, P.R., Slade, R., Slangen, A., Sokona, Y., Sörensson, A.A., Tignor, M., Van Vuuren, D., Wei, Y.-M., Winkler, H., Zhai, P., Zommers, Z., Hourcade, J.-C., Johnson, F.X., Pachauri, S., Simpson, N.P., Singh, C., Thomas, A., Totin, E., Arias, P., Bustamante, M., Elgizouli, I., Flato, G., Howden, M., Méndez-Vallejo, C., Pereira, J.J., Pichs-Madruga, R., Rose, S.K., Saheb, Y., Sánchez Rodríguez, R., Ürge-Vorsatz, D., Xiao, C., Yassaa, N., Alegría, A., Armour, K., Bednar-Friedl, B., Blok, K., Cissé, G., Dentener, F., Eriksen, S., Fischer, E., Garner, G., Guivarch, C., Haasnoot, M., Hansen, G., Hauser, M., Hawkins, E., Hermans, T., Kopp, R., Leprince-Ringuet, N., Lewis, J., Ley, D., Ludden, C., Niamir, L., Nicholls, Z., Some, S., Szopa, S., Trewin, B., Van Der Wijst, K.-I., Winter, G., Witting, M., Birt, A., Ha, M., Romero, J., Kim, J., Haites, E.F., Jung, Y., Stavins, R., Birt, A., Ha, M., Orendain, D.J.A., Ignon, L., Park, S., Park, Y., Reisinger, A., Cammaramo, D., Fischlin, A., Fuglestvedt, J.S., Hansen, G., Ludden, C., Masson-Delmotte, V., Matthews, J.B.R., Mintenbeck, K., Pirani, A., Poloczanska, E., Leprince-Ringuet, N., Péan, C., 2023. IPCC, 2023: Climate Change 2023: Synthesis Report. Contribution of Working Groups I, II and III to the Sixth Assessment Report of the Intergovernmental Panel on Climate Change [Core Writing Team, H. Lee and J. Romero (eds.)]. IPCC, Geneva, Switzerland. Intergovernmental Panel on Climate Change (IPCC). https://doi.org/10.59327/IPCC/AR6-9789291691647

Ivanov, I.N., Zachleder, V., Vítová, M., Barbosa, M.J., Bišová, K., 2021. Starch Production in Chlamydomonas reinhardtii through Supraoptimal Temperature in a Pilot-Scale Photobioreactor. Cells 10, 1084. https://doi.org/10.3390/cells10051084

Izumo, A., Fujiwara, S., Oyama, Y., Satoh, A., Fujita, N., Nakamura, Y., Tsuzuki, M., 2007. Physicochemical properties of starch in Chlorella change depending on the CO2 concentration during growth: Comparison of structure and properties of pyrenoid and stroma starch. Plant Science 172, 1138–1147. https://doi.org/10.1016/j.plantsci.2007.03.001

Jacques, P., Delannoy, L., Andrieu, B., Yilmaz, D., Jeanmart, H., Godin, A., 2023. Assessing the economic consequences of an energy transition through a

biophysical stock-flow consistent model. Ecological Economics 209, 107832. https://doi.org/10.1016/j.ecolecon.2023.107832

Jain, P., Singh, S., Arya, A., 2021. A student centric method for calculation of fatty acid energetics: Integrated formula and web tool. Biochemistry and Molecular Biology Education 49, 492–499. https://doi.org/10.1002/bmb.21486

Janssen, M., 2016. Chapter Four - Microalgal Photosynthesis and Growth in Mass Culture, in: Legrand, J. (Ed.), Advances in Chemical Engineering, Photobioreaction Engineering. Academic Press, pp. 185–256. https://doi.org/10.1016/bs.ache.2015.11.001

Kandilian, R., Pruvost, J., Legrand, J., Pilon, L., 2014. Influence of light absorption rate by Nannochloropsis oculata on triglyceride production during nitrogen starvation. Bioresource Technology 163, 308–319. https://doi.org/10.1016/j.biortech.2014.04.045

Kandilian, R., Taleb, A., Heredia, V., Cogne, G., Pruvost, J., 2019. Effect of light absorption rate and nitrate concentration on TAG accumulation and productivity of Parachlorella kessleri cultures grown in chemostat mode. Algal Research 39, 101442. https://doi.org/10.1016/j.algal.2019.101442

Kaplan, D.K., A.E. Richmond, Z. Dubinsky, S. Aaronson, 1986. Algal Nutrition, in: Handbook of Microalgal Mass Culture (1986). CRC Press.

Keeling, P.L., Myers, A.M., 2010. Biochemistry and Genetics of Starch Synthesis. Annual Review of Food Science and Technology 1, 271–303. https://doi.org/10.1146/annurev.food.102308.124214

Kim, D.G., Lee, C., Park, S.-M., Choi, Y.-E., 2014. Manipulation of light wavelength at appropriate growth stage to enhance biomass productivity and fatty acid methyl ester yield using Chlorella vulgaris. Bioresource Technology 159, 240–248. https://doi.org/10.1016/j.biortech.2014.02.078

Kim, Y.S., 1996. Suitability of Edible Bean and Potato Starches for Starch Noodles.

Knoll, A.H., Javaux, E.J., Hewitt, D., Cohen, P., 2006. Eukaryotic organisms in Proterozoic oceans. Philos Trans R Soc Lond B Biol Sci 361, 1023–1038. https://doi.org/10.1098/rstb.2006.1843

Kowallik, W., Schätzle, S., 1980. Enhancement of Carbohydrate Degradation by Blue Light, in: Senger, H. (Ed.), The Blue Light Syndrome, Proceedings in Life Sciences. Springer, Berlin, Heidelberg, pp. 344–360. https://doi.org/10.1007/978-3-642-67648-2_30

Kumar Tewari, A., Charan Tripathy, B., 1998. Temperature-Stress-Induced Impairment of Chlorophyll Biosynthetic Reactions in Cucumber and Wheat1. Plant Physiology 117, 851–858. https://doi.org/10.1104/pp.117.3.851

Latil de Ros, D., 2017. Microalgae as a new source of chitosans (http://hdl.handle.net/10803/402113). Universitat de Barcelona.

Leger, D., Matassa, S., Noor, E., Shepon, A., Milo, R., Bar-Even, A., 2021. Photovoltaic-driven microbial protein production can use land and sunlight more

efficiently than conventional crops. Proceedings of the National Academy of Sciences 118, e2015025118. https://doi.org/10.1073/pnas.2015025118

Levasseur, W., 2021. Biotechnological performances of acclimated green microalgae cultures : effect of light and its modulations (These de doctorat). université Paris-Saclay.

Levasseur, W., Perré, P., Pozzobon, V., 2023. Chlorella vulgaris acclimated cultivation under flashing light: An in-depth investigation under iso-actinic conditions. Algal Research 70, 102976. https://doi.org/10.1016/j.algal.2023.102976

Levasseur, W., Perré, P., Pozzobon, V., 2020. A review of high value-added molecules production by microalgae in light of the classification. Biotechnology Advances 41, 107545. https://doi.org/10.1016/j.biotechadv.2020.107545

Li, L., Aro, E.-M., Millar, A.H., 2018. Mechanisms of Photodamage and Protein Turnover in Photoinhibition. Trends in Plant Science 23, 667–676. https://doi.org/10.1016/j.tplants.2018.05.004

Li, T., Xu, J., Gao, B., Xiang, W., Li, A., Zhang, C., 2016. Morphology, growth, biochemical composition and photosynthetic performance of Chlorella vulgaris (Trebouxiophyceae) under low and high nitrogen supplies. Algal Research 16, 481–491. https://doi.org/10.1016/j.algal.2016.04.008

Libessart, N., Maddelein, M.L., Koornhuyse, NVd., Decq, A., Delrue, B., Mouille, G., D'Hulst, C., Ball, S., 1995. Storage, Photosynthesis, and Growth: The Conditional Nature of Mutations Affecting Starch Synthesis and Structure in Chlamydomonas. The Plant Cell 7, 1117–1127. https://doi.org/10.1105/tpc.7.8.1117

Liu, B.-H., Lee, Y.-K., 2000. Secondary carotenoids formation by the green alga Chlorococcum sp. Journal of Applied Phycology 12, 301–307. https://doi.org/10.1023/A:1008185212724

Liu, J., Hu, Q., 2013. Chlorella: Industrial Production of Cell Mass and Chemicals, in: Handbook of Microalgal Culture: Applied Phycology and Biotechnology. John Wiley and Sons, pp. 327–338. https://doi.org/10.1002/9781118567166.ch16

Lourdin, D., Putaux, J.-L., Potocki-Véronèse, G., Chevigny, C., Rolland-Sabaté, A., Buléon, A., 2015. Crystalline Structure in Starch, in: Nakamura, Y. (Ed.), Starch. Springer Japan, Tokyo, pp. 61–90. https://doi.org/10.1007/978-4-431-55495-0_3

Lourdin, D., Valle, G.D., Colonna, P., 1995. Influence of amylose content on starch films and foams. Carbohydrate Polymers 27, 261–270. https://doi.org/10.1016/0144-8617(95)00071-2

Malmir, S., Montero, B., Rico, M., Barral, L., Bouza, R., Farrag, Y., 2018. Effects of poly (3-hydroxybutyrate-co-3-hydroxyvalerate) microparticles on morphological, mechanical, thermal, and barrier properties in thermoplastic potato starch films. Carbohydrate Polymers 194, 357–364. https://doi.org/10.1016/j.carbpol.2018.04.056

Maningat, C.C., Seib, P.A., Bassi, S.D., Woo, K.S., Lasater, G.D., 2009. Chapter 10 - Wheat Starch: Production, Properties, Modification and Uses, in: BeMiller, J., Whistler, R. (Eds.), Starch (Third Edition), Food Science and Technology. Academic Press, San Diego, pp. 441–510. https://doi.org/10.1016/B978-0-12-746275-2.00010-0

Markou, G., Dao, L.H.T., Muylaert, K., Beardall, J., 2017. Influence of different degrees of N limitation on photosystem II performance and heterogeneity of Chlorella vulgaris. Algal Research 26, 84–92. https://doi.org/10.1016/j.algal.2017.07.005

Masojídek, J., Ranglová, K., Bečková, M., Torzillo, G., Knoppová, J., Benavides, A.M.S., Charvát, F., Komenda, J., 2022. Outdoor photoacclimation of two Chlorella strains characterized by normal and reduced light-harvesting antennas: photosynthetic activity and chlorophyll-protein organization. J Appl Phycol 34, 2339–2353. https://doi.org/10.1007/s10811-022-02803-1

Masojídek, J., Torzillo, G., Koblížek, M., 2013. Photosynthesis in Microalgae, in: Richmond, A., Hu, Q. (Eds.), Handbook of Microalgal Culture. John Wiley & Sons, Ltd, Oxford, UK, pp. 21–36. https://doi.org/10.1002/9781118567166.ch2

Mathiot, C., 2020. Measurement of photosynthetic linear and cyclic electron flows, CO2 capture in green microalgae (These de doctorat). Aix-Marseille.

Mathiot, C., Ponge, P., Gallard, B., Sassi, J.-F., Delrue, F., Le Moigne, N., 2019. Microalgae starch-based bioplastics: Screening of ten strains and plasticization of unfractionated microalgae by extrusion. Carbohydrate Polymers 208, 142–151. https://doi.org/10.1016/j.carbpol.2018.12.057

Meeus, J., 2009. Astronomical algorithms, 2. ed., [Nachdr.] with corr. ed. Willmann-Bell, Richmond, Va.

Metsoviti, M.N., Papapolymerou, G., Karapanagiotidis, I.T., Katsoulas, N., 2019. Effect of Light Intensity and Quality on Growth Rate and Composition of Chlorella vulgaris. Plants 9, 31. https://doi.org/10.3390/plants9010031

Middelberg, A.P.J., 1995. Process-scale disruption of microorganisms. Biotechnology Advances 13, 491–551. https://doi.org/10.1016/0734-9750(95)02007-P

Miyachi, Shigetoh, Miyachi, Shizuko, Kamiya, A., 1978. Wavelength effects on photosynthetic carbon metabolism in Chlorella1. Plant and Cell Physiology 19, 277–288. https://doi.org/10.1093/oxfordjournals.pcp.a075594

Müller, P., Li, X.-P., Niyogi, K.K., 2001. Non-Photochemical Quenching. A Response to Excess Light Energy1. Plant Physiology 125, 1558–1566. https://doi.org/10.1104/pp.125.4.1558

Münkel, R., Schmid-Staiger, U., Werner, A., Hirth, T., 2013. Optimization of outdoor cultivation in flat panel airlift reactors for lipid production by Chlorella vulgaris. Biotechnology and Bioengineering 110, 2882–2893. https://doi.org/10.1002/bit.24948

Nakamura, Y., Miyachi, S., 1982. Change in starch photosynthesized at different temperatures in Chlorella. Plant Science Letters 27, 1–6. https://doi.org/10.1016/0304-4211(82)90065-7

Němcová, Y., Kalina, T., 2000. Cell wall development, microfibril and pyrenoid structure in type strains of Chlorella vulgaris, C. kessleri, C. sorokiniana compared with C. luteoviridis (Trebouxiophyceae, Chlorophyta). Algological Studies/Archiv für Hydrobiologie, Supplement Volumes 95–105. https://doi.org/10.1127/algol_stud/100/2000/95

Neofotis, P., Temple, J., Tessmer, O.L., Bibik, J., Norris, N., Pollner, E., Lucker, B., Weraduwage, S.M., Withrow, A., Sears, B., Mogos, G., Frame, M., Hall, D., Weissman, J., Kramer, D.M., 2021. The induction of pyrenoid synthesis by hyperoxia and its implications for the natural diversity of photosynthetic responses in Chlamydomonas. eLife 10. https://doi.org/10.7554/eLife.67565

Nethravathy, M.U., Mehar, J.G., Mudliar, S.N., Shekh, A.Y., 2019. Recent Advances in Microalgal Bioactives for Food, Feed, and Healthcare Products: Commercial Potential, Market Space, and Sustainability. Comprehensive Reviews in Food Science and Food Safety 18, 1882–1897. https://doi.org/10.1111/1541-4337.12500

Nishida, I., Murata, N., 1996. CHILLING SENSITIVITY IN PLANTS AND CYANOBACTERIA: The Crucial Contribution of Membrane Lipids. Annu. Rev. Plant. Physiol. Plant. Mol. Biol. 47, 541–568. https://doi.org/10.1146/annurev.arplant.47.1.541

Nordin, N., Yusof, N., Maeda, T., Mustapha, N.A., Mohd Yusoff, M.Z., Raja Khairuddin, R.F., 2020. Mechanism of carbon partitioning towards starch and triacylglycerol in Chlorella vulgaris under nitrogen stress through whole-transcriptome analysis. Biomass and Bioenergy 138. https://doi.org/10.1016/j.biombioe.2020.105600

Obbard, R.W., Sadri, S., Wong, Y.Q., Khitun, A.A., Baker, I., Thompson, R.C., 2014. Global warming releases microplastic legacy frozen in Arctic Sea ice. Earth's Future 2, 315–320. https://doi.org/10.1002/2014EF000240

OECD, 2022. Global Plastics Outlook: Policy Scenarios to 2060. OECD. https://doi.org/10.1787/aa1edf33-en

Parker, M.S., Mock, T., Armbrust, E.V., 2008. Genomic Insights into Marine Microalgae. Annual Review of Genetics 42, 619–645. https://doi.org/10.1146/annurev.genet.42.110807.091417

Perrine, Z., Negi, S., Sayre, R.T., 2012. Optimization of photosynthetic light energy utilization by microalgae. Algal Research 1, 134–142. https://doi.org/10.1016/j.algal.2012.07.002

Peterhansel, C., Horst, I., Niessen, M., Blume, C., Kebeish, R., Kürkcüoglu, S., Kreuzaler, F., 2010. Photorespiration. arbo.j 2010. https://doi.org/10.1199/tab.0130

Peterhansel, C., Maurino, V.G., 2011. Photorespiration Redesigned. Plant Physiology 155, 49–55. https://doi.org/10.1104/pp.110.165019

Peters, D., 2006. Carbohydrates for fermentation. Biotechnology Journal 1, 806–814. https://doi.org/10.1002/biot.200600041

Petroutsos, D., Tokutsu, R., Maruyama, S., Flori, S., Greiner, A., Magneschi, L., Cusant, L., Kottke, T., Mittag, M., Hegemann, P., Finazzi, G., Minagawa, J., 2016. A blue-light photoreceptor mediates the feedback regulation of photosynthesis. Nature 537, 563–566. https://doi.org/10.1038/nature19358

Polman, E.M.N., Gruter, G.-J.M., Parsons, J.R., Tietema, A., 2021. Comparison of the aerobic biodegradation of biopolymers and the corresponding bioplastics: A review. Science of The Total Environment 753, 141953. https://doi.org/10.1016/j.scitotenv.2020.141953

Pulz, O., 2001. Photobioreactors: production systems for phototrophic microorganisms. Appl Microbiol Biotechnol 57, 287–293. https://doi.org/10.1007/s002530100702

Ramírez-Romero, A., Da Costa Magalhães, B., Dimitriades-Lemaire, A., Sassi, J.-F., Delrue, F., Steyer, J.-P., 2022. Chlorellaceae Feedstock Selection under Balanced Nutrient Limitation. Fermentation 8, 554. https://doi.org/10.3390/fermentation8100554

Ran, W., Wang, H., Liu, Y., Qi, M., Xiang, Q., Yao, C., Zhang, Y., Lan, X., 2019. Storage of starch and lipids in microalgae: Biosynthesis and manipulation by nutrients. Bioresource Technology 291, 121894. https://doi.org/10.1016/j.biortech.2019.121894

Raven, J.A., 2011. The cost of photoinhibition. Physiologia Plantarum 142, 87–104. https://doi.org/10.1111/j.1399-3054.2011.01465.x

Reumann, S., Weber, A.P.M., 2006. Plant peroxisomes respire in the light: Some gaps of the photorespiratory C2 cycle have become filled—Others remain. Biochimica et Biophysica Acta (BBA) - Molecular Cell Research, Peroxisomes: Morphology, Function, Biogenesis and Disorders 1763, 1496–1510. https://doi.org/10.1016/j.bbamcr.2006.09.008

Rich, P.R., 2003. The molecular machinery of Keilin's respiratory chain. Biochemical Society Transactions 31, 1095–1105. https://doi.org/10.1042/bst0311095

Robertson, T.M., Alzaabi, A.Z., Robertson, M.D., Fielding, B.A., 2018. Starchy Carbohydrates in a Healthy Diet: The Role of the Humble Potato. Nutrients 10, 1764. https://doi.org/10.3390/nu10111764

Rodolfi, L., Chini Zittelli, G., Bassi, N., Padovani, G., Biondi, N., Bonini, G., Tredici, M.R., 2009. Microalgae for oil: Strain selection, induction of lipid synthesis and outdoor mass cultivation in a low-cost photobioreactor. Biotechnology and Bioengineering 102, 100–112. https://doi.org/10.1002/bit.22033

Ross, I.L., Shah, S., Hankamer, B., Amiralian, N., 2021. Microalgal nanocellulose – opportunities for a circular bioeconomy. Trends in Plant Science 26, 924–939. https://doi.org/10.1016/j.tplants.2021.05.004

Ruggiero, M.A., Gordon, D.P., Orrell, T.M., Bailly, N., Bourgoin, T., Brusca, R.C., Cavalier-Smith, T., Guiry, M.D., Kirk, P.M., 2015. A Higher Level Classification of All Living Organisms. PLoS ONE 10, e0119248. https://doi.org/10.1371/journal.pone.0119248

Safi, C., Zebib, B., Merah, O., Pontalier, P.-Y., Vaca-Garcia, C., 2014. Morphology, composition, production, processing and applications of Chlorella vulgaris: A review. Renewable and Sustainable Energy Reviews 35, 265–278. https://doi.org/10.1016/j.rser.2014.04.007

Schansker, G., 2020. Chlorophyll Fluorescence and Photosynthesis: Simple Experiments with the JUNIOR-PAM Chlorophyll Fluorometer.

Secretariat of the Convention on Biological Diversity, 2012. Impacts of Marine Debris on Biodiversity: Current Status and Potential Solutions. CBD Technical Series No. 67 [WWW Document]. URL https://wedocs.unep.org/handle/20.500.11822/32622;jsessionid=6ADEF5710650E8AF2C5118DCB69D0E3B (accessed 2.16.24).

Shevela, D., Björn, L.O., Govindjee, 2018. Photosynthesis: Solar Energy for Life. WORLD SCIENTIFIC. https://doi.org/10.1142/10522

Shevela, D., Björn, L.O., Govindjee, 2017. The Ultimate: Artificial Photosynthesis, in: Photosynthesis: Solar Energy for Life. WORLD SCIENTIFIC, pp. 165–182. https://doi.org/10.1142/9789813223127_0009

Shi, M., Ge, T., Wang, Y., Zhao, L., 2022. Photorespiration is essential for acclimation to salt stress under high carbon availability in *Chlamydomonas*. Algal Research 64, 102687. https://doi.org/10.1016/j.algal.2022.102687

Slegers, P.M., van Beveren, P.J.M., Wijffels, R.H., van Straten, G., van Boxtel, A.J.B., 2013. Scenario analysis of large scale algae production in tubular photobioreactors. Applied Energy 105, 395–406. https://doi.org/10.1016/j.apenergy.2012.12.068

Slegers, P.M., Wijffels, R.H., van Straten, G., van Boxtel, A.J.B., 2011. Design scenarios for flat panel photobioreactors. Applied Energy, Special Issue of Energy from algae: Current status and future trends 88, 3342–3353. https://doi.org/10.1016/j.apenergy.2010.12.037

Soon Chow, W., Lee, H., Park, Youn–Il, Park, Yong–Mok, Hong, Y., Anderson, J.M., 2002. The role of inactive photosystem–II–mediated quenching in a last–ditch community defence against high light stress *in vivo*. Phil. Trans. R. Soc. Lond. B 357, 1441–1450. https://doi.org/10.1098/rstb.2002.1145

Spain, O., Funk, C., 2022. Detailed Characterization of the Cell Wall Structure and Composition of Nordic Green Microalgae. J. Agric. Food Chem. 70, 9711–9721. https://doi.org/10.1021/acs.jafc.2c02783

Suarez Ruiz, C.A., Baca, S.Z., van den Broek, L.A.M., van den Berg, C., Wijffels, R.H., Eppink, M.H.M., 2020a. Selective fractionation of free glucose and starch from microalgae using aqueous two-phase systems. Algal Research 46, 101801. https://doi.org/10.1016/j.algal.2020.101801

Suarez Ruiz, C.A., Kwaijtaal, J., Peinado, O.C., van den Berg, C., Wijffels, R.H., Eppink, M.H.M., 2020b. Multistep Fractionation of Microalgal Biomolecules Using Selective Aqueous Two-Phase Systems. ACS Sustainable Chem. Eng. 8, 2441–2452. https://doi.org/10.1021/acssuschemeng.9b06379

Takahashi, S., Murata, N., 2005. Interruption of the Calvin cycle inhibits the repair of Photosystem II from photodamage. Biochimica et Biophysica Acta (BBA) - Bioenergetics 1708, 352–361. https://doi.org/10.1016/j.bbabio.2005.04.003

Takeda, H., 1991. Sugar Composition of the Cell Wall and the Taxonomy of Chlorella (chlorophyceae)1. Journal of Phycology 27, 224–232. https://doi.org/10.1111/j.0022-3646.1991.00224.x

Templeton, D.W., Laurens, L.M.L., 2015. Nitrogen-to-protein conversion factors revisited for applications of microalgal biomass conversion to food, feed and fuel. Algal Research 11, 359–367. https://doi.org/10.1016/j.algal.2015.07.013

Tester, R.F., Karkalas, J., Qi, X., 2004. Starch—composition, fine structure and architecture. Journal of Cereal Science 39, 151–165. https://doi.org/10.1016/j.jcs.2003.12.001

Thompson, P.A., Guo, M., Harrison, P.J., 1992. Effects of Variation in Temperature. I. on the Biochemical Composition of Eight Species of Marine Phytoplankton1. Journal of Phycology 28, 481–488. https://doi.org/10.1111/j.0022-3646.1992.00481.x

Thunwall, M., Boldizar, A., Rigdahl, M., 2006. Compression Molding and Tensile Properties of Thermoplastic Potato Starch Materials. Biomacromolecules 7, 981–986. https://doi.org/10.1021/bm050804c

Torzillo, G., Vonshak, A., 2013. Environmental Stress Physiology with Reference to Mass Cultures, in: Handbook of Microalgal Culture. John Wiley & Sons, Ltd, pp. 90–113. https://doi.org/10.1002/9781118567166.ch6

Tran, T., Da, G., Moreno-Santander, M.A., Vélez-Hernández, G.A., Giraldo-Toro, A., Piyachomkwan, K., Sriroth, K., Dufour, D., 2015. A comparison of energy use, water use and carbon footprint of cassava starch production in Thailand, Vietnam and Colombia. Resources, Conservation and Recycling 100, 31–40. https://doi.org/10.1016/j.resconrec.2015.04.007

Tredici, M.R., 2010. Photobiology of microalgae mass cultures: understanding the tools for the next green revolution. Biofuels 1, 143–162. https://doi.org/10.4155/bfs.09.10

Tredici, M.R., 2004. Mass production of microalgae: photobioreactors, in: Handbook of Microalgal Culture: Biotechnology and Applied Phycology. Blackwell Science Ltd, Oxford, UK, pp. 178–214.

Van Kooten, O., Snel, J.F.H., 1990. The use of chlorophyll fluorescence nomenclature in plant stress physiology. Photosynth Res 25, 147–150. https://doi.org/10.1007/BF00033156

van Lun, M., Hub, J.S., van der Spoel, D., Andersson, I., 2014. CO2 and O2 Distribution in Rubisco Suggests the Small Subunit Functions as a CO2 Reservoir. J. Am. Chem. Soc. 136, 3165–3171. https://doi.org/10.1021/ja411579b

van Soest, J.J.G., Hulleman, S.H.D., de Wit, D., Vliegenthart, J.F.G., 1996. Crystallinity in starch bioplastics. Industrial Crops and Products 5, 11–22. https://doi.org/10.1016/0926-6690(95)00048-8

Varshney, P., Mikulic, P., Vonshak, A., Beardall, J., Wangikar, P.P., 2015. Extremophilic micro-algae and their potential contribution in biotechnology. Bioresource Technology, Advances in biofuels and chemicals from algae 184, 363–372. https://doi.org/10.1016/j.biortech.2014.11.040

Vitova, M., Bisova, K., Kawano, S., Zachleder, V., 2015. Accumulation of energy reserves in algae: From cell cycles to biotechnological applications. Biotechnology Advances 33, 1204–1218. https://doi.org/10.1016/j.biotechadv.2015.04.012

Vonlanthen, S., Dauvillée, D., Purton, S., 2015. Evaluation of novel starch-deficient mutants of Chlorella sorokiniana for hyper-accumulation of lipids. Algal Research 12, 109–118. https://doi.org/10.1016/j.algal.2015.08.008

Weissman, J.C., Goebel, R.P., Benemann, J.R., 1988. Photobioreactor design: Mixing, carbon utilization, and oxygen accumulation. Biotechnol Bioeng 31, 336–344. https://doi.org/10.1002/bit.260310409

Wellburn, A.R., 1994. The Spectral Determination of Chlorophylls a and b, as well as Total Carotenoids, Using Various Solvents with Spectrophotometers of Different Resolution. Journal of Plant Physiology 144, 307–313. https://doi.org/10.1016/S0176-1617(11)81192-2

Wingler, A., Lea, P.J., Quick, W.P., Leegood, R.C., 2000. Photorespiration: metabolic pathways and their role in stress protection. Philosophical Transactions of the Royal Society of London. Series B: Biological Sciences 355, 1517–1529. https://doi.org/10.1098/rstb.2000.0712

Wu, L., Birch, R.G., 2007. Doubled sugar content in sugarcane plants modified to produce a sucrose isomer. Plant Biotechnology Journal 5, 109–117. https://doi.org/10.1111/j.1467-7652.2006.00224.x

Xin, L., Hong-ying, H., Yu-ping, Z., 2011. Growth and lipid accumulation properties of a freshwater microalga Scenedesmus sp. under different cultivation temperature. Bioresource Technology 102, 3098–3102. https://doi.org/10.1016/j.biortech.2010.10.055

Xu, H., Yang, J., Wang, X., Peng, Q., Han, Y., Liu, X., Liu, K., Dou, S., Li, L., Liu, G., Yang, M., 2022. Starch accumulation dynamics and transcriptome analysis of Chlorella sorokiniana during transition of sulfur nutritional status. Frontiers in Marine Science 9.

Y. Shen, W. Yuan, Z. J. Pei, Q. Wu, E. Mao, 2009. Microalgae Mass Production Methods. Transactions of the ASABE 52, 1275–1287. https://doi.org/10.13031/2013.27771

Yagi, K., Hamada, K., Hlrata, K., Miyamoto, K., Miura, Y., Akano, T., Fukatu, K., Ikuta, Y., Nakamura, H.K., 1994. Stimulatory effect of red light on starch

accumulation in a marine green alga,chlamydomonas sp. strain MGA161. Appl Biochem Biotechnol 45, 225–232. https://doi.org/10.1007/BF02941801

Yamamoto, M., Fujishita, M., Hirata, A., Kawano, S., 2004. Regeneration and maturation of daughter cell walls in the autospore-forming green alga Chlorella vulgaris (Chlorophyta, Trebouxiophyceae). J Plant Res 117, 257–264. https://doi.org/10.1007/s10265-004-0154-6

Yao, C., Ai, J., Cao, X., Xue, S., Zhang, W., 2012. Enhancing starch production of a marine green microalga Tetraselmis subcordiformis through nutrient limitation. Bioresource Technology 118, 438–444. https://doi.org/10.1016/j.biortech.2012.05.030

Yap, B.H.J., Crawford, S.A., Dagastine, R.R., Scales, P.J., Martin, G.J.O., 2016. Nitrogen deprivation of microalgae: effect on cell size, cell wall thickness, cell strength, and resistance to mechanical disruption. Journal of Industrial Microbiology and Biotechnology 43, 1671–1680. https://doi.org/10.1007/s10295-016-1848-1

Yap, B.H.J., Dumsday, G.J., Scales, P.J., Martin, G.J.O., 2015. Energy evaluation of algal cell disruption by high pressure homogenisation. Bioresource Technology, Advances in biofuels and chemicals from algae 184, 280–285. https://doi.org/10.1016/j.biortech.2014.11.049

Ye, J., Yang, C., Xia, L., Zhu, Y., Liu, L., Cao, H., Tao, Y., 2023. Protoplast Preparation for Algal Single-Cell Omics Sequencing. Microorganisms 11, 538. https://doi.org/10.3390/microorganisms11020538

Yu, J.-K., Moon, Y.-S., 2021. Corn Starch: Quality and Quantity Improvement for Industrial Uses. Plants (Basel) 11, 92. https://doi.org/10.3390/plants11010092

Yuan, H., Zhang, Xinru, Jiang, Z., Wang, X., Wang, Y., Cao, L., Zhang, Xinxin, 2020. Effect of light spectra on microalgal biofilm: Cell growth, photosynthetic property, and main organic composition. Renewable Energy 157, 83–89. https://doi.org/10.1016/j.renene.2020.04.109

Yuan, Y., 2022. Phototropin links blue-light perception with starch accumulation in Chlamydomonas (Ph.D. thesis). Université Grenoble Alpes [2020-2022].

Yuan, Y., Liu, H., Li, X., Qi, W., Cheng, D., Tang, T., Zhao, Q., Wei, W., Sun, Y., 2018. Enhancing Carbohydrate Productivity of Chlorella sp. AE10 in Semi-continuous Cultivation and Unraveling the Mechanism by Flow Cytometry. Appl Biochem Biotechnol 185, 419–433. https://doi.org/10.1007/s12010-017-2667-1

Yuan, Y., Petroutsos, D., Li-Beisson, Y., 2023. Phototropin connects blue light perception to starch metabolism in green algae. https://doi.org/DOI available in the very next days

Zachleder, V., Brányiková, I., 2014. Starch Overproduction by Means of Algae, in: Bajpai, R., Prokop, A., Zappi, M. (Eds.), Algal Biorefineries. Springer Netherlands, Dordrecht, pp. 217–240. https://doi.org/10.1007/978-94-007-7494-0_9

Zachleder, V., Kselíková, V., Ivanov, I.N., Bialevich, V., Vítová, M., Ota, S., Takeshita, T., Kawano, S., Bišová, K., 2021. Supra-Optimal Temperature: An Efficient Approach for Overaccumulation of Starch in the Green Alga Parachlorella kessleri. Cells 10, 1806. https://doi.org/10.3390/cells10071806

Zhang, B., Xiong, S., Li, X., Li, L., Xie, F., Chen, L., 2014. Effect of oxygen glow plasma on supramolecular and molecular structures of starch and related mechanism. Food Hydrocolloids 37, 69–76. https://doi.org/10.1016/j.foodhyd.2013.10.034

Zhang, P., Xin, Y., He, Y., Tang, X., Shen, C., Wang, Q., Lv, N., Li, Y., Hu, Q., Xu, J., 2022. Exploring a blue-light-sensing transcription factor to double the peak productivity of oil in Nannochloropsis oceanica. Nat Commun 13, 1664. https://doi.org/10.1038/s41467-022-29337-x

Zhang, Y., Han, J.H., 2006. Mechanical and Thermal Characteristics of Pea Starch Films Plasticized with Monosaccharides and Polyols. Journal of Food Science 71, E109–E118. https://doi.org/10.1111/j.1365-2621.2006.tb08891.x

Zhang, Y., Rempel, C., Liu, Q., 2014. Thermoplastic Starch Processing and Characteristics—A Review. Critical Reviews in Food Science and Nutrition 54, 1353–1370. https://doi.org/10.1080/10408398.2011.636156

Zittelli, G.C., Biondi, N., Rodolfi, L., Tredici, M.R., 2013. Photobioreactors for Mass Production of Microalgae, in: Handbook of Microalgal Culture. John Wiley & Sons, Ltd, pp. 225–266. https://doi.org/10.1002/9781118567166.ch13